FLUID FLOW MEASUREMENT USING ELECTRICAL AND OPTICAL FIBRE STRAIN GAUGES

REKHA PHILIP-CHANDY

This research programme was sponsored by
Paul Instrument Fund, ROYAL SOCIETY

Ph.D. **1997**

FLUID FLOW MEASUREMENT USING ELECTRICAL AND OPTICAL FIBRE STRAIN GAUGES

REKHA PHILIP-CHANDY
(B.E)
[Government College of Technology, S.India]

A thesis submitted in partial fulfilment of the requirements

of **Liverpool John Moores University** for the degree of

Doctor of Philosophy

School of Electrical Engineering, Electronics and Physics

May 1997

ACKNOWLEDGEMENTS

I would like to thank my supervisors, Professor Roger Morgan and Dr. Patricia Scully, for giving me an opportunity to work in their team and for their support and encouragement all through this project. I am indebted to Professor Roger Morgan for all his valuable suggestions, patient guidance, constructive criticism and time spent for me in the execution of this work. I also take this opportunity to thank Dr. Patricia Scully for her guidance, words of encouragement and time spent for me.

I would like to express my gratitude to Sir Alan Cooke from the Royal Society for his encouragement and support.

I would like to thank Professor David Williams for his help and advice during the course of this work.

The financial support provided by the Paul Instrument Fund of the Royal Society and the Research Degrees Committee of Liverpool John Moores University is greatly appreciated.

I would like to thank Mr. Ron McGovern and Mr Brian Gray from the School's workshop for providing me with the equipment needed for this project.

I am thankful to the staff of the School of Engineering and Technology Management, for enabling me to use the wind tunnel, and the staff who helped me with the equipment near the wind tunnel, including Mr.John Carrier, Mr. Mark Jameson, and Mr. Harry Cranney.

I would like to thank Mr. M. Sokola, Mr. S.Alty, Mr Ibrahim.Z and Mr Liao.Y for all their help and Mr.B Deboux, Mr N.Schmitt and Mr D. Merchant from the Optical Fibre Sensors Research Group for their warmth and friendliness in the lab.

I am thankful to my husband, for his moral support, encouragement and prayers, and my parents, sister and in-laws for their prayers and advice.

Last, but not the least, I am ever grateful to my God and Heavenly Father, Jesus Christ, who, through the things He has done in my life during the course of this project work, has shown that the impossible can be made possible.

DEDICATED TO RAJIV, MY PARENTS,

SOWMY AND JOSHUA

ABSTRACT

The design, development and calibration of three flow sensors to measure the speed and direction of fluid flow is presented in this thesis. The force exerted by the fluid flow on the sensors are measured using strain gauges. Multidirectional fluid flow measurement has been made possible by vectorial addition of the orthogonal flow components. The fluid speed and direction are generated irrespective of each other.

Electrical resistance strain gauges are used as the force measuring device for the first version of the flow meter. These strain gauges are bonded to the four longitudinal surfaces of a square-sectioned, elastic, rubber cantilever having a drag element attached to its free end. An attempt has been made to optimise the shape and dimensions of the elastic beam to obtain a constant drag co-efficient over a wide flow range. Calibration of the electrical strain gauge flow sensor has been performed in a wind tunnel to measure air flow. The sensor has a repeatability of 0.02%, linearity within 2% and a resolution of 0.43 m/s. The most noteworthy feature of the flow sensor is its quick response time of 50 milliseconds. The sensor is able to generate a measurement of flow direction in two dimensions with a resolution of 3.6°. Preliminary measurements in a water tank enabled the speed of water to be measured with a resolution of 0.02 m/s over a range from 0 to 0.4 m/s.

An optical fibre strain sensor has been designed and developed by inserting grooves into a multimode plastic optical fibre. As the fibre bends, the variation in the angle of the grooves causes an intensity modulation of the light transmitted through the fibre. A mathematical model has been developed which has been experimentally verified in the laboratory.

The electrical strain gauge was replaced by the fibre optic strain gauge in the second version of the flow sensor. Two dimensional flow measurement was made possible by attaching two such optical fibre strain gauges on the adjacent sides of the square-sectioned rubber beam. The optical fibre flow sensor was successfully calibrated in a wind tunnel to generate both the magnitude and direction of the velocity of air. The flow sensor had a repeatability of 0.3% and measured the wind velocity up to 30 m/s with a magnitude resolution of 1.3 m/s and a direction resolution of 5.9°.

The third version of the flow sensor has used the grooved optical fibre strain sensor by itself without the rubber beam to measure the fluid flow. Wind tunnel calibration has been performed to measure two dimensional wind flow up to 35 m/s with a resolution of 0.96 m/s.

Table of contents *Page number*

INTRODUCTION 1

CHAPTER 1

TECHNIQUES OF FLOW MEASUREMENT

1.1 INTRODUCTION 4

1.2 FLUID FLOW THEORY 5

1.2.1 Properties of fluids 5

1.2.1.1 Real and perfect fluids 5

1.2.1.2 Viscosity 6

1.2.2 Reynolds number 7

1.2.3 Types of flow 8

1.2.3.1 Laminar and turbulent flows 8

1.2.3.2 Other classifications of flow 11

1.2.4 Fluid forces on a body 11

1.3 REVIEW OF THE FLOWMETERS IN CLOSED CONDUIT SYSTEMS 13

1.3.1 Volume flow meters 14

1.3.1.1 Variable area meters 14

1.3.1.2 Pressure difference meters 16

1.3.2 Mass flow meters 18

1.3.2.1 True mass flow meters 18

1.3.2.2 Inferential mass flow meter 20

1.3.3 Velocity meters 20

1.3.3.1 Point velocity meter : The pitot tube 20

1.3.3.2 Full flow velocity meter: Electromagnetic meter 22

1.3.3.3 Full flow velocity meter: Turbine meter 24

1.3.3.4 Full flow velocity meter: Vortex shedding meters 24

1.3.3.5 Full flow velocity meter: Ultrasonic meters 26

1.3.4 Miscellaneous flow metering techniques 28

1.3.4.1 Thermal flow meters 28

1.3.4.2 Laser Doppler Anemometer 30

1.4 TARGET FLOW SENSORS 31

1.4.1 Principle of operation of target flow sensors 31

1.4.2 Literature review of target flow sensors 33

CHAPTER 2

ELECTRICAL STRAIN MEASUREMENT

2.1 INTRODUCTION 37

2.2 BRIEF HISTORY 38

2.3 BASIC OPERATING PRINCIPLE 39

2.4 THE BONDED ELECTRICAL RESISTANCE STRAIN GAUGE 41

2.4.1 The grid 41

2.4.2 Backing 43

2.5 PERFORMANCE AND PROPERTIES OF FOIL-TYPE STRAIN GAUGES 44

2.5.1 Strain cycling 44

2.5.2 Drift, Creep and Stability 45

2.5.3 Resolution 45

2.5.4 Heat Dissipation 45

2.5.5 Thermal EMF's 47

2.5.6 Magnetic fields 47

2.5.7 Temperature Effects on gauge resistance 47

2.5.8 Elongation capability 48

2.5.9 Fatigue life 48

2.6 STRAIN GAUGE SELECTION PARAMETERS 49

2.6.1 Gauge length 49

2.6.2 Gauge resistance 49

2.7 STRAIN GAUGE INSTALLATION 51

2.8 STRAIN GAUGE INSTRUMENTATION 53

2.8.1 The sensing circuit 54

2.8.1.1 Quarter bridge operation 55

2.8.1.2 Half bridge 56

2.8.1.3 Full bridge 57

2.8.1.4: The sensing circuit used in this PhD project work 59

2.8.2 Bridge supply 59

2.8.3 Amplifiers 60

2.8.4 Real time processing and display 60

CHAPTER 3

ASSESSMENT OF THE SUITABILITY OF RUBBER AS THE SENSING BEAM MATERIAL FOR THE FLOW METER

3.1 INTRODUCTION 62

3.2 THE NATURE OF RUBBER 63

3.2.1 Thermoplastics 63

3.2.2 Thermosets 63

3.2.3 Elastomers 63

3.2.4 Discussion of the rubber used as the sensing beam material for air, water and oil flow measurements 64

3.3 RUBBER COMPOUNDING AND MANUFACTURE 66

3.3.1 Raw rubber 66

3.3.2 Vulcanisation 67

3.3.3 Reinforcement 69

3.3.4 Antidegradants 69

3.3.5 Other additives 69

3.3.6 The mixing and shaping processes 70

3.4 PHYSICAL PROPERTIES OF RUBBER AND HENCE THE SENSING BEAM OF THE FLOW SENSOR 72

3.4.1 Young's Modulus of the rubber beam of the flow sensor 72

3.4.2 Incompressibility and its effect on the sensitivity of the flow sensor 74

3.4.3 Strength of rubber and its effect on the dynamic range of the flow sensor 75

3.4.4 Hardness 75

3.4.5 Hysteresis 75

3.4.6 Effects of environment on rubber and the flow sensor 76

3.5 HOW TO ENSURE THE EFFECTIVENESS OF RUBBER AS A SENSING BEAM MATERIAL 78

CHAPTER 4

THE ELECTRICAL STRAIN GAUGE TARGET FLOW SENSOR

4.1 PRINCIPLE OF OPERATION OF THE FLOW SENSOR 80

4.1.1 Principle of one dimensional fluid flow measurement 80

4.1.2. Principle of two dimensional fluid flow measurement 83

4.2. ONE DIMENSIONAL AIRFLOW MEASUREMENT 83

4.2.1. Sensor design 83

4.2.2. Experiments in the wind tunnel 84

4.3. TWO DIMENSIONAL AIR FLOW MEASUREMENT 86

4.3.1. Design of the Elastic beam 86

4.3.2 The force measuring element 89

4.3.2.1 Specifications of the strain gauge used 89

4.3.2.2 Signal conditioning and amplification 89

4.3.3 Data acquisition and analysis 91

4.3.3.1 Labview 91

4.3.3.2 *Data acquisition* 91

4.3.3.3 *Data processing* 92

4.3.4 Experiments in the Wind tunnel 93

4.3.4.1 Magnitude of wind velocity 93

4.3.4.2 Direction of wind velocity 96

4.4. EXPERIMENTS ON SENSORS WITH DIFFERENT SENSING BEAM MATERIAL AND DIMENSIONS 97

4.4.1. Experimental Prototype 2: Hollow plastic beam 97

4.4.2. Experimental Prototype 3: A steel-spring sensing tube 98

4.4.3. Experimental Prototype 4: A rubber cylinder of circular cross-section 99

4.4.4. Experimental Prototype 5: A square-sectioned rubber sensing beam 101

4.4.5. Comparison of the different prototypes 103

4.5. COMPARISON OF THE THEORETICAL INVESTIGATION WITH THE EXPERIMENTAL RESULTS 103

4.5.1. Circular rubber beam 103

4.5.1.1 Theoretical investigation of the deflection behaviour of the flow sensor of circular cross-section 103

4.5.1.2 Determination of the drag co-efficient and Reynolds number 105

4.5.1.3 Comparison with the experimental results 107

4.5.2 Square-sectioned rubber beam 107

4.5.3 Optimisation of the shape and dimensions of the sensing element 108

4.6 ONE DIMENSIONAL WATER FLOW MEASUREMENT 109

4.7 EXTENDING THE TARGET FLOW SENSOR TO OTHER FLUIDS 111

4.8 DISCUSSION 113

CHAPTER 5

PERFORMANCE CHARACTERISTICS OF THE ELECTRICAL STRAIN GAUGE FLOW SENSOR

5.1 INTRODUCTION 114

5.2 STATISTICS FROM THE FLOW SENSOR EXPERIMENTS 115

5.2.1 Brief introduction 115

5.2.2 Results from the present work on the flow sensor 116

5.3 OPERATING CHARACTERISTICS OF THE FLOW SENSOR 117

5.3.1 Measurement 118

5.3.2 Operation 118

5.3.3 Environmental effects 119

5.3.4 Operating characteristics of the flow sensor 119

5.4 STATIC CHARACTERISTICS OF THE FLOW SENSOR 120

5.4.1 Accuracy 120

5.4.2 Repeatability/Reproducibility 122

5.4.3 Hysteresis 123

5.4.4 Linearity 123

5.5 DYNAMIC CHARACTERISTICS OF THE FLOW SENSOR 124

5.5.1.Step response 124

5.5.2 Wind tunnel experiments 128

5.5.3 Dropping weight experiments 129

5.6 DISCUSSION 131

CHAPTER 6

A REVIEW OF OPTICAL FIBRE SENSORS

6.1 INTRODUCTION TO OPTICAL FIBRE SENSORS 132

6.2 TRANSDUCTION MECHANISMS 135

6.2.1 Intensity modulated Sensors 135

6.2.1.1 Microbending Sensors 136

6.2.1.2 Breakage or crack sensors 138

6.2.1.3 Transmission-Reflection modulation sensors 138

6.2.1.4 Sensors based on refractive index changes 140

6.2.1.5 Modulation by evanescent wave coupling 140

6.2.1.6 Absorption and light scattering sensors 142

6.2.1.7 Modified cladding 142

6.2.2 Polarisation modulated sensors 144

6.2.3 Wavelength and frequency modulated sensors 146
6.2.4 Phase Modulated sensors 147
6.2.4.1 Principle of interferometry *147*
6.2.4.2 Two beam interferometers *148*
6.2.4.3 Multiple beam interferometers. *150*
6.3 REVIEW OF OPTICAL FIBRE FLOW SENSORS 150
6.3.1 Variable area optical flowmeters 150
6.3.2 Fibre optic Impeller devices 151
6.3.3 Vortex shedding optical flow sensors 153
6.3.3.1 Pressure based vortex sensors *153*
6.3.3.2 Strain based vortex sensors *155*
6.3.4 Thermal flowmeters 155
6.3.5 Ultrasonic optical flowmeters 157
6.4 DISCUSSION 158

CHAPTER 7

THE FIBRE OPTIC STRAIN GAUGE

7.1 THE POLYMER FIBRE STRAIN SENSOR FABRICATION 159
7.1.1 Why Plastic Fibres? 159
7.1.2 The Fibre Groove 161
7.2 PRINCIPLE OF OPERATION OF THE OPTICAL FIBRE STRAIN GAUGE 161
7.2.1 Definition of strain sensitivity 163
7.2.2 Gauge factor for multiple grooves. 165
7.2.3 The effect of groove closing 167
7.3 EXPERIMENTAL VERIFICATION OF THE THEORY 167
7.3.1 Experimental arrangement 167
7.3.2 Thermal effects 168
7.3.3 The measurement process 169
7.3.4 The effect of continuous bonding 171
7.4 OPTIMISATION OF THE NUMBER OF GROOVES 172
7.5 COMPARISON OF THE OPTICAL FIBRE STRAIN GAUGE WITH THE ELECTRICAL RESISTANCE STRAIN GAUGE 174
7.6 DISCUSSION 175

CHAPTER 8

THE OPTICAL FIBRE STRAIN GAUGE FLOW SENSOR

8.1 THE OPTICAL FIBRE FLOW SENSOR WITH RUBBER CANTILEVER 177
8.1.1 Construction of the optical fiber flow sensor in one dimension 177
8.1.2 Principle of operation of the optical fiber flow sensor 179
8.1.3 Referencing of the optical sensor system 179
8.2 PRINCIPLE OF OPERATION OF THE FLOW SENSOR IN TWO DIMENSIONS 181
8.3 WIND TUNNEL EXPERIMENTS 184
8.3.1 Flow sensing and display 184
8.3.2 Magnitude of wind speed: First prototype of the optical fibre flow sensor 185
8.3.3 Magnitude of wind speed: Second prototype of the optical fibre flow sensor 185
8.3.4 Direction of wind velocity 190
8.4 STATIC CHARACTERISTICS OF THE OPTICAL FIBRE FLOW SENSOR 190
8.5 DYNAMIC CHARACTERISTICS OF THE OPTICAL FIBRE FLOW SENSOR 194
8.6 AN OPTICAL FIBRE FLOW SENSOR WITHOUT RUBBER CANTILEVER. 195
8.6.1 Development of the flow sensor 196
8.6.2. Experiments in the Wind Tunnel 196
8.7 DISCUSSION OF THE RESULTS 198

CHAPTER 9

CONCLUSION: SENSOR FEATURES AND APPLICATION AREAS

9.1 NOVEL FEATURES OF THE FLOW SENSORS 200
9.1.1 The novelty of the research undertaken to develop the target flow sensors 200
9.1.2 Improved features of these flow sensors over others 201
9.2 APPLICATION AREAS 202
9.2.1. Meteorology 202
9.2.2. Hydrology 202
9.2.3. Marine studies 202
9.2.4 Oil and gas industry 203
9.2.5 Automobile Industry 203
9.2.6 Domestic water metering 203

9.2.7 Steam measurement 204
9.2.8 Multi-phase flow 204
9.3 SUGGESTIONS FOR FURTHER WORK 205

REFERENCES

APPENDICES

PUBLICATIONS

GLOSSARY

μ	dynamic viscosity of the fluid (Ns/m^2)
ν	kinematic viscosity of the fluid (m^2/s)
ρ	Density of the fluid (Kg/m^3)
τ	frictional shearing stress (N/m^2)
du/dy	velocity gradient
Re	Reynolds number
Q	Volume/unit time
C_d	discharge co-efficient
P_s	Impact or stagnation pressure (N/m^2)
P_1	Static pressure (N/m^2)
c	Velocity of sound (m/s)
δ	fringe spacing
λ	wavelength of laser light (nm)
F_D	total drag (N)
F_F	friction drag (N)
F_P	pressure drag (N)
C_D	drag co-efficient
V	velocity of fluid flow (m/s)
R	Resistance of a conductor(Ω)
L	Length of conductor (m)
A	cross-sectional area of conductor (m^2)
ρ	specific resistance
ν	Poisson's ratio
σ	Stress in the conductor (N/m^2)
ε_a	axial strain in the conductor
ε_t	transverse strain in the conductor
S_A	electrical strain sensitivity
E_B	bridge excitation voltage (volts)
R_G	gauge resistance (Ω)
ε	actual strain
$\hat{\varepsilon}$	indicated strain

E	Young's modulus
A	Area of the drag element (m^2)
a	beam thickness (m)
b	beam width (m)
U	magnitude of wind velocity (m/s)
U_x	x-component of wind velocity (m/s)
U_y	y-component of wind velocity (m/s)
θ	direction of wind velocity (degrees)
$Strain_x$	x-component of strain
$Strain_y$	y-component of strain
V_{init}	unstrained voltage of the strain gauge (volts)
V_{sg}	voltage read from the strain gauge (volts)
n_1	refractive index of the core
n_2	refractive index of the cladding
θ_m	ray propogation angle (degrees)
a	depth of the groove in the POF (m)
$2z_0$	width of the groove in the POF prior to straining(m)
2z	width of the groove in the POF after application of strain (m)
$2\theta_0$	apex angle of the groove prior to straining (degrees)
$2\theta_x$	apex angle of the groove after strain (degrees)
P_i	Power transmitted through the POF before grooving (W)
P_0	Power transmitted through the POF after grooving at zero strain (W)
P_x	Power transmitted through the POF after grooving at strain 'x'(W)
P_{L0}	Light lost from a groove at zero strain (W)
P_{Lx}	Light lost from a groove at strain 'x'(W)
S_0	optical strain sensitivity
n	number of grooves

INTRODUCTION

The measurement of fluid flow is vital for a wide range of industrial processes and environmental applications. Looking at the history of flowmeters, one can learn that it is only in the past twenty years that some techniques have been perfected while others are showing significant promise for the future. This thesis describes the design, development and calibration of three flow sensors, all of which are based on the principle of cantilever beam deflection. The first flow sensor has used conventional resistance strain gauges while the latter two have used optical fibre strain gauges to sense the deflection. These sensors were specifically designed to measure fluid flow in the natural environment and in industry.

Conventional electrical resistance strain gauges have been in the market for the last five decades. Continuous commercial development, and extensive industrial and research investigations, have resulted in excellent performance characteristics particularly in stability, temperature compensation, and creep. Such advantages in turn has led to the resistance strain gauge becoming the basic sensing element of very high precision load transducers and weighing systems. In this project the resistance strain gauge has been used to sense the deflection of a rubber cantilever due to force exerted by fluid flow. The combination of the two have led to the development of the resistance strain gauge target flow sensor to measure the speed and direction of two dimensional fluid flow.

A novel method to measure strain using plastic optical fibres will be discussed in this thesis. While resistance strain gauges are one of the few accurate, sensitive, versatile and easy-to-use sensors available today, they have problems in hazardous environments. The optical fibre strain gauge that has been developed, optimised and calibrated in this project could be used in such hostile areas and where there is a need for immunity to electromagnetic interference or corrosion. The fibre optic strain gauge has been used to measure fluid flow by attaching it to the surface of a rubber cantilever. The deflection of the rubber cantilever produces a change in the intensity of light transmitted through the optical fibre which can be related to the velocity of the fluid. The measurement of two dimensional fluid flow has been made possible by attaching two such fibres on the two adjacent sides of the rubber beam. This has enabled the speed and direction of the fluid

flow to be measured. The third flow sensor that has been developed and calibrated, has used the above mentioned optical fibre strain gauge itself as the drag element, by completely removing the rubber beam. This configuration of the optical fibre flow sensor has better performance characteristics than the optical fibre flow sensor with the rubber cantilever.

The structure of the thesis is as follows:

Chapter One reviews the flow measurement techniques where a background of concepts is built up from first principles, which may be utilised in the application of fluid dynamics to problems in different fields of engineering. This chapter also reviews the various flowmeters that have been in the market with a brief description of their working principle. In particular, a literature review on the target flow sensors has been discussed.

Chapter Two discusses the resistance strain gauges that have been in use since 1940. In this chapter, the operating principle, installation and instrumentation used by the strain gauges are reviewed.

The choice of a suitable material for the sensing beam of the flow sensor described in this thesis was an important aspect in the design of the flow sensor. Chapter Three assesses the suitability of rubber as the material for the sensing beam. Compared to other materials, rubbers offer the most useful range of moduli and many different types are available. The unique combinations of useful properties which rubbers exhibit make them the ideal material for the sensing beam of these flow sensors.

Chapter Four describes the design, development and calibration runs of the resistance strain gauge flow sensor to measure one and two dimensional air flow, which in turn measures the speed and direction of wind velocity. The results of the experiments performed in a wind tunnel and preliminary experiments in a water tank to measure one dimensional water speed are presented.

Chapter Five investigates the performance characteristics of the resistance strain gauge target flow sensor to evaluate both the static and dynamic characteristics of this flow sensor.

Chapter Six reviews the optical fibre sensor development with particular attention to the optical fibre flow sensors that have been in the market. Some of these optical fibre flow

sensors are based on the existing conventional techniques of flow measurement discussed in Chapter One.

Chapter Seven investigates the construction and optimisation of a fibre optic strain gauge where a novel intensity based sensor using a plastic optical fibre has been developed. A mathematical theory has been postulated which has been confirmed by experiments performed in the lab.

Chapter Eight evaluates the design and operation of two optical fibre flow sensors, both of which have used the optical fibre strain sensor described in the previous chapter. The first optical fibre flow sensor has sensed the deflection caused by the fluid using the rubber cantilever on which the strain sensor is attached. The second flow sensor has used unsupported sensitised 1mm diameter plastic optical fibre sans the rubber beam to measure the fluid induced deflection.

Finally, in Chapter Nine, the novel features and application areas of these flow sensors are discussed.

CHAPTER 1

TECHNIQUES OF FLOW MEASUREMENT

1.1 INTRODUCTION

Flow measurement is important to the economy of any business where fluids of all types are bought and sold. There is an ever increasing need for accurate and reliable flow measurement at realistic cost. The importance of measuring the flow of fluid is apparent in some areas, such as oil and gas, but there are many other less obvious ones where it is equally important, such as power generation and the chemical and process industries. The impact of flow measurement is universal. At one end of the scale, it challenges us in spacecraft, not only in ensuring correct fuelling of the thruster motors but also in accurately ventilating the spacesuits of the occupants. In more mundane affairs, it has a widespread use on land and on sea; so much so that flow and its measurement form part of our daily lives.

In any assessment the form taken by the fluid also assumes an important part. We have purely liquid and purely gas states at a variety of pressures and temperatures. To these multi-phase versions must be added, some being liquids or gases containing particulate solids or liquids containing gases, gases with traces of liquid, or mixtures of liquids or gases, etc. All this adds to the complexity of the operational procedures and computational techniques which must be applied in a specific situation, whether in an open channel or a closed duct. Now, more than ever, the need for the conservation and the efficient utilisation of the reserves of energy existing on this planet are coming to be realised. Once again flow measurement is to be found on the forefront as an essential constituent in metering consumption.

This introductory chapter deals initially with the fluid flow theory, where a background of concepts is built up from first principles, which may be utilised in the application of fluid dynamics to problems in different fields of engineering. This is followed by a review of the different flowmeters which have been in use over the past century, with a brief description of their theory along with their advantages and disadvantages in industry.

Finally this chapter will focus on the target flow sensor by presenting a literature review on the different drag-force sensing techniques that have been published.

1.2 FLUID FLOW THEORY

1.2.1 Properties of fluids

The science of fluid dynamics concerns itself with the determination of the characteristics of the flow past bodies of various shapes. Before proceeding with the analysis of flow problems, it is necessary to have an understanding of the fluid medium with which we are dealing. Fluids are of two types, liquid and gaseous. In this project, we are concerned with a gaseous fluid, air, but many of the concepts apply equally well to the flow of liquids.

1.2.1.1 Real and perfect fluids

Most theoretical investigations in the field of fluid dynamics are based on the concept of a perfect, i.e. frictionless and incompressible, fluid. In the motion of such a perfect fluid, two contacting layers experience no tangential forces (shearing stresses) but act on each other with normal forces (pressures) only. This is equivalent to stating that a perfect fluid offers no internal resistance to a change in shape. The theory describing the motion of a perfect fluid is mathematically very far developed and supplies in many cases a satisfactory description of real motions, such as the motion of surface waves or the formation of liquid jets. On the other hand the theory of perfect fluids fails completely to account for the drag of a body. In this connection it leads to the statement that a body which moves uniformly through a fluid which extends to infinity, experiences no drag (d'Alembert's paradox). [1.1] This unacceptable result of the theory of a perfect fluid can be traced to the fact that the inner layers of a real fluid transmit tangential as well as normal stresses, this being also the case near a solid wall wetted by a fluid. These tangential or friction forces in a real fluid are connected with a property which is called the *viscosity* of the fluid.

Because of the absence of tangential forces, on the boundary between a perfect fluid and a solid wall there exists, in general, a difference in relative tangential velocities, i.e. there is slip. On the other hand, in real fluids the existence of intermolecular attractions causes the fluid to adhere to a solid wall and this gives rise to shearing stresses [1.1].

The existence of tangential (shearing) stresses and the *condition of no slip* near solid walls constitute the essential differences between a perfect and a real fluid. Fluids like water and air, which are of great practical importance, have very small coefficients of viscosity, but unlike in perfect fluids, the condition of no slip near a solid boundary prevails. A perfect fluid may be defined as non-viscous or inviscid; thus no shear stresses exist for this fluid when it is in motion.

1.2.1.2 Viscosity

The viscosity of a fluid is a measure of its resistance to flow. It is this property of all real fluids that distinguishes them from ideal or non-viscous fluids. A gas consists of a large number of molecules each of which has a random motion. If a gas is in motion with a velocity 'v', then each molecule has in addition to its random speed 'c' an ordered velocity 'v'. The concept of viscosity has meaning only for gases that have an ordered velocity. The viscosity of a fluid is manifested itself by its tendency to adhere to a surface. [1.1] The nature of viscosity can best be visualised with the aid of the following experiment: Consider the motion of a fluid held captive between two very long, parallel plate; one at rest, the other moving with a constant velocity parallel to itself as shown in Figure 1.1. Let the distance between the plates be 'h', the pressure being constant throughout the fluid.

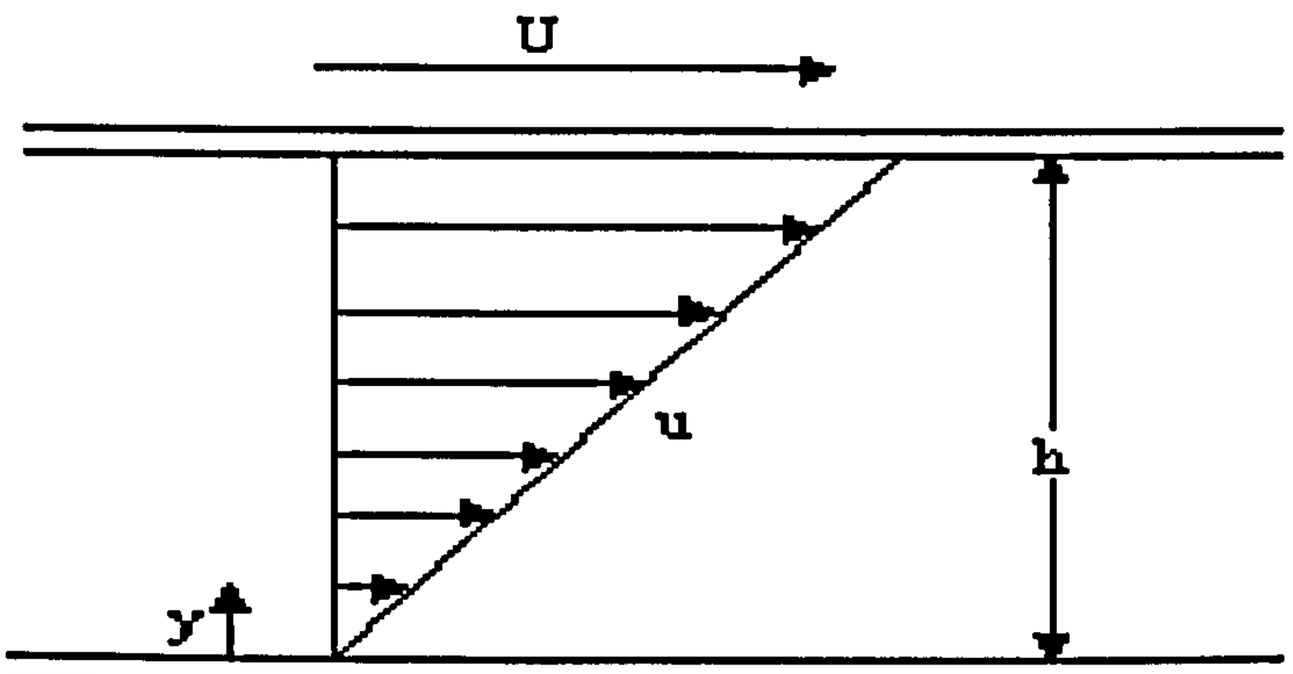

Figure 1.1 : Velocity distribution in a viscous fluid between two parallel flat walls (Couette flow)

Experiment [1.1] teaches that the fluid adheres to both walls, so that its velocity at the lower plate is zero, and that at the upper plate is equal to the velocity of the plate, U. Furthermore, the velocity distribution in the fluid between the plates is linear, so that the fluid velocity is proportional the distance 'y' from the lower plate, and we have

$$u(y) = \frac{y}{h}U \qquad (1.1)$$

In order to support the motion it is necessary to apply a tangential force to the upper plate, the force being in equilibrium with the frictional forces in the fluid. This force, frictional shearing stress, τ, resists the motion of the upper plate and is proportional to the velocity U of the upper plate, and inversely proportional to the distance 'h', which in general can be substituted by du/dy, the velocity gradient. Therefore,

$$\tau = \mu \frac{du}{dy} \qquad (1.2)$$

where μ is a factor of proportionality known as *dynamic viscosity* which depends on the nature of the fluid. The dimensions of μ, the dynamic viscosity are $ML^{-1}T^{-1}$ and its units in the SI system of units is Ns/m^2 and in the cgs system, the poise [0.1 Ns/m^2]. The dynamic viscosity of water at 20°C is approximately 1.002×10^{-3} Ns/m^2 and that of air at 20°C is 18.2×10^{-6} Ns/m^2. It was Newton who postulated that the shear stress, τ, is proportional to the velocity gradient and consequently Equation 1.2 is referred to as *Newton's law of friction*, and the fluids that conform to this law are considered to be *Newtonian fluids*.[1.1]

In all fluid motions in which frictional and inertial forces interact, it is important to consider the ratio of the viscosity,μ, to the density,ρ , known as the *kinematic viscosity*, ν.

$$\nu = \frac{\mu}{\rho} \qquad (1.3)$$

The dimensions of the kinematic viscosity are L^2T^{-1} and the units are m^2/s. Water, air and gas are essentially Newtonian fluids because linearity exists between shear stress, τ and velocity gradient.

1.2.2 Reynolds number

A very important dimensionless parameter used to define the regions within the operating flow range of a meter, where the meter performance is sensitive or insensitive to fluid parameters, is the Reynolds number. The Reynolds number is a ratio of the inertial force to the viscous force acting on the body. The viscous force is that needed to

maintain motion through the fluid. The inertial force is the force that would be needed to stop the body which is moving along steadily with its own inertia. [1.2]

The inertial force (F_I)of a parcel of air or water is proportional to the square of its speed, U^2, divided by its length scale, d. The frictional or viscous force(F_V) working on an object of diameter d moving through a fluid at speed U is given as

$$F_V = \frac{U\nu}{d^2} \qquad (1.4)$$

where ν is the kinematic viscosity of the fluid and

$$F_I = \frac{U^2}{d} \qquad (1.5)$$

The ratio of these forces , Re, is a dimensionless parameter given by

$$Re = Ud/\nu \qquad (1.6)$$

Two flow regimes are considered identical if they have the same Reynolds number. This allows the flow around an obstacle to be modelled in a tank or tunnel simply by choosing U, d and ν so that Re is the same as in the atmosphere or ocean.

1.2.3 Types of flow

Experimental observations have shown that two distinct types of flow can exist; the laminar or streamline flow and turbulent flow.

1.2.3.1 Laminar and turbulent flows

The first type of flow is **laminar** or **streamline** or **viscous** flow. Laminar flow is defined as flow under conditions where forces due to viscosity are more significant than forces due to inertia. This is shown for a circular pipe in Figure 1.2. This type of flow has the characteristic of having adjacent fluid particles move along essentially parallel paths in a highly ordered manner. Thus laminar flow in a circular pipe can be considered as a number of annular layers: the velocity of these layers increases from zero at the pipe wall to maximum at the pipe centre with significant viscous shear stresses between each layer. Figure 1.2 shows the resulting velocity profile; a graph of layer velocity, v, versus distance, r, of layer from centre, which is parabolic in shape.

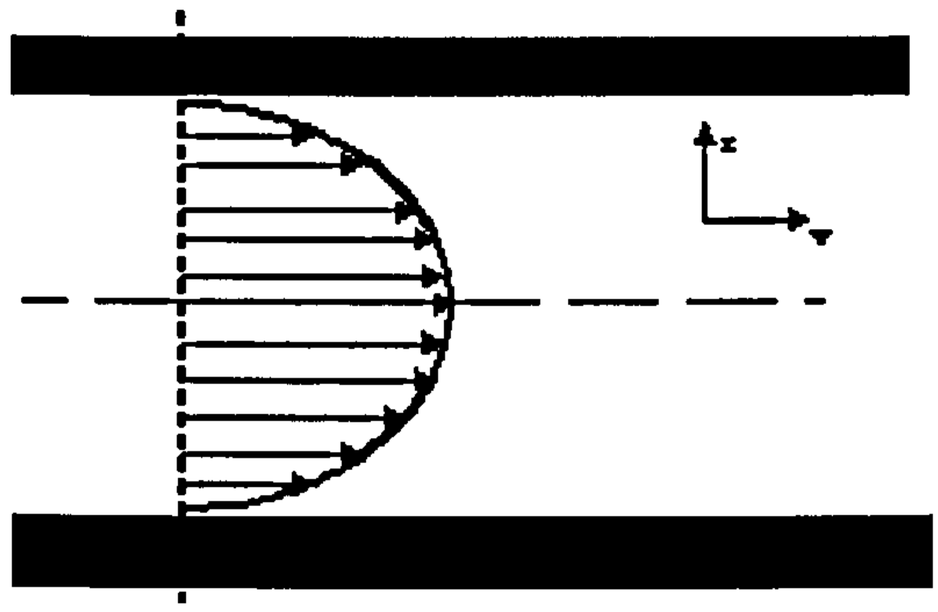

Figure 1.2 : Velocity profile of laminar flow in a circular pipe

Measurements show that the type of motion through a circular pipe in which the velocity distribution is parabolic exists only at low and moderate Reynolds number. The second type of flow, **turbulent flow**, is shown in Figure 1.3. This is highly disordered; each particle moves randomly in three dimensions and occupies different relative positions in successive cross sections. As a result, the velocity and pressure at a given point in the pipe are both subject to small random fluctuations with time about their mean values. The viscous friction forces which cause the ordered motion in laminar flow are much smaller in turbulent flow.

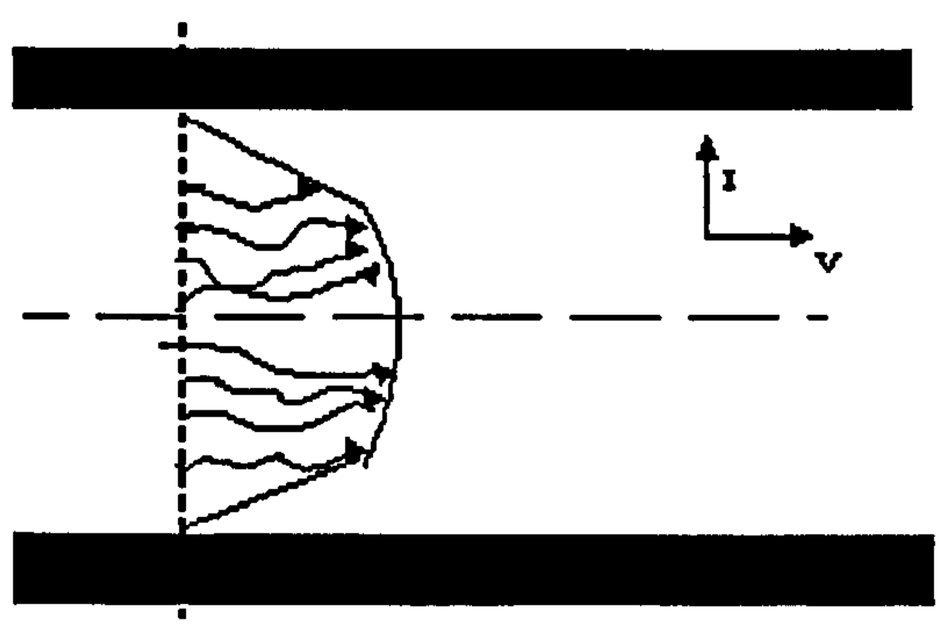

Figure 1.3 : Velocity profile of turbulent flow in a circular pipe

O.Reynolds (1842-1912) demonstrated in his classic paper, that this characteristic of the motion can be made clearly visible by introducing a dye into the stream and by discharging it through a thin tube[1.3]. At the moderate Reynolds number associated with laminar flow, the dye is visible in the form of a clearly defined thread extending over the whole length of the pipe. By increasing the flow velocity, it is possible to reach a stage when the fluid particles cease to move along straight lines and the regularity of the motion breaks down. The coloured thread becomes mixed with the fluid, its sharp outline becomes blurred and eventually the whole cross section becomes coloured. There are now superimposed irregular radial fluctuations which effect the mixing. Such a flow

pattern is called turbulent. Reynolds ascertained that the transition from the laminar to turbulent type of motion takes place at a definite value of the Reynolds number called the critical Reynolds number.

The actual value of the critical Reynolds number depends further on the details of the experimental arrangement, in particular on the amount of disturbance suffered by the fluid before entering the pipe. With an arrangement that is as free from disturbances as possible, a critical Reynolds number exceeding 10^4 can be attained. With a sharp edged entrance the critical Reynolds number becomes approximately

$$R_{crit} = \left(\frac{\bar{u}d}{\nu}\right)_{crit} \approx 2300 \text{ (pipe)} \qquad (1.7)$$

where $\bar{u}$ denotes the mean velocity averaged over the cross-sectional area.

This value can be regarded as the *lower limit for the critical Reynolds number* below which even strong disturbances do not cause the flow to become turbulent. Accordingly, flows for which the Reynolds number $Re < R_{crit}$ are supposed to be laminar, and flows for which $Re > R_{crit}$ are expected to be turbulent. The numerical value of the critical Reynolds number depends very strongly on the conditions which prevail in the initial pipe length as well as in the approach to it. Reynolds postulated that the critical Reynolds number increases as the disturbances in the flow before the pipe are decreased. This fact was confirmed experimentally by Barnes [1.4] and later by Schiller [1.5] who obtained critical values of the Reynolds number of up to 20,000. Ekman [1.6] succeeded in maintaining laminar flow up to a critical Reynolds number of 40,0000 by providing an inlet which was made exceptionally free from disturbances. The *upper limit* to which the critical Reynolds number can be driven, if extreme care is taken to free the inlet from the disturbances, is not known at present.

Experiments [1.7] show that it is possible to maintain laminar flow to very high Reynolds numbers if care is taken to increase the flow gradually, but normally the slightest disturbance will destroy the laminar boundary layer if the value of Reynolds number is greater than 4000. Similarly, flow initially turbulent can be maintained with care to very low Reynolds numbers, but the slightest upset will result in laminar flow if the Reynolds number is less than 2000. The Reynolds number range between 2000 and 4000 is known

as the critical zone. Flow in the zone is unstable, and designers of piping systems must take this into account.[1.7].

1.2.3.2 Other classifications of flow

Various types of flow can be distinguished. For example, flow may be steady, unsteady or pulsating, compressible or incompressible and subsonic or supersonic.

Flow is **steady** when conditions do not vary in time, or when, in the case of turbulent flow, the statistical parameters (mean value and standard deviation) do not vary in time. The steady flows observed in pipes are, in practice, flows in which quantities (such as velocity, pressure, mass, density and temperature) vary in time about mean values which are independent of time; these are actually "statistically steady flows".

Unsteady flow, on the other hand, is a flow in which the flow rate fluctuates randomly with time and for which the mean value is not constant.

Pulsating flow is defined as having a flow rate that varies with time, but for which the mean flow rate is constant when obtained over a sufficiently long period of time.

Flow is **incompressible** if there are no or negligible density changes. Compressible effects can occur in gas flows at high velocities.

Subsonic flows involves flow with velocity less than sound. (Sonic speeds in air at STP is 330 m/s. Mach number(M) is a dimensionless quantity used to define if the flow is subsonic or supersonic. It is the ratio of the fluid speed to the local speed of sound. When $M<1$, the flow is subsonic and if $M>1$, the flow is **supersonic**. For $M<0.3$, the flow is incompressible.

1.2.4 Fluid forces on a body

A body in the flow experiences a fluid force when there is a relative motion between the fluid and the body. Relative motion means that there exists a velocity difference between the body and the fluid; i.e. the body may be at rest or moving at a velocity lower or higher than that of the flow. The fluid force acting in the direction of the motion of the body is known as the drag force. The fluid force acting normal to the direction of motion of the body is called the lift force. Theoretical determination of the fluid forces is not yet possible. The usual approach is to determine the fluid forces via

the introduction of the drag and lift coefficients (C_D and C_L), which are determined experimentally. Since the flow around a body may be in the laminar, turbulent or transitional regime, the fluid forces (or better the drag and lift coefficient) are strongly related to the type of flow which is characterised by the Reynolds number (Re). Thus C_D and C_L are functions of Re. C_D, the drag coefficient, depends on:

1. the shape of the body
2. the roughness of the body surface
3. the type of flow characterised by the Reynolds number.

Figure 1.4 shows the experimentally determined drag coefficients, as a function of Re, for smooth bodies of different shapes.

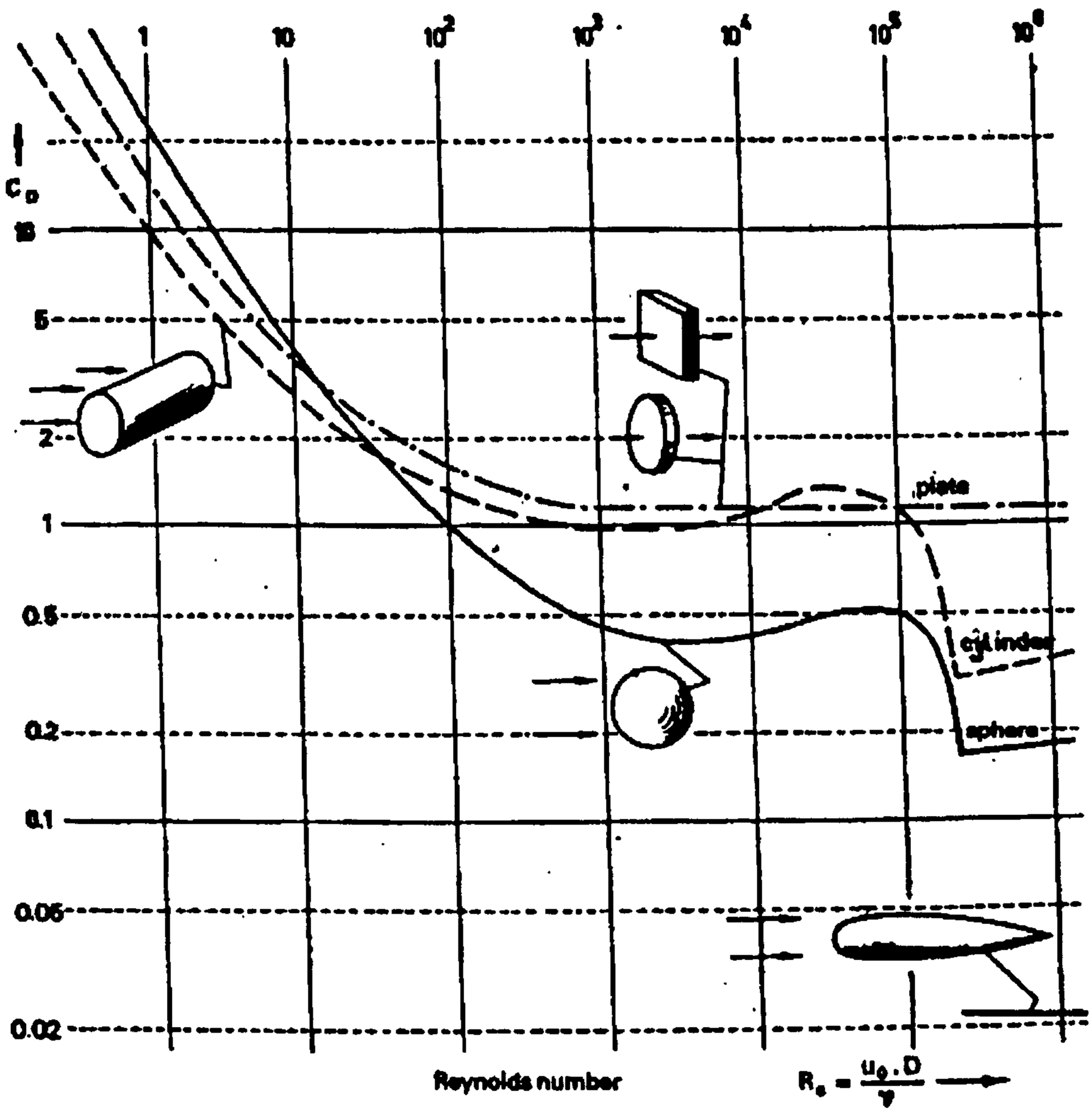

Figure 1.4 : Drag coefficient of smooth bodies. (Courtesy Delft Hydraulics, 1981)

1.3 REVIEW OF THE FLOWMETERS IN CLOSED CONDUIT SYSTEMS

A flow meter is a device for measuring the quantity or rate of flow of a moving fluid in a pipe or open channel. It may consist of a primary device and a secondary device. The primary device generates a signal responding to the flow from which the flow rate may be inferred. A secondary device receives a signal from the primary device and displays, records, and/or transmits the signal as a measure of the flow rate. In most cases, the primary device is wetted by the fluid and the secondary device is outside the process. This section is a critical review of the major types of pipe-mounted flowmeters in current use in closed conduit systems; most of the details taken from references from Brain (1982)[1.8] and Furness (1986)[1.9]. For each flowrate sensing element considered, physical descriptions are presented together with the flow meter's operating principles and their theoretical derivation. Measurements of both liquid and gas flowrates are considered and for each meter, guidelines are offered giving typical accuracies attainable and pointing out their advantages and pitfalls.

In Table 1.1, an attempt has been made to list the more widely available flow meters in their respective groups. These groups fall conveniently into two basic categories, those which extract energy from and those which add energy to the fluid being metered. The extractive approach involves the placing of an obstruction into the flow. This obstruction may be a rotor, a bluff body or merely a change of section. The potential energy of the stream is converted into kinetic energy and this is used to infer flow. In the additive approach, the addition could be in the form of a magnetic field, ultrasound or light. The flowing fluid acts on this addition and any change from the input value is used to infer flowrate.

Table 1.1: Flow meter classification

Group 1: Volume flow meters	
1a: Variable area meters	1b: Pressure difference meters
1a: (1) Tapered tube and Float meter	1b:(1) Orifice plate
	(2) Nozzles
	(3) Venturi tube
	(4) Elbow meter
Group 2: Mass flow meters	
2a: True mass flow meters	2b: Inferential mass flow meters
(1) Full momentum mass meters	(1) Coriolis mass meters
Group 3: Velocity flow meters	
3a: Point velocity meters	3b: Full flow velocity meters
(1) Pitot tube	(1) Electromagnetic flow meters
	(2) Turbine flow meters
	(3) Vortex-shedding flow meters
	(4) Ultrasonic flow meters
	(5) Target flow meters

1.3.1 Volume flow meters

The main methods of measuring the volumetric flow rate of liquids can be divided under the headings 'variable area' and 'pressure difference'.

1.3.1.1 Variable area meters

In Figure 1.5 the more widely used form of variable area meter is shown. In this tapered tube and float meter, the fluid flows upwards in a vertical tube which tapers downwards.

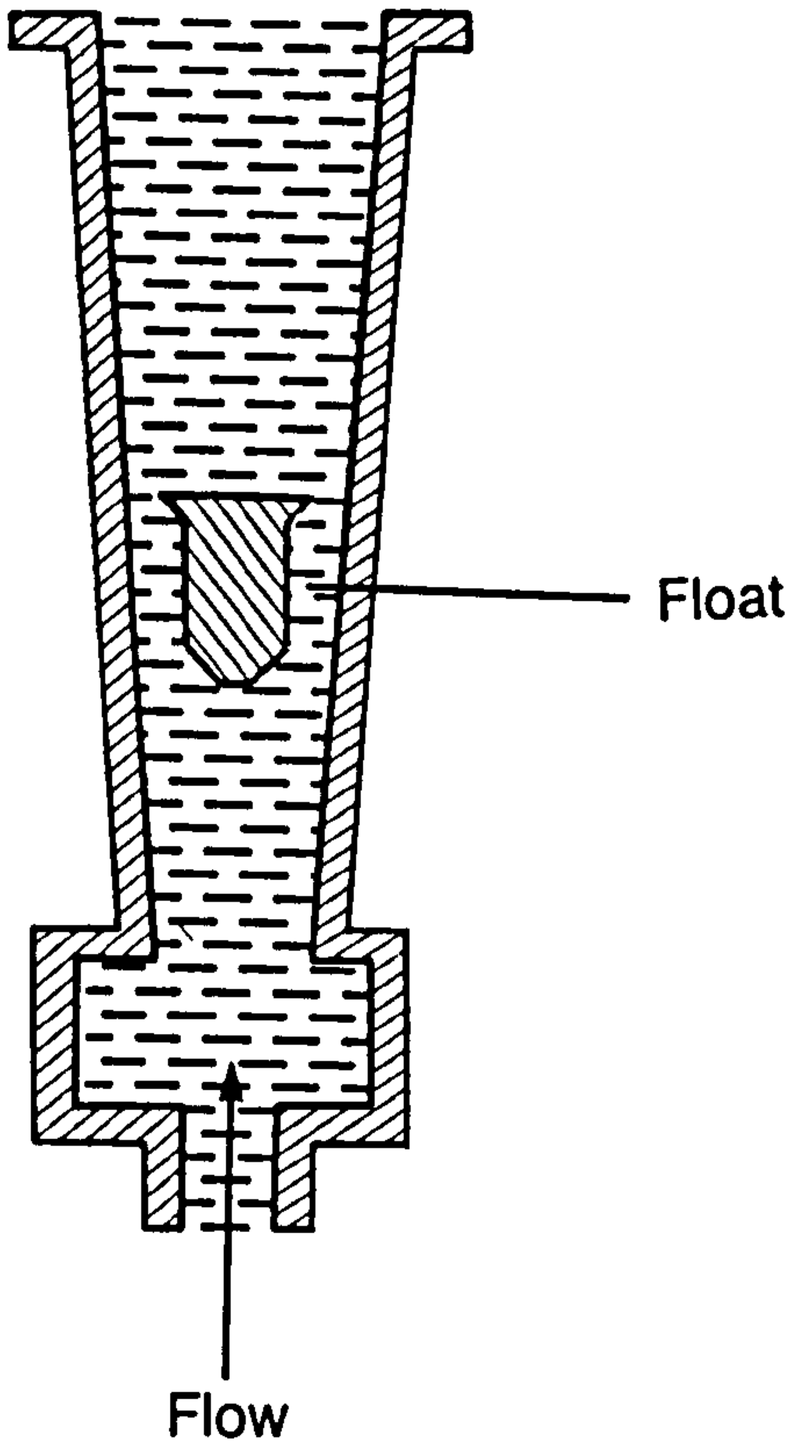

Figure 1.5: Basic tapered tube and float meter (Morris A S: 1993)

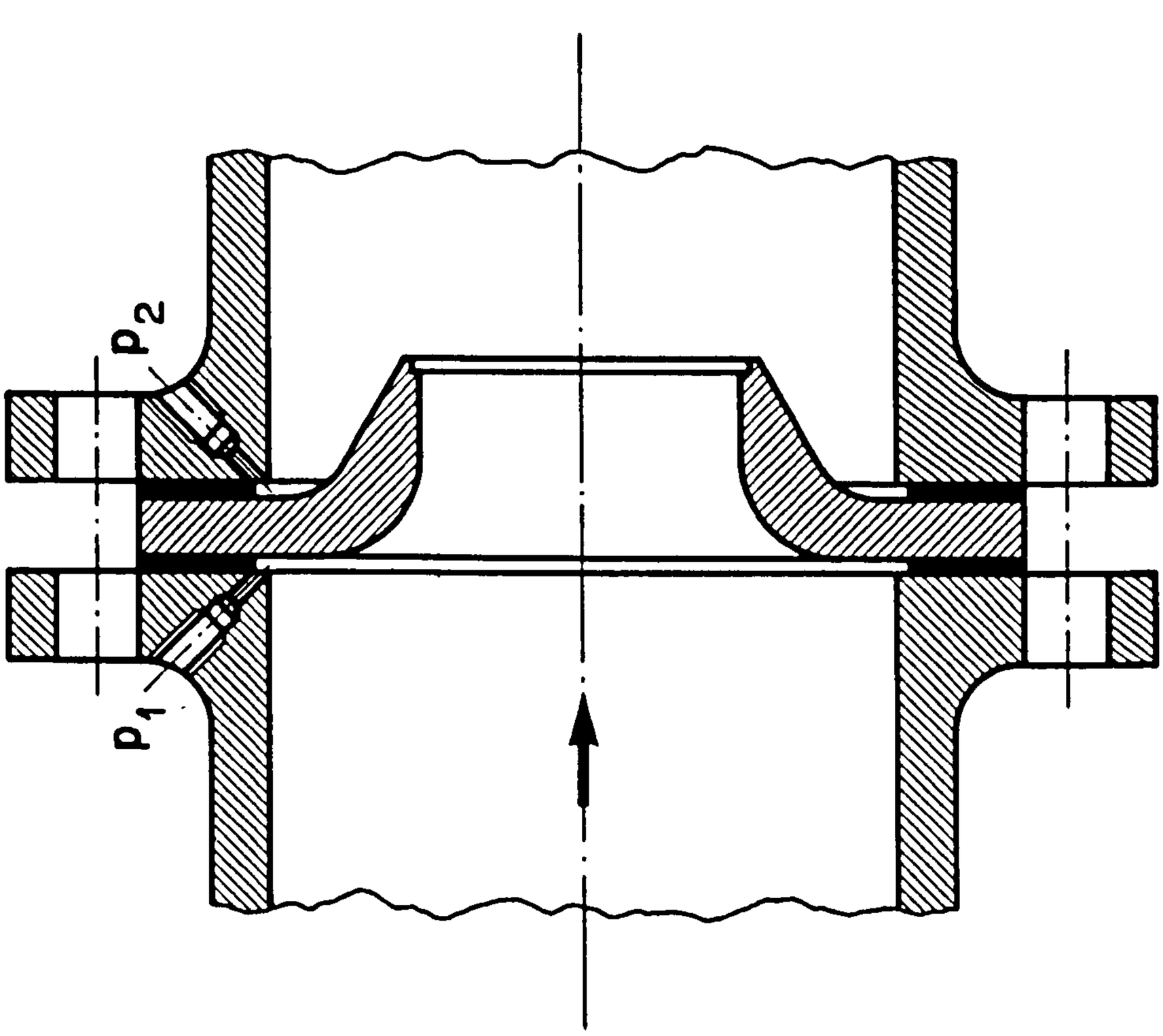

Figure 1.6 a :Nozzle (Escudier M P: 1983)

The flow supports a float, which is often provided with slots that cause the float to rotate in order to give it central stability. Since the tube is tapered, at a given flowrate the velocity of the fluid varies along the length of the tube, and the float assumes an equilibrium position, at a height within the tube dependant on the rate of flow. If the tube is made of a transparent material, such as glass, the equilibrium position of the float can be observed directly against a scale. Since the variable area meters give a direct indication of the rate of flow at the instant of observation, they are well suited for process control applications. The flow measurement accuracy claimed for such meters is usually within ±2% of full scale reading. They cover flowrates which range from near zero to 0.5 m^3/s for gases and 0.1 m^3/s for liquids.

1.3.1.2 Pressure difference meters

To meter flow using a pressure difference method, a constriction is introduced to the flow, causing the velocity of the fluid to increase as it passes through the constriction. Owing to this increase in velocity, the static pressure of the fluid decreases as the fluid stream contracts and a pressure difference is created between the pressure upstream of the contracting fluid and the pressure at the constriction. Flowrate is determined by measuring this pressure difference as well as the density and static pressure of the flowing liquid. The pressure difference meters are nozzles, orifice plates and venturi tubes.

A nozzle is a pressure difference device with a shaped convergent entry, which is often followed by a short cylindrical throat. The pressure difference across the nozzle is measured using pressure tappings and the volume/ unit time is given by Equation 1.8.

Orifice plate: A restricted opening through which fluid flows is known as an orifice. An orifice meter consists of a plate with a sharp edged circular hole that is inserted between two flanges of a piping system. Figure 1.6 shows a typical arrangement for an orifice plate. The volume/ unit time, Q is given by Equation 1.8.

$$Q = C_d \frac{A_2}{\sqrt{1-\left[A_2/A_1\right]^2}} \sqrt{\frac{2(p_1 - p_2)}{\rho}} \qquad (1.8)$$

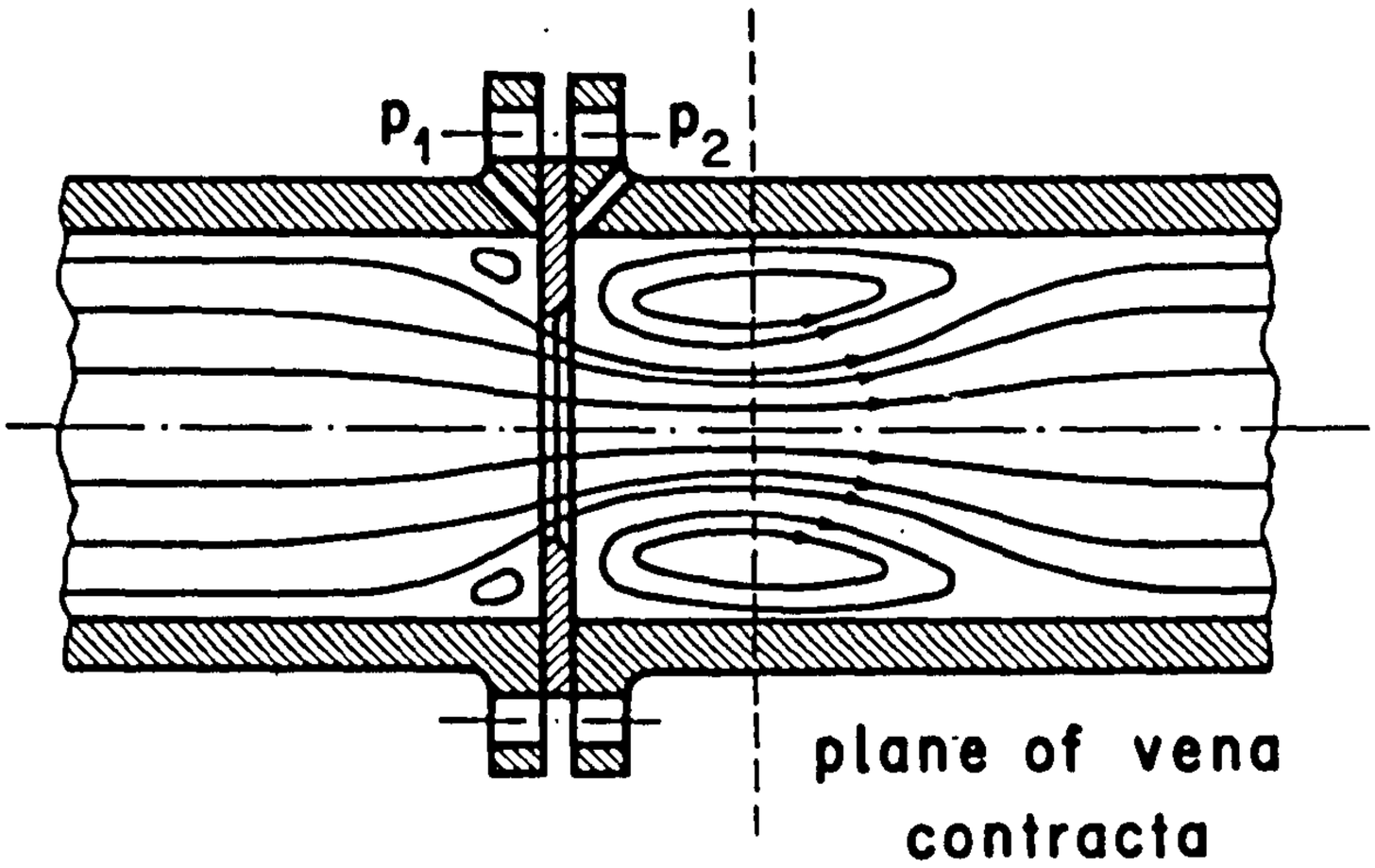

Figure 1.6 b: Orifice plate (Escudier M P: 1983)

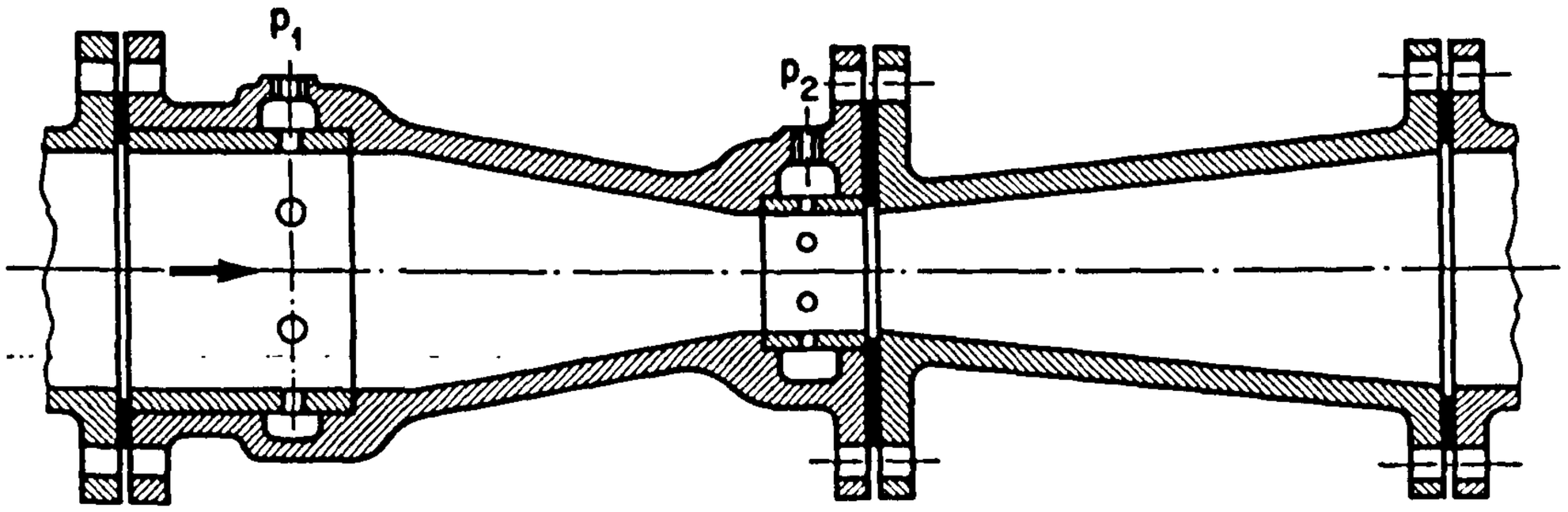

Figure 1.7: Venturi tube (Escudier M P: 1983)

where C_d is the discharge coefficient, A_1 and A_2 are the cross sectional area of flow, p_1 and p_2 are the pressures where A_1 and A_2 are measured and ρ is the fluid density.

$$C_d = \frac{Q_{actual}}{Q_{theoretical}} \qquad (1.9)$$

A standard venturi tube is shown in Figure 1.7 where it can be seen that the pressure difference is determined using tappings at the inlet and throat. Since this device has a diffuser section at its exit, it allows the fluid pressure to recover smoothly and hence it gives excellent pressure recovery when compared with orifice plates or nozzles, which cause substantial pressure head loss.

1.3.2 Mass flow meters

Mass flow meters can be divided into two main groups: true mass flow meters and inferential mass flow meters. A true mass flow meter is one in which the reaction of the basic sensing element is dependant on the mass flow of liquid through the device. In inferential mass meters, volumetric fluid flowrate and density at line conditions are measured and by multiplying flowrate by density, mass flowrate is obtained.

1.3.2.1 True mass flow meters

In this review we will restrict our attention to the main types of true mass flow meters in current use - fluid momentum meters. An example of this category is the Axial flow transverse momentum mass flow meter. The basic principle of this flow meter, first introduced by Orlando and Jennings (1954) [1.10] can be described with the assistance of Figure 1.8, where it can be seen that the main components are a constant speed motor, an impeller and a turbine arranged as shown. The fluid enters the annular space of the impeller, and the fluid is given an angular momentum by an impeller driven at constant speed and then its rotational velocity is brought to zero by a second rotor whose movement is restrained by a spring. The mass flowrate is measured by the angular displacement of the second rotor. These meters give a direct indication of the mass flowrate, provided they are operated within the density ranges specified by the manufacturers. However, their construction is rather complex, they tend to be expensive to buy and are susceptible to wear; also they require rotating seals as well as an accurate

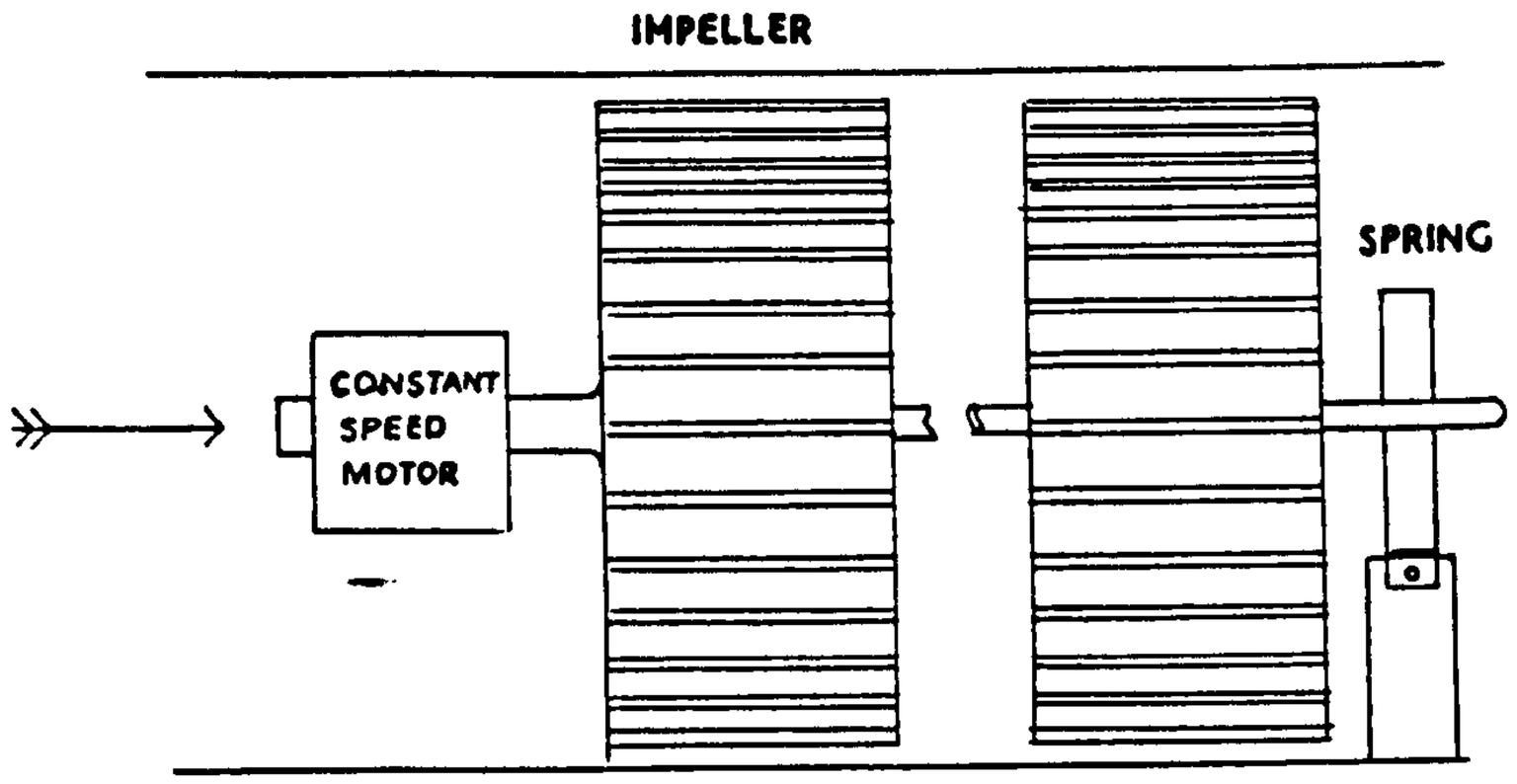

Figure 1.8 Axial flow transverse momentum mass flow meter (Medlock R S: 1983)

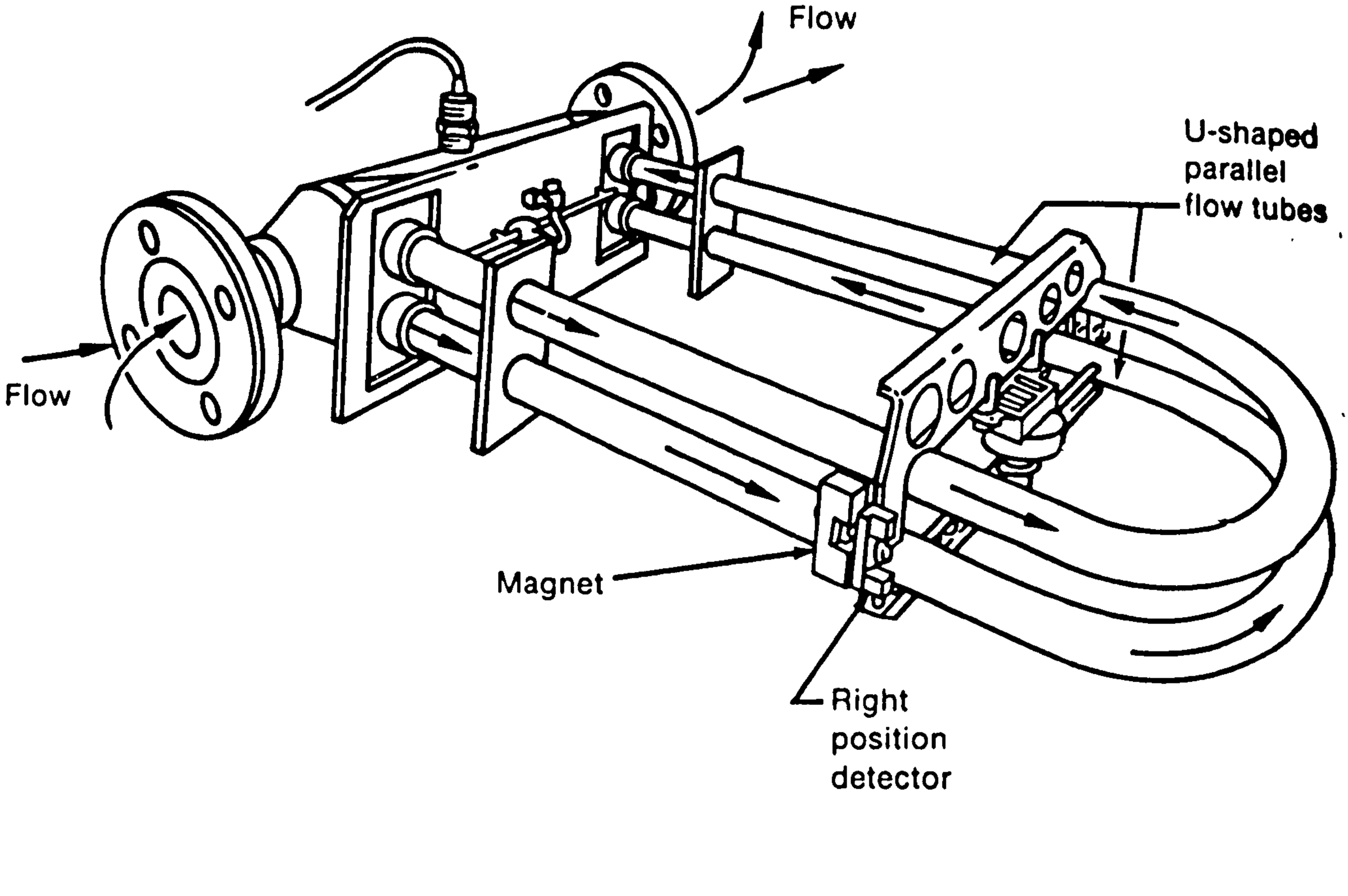

Figure 1.9: Coriolis mass flow meter (Furness and Heritage: 1986)

constant speed driving motor. These meters can be used for both gases and liquids and accuracies of better than ±1% of reading can be achieved over a 10 to 1 flow range.

1.3.2.2 Inferential mass flow meter

An example of the inferential mass flow meter is the Coriolis mass flow meter, shown in Figure 1.9. In Coriolis mass flow meters, measurement of the torque required to give the fluid stream a Coriolis acceleration gives a measure of the mass flowrate of the fluid.

The fluid is passed through a U-shaped tube which is mounted so that the tube can be vibrated at its resonant frequency. At zero flow the two legs of the U-shaped tube remain parallel but owing to the coriolis component the legs depart from parallelism by an amount dependant on the mass flow through them. The subsequent angular vibration is measured by two optical sensors, whose output is processed electronically to generate a mass flow signal.

These meters have not yet been developed successfully for gas measurements but they can be used to meter liquids (single and multi-phase), slurries and solid particle/liquid mixtures. Accuracies of within ±0.4% of reading are claimed and each meter has a rangeability of approximately 25 to 1.

1.3.3 Velocity meters

1.3.3.1 Point velocity meter : The pitot tube

The pitot tube primary element is simply a tube having a short section of one end bent toward the flow direction, thereby allowing the flow to impact the tube opening as shown in Figure 1.10. In operation, the differential pressure between the stagnation or impact pressure and the static pressure at the wall of the closed conduit is measured. The secondary element employed to measure the differential pressure may be simply a U-tube manometer or any one of the various forms of differential pressure measuring instruments. The differential pressure is proportional to the square of the velocity. A device of this type is normally employed in large conduits. Advantages of the pitot tube over other forms of flow meter used for this application are its low cost and its slim form, which allows insertion into the conduit through a small opening. Disadvantages

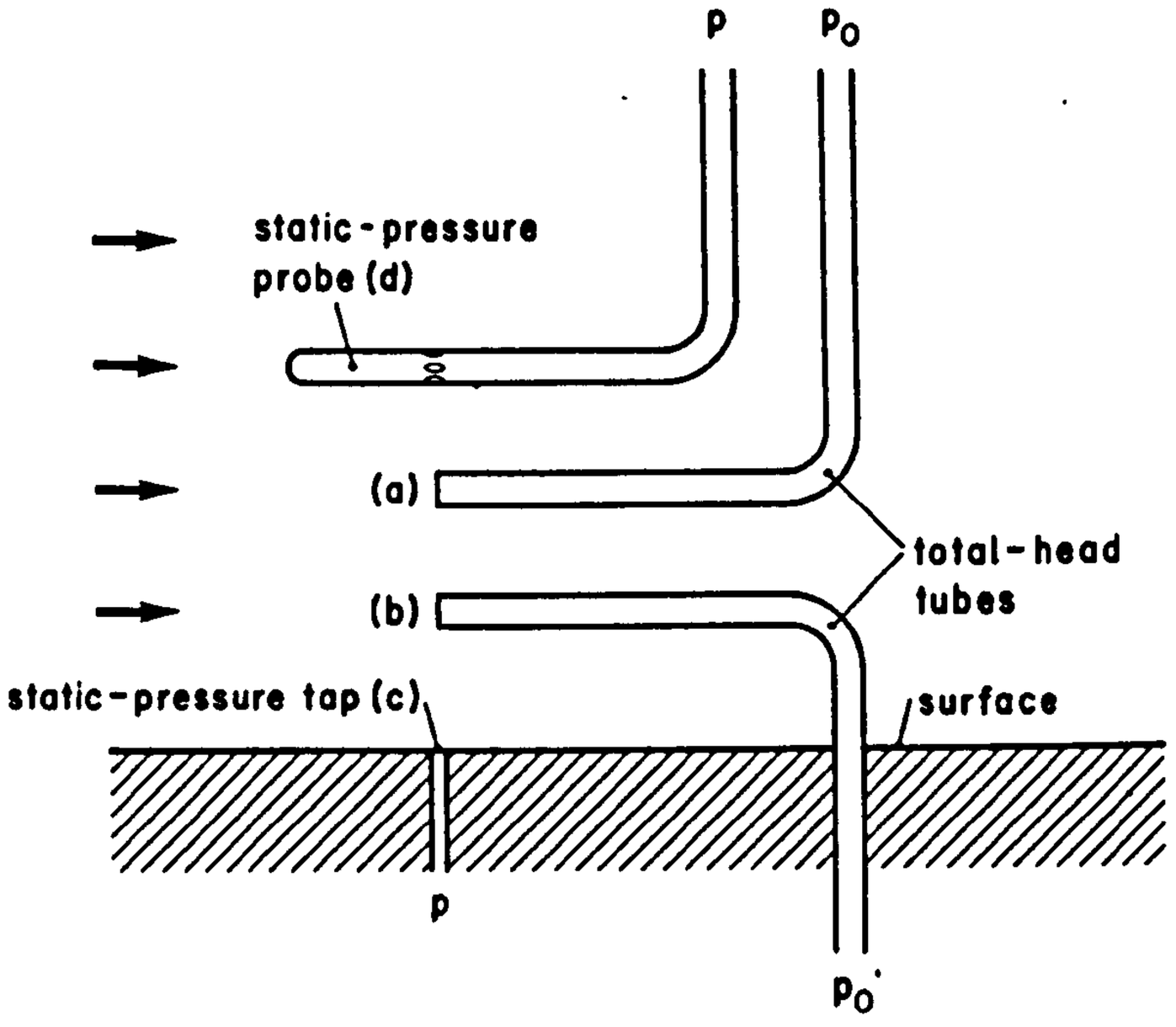

Figure 1.10 A basic Pitot or impact tube (Escudier M P: 1983)

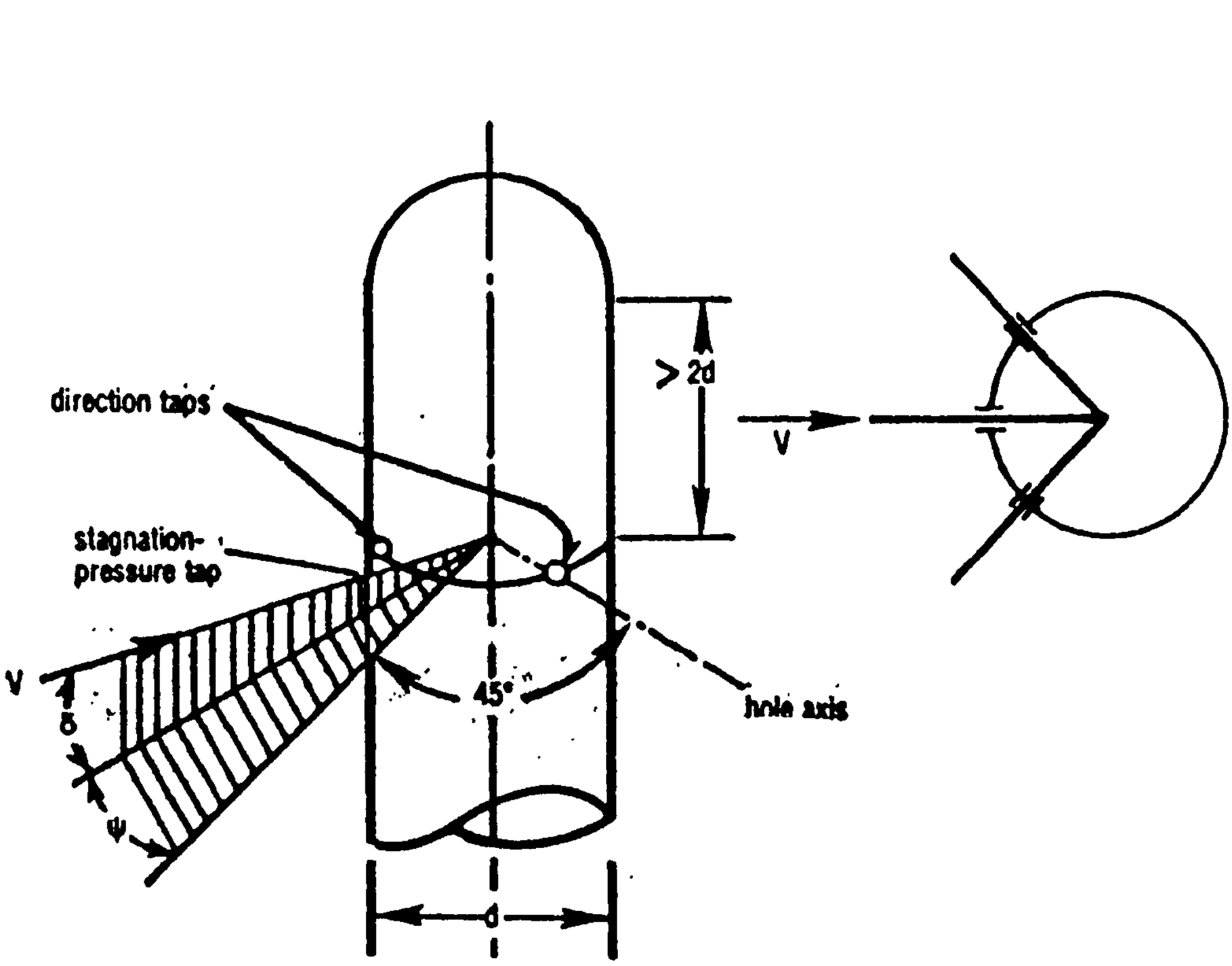

Figure 1.11: Flow-Direction measuring Pitot Probe (De Carlo: 1984)

are its ability to measure the flowrate only at a point (the impact pressure point), its susceptibility to clogging in dirty fluids, and its sensitivity to the relative direction of flow. To overcome the disadvantage of a single point measurement, several ports are placed along a tube in an attempt to measure an average impact pressure. Although devices of this type are reported to be flow-rate averaging devices, they are affected by nonsymmetrical flow velocity profiles.

Pitot static tubes are used for **flow direction measurement** as well as flow rate magnitude. A simple, rugged, two dimensional direction probe configuration is comprised of a cylinder inserted normal to the plane of the angle measurement. As seen in Figure 1.11, the three-hole direction probe is constructed with a stagnation pressure tap between the two direction taps. To provide for maximum sensitivity, the direction taps are located at 45^0 on either side of the stagnation-pressure tap. If the probe is rotated in the fluid stream until the pressure difference between the two direction taps is zero, the bisector of the angle between the holes gives the flow direction and the stagnation pressure tap gives the true impact pressure. The differential pressure between the impact pressure and the static pressure, as measured by one of the directional taps, provides the true velocity measurement. The device has been useful for measurements to within 0.1^0 at velocities over 33 m/s.

The velocity using the pressure measurements taken with a pitot or pitot-static tube is

$$V_1 = \sqrt{\frac{2P_s - P_1}{\rho_1}} \qquad (1.10)$$

where V_1 is the velocity of the fluid stream at the location of the probe tip, P_s is the stagnation or impact pressure measured at the probe tip, P_1 is the static pressure and ρ_1 is the density of the fluid at the location of the static pressure.

1.3.3.2 Full flow velocity meter: Electromagnetic meter

These meters utilise the principle of induction discovered by Michael Faraday in 1832. When an electrically conducting fluid flows through a magnetic field, a voltage is induced in the axis perpendicular to the axis of the flow direction and magnetic field. The strength of the induced voltage, which is proportional to the flowrate is measured

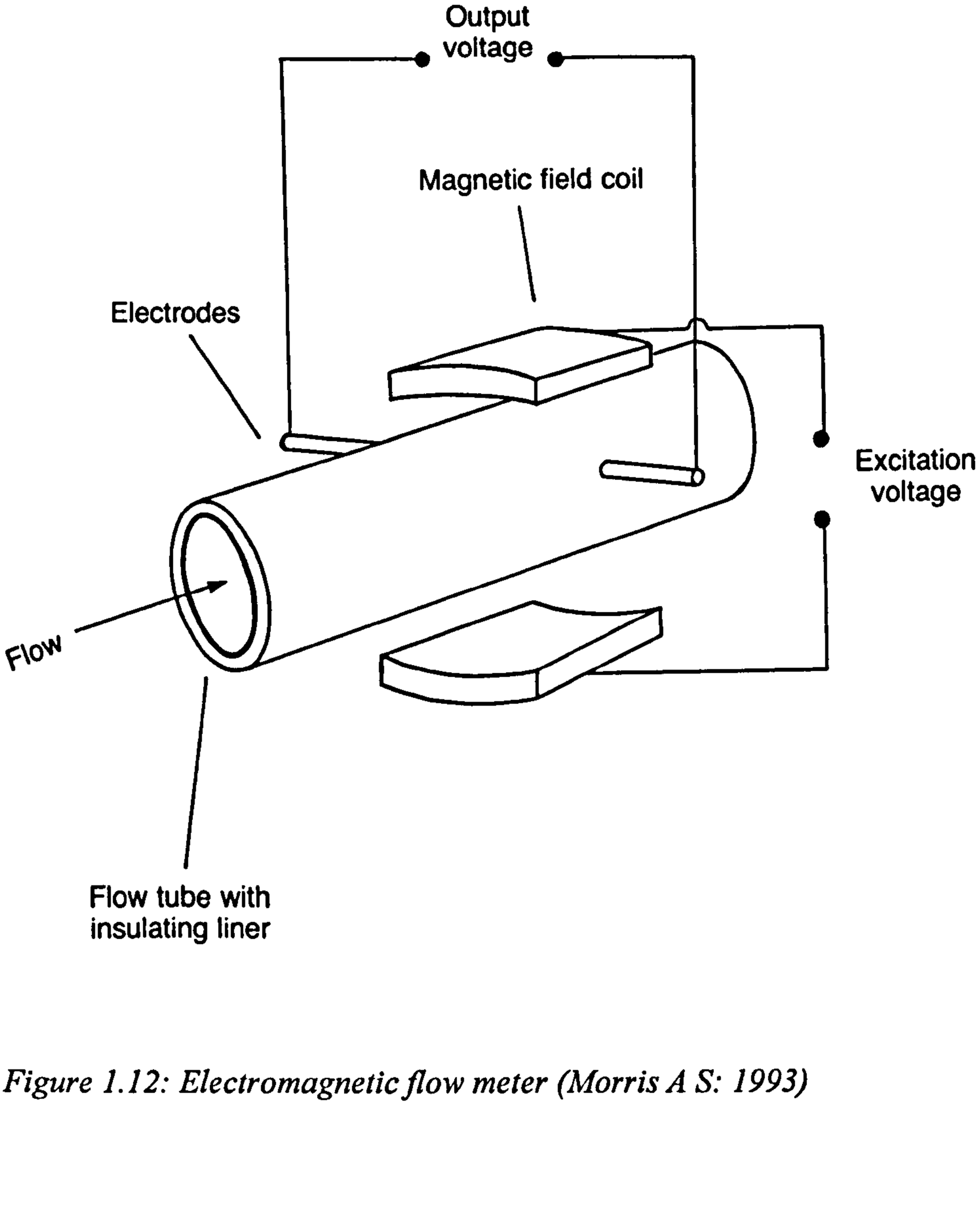

Figure 1.12: Electromagnetic flow meter (Morris A S: 1993)

using the electrodes on the pipe wall. This type of meter (Figure 1.12) is non-invasive and is used extensively on large water flows, slurries and corrosive liquids. Another advantage is the wide size range available (2.5mm to >3000mm). The problems associated with this flow meter are the possibility of polarisation at, or corrosion or erosion of the electrodes. A novel development is a meter with contactless electrodes (Al-Khazraji, 1979) [1.11] i.e. the electrodes are physically isolated from the fluid being metered. This design of the meter is, however, more sensitive than others to external interference effects because of the high source impedance feature. The electromagnetic flow meter is relatively expensive in the larger sizes. Typical accuracies are ±1% of full scale flow for more conventional AC types and approximately half that for DC versions. Flow rangeability is typically 10 to 1 for each velocity range setting.

1.3.3.3 Full flow velocity meter: Turbine meter

The turbine meter is a first choice meter in batching, blending and bottling applications for liquids[1.8]. From Figure 1.13 it will be seen that a turbine rotor is mounted centrally in the fluid stream in the pipeline to act as the transducing element of the meter. Rotary motion takes place through the fluid stream impinging upon the blades of the rotor and thus producing an equivalent angular velocity. The rotational speed of the turbine is proportional to the fluid velocity over a wide range of volumetric flowrates. An externally mounted pick-off unit senses this rotational speed as the meter output signal. Functionally, the pick-off arrangement may be electro-magnetic, RF type or opto-electronic.

One manufacturer quotes the flow range of his production range as between 9 to 1 and 27 to 1 depending on meter size. In calibration, repeatabilities of around ±0.1% are not uncommon and accuracies of ±0.5% of actual flow over the normal operating range of the meter are typical in modern equipment.

1.3.3.4 Full flow velocity meter: Vortex shedding meters

The vortex-shedding flow meter [1.8] is a modern practical application of a natural phenomenon which has been known to man for centuries. The meter relies on the principle (Figure 1.14) that when a bluff (non-streamlined) body is located in a fluid stream, vortex shedding occurs. As the flow round the body separates from its surface,

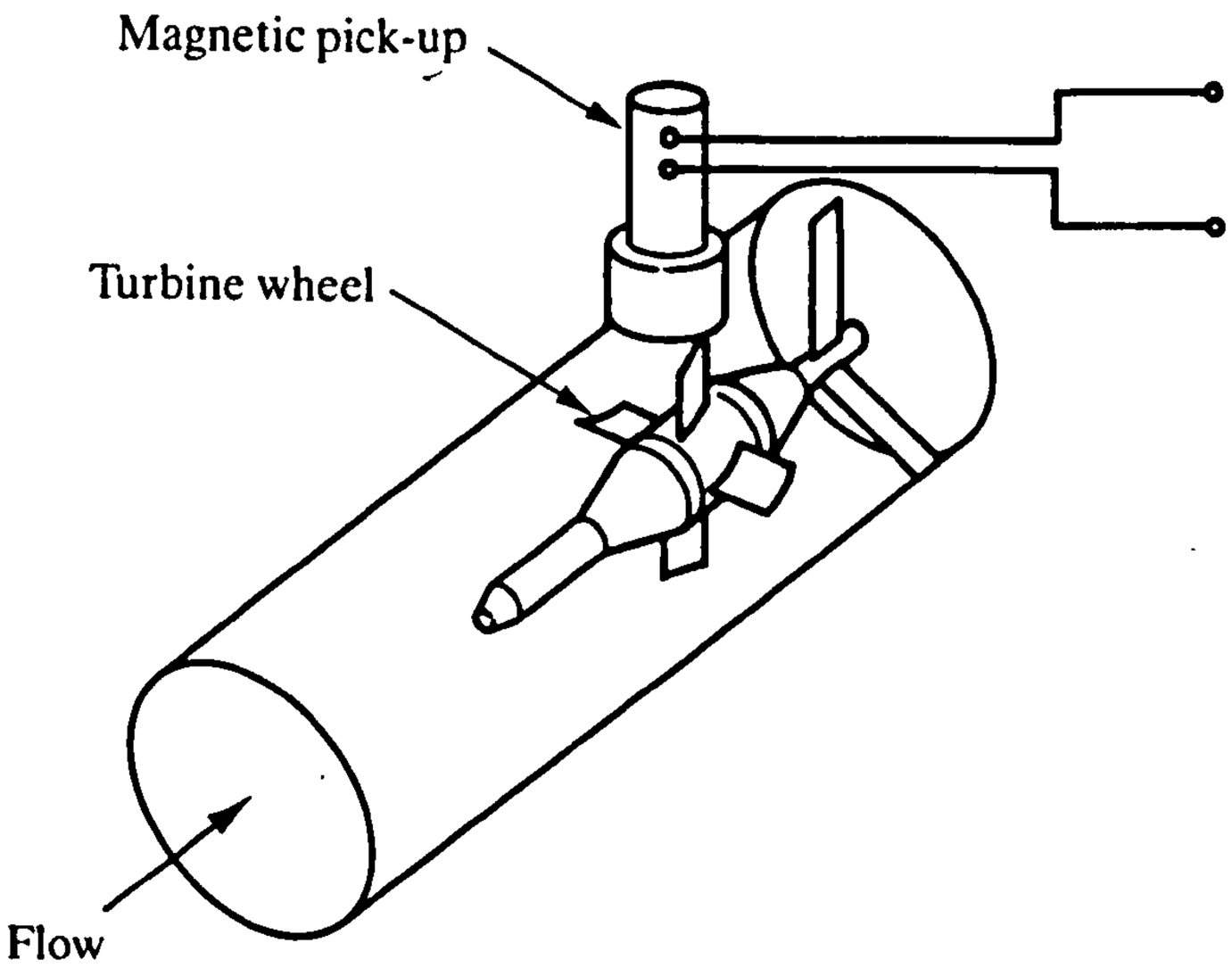

Figure 1.13: Turbine flow meter (Morris A S: 1993)

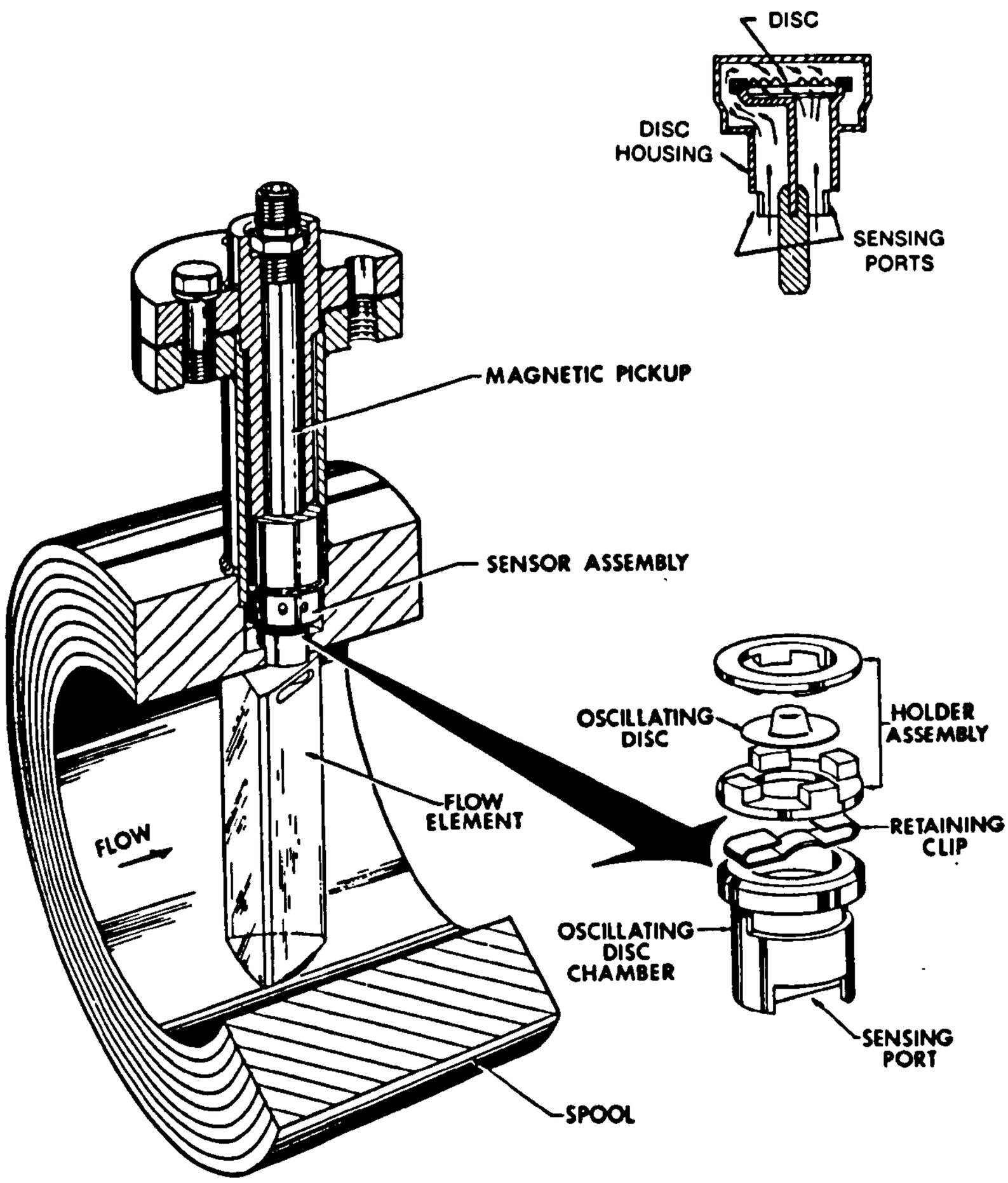

Figure 1.14 : Principle of vortex shedding flow meter (Neptune Eastech, Edison, NJ)

circular eddies are set up and under favourable conditions a pressure feedback system results in synchronising these eddies and producing a regular shedding pattern from alternate sides of the body. This alternating, contra-rotational pattern is known as a Von Karman vortex street. Vortex shedding is generally characterised by the Strouhal number, S = fd/v, where f is the shedding frequency, d a representative dimension of the bluff body and v the fluid velocity. Many experiments have been carried out to procure the optimum shape of the bluff body, to give a relatively constant value of Strouhal number over a wide range of Reynolds numbers. This means that the flow meter exhibits a linear relationship between shedding frequency and fluid velocity. At low Reynolds number, there is a cut off point below which the vortex shedding frequency becomes irregular and therefore, unreliable, for metering purposes. Mechanical, electrical or thermal sensors are among the options available for frequency sensing. The electrical method is the capacitive pick-up system. Mechanical devices are based on pressure sensing strain gauges, since the formation of the vortices is accomplished by a series of pressure pulses resulting from high and low pressures alternating on either side of the body. The thermal sensors are described in Section 1.3.4.1.

The repeatability of vortex shedding flow meters is generally good(0.1%) and a representative accuracy is ±0.5% of point for a frequency output system. A flow rangeability of up to 15 to 1 has been quoted.

1.3.3.5 Full flow velocity meter: Ultrasonic meters

The most commonly encountered types in this group are the Doppler meter and the transit time meter. The transit time method of measurement is based on the time it takes for sound to travel between two transducers. (Figure 1.15). The transit times are dependant on whether the sound is travelling with or against the direction of the flow and the difference between these is used to calculate the velocity of the fluid. [1.9].

If t_0 is the time for signal to travel distance L at speed c, then

$$t_0 = L/c \qquad (1.11)$$

If fluid is flowing at velocity V in the direction of sound travel, time for signal to travel

$$t = L/(c+V) \approx L/c(1-V/c) \qquad (1.12)$$

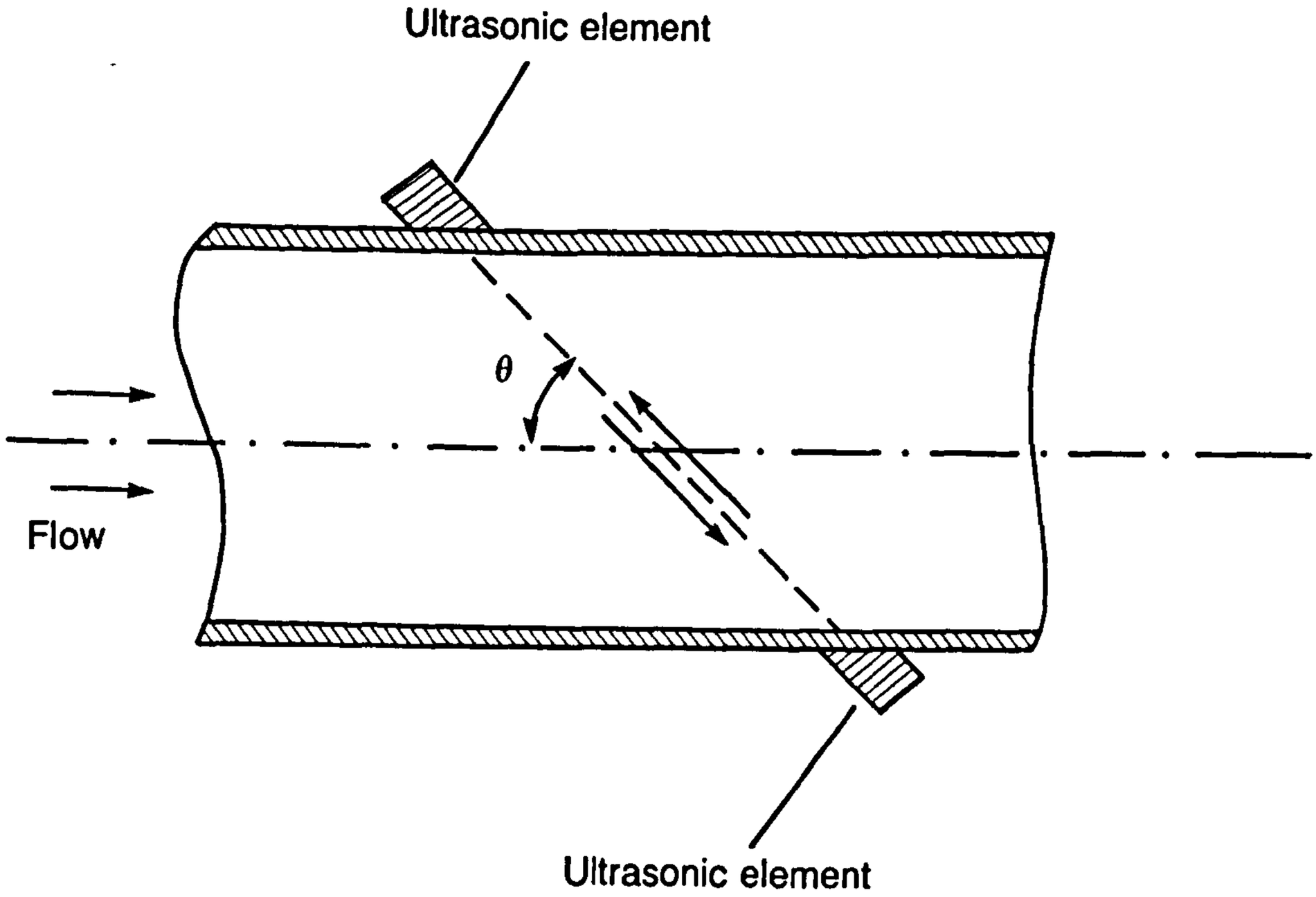

Figure 1.15: Transit time Ultrasonic flow meter (Morris A S: 1993)

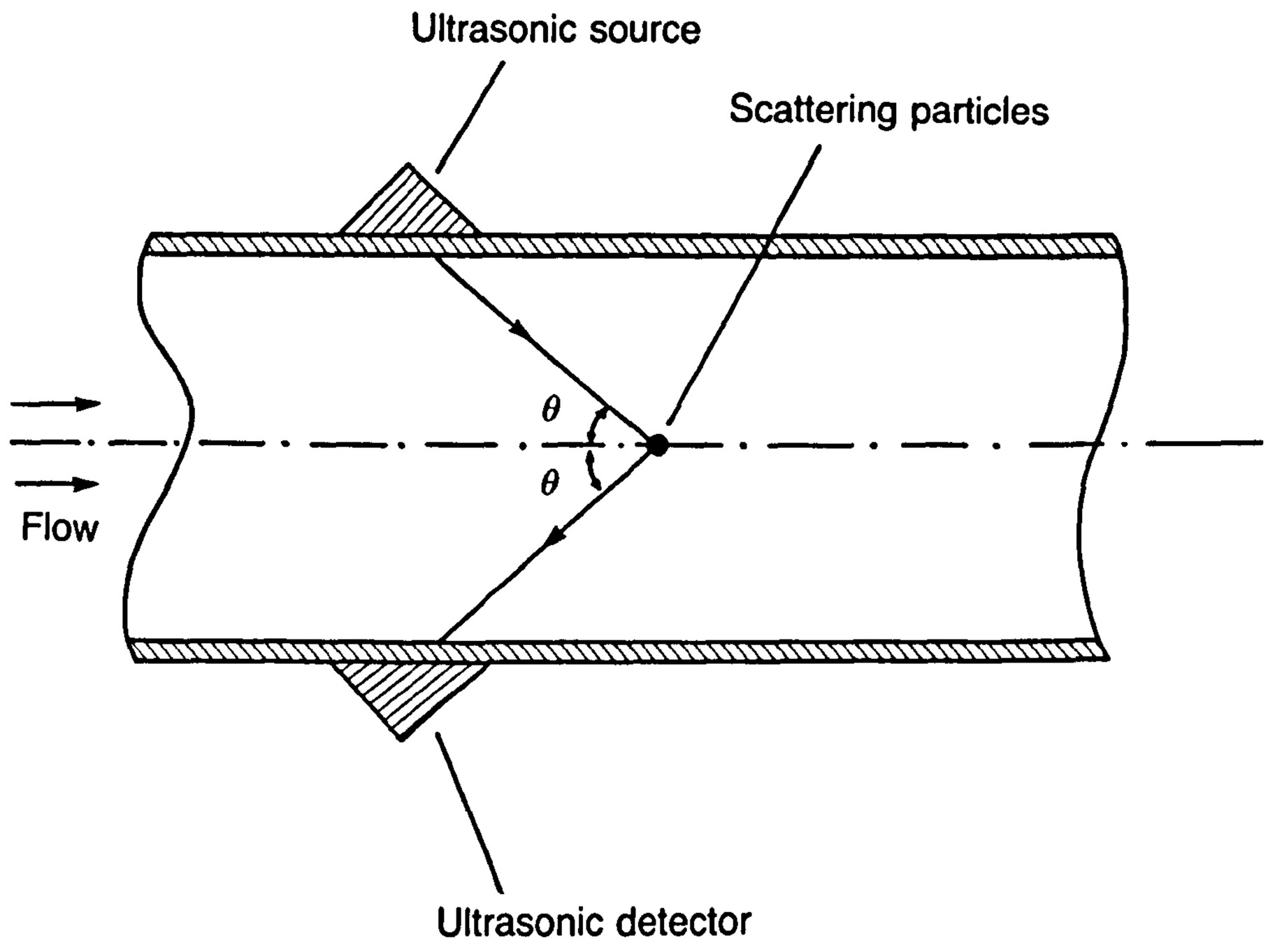

Figure 1.16: Doppler Ultrasonic flow meter (Morris A S: 1993)

Hence

$$\Delta t = t - t_0 = LV/c^2 \ \alpha \ V \qquad (1.13)$$

Transit times are suitable for clean liquids and although they are susceptible to distorted velocity profiles this effect can be reduced by using two or more acoustic paths (i.e. multi-beam systems). Accuracies can be around 0.5% of reading with the sophisticated multi-channel systems.

Doppler types depend on the change in frequency caused when sound is reflected by a moving object in the fluid. (Figure 1.16). The frequency change is approximately 2fV/c, where f is the frequency of the incident beam and V is the velocity of the scattering centre. The frequency shift is related to the velocity of the object and therefore is a measure of the fluid velocity if they are both moving at the same speed. Doppler devices are usually clamp-on and they are inherently much less accurate than transit time meters, their accuracy being typically 5-10% of rate devices.

1.3.4 Miscellaneous flow metering techniques

1.3.4.1 Thermal flow meters

The hot wire and hot film anemometers are the two major sensors belonging to the category of the thermal flow sensors [1.12]. The hot wire anemometers (Figure 1.17) commonly are made in two basic forms: the constant current type and the constant temperature type. Both utilise the same physical principle but in different ways. In the constant-current type, a fine resistance wire carrying a fixed current is exposed to the flow velocity. The wire attains an equilibrium temperature when the i^2R heat generated in it is just balanced by the convective heat loss from its surface. Since the convection film coefficient is a function of flow velocity, the equilibrium wire temperature is a measure of velocity. The wire temperature can be measured in terms of its electrical resistance. In the constant-temperature type, the current through the wire is adjusted to keep the wire temperature (as measured by its resistance) constant. The current required to do this then becomes a measure of flow velocity.

For equilibrium conditions, the energy balance for a hot wire can be written as

$$I^2R = h\,A\,(T_w - T_f) \qquad (1.14)$$

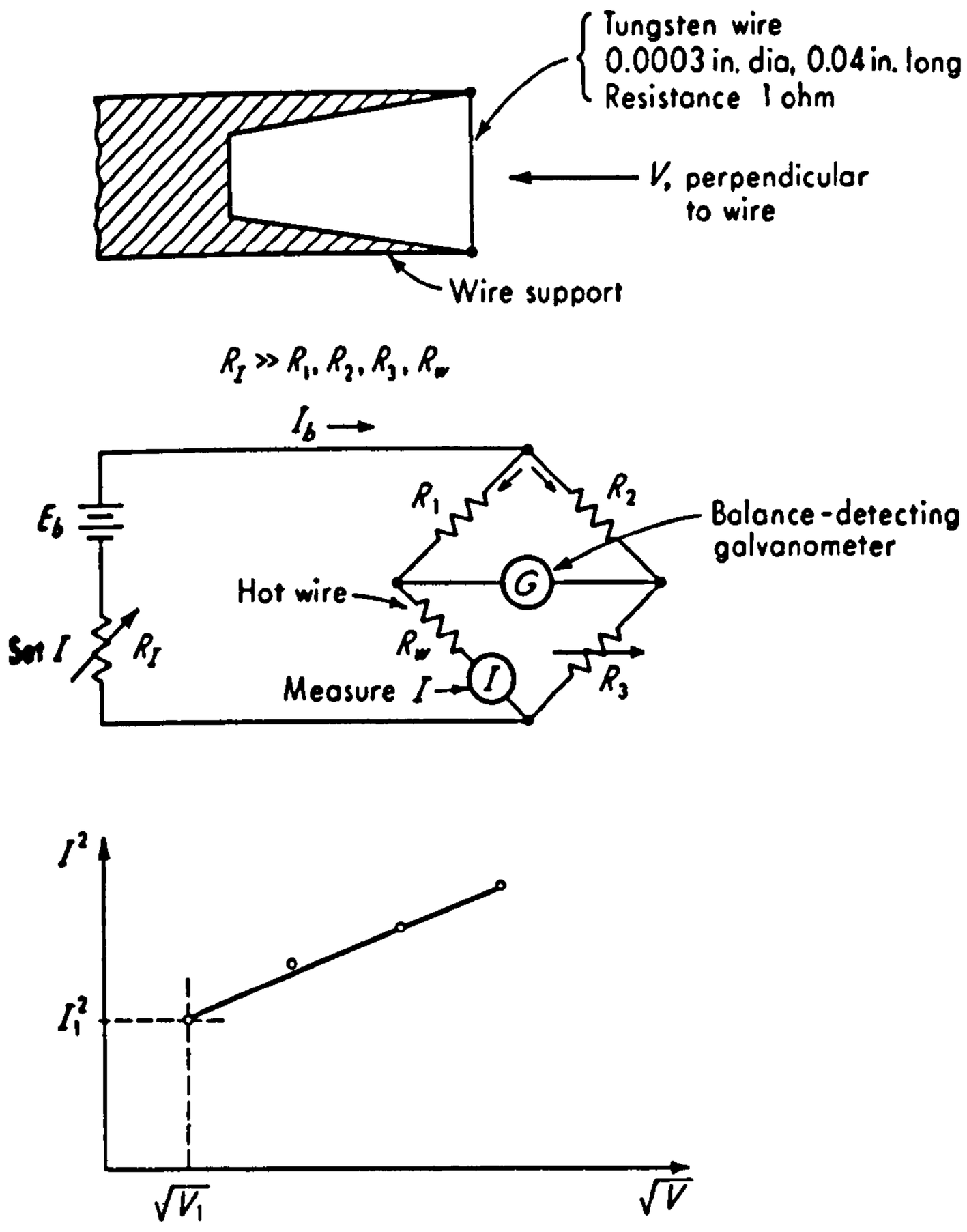

Figure 1.17: Hot wire anemometer (Doebelin E O: 1990)

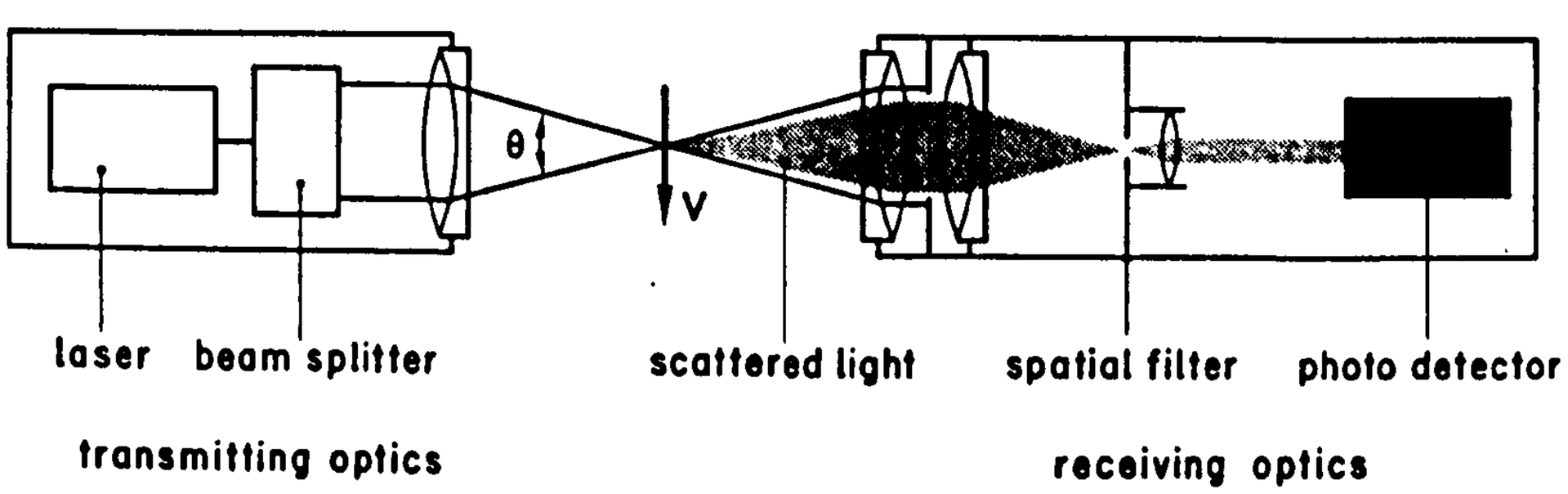

Figure 1.18: Schematic of the Laser Doppler Anemometer (Escudier M P: 1983)

where I is the wire current, R_w is the wire resistance, T_w is the wire temperature, T_f is the temperature of the flowing fluid, h is the film coefficient of heat transfer and A is the heat transfer area. For a given fluid density h is mainly a function of flow velocity. This function (called King's law) has the general form

$$h = C_0 + C_1\sqrt{V} \tag{1.15}$$

So I^2R is a function of $\sqrt{V}$, V being the fluid velocity.

Hot wire sensors are fabricated from platinum, platinum coated tungsten or a platinum-iridium alloy. Since the wire sensor is extremely fragile, hot wire anemometers are usually used only for clean air or glass applications.

A variation of the hot-wire anemometer, intended to extend its utility, is the hot-film transducer [1.12]. Here, the resistance element is a thin film of platinum deposited on a glass base. The film takes the place of the hot wire. The film transducers have greater mechanical strength and may be used at very high temperatures by constructing them with internal cooling-water passages.

1.3.4.2 Laser Doppler Anemometer

The hot wire anemometer first came into use in the 1920s and is now a standard laboratory instrument. In contrast, the laser Doppler anemometer was first applied to flow measurement only in the early 1960s [1.13]. A schematic diagram of a typical dual-beam forward scatter LDA system is shown in Figure 1.18. Low power (5mW) Helium-Neon lasers are commonly used as the coherent light source, although some systems, especially those designed for the simultaneous measurement of two velocity components, use high power (5W) Argon-ion lasers which have the useful property of roughly equal power at two different wavelengths (488.0 nm-blue and 514.5 nm-green). For a given velocity component, the laser beam is split into two parallel beams which are then brought to a common focus. Particles passing through the region where the two beams cross scatter light as they cross the light interference fringes in that region. The scattered light is focused on to a photodetector. The fringe spacing, δ is given by Equation 1.16.

$$\delta = \frac{\lambda}{2\sin(\alpha/2)} \tag{1.16}$$

where λ is the wavelength of the laser light, and α is the angle between the two beams in the flowing medium. The beat frequency of the scattered light is then

$$f = \frac{2V \sin(\alpha/2)}{\lambda} \tag{1.17}$$

where V is the component of the particle velocity orthogonal to the fringes.

Evident advantages of the LDA over the hot-wire anemometer, are that it is an absolute measuring instrument requiring no calibration and is a non intrusive device producing virtually no disturbance to the flow. A drawback is that access is often difficult and in most practical applications limited to one side so that the instrument must be used in the back-scatter mode.

1.4 TARGET FLOW SENSORS

Since the work undertaken for this project involves a category of target flow sensors, an entire section has been devoted to describe this type of flow sensor in greater detail. Since its introduction several decades ago, the target flowmeter has proven to be one of the most reliable, versatile and easy to use flowmeters [1.14]. The inherent flexibility of the target flowmeter provides many advantages to the user when compared to the other types of flowmeters. Certain types of target flowmeters can handle wide temperature and pressure ranges. They also can use special alloy materials compatible with almost any fluid, and can be easily field calibrated.

1.4.1 Principle of operation of target flow sensors

The target flowmeter utilises the principle of fluid drag on a three-dimensional body. [1.14]. The total drag on any three-dimensional body suspended in a fluid stream, gas or liquid is the sum of the friction drag and the pressure drag.

$$F_D = F_F + F_P \tag{1.18}$$

The friction drag is due to the shearing stresses in the thin layer of fluid near the surface of the body called the boundary layer. The pressure drag or form drag is due to the disturbance of the flow stream as it passes the body, creating a turbulent wake. The characteristics of the disturbance are dependant on the form of the body and sometimes on the Reynolds number of flow and the roughness of the surface. The pressure drag is

therefore equal to the integration of the components in the direction of motion of all the pressure forces acting on the body's surface. For different shapes the distribution of the total drag between friction drag and pressure drag varies widely. For a flat plate or cylinder placed perpendicular to the flow, pressure drag produces nearly all the drag. For a well-streamlined shape, friction becomes more significant. When considering an equation to describe the response of the target flowmeter, only the total drag is of interest, which in this case is the pressure drag and the equation becomes,

$$F_D = C_D \rho A \frac{V^2}{2} \qquad (1.19)$$

where C_D is the overall drag coefficient, ρ is the fluid density, V is the fluid's velocity at the point of measurement, and A is the projected area of the body normal to flow. In addition to the form of the body, three other parameters have an effect on the pressure drag coefficient and hence on the overall drag coefficient. These are the Reynolds number, the surface roughness of the body, and the degree of turbulence in the free fluid stream. [1.15] Effects of variation in Reynolds number on drag coefficient are small for Reynolds number greater than 10,000. [1.16] Effects of variation in Mach number are also small for Mach numbers less than 0.75. [1.16] However, at transonic Mach numbers, variations in drag coefficient are not negligible and cause a non-linear relation between drag force and velocity. The drag coefficient is relatively insensitive to flow angle for angles to within 20^0 of normal to the beam surface. [1.17] The overall drag coefficient is determined by empirical data.

For very low flow rates i.e. for Reynolds numbers less than 1.0, the drag is almost entirely due to friction and so the drag becomes a function of viscosity and is described by Stoke's law,

$$F_D = 3\pi\mu DV \qquad (1.20)$$

where μ is the dynamic viscosity and D is the body's diameter. If Equation 1.20 is expressed in the form involving a drag coefficient, the resulting value of C_D is given as

$$C_D = \frac{24}{\mathrm{Re}} \qquad (1.21)$$

This plots as a straight line at the left of Figure 1.4. During this linear portion of the curve, the boundary layer becomes attached to the body and very little turbulent wake is produced. As the Reynolds number increases, separation occurs and pressure drag becomes more significant. Those shapes which have sharp edges always cause the boundary layer to separate at the same place. [1.15] Therefore, the drag coefficient for these shapes, and hence for the beam used in this project is nearly independent of the Reynolds number.

1.4.2 Literature review of target flow sensors

The target flowmeter is a force transducer since the drag is essentially a force. Three primary transducers have been used to measure the force or the deflection that occurs to the target body during flow [1.14]. They are:

- measurement of the displacement of the body immersed in the fluid,
- measurement of the balance force, and
- measurement of the strain produced in the sensing element.

The simplest form of the target flow sensor is the vane meter which utilises the first method of measurement of the physical displacement that the body undergoes. A linear variable differential transformer (LVDT) is used to measure this small deflection. The limitation to this approach is the required sensitivity to very small displacements, and the requirement for ac excitation which does not lend itself to two-wire direct current loops. De Carlo[1.18] describes a simple form of this type of meter called the **vane-type flowmeter** shown in Figure 1.19. Fluid flowing through the device causes a plate to swing outward, away from the fluid jet. At no flow, the plate rests against the end section of the meter. In its simplest form, the device is used as a flow indicator only and no flow scale is provided. However, the meter may be provided with a scale for the determination of flow rate, where the scale might be the angle through which the target or vane swings.

In the force balance approach, the target is returned to its original position. This restoring force is the measurand of the force balance system. A feedback force is

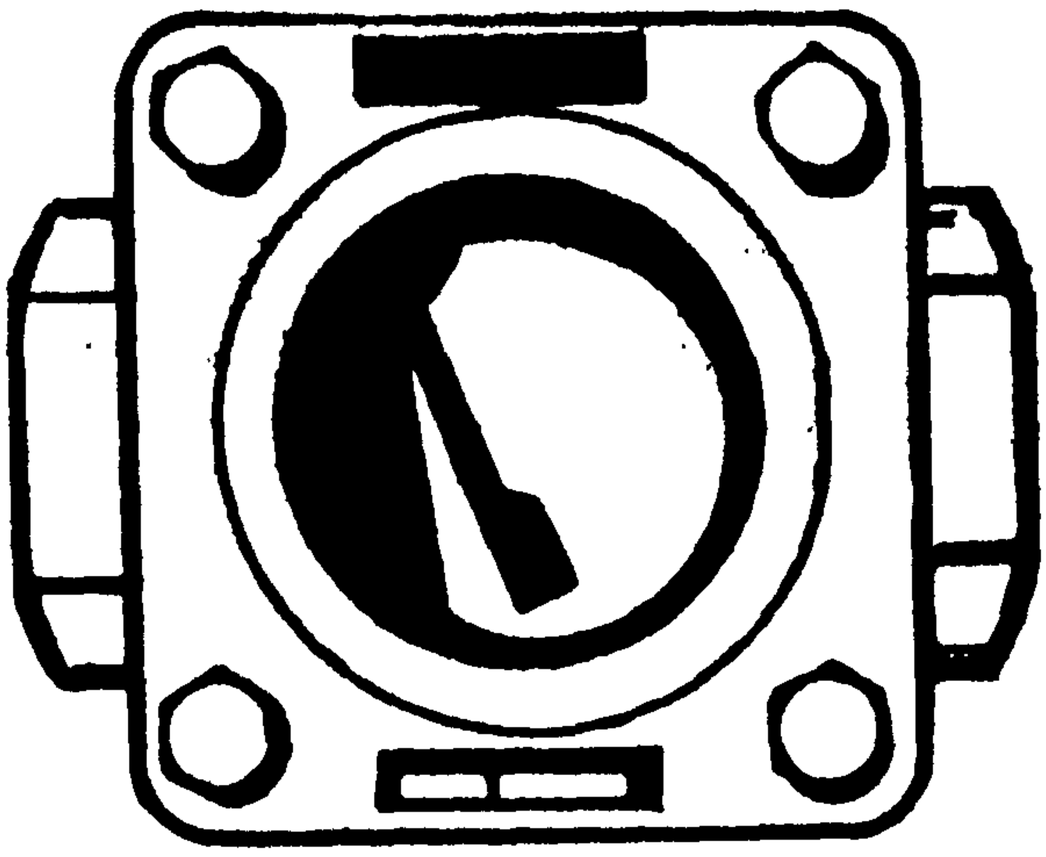

Figure 1.19: Vane type flowmeter (De Carlo: 1984)

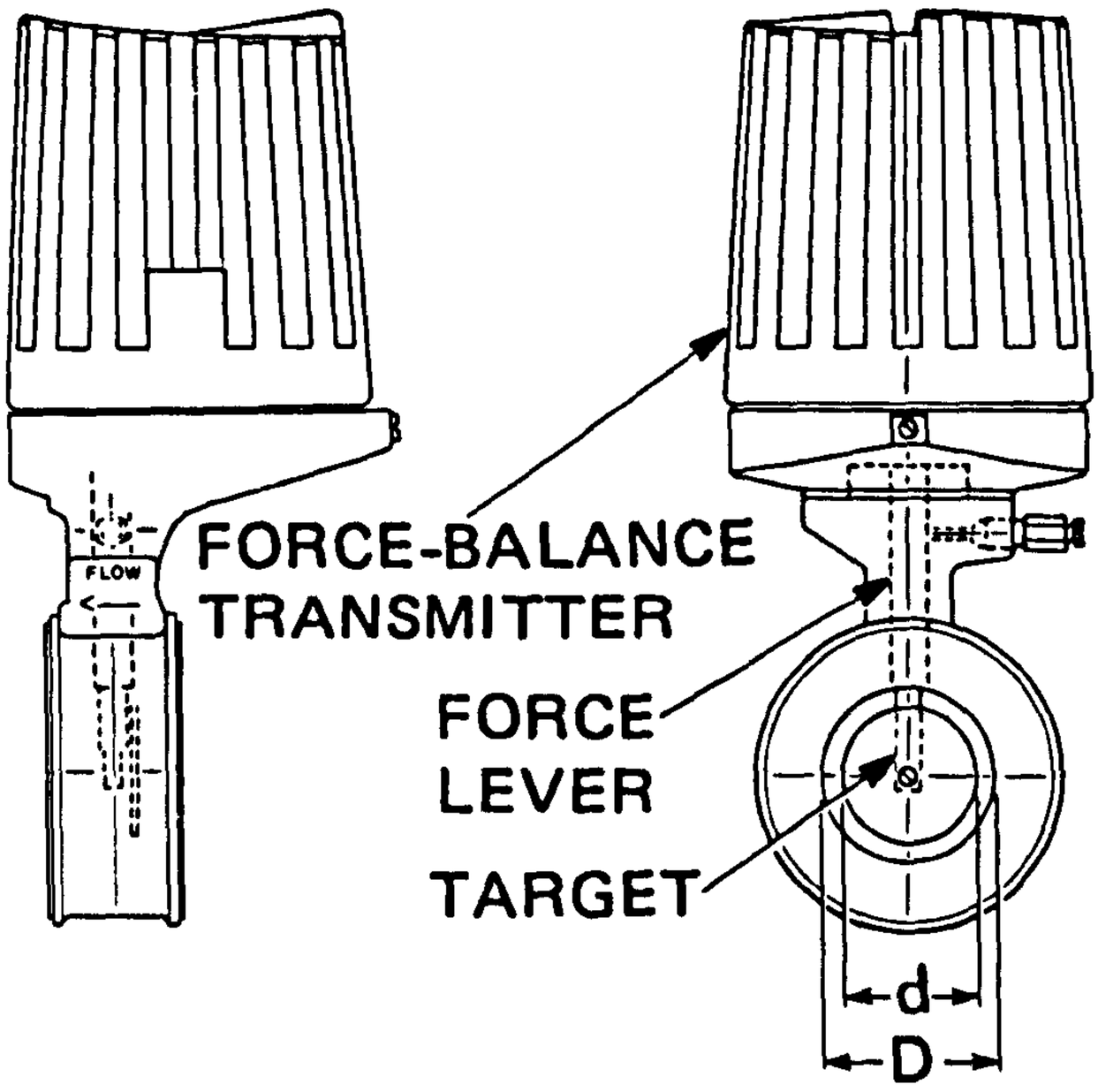

Figure 1.20: Force balance target flowmeter (De Carlo: 1984)

applied and senses the equilibrium position. A literature search on this approach has once more pointed to De Carlo [1.18] where a target or disk is mounted perpendicular to the flow direction and a secondary element measures the force on the target by means of the force balance system (Figure 1.20). An annular orifice configuration is formed by the disk shaped target in the circular pipe and the target is fixed to a rod which transfers the force to the force balance mechanism.

De Carlo emphasises the point that target flow sensors were 'explored for application on dirty, sediment-laden and high melting point liquids that could not be measured by other head-class devices, like the orifice plate'. He also mentions that at that time (1984) it was the known meter to be specified when difficult applications arise and when repeatability or precision is the main concern rather than absolute accuracy. However, he decided that with proper calibration and installation, the device provided accuracies comparable to other head class flowmeters.

Although, there are many applications where the force balance and LVDT approaches will work satisfactorily, the strain measuring approach is by far the most versatile and reliable. Waldron et al [1.19] used a semi-conductor strain gauge as a sensing element to provide a quantitative measure of turbulent velocity fluctuations in a marine water column. The noise performance of the instrument was poorer than that of contemporary instruments using ultrasonics, hot film anemometry and doppler scatter techniques.

A strain gauge target flow meter [1.14] was developed to meter the production of heavy water where high strength materials were used for the target rod and sensing tube. This meter was used to measure bi-directional fluid flow in one dimension. The sensor has a number of noteworthy performance characteristics like a rapid response time making it possible to throttle a pulse as small as 10 milliseconds, extreme accuracy and repeatability over a wide flow range, long term reliability and stability and ability to handle temperature ranges of -320^0 F to 650^0 F with a high degree of reliability.

Krause and Fralick [1.17] describes a drag-force anemometer which measures unsteady as well as steady state velocity head. This sensor also measures the flow angle in the inlet of a turbofan engine during transient flow conditions for which two beams are required.

The various force and strain measurement techniques for target flowmeters have been reviewed in this chapter to give the reader a better understanding of the novelty of the

target flow sensors that have been developed in this PhD project and discussed in Chapters 4 to 8 of the thesis. The flow meters that have been developed by the author measures two dimensional wind and water flow with successful calibration performed for two dimensional air flow measurement and one dimensional water flow measurement. An advantage of the instruments is that they can be made to generate a measurement of flow direction in two dimensions, or even in three dimensions. Provided that the deflecting forces are independent in the sensing directions, the resulting outputs can be added vectorially to generate values for speed and direction of fluid flow which are independent of each other. This approach of vectorially adding the fluid components to generate both the speed and direction is a novel drag-force sensing technique when compared to the existing techniques used in target flow sensors [1.14 - 1.19].

CHAPTER 2

ELECTRICAL STRAIN MEASUREMENT

2.1 INTRODUCTION

The bonded electrical resistance strain gauge has been the most powerful single tool in the field of experimental stress analysis since 1940. It is one of the most accurate, sensitive, versatile and easy-to-use sensors available. The strain gauge is relatively low in cost, is linear in output, is easily installed, and is available in a broad variety of configurations, sizes and materials, to meet a very large spectrum of measurement requirements.

The strain gauge has become the basic sensing element of very high precision load transducers because of its exceptional performance characteristics particularly in stability, temperature compensation, and creep. In spite of the relative ease with which strain gauges can be employed, the proper and effective use of them requires a thorough understanding of their characteristics and performance, and of application techniques and associated instrumentation. This chapter is devoted to those features which affect the behaviour of the resistance strain gauge, the adhesives, installation and protection techniques and instrumentation.

It is essential to record the following definitions from the British Standards [2.1] before proceeding further: Strain is the change in length per unit length in a specified direction of a specimen of a material, i.e. dL/L, where L is the initial length in the specified direction and dL is the dimensional change in that direction. Strain is normally expressed in micrometers per meter colloquially known as microstrain ($\mu\varepsilon$).

The bonded electrical resistance strain gauge is a device which when strained after bonding to a surface gives a change in electrical resistance proportional to change in the length.

2.2 BRIEF HISTORY

The electrical resistance strain gauge is based on principles established by Lord Kelvin [2.2] in a classic series of experiments conducted in 1856. In these experiments, Lord Kelvin proved that :

1. Wires subjected to loads and/or strains change resistance.

2. Wires fabricated from different materials exhibit different strain sensitivities.

3. Resistance changes in the wires resulting from the imposed strains are small, but they can be accurately measured with a Wheatstone bridge.

The bonded electrical resistance strain gauge was first used in the USA in 1938. Simmons at the California Institute of Technology and Ruge at the Massachusetts Institute of Technology both discovered that small diameter wires made of electrical resistance alloys, such as copper-nickel, could be adhesively bonded to a structure to measure surface strain.

The strain sensitivity of resistance wires was first utilised some years prior to this in the unbonded wire strain gauge. This consisted of an arrangement of wire, wound around a series of pins actuated by linkages, any movement of which stretched the wire and changed its resistance. [2.3] This was essentially an electrical extensometer, and the principle is still used today in some special types of transducers.

Following the development of the techniques for bonding resistance wires to structures, discovered by Simmons and Ruge, strain gauge measurements were adopted for structural testing during the rapidly growing aircraft development programmes of World War II. Metal-foil strain gauges were first developed by Saunders and Roe in England in 1952 as the requirements of the aircraft industry increased. At that time, printed circuit techniques were appearing, and Saunders-Roe developed the idea of making a strain gauge by etching the grid from a thin foil of the appropriate resistance material. This permits miniaturisation of the grids, versatility of the grid configuration, economies of production, and enhanced control of quality of the gauge.

Semiconductor strain gauges were developed as a by-product of research at Bell Telephone Labs. The characterisation of semiconducting silicon and germanium

provided the foundations for the commercial development of piezoresistive strain gauges that became available in the 1960s.

The metal alloys used in the production of metal-foil electrical resistance strain gauges have maximum strain limits of approximately ±5%. For very-large-strain applications where specimen elongations of 100% may be encountered, liquid-metal strain gauges which is made of a rubber tube filled with mercury or a gallium-indium-tin alloy have been developed.

2.3 BASIC OPERATING PRINCIPLE

Lord Kelvin [2.2] first observed that a change in the strain imposed on a wire is accompanied by a change in resistance ΔR of the wire. The relationship between resistance change ΔR and strain ε can be derived by considering a uniform conductor of length L, cross-sectional area A, and specific resistance ρ. The resistance R of such a conductor is given by the expression

$$R = \frac{\rho L}{A} \qquad (2.1)$$

Differentiation of Equation (2.1) and division of the result by R gives

$$\frac{dR}{R} = \frac{d\rho}{\rho} + \frac{dL}{L} - \frac{dA}{A} \qquad (2.2)$$

However, as indicated in Equation A-4 in the Appendix,

$$\frac{dA}{A} = -2\nu\frac{dL}{L} + \nu^2\left(\frac{dL}{L}\right)^2 \qquad (2.2a)$$

where ν is the Poisson's ratio of the metal used for the conductor, provided that the deformation of the conductor is elastic. All electrically conductive materials possess a strain sensitivity S_A defined as the ratio of the relative electrical resistance change of the conductor to the relative change in its length.

$$S_A = \frac{dR/R}{dL/L} \qquad (2.3)$$

Substituting Equations. (2.2) and (2.2a) into Equation. (2.3) yields

$$S_A = \frac{d\rho/\rho}{dL/L} + 1 + 2\nu - \nu^2\left(\frac{dL}{L}\right) \qquad (2.4)$$

The last three terms in Equation. (2.4) are due to the dimensional changes in the conductor (dL and dA). The first term is due to the change in the specific resistance with strain. The change in specific resistance is due to variations in the number of electrons and their increased mobility with applied strain. From Equation. (2.1) and (2.3), the basic strain sensitivity can be established due to the dimensional changes, assuming that the resistivity remains constant. If the conductor is stretched elastically, for a given change in length (ΔL) there will be an associated reduction in cross-sectional area due to the Poisson effect. These two effects are additive in increasing the resistance of the conductor, and assuming a Poisson's ratio of 0.3 (which is approximately the same for most resistance materials) the sensitivity factor (S_A) is about 1.6, i.e. ($1 + 2\nu \approx 1.60$). The last term is usually neglected for elastic strains in metals since it is small ($<0.1\ \varepsilon$) compared to the two middle terms ($1 + 2\nu \approx 1.60$). Therefore,

$$S_A = \frac{d\rho/\rho}{dL/L} + 1 + 2\nu \qquad (2.5)$$

Tests on various resistance materials [2.3] have shown that they exhibit widely different values of strain sensitivity (Table 2.1). These variations indicate that the specific resistivity (ρ) of the materials must be affected by strain, or perhaps more directly by the associated internal stress in the material. Strain sensitivity is, therefore, a combination of the effects of geometric changes plus a resistivity change due to changing internal stresses.(Equation 2.5)

Beyond the elastic limit of the material, however the change in internal stress approaches zero, and Poisson's ratio approaches 0.5. In this case, resistance changes due to strain are primarily due to dimensional changes and the strain sensitivity ($S_A = 1+2\nu$) approaches 2.0. This means that materials which have a strain sensitivity appreciably different from 2.0 in the elastic range will have values approaching 2.0 in the plastic range, with the associated non-linearity which this variation implies. So only those alloys which have a sensitivity of approximately 2.0 in the elastic range will remain essentially linear over a wide strain range, and this is generally true of the most commonly used strain gauge materials. Some materials which have an attractively high sensitivity in the

elastic range are in fact highly non-linear, which means that the sensitivity varies with strain, rendering them undesirable for strain gauge purposes.

Table 2.1: Strain sensitivity of various materials
(Courtesy of Window A L & Holister G S)

Material	Trade name	Typical strain sensitivity
Copper-nickel (55-45)	Constantan	+2.1
Nickel-chromium(80-20)	Nichrome V	+2.2
Nickel-chromium(75-20) + iron and aluminium	Karma	+2.1
Iron-chromium-aluminium(70-20-10)	Armour D	+2.2
Nickel-chromium-iron-molybdenum (36-8-55.5-0.5)	Isoelastic	+3.5
Platinum-Tungsten (92-8)	-	+4.0
Copper-nickel-manganese (84-4-12)	Manganin	+0.6
Nickel	-	-12.0
Iron	-	+4.0

2.4 THE BONDED ELECTRICAL RESISTANCE STRAIN GAUGE

The bonded electrical resistance strain gauge in its present form consists of a strain sensing element (the grid), a thin film that serves as an insulator and a carrier for the strain sensing element (the backing) and tabs (or terminals) for lead-wire connections.

2.4.1 The grid

The strain sensing element (shown in Figure 2.1) consists of a grid that is either stamped or photoetched from a very thin sheet of metallic foil. The grid configuration is used to develop the required resistance ($\approx 100\ \Omega$) of the sensing element while keeping the length l_o and the width w_o of the gauge small. The size of the grid is adjusted by the

manufacturer to suit a wide variety of applications. Gauge lengths are available throughout the range from 0.178 mm to 150 mm. [2.4] The size of the sensing element is selected by the experimentalist to minimise error due to non-linear strain gradients and the alloy is selected to accommodate test conditions, including temperature, duration of the measurement, and dynamic or cyclic loading.

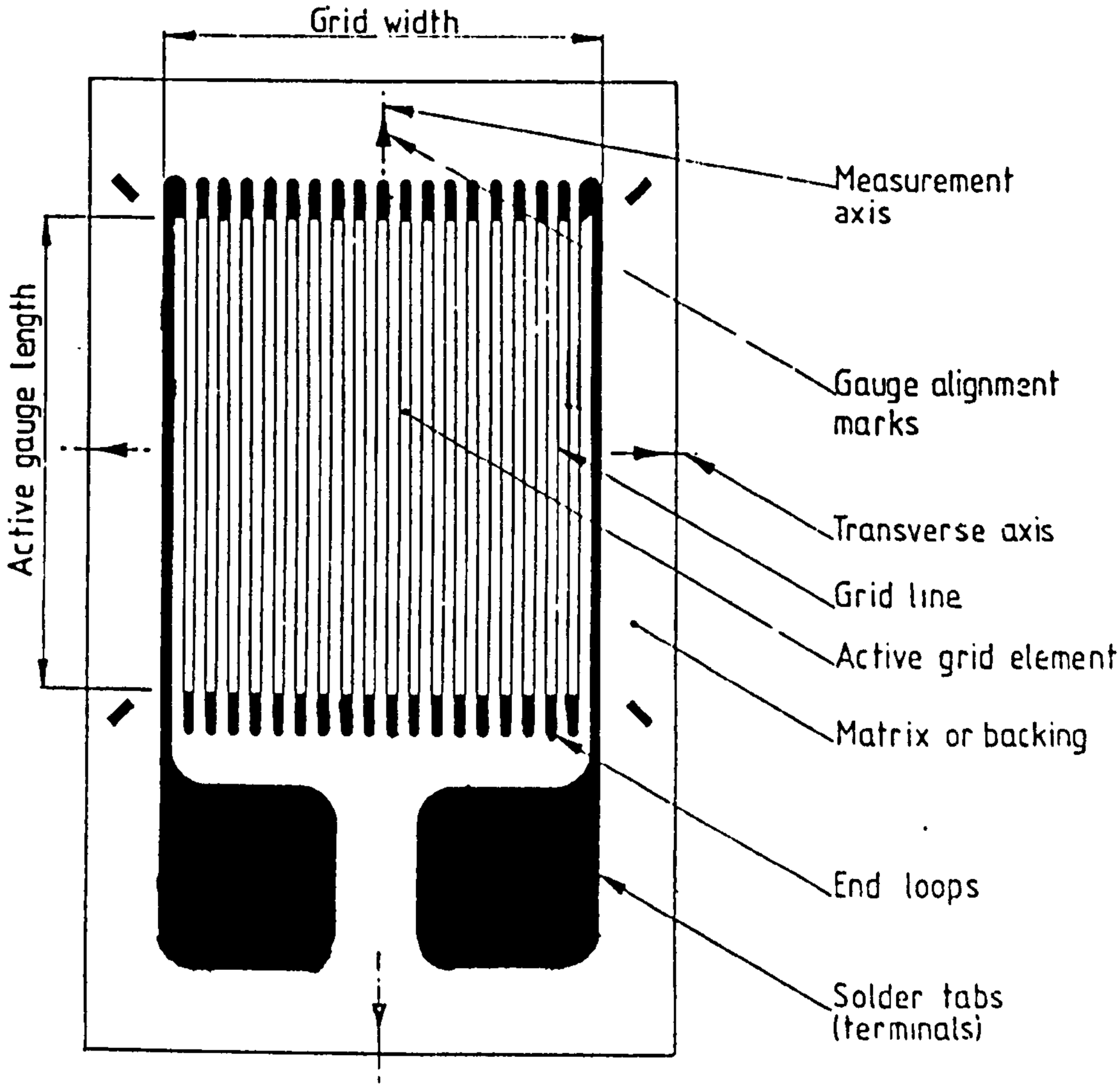

Figure 2.1: Outline view of the bonded electrical resistance strain gauge

Some of the features of a strain sensitive resistance element are:

1. Linear strain sensitivity in the elastic range - for accuracy and repeatability.

2. High resistivity - for smaller size.

3. Low hysteresis - for accuracy and repeatability.

4. High strain sensitivity - for maximum electrical output for a given strain.

5. Low and controllable temperature coefficient of resistance - for good temperature compensation.
6. Wide operating temperature range - for the widest range of applications.
7. Good fatigue life - for dynamic measurements.

Table 2.1 summarises the strain sensitivity of a number of resistance materials which might be considered for strain gauge purposes, In practice, only a few alloys come close to meeting the most desirable features.

2.4.2 Backing

The strain sensing foils are extremely thin (approximately 0.0025 mm) and very fragile. Therefore, they must be supported by a thin film that is bonded to the foil prior to photoetching. The backing or carrier material [2.3] of a strain gauge serves several important functions, including the following:

1. The film serves as a carrier during production and testing before packaging and for handling the sensing element prior to installation;
2. The carrier also serves as an insulator between the grid and the test material after installation;
3. The backing provides a readily bondable surface for bonding the gauge to the test material;
4. The film faithfully transmits the strain from the test material via the adhesive to the gauge grid.

These primary functions lead to the need for some very specific properties of the backing to achieve optimum overall strain gauge performance, and these are:

1. High shear modulus with minimum thickness, to ensure complete strain transmission;
2. Strength and flexibility, to reduce the possibility of damage during installation;
3. High elongation capability, for use at high strain levels into the plastic range;
4. Good bondability, for good 'peel' strength between the grid and backing, and good adhesion between the backing and test material;

5. Inherently high insulation resistance, to eliminate measurement problems and inaccuracies due to shunting effects of low insulation;

6. Good stability, with minimum creep;

7. Retention of all the above characteristics over as wide a temperature range as possible.

The different materials [2.4] employed as backing in gauge construction include acrylic, polyimide, polyimide-epoxy, epoxy, epoxy-phenolic, epoxy-glass, phenolic, phenolic glass, and paper. The carrier material employed with the wire gauges of the 1940's was paper; but now, in most instances, paper has been replaced with thin-film polymers. Polyimide, a carrier material that is flexible, tough, and compatible with most adhesive systems, is used for most general purpose strain gauges. A very thin epoxy film is used for gauges designed for transducer applications. The linear elastic behaviour of this carrier material helps the designer to meet the tight linearity and hysteresis specifications normally imposed on transducer performance. Glass-fibre-reinforced polymers are used for gauges that will be exposed to large magnitude cyclic strains. Glass-fibre-reinforced epoxy and phenolic carriers are used for strain gauges that will be exposed to elevated temperatures.

In certain field applications, it is advantageous to employ encapsulated strain gauges where environmental conditions are very severe [2.4]. These encapsulated gauges protect the gauge from weather and abuse. During fabrication, the gauges are mounted on a thin sheet of stainless steel or brass and then covered with sheet metal, rubber or polycarbonate.

2.5 PERFORMANCE AND PROPERTIES OF FOIL-TYPE STRAIN GAUGES

2.5.1 Strain cycling

One measure of the performance of a strain gauge system ("system" here implies gauge, adhesive and instrumentation) involves considerations of linearity, hysteresis and zero shift. These three factors, which are interrelated, are functions of the characteristics of the strain sensitive alloy, the backing material, strain level, and adhesive cure. For experimental stress analysis, modern high performance strain gauges with well-cured adhesives can generally be considered free from these effects. For properly installed

gauges, deviations from linearity will generally be between 0.05 and 0.1% of the maximum strain, and hysteresis and zero shift less than 0.2% of the maximum strain.

In high performance transducers, small deviations of this order are significant, and can be minimised by post-curing the adhesive at a temperature higher than the maximum operating conditions, and by load cycling 4 or 5 times over the working range.

2.5.2 Drift, Creep and Stability

Drift is a time dependent and generally irreversible change in gauge resistance with time at constant temperature under no-load conditions (i.e. with zero applied strain). Properly manufactured modern foil gauges are capable of showing resistance drift of only a few parts per million per year. All strain gauge alloys, however, display increased drift rates as temperatures are increased.

Creep differs from drift in that it is a change of resistance with time at constant temperature, but under load (with applied strain), and is a function of the behaviour of the organic backing and adhesive materials. It can generally be minimised by post-curing the gauge installation above its maximum operating temperature, and is frequently less than the creep in the material being tested.

Stability can be defined as the lack of drift or creep over long periods of time, typically months or years. Experiments have shown stability to within thirty parts per million (equivalent to a strain of 0.003%) over 900 days for Karma alloy with glass fibre reinforced epoxy-phenolic backing and a well cured epoxy adhesive system.

2.5.3 Resolution

Resolution or the ability of the gauge to detect small changes in strain, could be considered as being infinite. But, limitations of instrumentation and other performance characters generally mean that a resolution of 0.1 microstrain (one part in ten million) is about the smallest practical value attainable.

2.5.4 Heat Dissipation

It is necessary to pass an electrical current through a resistance strain gauge to provide an output which, in turn, is proportional to the gauge excitation level. For maximum sensitivity and resolution, the highest practical excitation level is desirable, although the

resulting current in the gauge can produce undesirable self-heating effects. This is a function of the gauge size, resistance, type of backing and adhesive used, velocity of air flowing over the gauge installation and heat sink capability of the test specimen. Under normal conditions, all the heat developed in the gauge flows through the backing and adhesive into the specimen. Metallic specimens are fair-to-excellent heat sinks, depending on their size, shape and thermal conductivity. Unfilled plastics are thermal insulators rather than heat sinks, so that much of the heat from the gauge must be transferred to the surroundings by convection.[2.3].

Errors due to self-heating effects show up as instability in readings of the gauge output. Voids in the adhesive glue line, or imperfections in the gauge grid, will result in local 'hot spots' with consequent reductions in performance. In the case of plastic specimens, the self-heating of the gauge installation may cause a severe local loss in specimen properties (e.g. elastic modulus), leading to inaccurate and misleading results [2.3]. By knowing the approximate levels of power density for various specimen and test conditions, the corresponding excitation voltages can be obtained using the formula:

$$\text{Power density in grid} = \frac{E_B^{\,2}}{4 R_G A_G} \qquad (2.6)$$

where E_B = bridge excitation voltage; R_G = gauge resistance; A_G = grid area [(active gauge length) X (grid width)]

Table 2.2 lists typical power density recommendations for foil strain gauges.

The maximum gauge excitation can be experimentally determined [2.5] by gradually increasing the bridge excitation under zero-load conditions until a definite zero instability is observed. The excitation should then be reduced until the zero reading becomes stable again, without a significant offset from the low excitation zero reading. For most applications, this value of bridge voltage is the highest that can be used safely without significant performance degradation.

Table 2.2: Allowable power densities (Courtesy of Kobayaski A, 1987)

Specimen conditions	Power density W/mm^2
Heavy Aluminium or copper sections	0.008-0.016
Heavy steel sections	0.003-0.008
Thin steel sections	0.0015-0.003
Fibreglass, glass, ceramics	0.0003-0.0008
Unfilled plastics	0.00003-0.00008

2.5.5 Thermal EMF's

It is possible for a thermocouple junction to be formed by the presence of dissimilar metals where strain gauge lead wires are attached to the gauge tabs. When copper lead wires are used with a copper-nickel gauge, a typical thermocouple combination arises, such that changes in temperature can produce small d.c. voltages. Normally these effects tend to cancel out because of the two opposing lead wire connections on a standard strain gauge, provided that both connections are at the same temperature. With modern strain gauges and protective coatings where this is generally the case, the effects can be ignored.

2.5.6 Magnetic fields

Errors can be introduced in strain gauge measurements by strong magnetic fields. There are various ways of overcoming this problem by paying particular attention to the gauge wiring and shielding. Another method is by using a special strain gauge consisting of two identical grids superimposed on top of each other, separated by an insulating layer, and then connected in series. This arrangement results in almost complete cancellation of the voltages which may be induced in the gauge due to magnetic fields.

2.5.7 Temperature Effects on gauge resistance

All electrical conductors have a temperature coefficient of resistance, which means that a strain gauge made from these materials will undergo a change in resistivity with temperature. In a bonded electrical resistance strain gauge there is an additional effect

producing a change in resistance with temperature. When a gauge is bonded to a test material which has an expansion coefficient different from that of the gauge material, a change in temperature will produce a strain in the gauge and hence a resistance change due to the difference in expansion. The combination of these changes of resistance which occur, is interpreted as a mechanical strain and is referred to as temperature induced 'apparent strain'. This is one of the most serious potential sources of error in the practice of static strain measurements with strain gauges. Some strain gauge alloys exhibit large 'apparent strain' errors but others can be processed to produce very small resistance changes with temperature. Both copper-nickel and modified nickel-chromium can be processed by heat treatment to adjust the basic temperature coefficient of resistance to compensate for the resistance change due to differential expansion effects on various materials. These are referred to as self-temperature compensated gauges (STC).

2.5.8 Elongation capability

All bonded strain gauges are limited in the maximum strain level that can be applied before failure by characteristics of the grid, the alloy, the backing and the adhesive. High performance gauges with glass fibre reinforced backings are usually limited to maximum strains of 1 to 2%. General purpose STC gauges with copper-nickel grids are normally capable of measuring strains of up to 5% in other than very small grid sizes.

2.5.9 Fatigue life

In common with all metals, strain gauge grids will eventually fail in fatigue due to cyclic straining at reasonably high strain levels. Wire gauges become completely open-circuited within a few cycles of attaining their fatigue limit. Foil gauges usually remain intact for hundreds or thousands of cycles before complete grid failure occurs because cracks at the line edges progress gradually across the width. This first manifests itself as an irreversible increase in resistance, producing a positive zero shift, which increases with additional cycling. The presence of these cracks in the foil grid also produces an apparent increase in sensitivity. This is because the opening and closing of the cracks produces change in resistance which is not proportional to the normal resistance changes due to strain. This phenomenon is referred to as super-sensitivity. Because of all this, the fatigue limit for foil strain gauges is normally defined as that point at which the zero shift has a value of between 100 and 300 microstrain, depending on the required test accuracy.

2.6 STRAIN GAUGE SELECTION PARAMETERS

The installation and operating characteristics of a strain gauge are influenced by all of the various parameters which have already been reviewed. The process of selecting a gauge for a particular measurement situation consists of determining the compromise of the combination of parameters which are compatible with environmental and other operating considerations allied to the installation and operating requirements, such as accuracy, stability, maximum elongation, test duration, cyclic endurance, simplicity and ease of installation. Table 2.3 lists the influence of size, resistance and end loop size on some of the main performance criteria which have already been discussed.

2.6.1 Gauge length

Gauge length is an important consideration in strain gauge selection. Strain measurements are usually made at the most critical or highly stressed points on a machine part or structure. These highly stressed points are associated with stress concentrations, where the strain gradient is quite steep, and the area of maximum strain restricted to a very small region. Since the strain gauge tends to integrate or average the strain over the area covered by the grid, and since the average of any non-uniform strain distribution is always less than the maximum, a strain gauge which is larger than the maximum strain region will indicate a strain magnitude which is too low.[2.3].

Larger gauges have several advantages like being easier to handle (in gauge lengths up to about 13 mm) and providing improved heat dissipation because they introduce, for the same nominal gauge resistance, lower wattage per unit of grid area. This consideration can be very important when the gauge is installed on plastic or other material with poor heat transfer properties.

2.6.2 Gauge resistance

Strain gauges are generally available with two grid resistances - typically 120 ohms and 350 ohms. When the choice exists, the higher resistance gauge is preferable in reducing the heat generation rate by a factor of three (for the same applied voltage across the gauge). Higher gauge resistances is also advantageous in decreasing lead wire effects such as spurious signals caused by lead wire resistance changes with temperature fluctuations. In addition, the signal to noise ratio can be improved with high resistance

gauges (by using higher voltages) when the gauge circuit includes switches, sliprings or other sources of random resistance change. [2.3].

Table 2.3: Effects of gauge size, resistance and end loop length on foil gauge performance criteria. (Courtesy of MicroMeasurements)

Performance	Desirable for optimum performance		
criterion	Gauge size	Gauge resistance	End loop length
Gauge factor (a) uniformity	Large	Medium	Medium
(b) maximum	Medium	High	Long
Low transverse sensitivity	Small	High	Long
Apparent strain uniformity	Medium	Medium	Medium
High strain	Medium	Low	Short
High fatigue life	Large	Low	short
Low creep	Medium	Medium	Medium
Maximum temperature limit	Large	High	Long
Low self heating	Large	High	Medium
Ease of installation	Medium	Low	-
Low noise	-	High	-
Low cost	Medium	Low	-

2.7 STRAIN GAUGE INSTALLATION

Because the strain gauge is an extremely sensitive device capable of registering the smallest effects of an imperfect bond, considerable attention to detail need to be taken to assure reliable, creep-free installations. The first step to be taken before installing a gauge is the selection of the adhesive. The strain in the test surface is faithfully transmitted through the adhesive layer into the gauge grid. Resistance strain gauge theory assumes that the strain appearing in the gauge grid is identical to that occurring on the surface to which the gauge is bonded. In addition, the adhesive has a significant influence on many installation properties such as gauge factor, creep performance, linearity, hysteresis, zero shift with temperature and heat dissipation characteristics. An adhesive must be selected that has the most appropriate combination of characteristics for the installation to be undertaken. The two adhesives that are in common use today are cyanoacrylate and epoxy. Cyanoacrylate is simple to use being single part and hence requires no mixing. It is very fast curing as polymerisation takes place in less than one minute when the material is spread into a thin film. Its main limitations are a restricted operating temperature range of -5°C to 50°C and also it is not very waterproof. Therefore the cyanoacrylates should not be used for long term installations. On the other hand, epoxies and epoxy phenolics have been widely used for the installation of strain gauges for many years. A wide selection is available in both room temperature curing form using an amine catalyst and hot curing form using an acid anhydride catalyst. These are sometimes modified with phenolics for improved performance up to 300°C.

After having selected the appropriate adhesive, the material surface must be properly prepared. The purpose of surface preparation is to develop a chemically clean surface having a roughness appropriate to the gauge installation requirements, a surface alkalinity of the correct pH, and visible gauge layout lines for locating and orienting the strain gauge.[2.6]

The next step in the installation of the strain gauge is the bonding itself. The performance of the electrical resistance strain gauge is absolutely dependent on the bond between itself and the test part. Practical considerations dictate that the strain gauge be mounted in the area of the highest strain. This produces the maximum allowable signal output consistent with the strength of the beam. At the same time, it minimises the likelihood of

fatigue originating at points of stress concentration outside of the designated gauging site. For a straight beam, the gauge location should be 1/2 to 1 "W" away from the clamped end of beam (where "W" is the width of the beam) to reduce the influence of clamping force on the strain distribution in the gauge area. [2.7]. The strain gauge is carefully removed from its acetate envelope and placed on a chemically clean glass plate. Using a cellophane tape the gauge is lifted from the glass plate and positioned on the test specimen. For applying the adhesive, the end of the tape opposite the solder tabs are lifted at a shallow angle until the gauge and terminal are free of the specimen. The loose end of the tape is tacked under and pressed to the surface so that the gauge lies flat with the bonding side exposed. After applying the adhesive on the gauge, the tape and gauge is pressed down into position, wiping excess adhesive to the outside edges of the gauge to leave a thin film of adhesive between the specimen and the gauge.

Care should be taken to see that there are no air bubbles between the adhesive and the gauge. Force is applied till the adhesive has set for 5-6 hours. Then the clamps are removed, the tape is pulled back directly over itself , peeling it slowly and steadily off the surface.

After the strain gauge has been installed and the adhesive cured, there are several quick tests that can be made to ascertain that the gauge will function properly. [2.8] First, the gauge resistance is checked. If it shows an open circuit but all soldered connections are conductive, the gauge may have been damaged during installation and is therefore useless. If, on measuring the gauge resistance, a value noticeably different from the manufacturer's specifications is obtained, the gauge should be regarded with extreme suspicion, for this, too, indicates probable damage in handling or bonding of the gauge. Next, the resistance between the strain gauge filament and the metal surface to which the gauge is attached should be measured. A thoroughly cured gauge will show a resistance of 1000 megohms or higher but a minimum of 50 megohms is considered necessary for accurate, stable functioning of the gauge. A final check on the gauge bond is done by connecting the gauge to a static strain indicator, balance the bridge (described in Section 2.8.1) and then press lightly on the strain gauge. When this pressure is applied, the needle should show a slight deviation, but when the pressure is

released, the meter needle should return to zero or nearly so. If the pointer fails to return at all or becomes unsteady, then the gauge is either imperfectly bonded (which might be caused by an air bubble under the gauge) or accidentally damaged and will have to be replaced.

2.8 STRAIN GAUGE INSTRUMENTATION

The definition of strain gauge instrumentation is everything from the energising of the strain gauge to the production of test results in the required form. Figure 2.2 shows the strain measurement system in the form of a Venn diagram. The instrument can provide all the components of the sensing circuit except the active strain gauges, and may also include analog-to-digital conversion of the amplified signal.

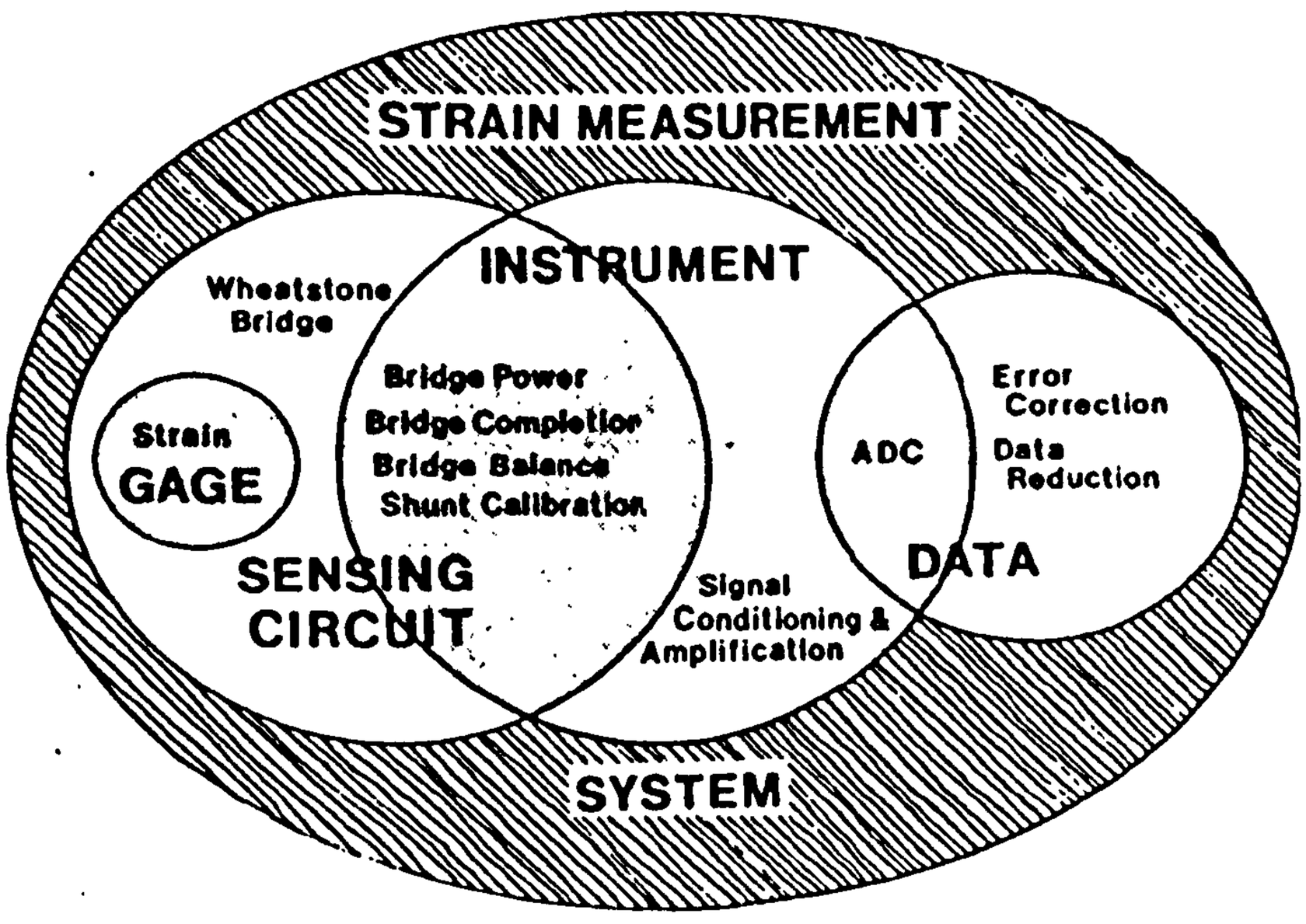

Figure 2.2: The Strain Measurement system (Courtesy of Micromeasurements Group)

Strain instrumentation consists of complex equipment that can perform any or all of the following functions :

1. Supply bridge power

2. Provide bridge completion for quarter and half - bridge installations

3. Zero - balance the bridge

4. Shunt - calibrate the system of gauges

5. Condition and amplify the signal from the bridge

6. Set gauge factor for direct readout of strain, or gain for scaling output signal from the instrument

7. Provide analog - to - digital conversion of the signal

2.8.1 The sensing circuit

The Wheatstone bridge is the sensing circuit utilised to measure the resistance changes produced when active gauges are exposed to strain. The bridge, in effect a dual voltage divider, is normally powered by a constant voltage source of a few volts dc. It converts very small resistance changes in the gauge into millivolt electrical signals suitable for amplification and processing. The classical Wheatstone bridge arrangement has been used for many years for the accurate measurement of a single unknown resistance; and in such instruments, the bridge is balanced at the time of measurement by adjusting the resistances of the other arms. The bridge circuit found in most strain indicators, on the other hand, is unbalanced by the varying gauge resistances at the time of making the measurement, and is therefore commonly referred to as the "unbalanced Wheatstone bridge". The output voltage obtained from the "unbalanced" Wheatstone bridge is a function of the amount of unbalance, and is therefore directly related to the strain applied to the strain gauge. However, under certain conditions frequently encountered in actual practice, the bridge output voltage is a non-linear function of the resistance change in the bridge arms; and when this occurs, the strain readings will be somewhat in error.

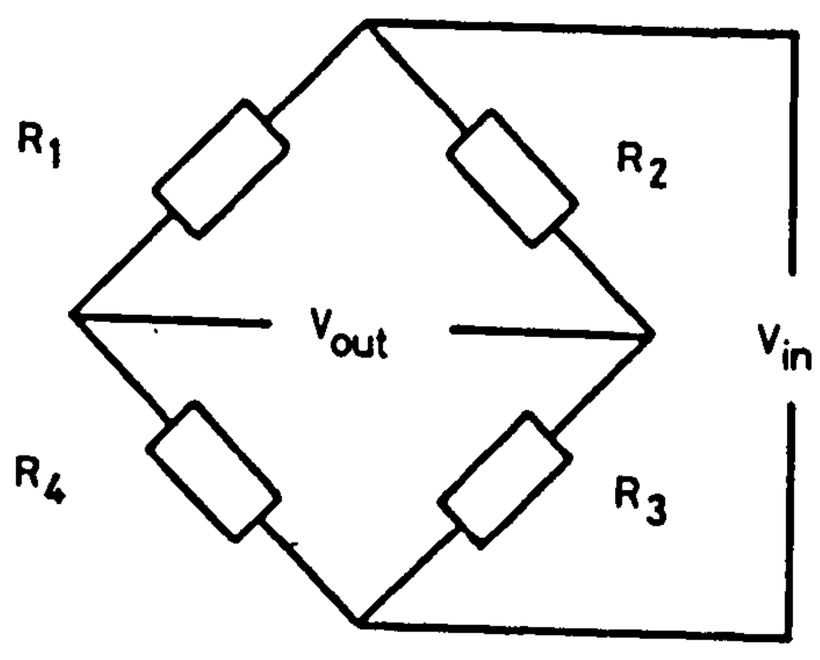

Figure 2.3 : The Wheatstone bridge

Consider Figure 2.3 in which R_1, R_2, R_3, R_4 are resistors. Assuming that the condition $R_1/R_4 = R_2/R_3$ is satisfied then the output voltages V_{out} will be zero, i.e. the bridge is balanced. A change in resistance in R_1 will unbalance the bridge and produce a voltage across the output terminals.

If a similar change, in both magnitude and polarity occurs in an adjacent arm of the bridge, say R_4, then the voltage V_{out} will remain at zero and the bridge will remain in a balanced condition.

If, in adjacent arms, resistance changes occur of equal magnitude but opposite polarity, then the voltage V_{out} will be twice that due to resistance changes in one arm. For strain gauge purposes, the output equation for the bridge is

$$V_{out} = \frac{F\varepsilon\, N\, V_{in}}{4} \qquad (2.7)$$

where F is the gauge factor, V_{in} is the bridge volts, ε is the strain and N is the number of active arms of the bridge.

The output voltage, V_{out}, is also dependent on the resistance or impedance of the circuit that is connected across the output terminals of the bridge. In early instruments this could have been a low impedance galvanometer or meter and its effect on the output voltage would have been severe. With modern amplifiers of extremely high impedances there is little or no 'loading' effect on the bridge, i.e. the current consumed by the external circuit is negligible.

There are three types of input configurations: the quarter bridge operation, the half bridge and the full bridge.(Figure 2.4)

2.8.1.1 Quarter bridge operation

When a single gauge is used at the measurement point with resistors within the strain indicator completing the bridge, then that is termed 'quarter bridge operation'. The lead wires connecting the gauge into the bridge form part of the measurement circuit and must be treated with care. To this end the three wire system is recommended as the resistance of the lead wire, irrespective of length does not unbalance the bridge because there are similar lead wires in adjacent arms of the bridge and their effects will cancel. The other two advantages of the lead wire system are that the resistance changes of the

lead wires produced by temperature changes are cancelled out in the bridge and that the desensitisation effects of the lead wires are halved.

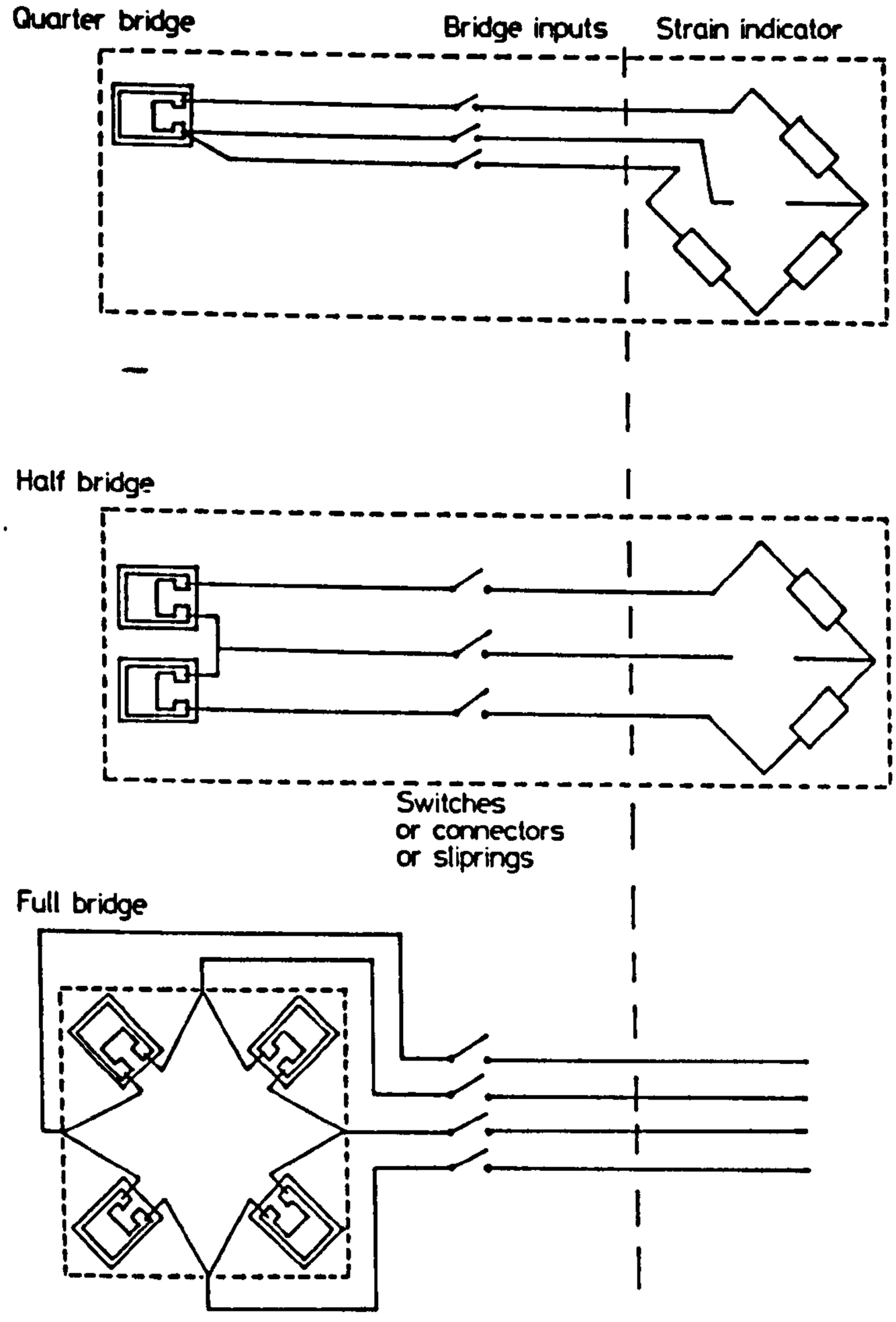

Figure 2.4: Bridge configurations-measuring circuit: All items within the dotted boundaries are in the bridge (measuring) circuit and will directly affect the measurement. (Courtesy of Window A L and Holister G S)

2.8.1.2 Half bridge

When two gauges are used in adjacent arms of the bridge, it is known as a half bridge system. For this to work one gauge must see tension and the other compression, i.e. one increasing and the other decreasing in resistance, or one gauge must see zero

mechanical strain. With the two gauges wired as shown in Figure 2.4 then resistance changes of the same sign caused by temperature changes will not unbalance the bridge.

The use of the half bridge in any form does not ensure complete and automatic temperature compensation and it relies on the two gauges having well-matched temperature/resistance characteristics. One example of a half bridge system is a cantilever beam with one gauge on top and one directly underneath wired [Chapter 4]. If the output is measured and Equation 2.7 rearranged to compute the strain, then with N=2 the average of the two surface strains will be recorded, with N=1 the sum of the two surface strains will be recorded.

2.8.1.3 Full bridge

The full bridge using gauges as all four arms of the Wheatstone bridge, is a logical extension of the half bridge and can be used to further increase the sensitivity of a measuring system. Putting two gauges on each side of a beam instead of one, gives a value of N=4 i.e. the output is four times that of a single quarter bridge installation, with possible improved temperature compensation, and the cancellation of unwanted signals. The greatest advantage of the full bridge system is that all the lead wires from the measuring point to the instrumentation including plugs, connectors and sliprings if used, are outside the measuring circuit and contribute minimal errors to the system. (Figure 2.4) The full bridge is therefore often used for installations where the measuring point is a long way from the reading instruments, particularly for 'on-site' work where there are large temperature and other environmental variations.

Table 2.4 gives the output voltage as a function of the applied strain for a variety of cases representing different strain states and different arrangements of gauges on the structural member and within the Wheatstone bridge. It will be noted from this table that only certain bridge configurations produce a linear output for a linear surface strain effect. The only configurations that do produce a completely linear output (output is a linear function of the strain) are those employing bridges with equal and opposite arms, i.e. two fully active arms and four fully active arms, when the resistance changes are such that the currents in the bridge arms remain constant - that is when $\Delta R_1/R_1 + \Delta R_4/R_4 = 0$ and $\Delta R_2/R_2 + \Delta R_3/R_3 = 0$ (the third , sixth and seventh cases). Table 2.4 also

Table 2.4 : Output voltage for different strain states and arrangements (Courtesy of Micromeasurements Group)

Description	output equation in mV/V	$\frac{\text{actual strain}}{\text{indicated strain}} = \frac{\varepsilon}{\hat{\varepsilon}}$	Comments
Single active gauge in uniaxial tension or compression	$\frac{E_o}{E} = \frac{F\varepsilon\, X10^{-3}}{4+2F\varepsilon\, X10^{-6}}$	$1+\frac{F\hat{\varepsilon}\, X10^{-6}}{2-F\hat{\varepsilon}\, X10^{-6}}$	Non-linear
Two active gauges in uniaxial stress field-one aligned with max. principal strain, one "Poisson gauge"	$\frac{F\varepsilon\ (1+\nu)\, X10^{-3}}{4+2F\varepsilon\,(1-\nu)X10^{-6}}$	$1+\frac{F\hat{\varepsilon}\,(1-\nu)X10^{-6}}{2-F\hat{\varepsilon}\,(1-\nu)X10^{-6}}$	Non-linear
Two active gauges with equal and opposite strains- bending beam.	$\frac{F\varepsilon\, X10^{-3}}{2}$	$\frac{\varepsilon}{\hat{\varepsilon}} = 1$	Linear
Two active gauges with equal strains of same sign-used on opposite sides of column with low temperature gradient: (bending cancellation)	$\frac{E_o}{E} = \frac{F\varepsilon\, X10^{-3}}{2+F\varepsilon\, X10^{-6}}$	$1+\frac{F\hat{\varepsilon}\, X10^{-6}}{2-F\hat{\varepsilon}\, X10^{-6}}$	Non-linear
Four active gauges in uniaxial stress field-two aligned with max. principal strain, two Poisson gauges: column	$\frac{F\varepsilon\ (1+\nu)\, X10^{-3}}{2+F\varepsilon\,(1-\nu)X10^{-6}}$	$1+\frac{F\hat{\varepsilon}\,(1-\nu)X10^{-6}}{2-F\hat{\varepsilon}\,(1-\nu)X10^{-6}}$	Non-linear
Four active gauges in uniaxial stress field-two aligned with max. principal strain, two "Poisson" gauges: beam	$\frac{F\varepsilon\ (1+\nu)\, X10^{-3}}{2}$	$\frac{\varepsilon}{\hat{\varepsilon}} = 1$	Linear
Four active gauges with pairs subjected to equal and opposite strains: beam in bending or shaft in torsion.	$F\varepsilon\ X\ 10^{-3}$	$\frac{\varepsilon}{\hat{\varepsilon}} = 1$	Linear

includes, for each case, the ratio of the actual strain to the indicated strain, permitting correction of indicated strains with these formulas in the non-linear cases.

2.8.1.4: The sensing circuit used in this PhD project work

For the sensor that was developed in this PhD project (Chapter 4), the strain arrangement used was the third case, in which the output is a linear function of strain. The half bridge was preferred to the quarter bridge, as automatic temperature compensation was ensured by using two gauges having well-matched temperature/ resistance characteristics. The full bridge would have been a better alternative to the halfbridge arrangement as far as the sensitivity of the device was concerned but owing to the fact that the elastic beam used was not very wide (0.0135 m), it would not have been practical to install and wire two gauges on the same side of the beam. Hence the half bridge arrangement was preferred and chosen.

2.8.2 Bridge supply

So far the Wheatstone bridge has been discussed, as if powered by a direct current, constant voltage supply. There are other means of supplying bridge power. The advantages of d.c over a.c supply are simpler circuitry, a more stable amplifier gain and hence stable system sensitivity, better system linearity and absence of cable capacitive or inductive effects. In contrast the a.c supply is less sensitive to electromagnetic interference, system zero is not affected by any amplifier zero drift and thermocouple voltages are not measured.

A strain gauge is essentially a resistance which, when a current is passed through it, has to dissipate the heat generated. Most of the heat is dissipated by conduction through the material to which the gauge is bonded. If the voltage supply to the bridge is increased, the current through the arms of the bridge will increase in proportion, and the power dissipated in them will increase in proportion to the square of the voltage. If the heat is not conducted away at a sufficient rate then the gauge temperature rises and its resistance changes. If the gauges are not mounted so that they all lose heat equally, a bridge output will be produced. The effect then is a continuing drift on the output. Excessive currents can produce so much heat in a gauge that the foil melts and becomes an open circuit. To prevent gauge failure due to overheating, and to limit the spurious

bridge output to acceptable proportions, manufacturers specify a maximum current for any given gauge, and this sets a maximum on the bridge supply voltage. Even within this limit, it is essential to ensure that any heating that does occur produces a negligible output in any particular application.

So the problem, then, is how to indicate strains in the order of 1 or 2 microstrain when the output voltage of the bridge must be limited, to be of the order of tens or hundreds of microvolts. The solution is to amplify these small changes of voltage into much larger proportional changes of voltage, which can then be used to activate some indicating or recording device.

2.8.3 Amplifiers

An amplifier is defined as a device which can consist of a number of stages. A strain gauge amplifier is assumed to include bridge completion resistors suitable for quarter and half bridge use, balance facilities, and a power supply for the bridge. The type of amplifier is usually dictated by the nature of the task, i.e. static or dynamic measurements. With static measurements it is usually possible to use only one amplifier and, if more than one measurement point is needed, then a number of gauges can be switched, feeding one at a time to the amplifier. In dynamic work correlation between different measurement points is usually required which means simultaneous amplification and recording and hence one amplifier per measurement point. In addition, the amplifier will be designed to have a wide frequency response and low internally generated noise.

2.8.4 Real time processing and display

The output of the strain gauge amplifier is a voltage which is directly proportional to the strain change at the gauge position. Real time processing is carried out during the testing, as opposed to post processing which is carried out remote from the test using stored data. Real time processing ensures that the pertinent data is immediately available to the operator in readily understood units. Analogue or digital processing may be used. Analogue processing in strain gauge testing, is the manipulation and testing of the signal voltage. For digital processing, the analogue signals are passed through an analogue-to-digital converter (ADC) which provides a suitable coded output for access to a computer. With the analogue signal processed in an ADC, the signal may be displayed or printed in a convenient, understandable form, stored in digital form for ease of

computerised post processing, or processed by a computer or processor in the real-time of the test programme.

CHAPTER 3

ASSESSMENT OF THE SUITABILITY OF RUBBER AS THE SENSING BEAM MATERIAL FOR THE FLOW METER

3.1 INTRODUCTION

Natural rubber is a very versatile and adaptable material which has been successfully used in engineering for over a hundred years. Good weathering resistance, achieved by means of modern protective agents, ensures that natural rubber lasts for many years. Unlike metal, rubber possesses some inherent damping, which is particularly beneficial when resonant vibrations are encountered, and it can store more energy than steel.

The need for a suitable material for the sensing beam of the flow sensor described in this thesis arose as this was an important aspect in the design of the flow sensor. Compared to other materials, rubbers offer the most useful range of moduli and many different types are available. The unique combinations of useful properties which rubbers exhibit making them the ideal material for the sensing beam of this flow sensor are as follows:

- The first and foremost property is elasticity, the ability to deform substantially by stretching, compression or torsion and then snap back to almost their original shape after removal of the force causing the deformation;
- Low permeability to air, several gases, water and steam;
- Good electrical and thermal insulation;
- Good mechanical properties;
- The capability of adhering to various fibres, metals and rigid plastics.

This chapter describes the various steps taken to process natural rubber and the effect of various external conditions on rubber. This information enables the suitability of natural rubber as a sensing beam material to be assessed, and preliminary design to be carried out.

3.2 THE NATURE OF RUBBER

Natural rubber is a member of the class of substances known as high polymers. The distinguishing feature of polymers is the long length of the molecular chain. Polymers can be grouped into three general categories:

3.2.1 Thermoplastics

These materials can be softened and resoftened indefinitely by the application of heat, provided the temperature is not so high as to cause decomposition. The term thermoplastic implies that the material becomes plastic when heated. [3.1] Such polymers are made up of long-chain molecules that are not chemically joined to each other. The atoms in the molecules are held together by strong covalent bonds and only very weak secondary bonds operate between the molecules. An important characteristic of these long molecules is that they are not straight and stiff; the molecules can be bent easily which is why thermoplastics are ductile. Examples of common thermoplastics are nylon, polystyrene, perspex; vinyls based on vinyl chloride(PVC) and vinyl acetate; polyolefins based on polyethylene and polypropylene; polyamides, polyacetals, polycarbonates and cellulosics.

3.2.2 Thermosets

These materials are rigid and not softened by the application of heat. Such polymers have molecular structures which are chemically cross-linked to one another during polymerisation to form a continuous and quite rigid framework. The cross-links are called covalent bonds. Because of this, when heat causes bonds to break, the effect is not reversible on cooling. Examples are phenolics, amino resins, epoxies, bakelite, melamine, Formica and adhesives such as Araldite.

3.2.3 Elastomers

Elastomers can be characterised according to the form of their polymer chains, as follows:

- Only carbon in the backbone of the polymer chain. This includes natural rubber, butadiene-styrene, butadiene acrylonitrile and butyl rubbers.
- Polymer chains with oxygen in the backbone. Polypropylene oxide is an example.

- Polymer chains with silicon in the backbone. Fluorosilicone is an example.
- Polymer chains having sulphur in the backbone. Polysulphide is an example.
- Thermoplastic elastomers, which are block copolymers with alternating hard and soft blocks. Examples are polyurethane, ethylene vinyl acetate and styrene-butadiene-styrene. Such elastomers can be processed by thermoplastic moulding methods such as injection and blow moulding. They, like thermoplastics, can be repeatedly softened by heating, unlike elastomers.

3.2.4 Discussion of the rubber used as the sensing beam material for air, water and oil flow measurements

The chemical formula of natural rubber is $(C_5H_8)_n$ where n is about 10,000 and C_5H_8 is the monomer isoprene [3.3]. The configuration of each isoprene unit is in accord with a definite and unique geometrical pattern. (Figure 3.1). Any other arrangement would give a material of quite different properties. In natural rubber the arrangement is designated *cis*, hence the chemical name for natural rubber: cis-polyisoprene.

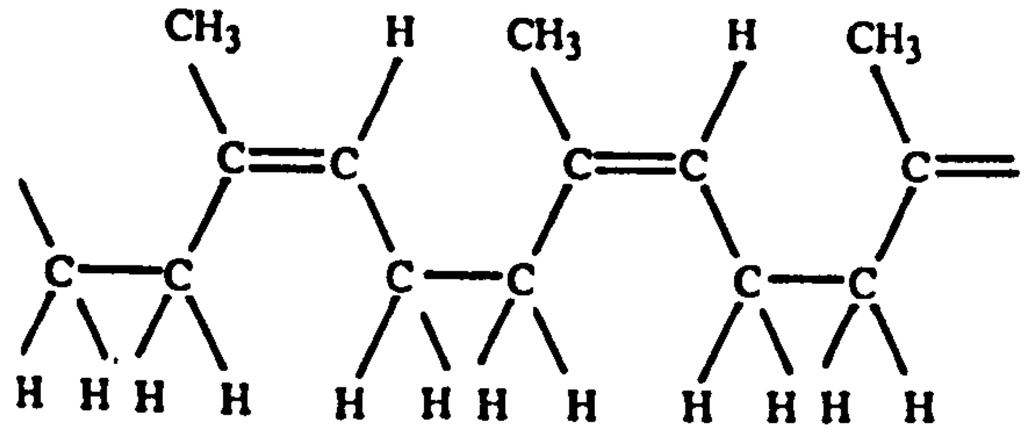

Figure 3.1: Cis-polyisoprene, the natural rubber chain before vulcanisation. (Courtesy Bolton W, 1989)

General purpose elastomers include styrene-butadiene rubber (SBR), butadiene rubber (BR) and polyisoprene - both natural rubber (NR) and synthetic (IR).

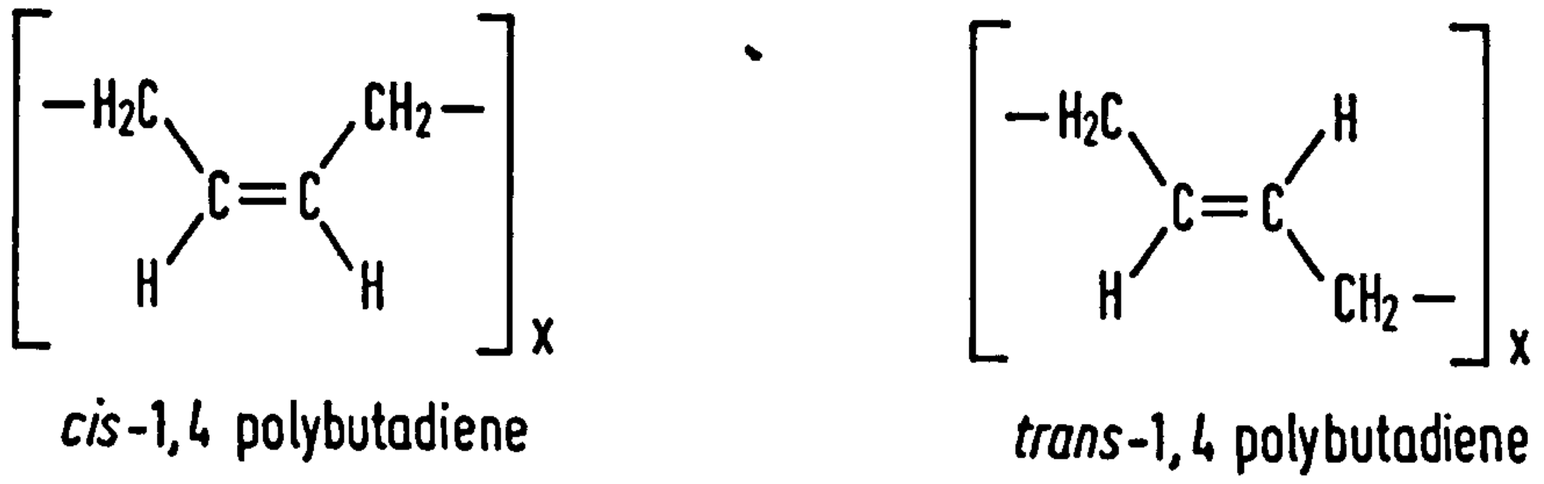

Figure 3.2: Possible configurations of 1,4 polybutadiene: the sensing beam material.(Courtesy Nagdi K, 1993)

The polymer used as the material for the sensing beam of the flow sensor was polybutadiene (BR) which was unfilled and vulcanised supplied by the Malaysian Rubber Company. Figure 3.2 shows the basic structure of this polymer. BR is a homopolymer of butadiene shown in Equation 3.1. [3.2] The high cis grades contain approximately 97-98% cis-1,4 butadiene units. Oil extended grades (with and without carbon black) are also available.

$$CH_2=CH-CH=CH_2 \xrightarrow{\text{polymerisation}} [-CH_2-CH=CH-CH_2-]_X \quad (3.1)$$

Polybutadiene polymers are more difficult to process than NR or SBR. Therefore, they are normally used in blends with other rubbers such as NR, IR or SBR to improve the abrasion resistance, resilience and low temperature flexibility. The blends usually contain less than 50% of BR and often only 10-25%. The vuncanizates of 100% BR have high abrasion resistance, the highest resilience (the ability of an elastomeric part to return quickly to its original shape after a temporary deflection, which indicates the speed of recovery for the rubber and negligible zero drift for the flow sensor) of all known polymers and the lowest glass temperature (Tg) of about -100^{0}C.[3.2].

Nagdi K [3.2], in his ratings on rubber polymers based on their general chemical resistance, has quoted that water has the least effect on polybutadiene polymer. Therefore this polymer would be the ideal material for water flow measurements. Almost all elastomers (with suitable compounding ingredients) can be used in cold water. Suitably formulated NBR compounds (acronitrile-butadiene rubbers) can be used in hot water up to 100^{0}C. For higher hot water temperatures, peroxide cured EPDM compounds (ethylene-propylene rubbers) provide the highest resistance. The recommended material for petroleum or mineral oil flow measurements are the polar elastomers like NBR, hydrogenated NBR (HNBR),chloroprene rubbers (CR), polyacrylate rubbers(ACM), ethylene-acrylic rubbers(AEM), fluorocarbon rubbers(FPM), fluorosilicone rubbers(FMQ), polyurethane rubbers(AU/EU), epichlorohydrin rubbers (CO, ECO), and chlorosulphonated polyethylene rubbers (CSM) which are consistently more resistant to a wide variety of mineral-oil-based fluids at different temperature ranges. All nonpolar hydrocarbons elastomers like natural rubber, synthetic rubber and styrene-butadiene-styrene polymers are badly swollen by mineral oils and should be avoided when used to measure oil flow. Water-in-oil emulsions consist of approximately 40% water dispersed in a continuous phase of mineral oil. For

such measurements, properly formulated NBR elastomers can be used. For air flow measurements up to 70^{0}C, the polybutadiene rubber(BR) used in this PhD project is recommended but for higher air temperatures, this rubber is not recommended and should be replaced by AEM or ACM rubbers for temperatures up to 150^{0}C and by FPM rubber for temperatures up to 200^{0}C.

This section has discussed the ideal rubber material that could be used in the different fluids and over different temperature ranges. Therefore, depending on the fluid that will be measured and the temperature range that would be encountered during the measurement process, the appropriate rubber polymer from those mentioned above could be selected and used for the design of the flow sensor.

3.3 RUBBER COMPOUNDING AND MANUFACTURE

Over the past decade the rubber industry has faced an ever increasing demand for improved product performance. This challenge has been met by improved product design procedures, by improved materials, and by improved manufacturing. The rising tide of automation and computer-controlled systems has affected all areas of rubber processing. The addition to raw rubber of various chemicals, to impart desirable properties, is termed rubber compounding or formulation. Typical ingredients include crosslinking agents (also called curatives), reinforcements, antidegradants, process aids, extenders, and speciality additives, such as tackifiers, blowing agents, or colourants.

3.3.1 Raw rubber

Rubber latex occurs beneath the bark of certain trees, notably '*Hevea brasiliensis*', which is cultivated in the plantations of Malaysia and other tropical countries. Rubber trees are tapped for latex every other day, producing nearly three million tons of rubber each year. The latex is coagulated then processed into blocks or sheets for shipping in compressed bales. At this stage it is still raw rubber and has little practical use. It flows under load as the long molecules slide over each other, thus preventing recovery when the load is removed, it crystallises readily at temperatures around 0^{0}C and below, and it becomes soft and sticky in hot weather. [3.3]

3.3.2 Vulcanisation

In order to make it practical to use, raw rubber has to undergo a chemical reaction known as vulcanisation, a process discovered by Charles Goodyear in 1839. A raw elastomer is a high molecular weight liquid with low strength. Goodyear found that when raw rubber was masticated, mixed with sulphur and then heated, the doughlike mixture was converted into an elastic material, becoming stable over a much wider temperature range and resistant to flow under load. Vulcanisation or curing causes the chains to be chemically linked together to form a network, thereby transforming the elastomeric liquid into an elastic solid. Strength and modulus increase while set and hysteresis decrease. Figure 3.3 shows the structure of vulcanised rubber, sulphur linked polyisoprene chains.

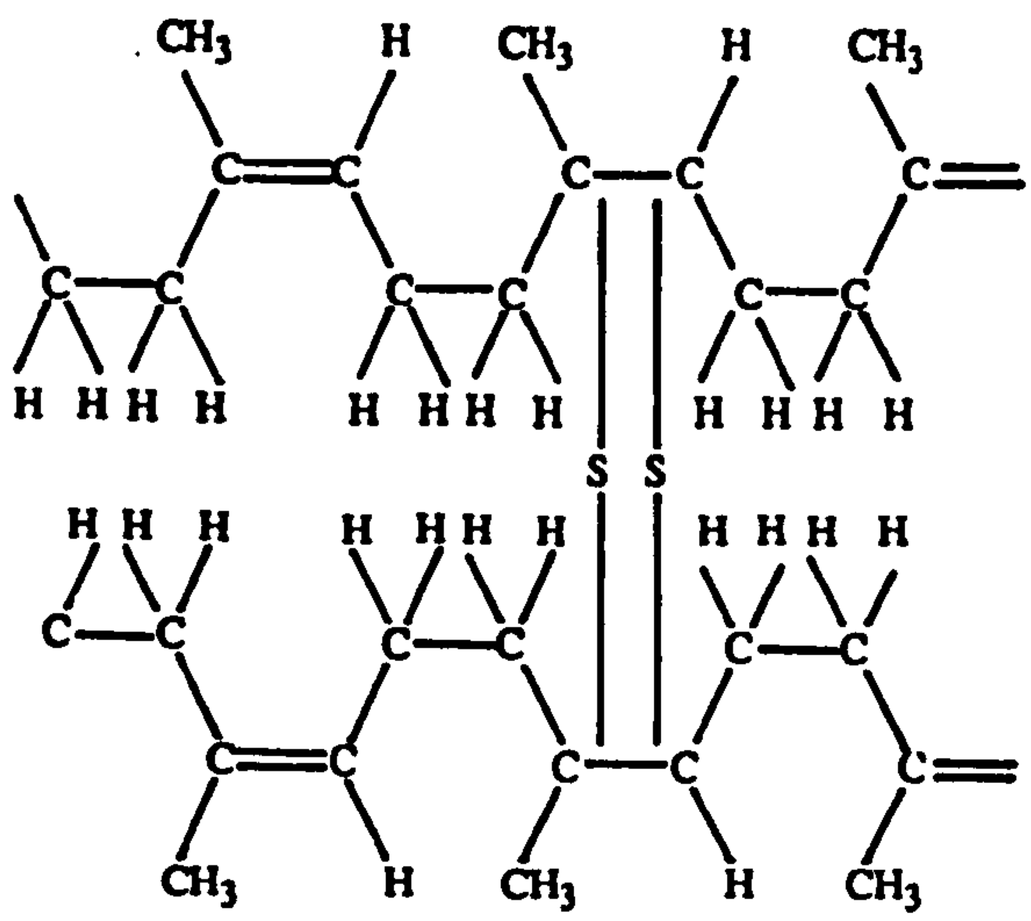

Figure 3.3: Structure of vulcanised rubber (Courtesy: Bolton W, 1989)

During vulcanisation, the long chain molecules of rubber are chemically linked, usually by sulphur, at intervals along their lengths with adjacent rubber chains. The type of crosslink produced depends upon the curing conditions (time and temperature) as well as the amount and type of vulcanising ingredients in the compound. The chemical nature of the various types of crosslinks influences the properties of the rubber.

The most widely used vulcanising agent is sulphur.(Figure 3.4a). Crosslinking with sulphur alone is quite inefficient and requires curing times of several hours.[3.4] For

every crosslink, 40-55 sulphur atoms are combined with the rubber. The structure contains polysulfide linkages, dangling sulphur fragments, and cyclic sulphides. Much of the sulphur is not involved in crosslinks between chains. The network is unstable and has poor ageing resistance. By adjusting the sulphur content the number of crosslinks can be controlled; the more crosslinks there are, the stiffer and harder is the rubber. The rubber in a car tyre may contain between 3 and 5 % sulphur; the vulcanised rubber case of a car battery may contain as much as 40% sulphur and is much harder than the rubber in a car tyre.

To increase the rate and efficiency of sulphur crosslinking, accelerators are normally added. [3.4]. These are organic bases. Accelerated sulphur (Figure 3.4b) curing is more efficient when the activators zinc oxide and stearic acid are added. It is thought that these combine to create soluble zinc ions that activate the intermediate reactions involved in crosslink formation. A common instrument used to determine the kinetics of crosslinking is the oscillating disk rheometer.

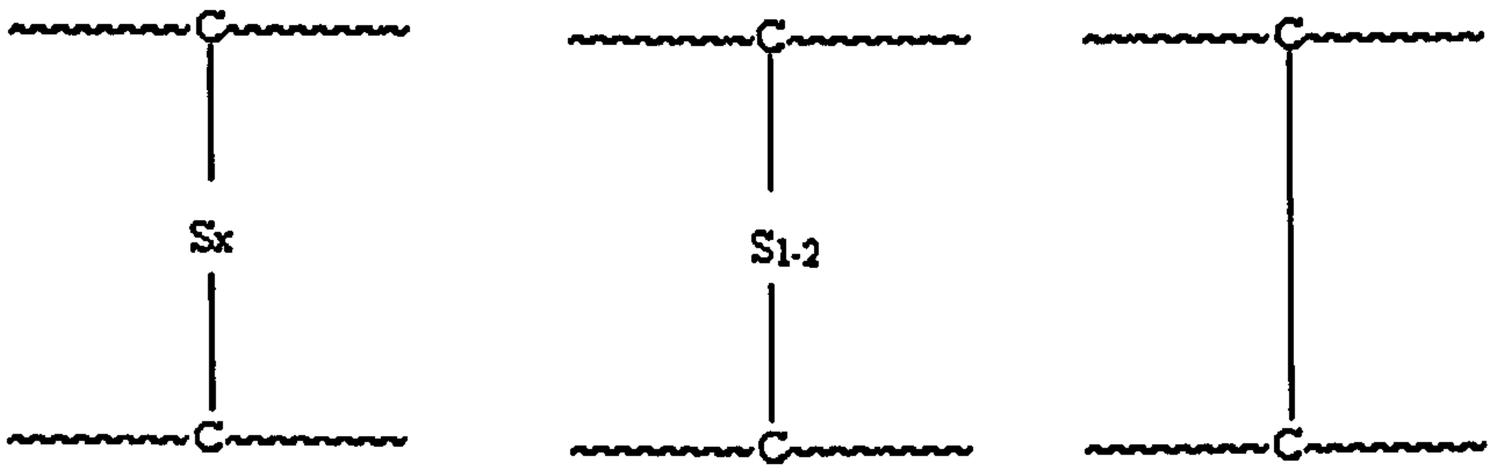

polysulphidic crosslinks (x≥2) conventional accelerated-sulphur vulcanizate (a)

mono and di sulphidic crosslinks (b)

carbon-carbon crosslinks (c)

Figure 3.4 Various types of crosslinks used in rubber compounding

Peroxides are another type of curing agent for elastomers. (Figure 3.4c). Unlike sulphur curing, double bonds are not required for peroxide vulcanisation, and thus, they may be used to crosslink saturated rubbers like silicone rubber. Peroxide curing occurs by a free radical mechanism and leads to carbon-carbon crosslinks, which are quite stable and result in vulcanizates with good ageing and compression set resistance.[3.4].

3.3.3 Reinforcement

Particulate fillers can increase the strength of an amorphous rubber more than 10 fold. For a filler to cause significant reinforcement, it must possess high specific surface area; that is, the particles must be small (≤1μm). Small particles have large surface area to interact with the rubber and diminished particle-to-particle distance. Two types of filler that have been the most effective for reinforcing rubber are carbon black and silica. To be effective, filler particles must be well dispersed. This requires mixing in a high shear field and at an elevated temperature. The viscosity of rubber must not be too low, or shear stresses will be insufficient to break apart filler agglomerates. Thus, when oil is to be added to a stock, it is added toward the end of the mixing cycle-after the carbon black has already been incorporated and dispersed.

3.3.4 Antidegradants

Oxygen and ozone can react with elastomers and alter network structure by causing chain scission and/or crosslinking. If chain scission dominates, the elastomer softens and eventually may become sticky with ageing. Most elastomers, however, harden and eventually embrittle during oxidation- a consequence of crosslinking dominance. Even when present in the atmosphere at only a few parts per hundred million, ozone readily cleaves carbon-carbon double bonds in elastomers. An unsaturated vulcanizate that has been strained and exposed to ozone quickly develops cracks. The severity of cracking increases rapidly with strain. Antioxidants and antiozonants, which can function chemically or physically, have been developed to inhibit the action of these degradants. Paraphenylenediamines (PPD) are effective in "diene" rubber to reduce ozone cracking. Organic phosphites are preventive antioxidants and are nonstraining.

3.3.5 Other additives

Rubbers almost invariably contain not only a polymeric material, but also additives. Other than fillers and antidegradants, the other additives used are:

1. Plasticizers to enable molecular chains to slide more easily past each other, hence making the material more flexible.

2. Stabilisers to enable the material to resist degradation better.

3. Flame retardants to improve the fire resistance properties.

4. Lubricants and heat stabilisers to assist the processing of the material.

5. Pigments and dyes to give colour to the material.

3.3.6 The mixing and shaping processes

Figure 3.5 shows the cumulative steps of manufacture which determine the product performance. All rubber product manufacture begins with a mixing process, and the behaviour of a rubber compound, both in the downstream processes and in the final product is influenced strongly by the treatment it receives in this process. Rubber mixing is dominated by batch processes, so there is an opportunity to vary the mixing treatment over a wide range through the manipulation of operational variables, in contrast to continuous mixing, where the mixing treatment is much more strongly influenced by the mixer geometry. This gives the processor the essential capability of mixing a wide range of compounds with a single mixing system.[3.5]

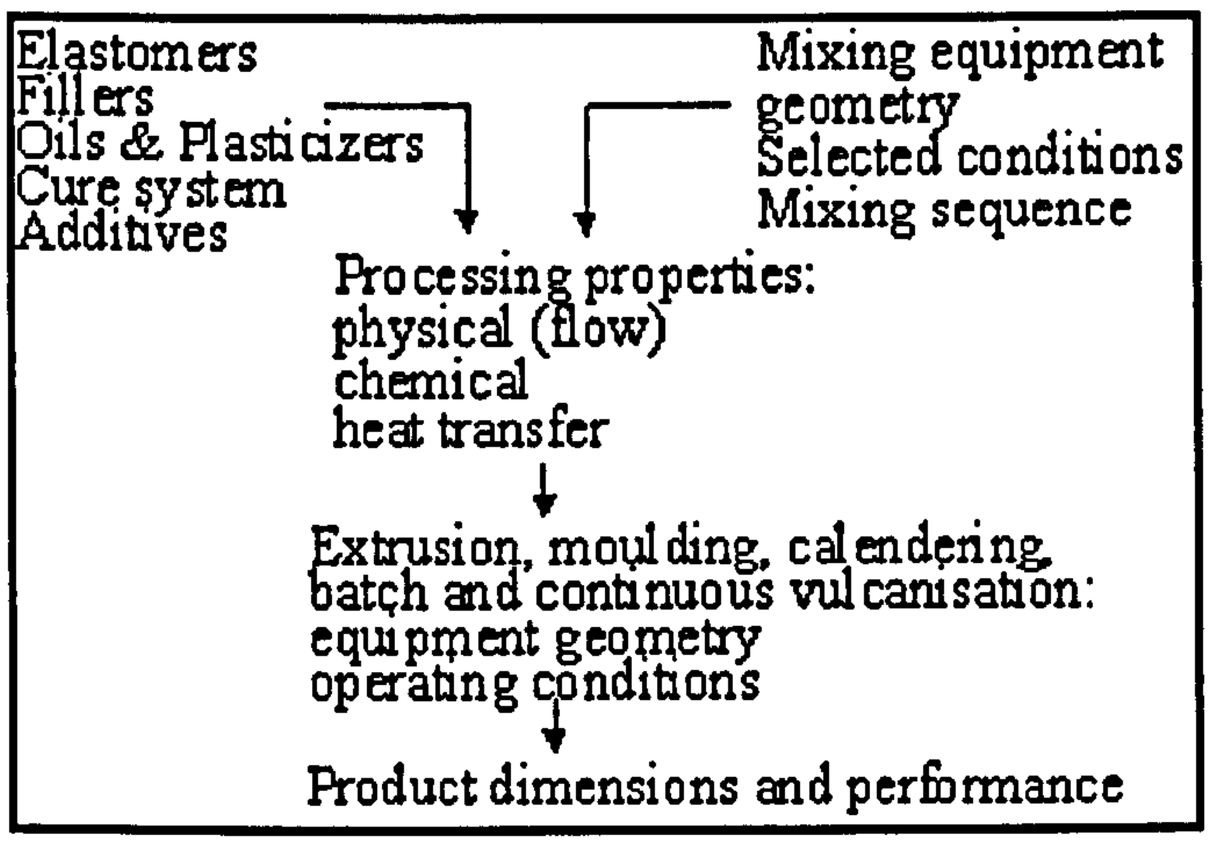

Figure 3.5: The cumulative steps of rubber manufacture

Rubber compounding is generally carried out on open mills or in internal mixers. An open mill (Figure 3.6) consists of two adjacent, smooth, hardened-steel rolls set horizontally. They rotate in horizontal directions, toward each other. Mixing is achieved by the shearing action induced in the space between the rolls, which is adjustable. The mixing process on an open mill involves masticating or breaking down the crude rubber until an even and smooth band is formed around the front roll. When the crude rubber becomes soft and plastic, the fillers and other ingredients are added and worked in, following a definite time, temperature range and sequence schedule. During the mixing

operation, cutting and blending is carried out in order to obtain a thorough and uniform dispersion of the ingredients in the rubber mix.[3.2]

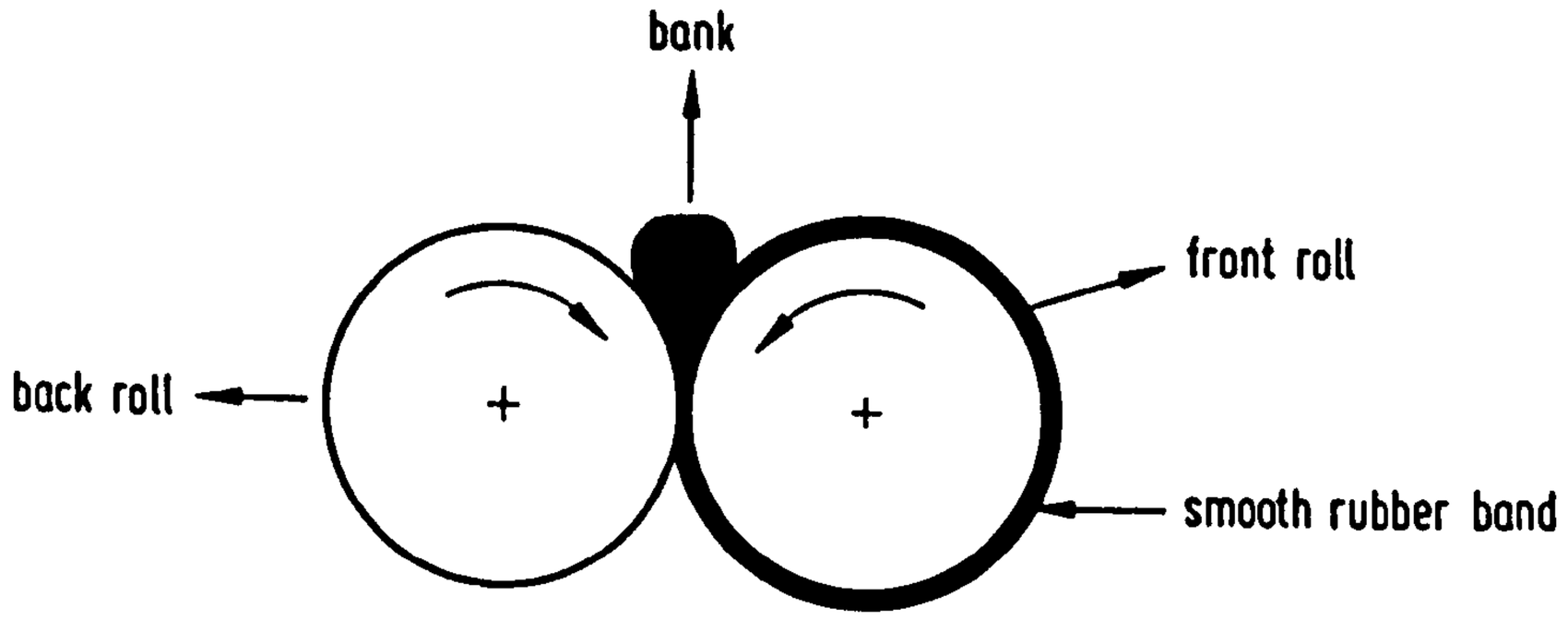

Figure 3.6: Open mill (Courtesy Nagdi K, 1993)

An internal mixer consists of an enclosed chamber and two rotors with small clearance between them and the enclosing wall (Figure 3.7). As with the open mill, the rotors rotate in opposite directions. The mixed batch is dropped from the bottom of the internal mixer onto a sheeting mill and then taken off for storage until further processing.

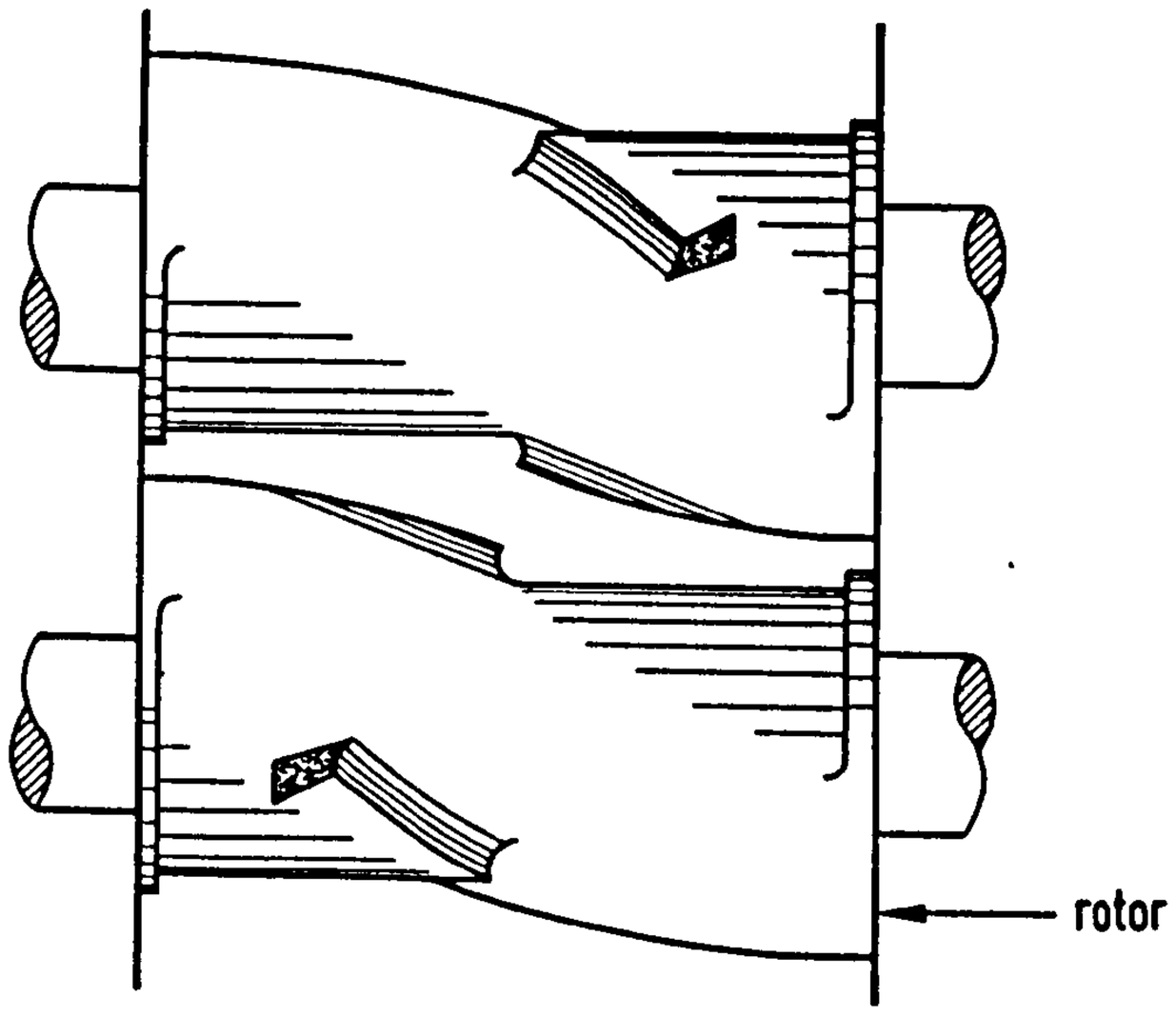

Figure 3.7: Internal mixer (Courtesy Nagdi K, 1993)

After mixing, the green stock requires shaping (forming) into blanks of suitable dimensions. At this stage the stock will retain the shape imposed on it because it is predominantly plastic. The basic processing machines used for forming rubber stocks are the *calenders* and *extruders*. The calender is used essentially for producing rubber sheets of various lengths and thickness. An extruder is used for continuous shaping of a material by passage through an orifice called a die. The stock is fed in at one end and the material becomes hot and plastic as it moves to the exit end of the extruder. It is then pushed through a die having the desired shape. Extrusion is generally used for manufacturing products such as rubber tubes, insulated cables and weather sealing strips.

For process monitoring, quality control and optimisation of rubber manufacture, the multivariable nature of rubber compounds and rubber processes has prompted the adoption of statistical experiment design and optimisation packages by a number of companies.

3.4 PHYSICAL PROPERTIES OF RUBBER AND HENCE THE SENSING BEAM OF THE FLOW SENSOR

3.4.1 Young's Modulus of the rubber beam of the flow sensor

Vulcanised rubber is a solid, three-dimensional network. The more crosslinks there are in the network the greater is the resistance to deformation when a force is applied. Certain fillers, notably the reinforcing blacks, create a structure within the rubber which further resists deformation.

The load versus deflection curves for rubber in tension and compression are approximately linear for strains of the order of a few percent, and values of Young's modulus can be obtained from these linear regions. The tensile test serves as the basis for determining several important mechanical properties of materials. In this test, the yield strength, tensile strength, elongation, modulus of resilience, modulus of toughness and modulus of elasticity are determined. In the tensile test, the specimen is loaded in uniaxial tension until the specimen fractures. [3.6]. The specimen is clamped at one end and weights are added on the other: first in an ascending order from 1kg up to 6 kg and then reduced to 1 kg. The change in length and diameter of the rubber beam is noted.

Stress is defined as the applied force, F, per unit original undeformed cross-sectional area (a) of the specimen,

$$\sigma = F/a \qquad (3.2)$$

and strain is

$$\varepsilon = (l - l_o)/l_o \qquad (3.3)$$

where 'l_o' is the length of the beam prior to the application of the load and 'l' is the length of the beam after the load is applied. The stress-strain curve of a material will depend on many factors, such as chemical composition, heat treatment, prior plastic deformation, strain rate and temperature. Because of the difficulty in determining the elastic limit, it is commonly replaced by the proportionality limit, which is the stress at which the stress-strain curve is out of linearity. The modulus of elasticity or the Young's modulus, E, a measure of the stiffness of the material, is the slope of the curve below the proportional limit. (Figure 3.6) Lower the Young's modulus, the less stiffer it is and smaller is the elongation it can withstand.[3.7]

$$E = \frac{stress}{strain} = \frac{\sigma}{\varepsilon} = \frac{F/a}{\Delta l / l} \qquad (3.4)$$

This project made use of rubber beams in the construction of the flow sensors developed during the work. Initially, therefore, experiments were done to determine the value of Young's modulus for the rubber to be used. Figure 3.8 shows the stress-strain characteristic of the rubber cylinder which was used as the sensing beam of the flow sensor developed in this PhD project and described in Chapter 4.4.3. The experiments were performed for both increasing and decreasing load.

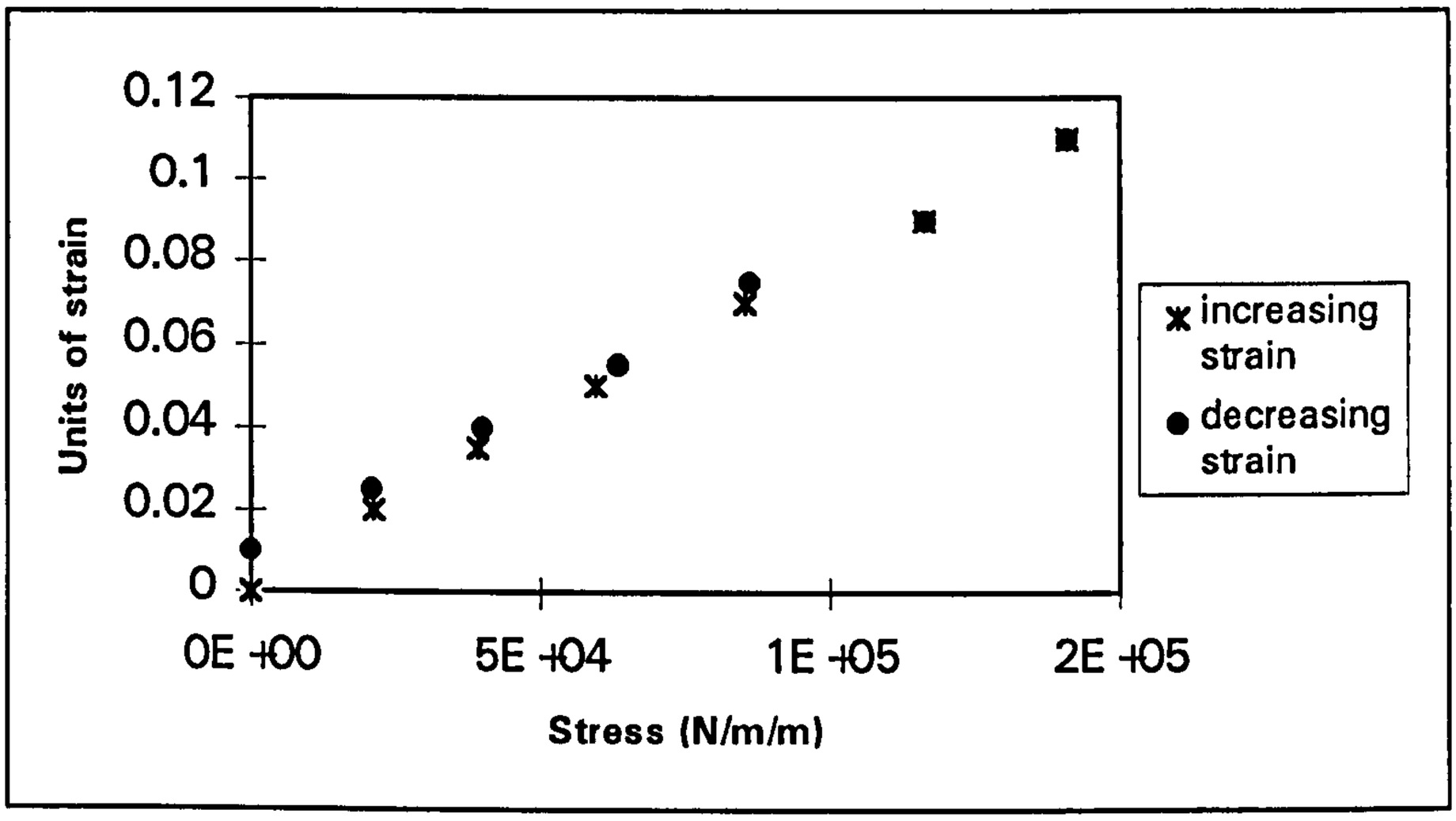

Figure 3.8 : Stress- strain curve for the polybutadiene rubber beam.

From the graph, the modulus of elasticity or the Young's modulus of the sensing beam is found to be 1.2×10^6 N/m^2. As the curves are continuous through the origin, the values of Young's modulus in tension and compression are approximately equal. Two features lead to the increased stiffness of high strains: one is due to the sections of molecules between adjacent crosslinks approaching their limiting extension; the other is strain induced crystallisation which occurs only in a few rubbers, notably natural rubber.

Shear modulus (G) can be obtained in a manner similar to the Young's modulus. The shear modulus is about one-third to one-quarter of the Young's modulus. So for the sensing beam used in this PhD project, the shear modulus is approximately 0.37 MN/m^2.

3.4.2 Incompressibility and its effect on the sensitivity of the flow sensor

One of the important features of rubber is its flexibility, which is given by its bulk modulus. A small bulk modulus usually implies a rubber of low stiffness, which in this case will allow the sensor to achieve a good sensitivity. The bulk modulus of rubber E_∞ (1000-2000 MN/m^2) is many times larger than its Young's modulus and Poisson's ratio (which can be taken as 1/2). The very high bulk modulus means that rubber hardly changes in volume even under high loads, so that for most types of deformation there must be space into which the rubber can deform. The more restriction that is made on its freedom to deform, the stiffer it will become. This is a feature used in the design of compression springs and should be avoided for this sensor. The bulk modulus of the

rubber used for the flow sensor described in this PhD thesis is 1000 MN/m^2, which is about the lowest possible value for rubbers, indicating a sensor with maximised sensitivity to force exerted by the fluid flow.

3.4.3 Strength of rubber and its effect on the dynamic range of the flow sensor.

The breaking stress of rubber in tension is about 14-28 MN/m^2 when calculated on the original cross-sectional area. When calculated on the cross-section at break, the breaking stress may be as high as 200 MN/m^2 which is only a factor of five or so below the corresponding value for steel. A stress well in excess of 160 MN/m^2 is required to cause the failure of rubber in compression. This indicates that the sensing beam of the flow sensor, when made of rubber, can withstand very high wind speeds without the failure of the rubber. This enables the dynamic range of the flow sensor to be extended to a very high value.

3.4.4 Hardness

Hardness measurements are generally used to characterise vulcanised rubbers. For rubber, hardness is essentially a measurement of the reversible, elastic deformation produced by a specially shaped indentor under a specified load and is therefore related to the Young's modulus of the rubber, unlike metal hardness which is a measure of an irreversible, plastic indentation. The unit of the hardness values are given as International Rubber hardness degrees (IRHD) or the British standard Hardness degrees (^{0}BS). The hardness of the rubber used as the sensing beam can be found in relation to its Young's modulus and is 35 ± 2 IRHD.

3.4.5 Hysteresis

Hysteresis, which is the work represented by the area between the loading and unloading curves in a load deformation cycle, occurs with all rubbers. For natural rubber containing no filler there is little hysteresis up to moderate extensions; fillers increase hysteresis. At high extensions, not normally used in practical applications, the hysteresis is much greater. This is associated with the crystallisation taking place on extension and is responsible for the high strength of natural rubber. Therefore, although the high strength of rubber indicates a flow sensor with a wide dynamic range, there is likely to be an increase in hysteresis if the dynamic range is extended without calibration. Tests for

hysteresis of the flow sensor have indicated negligible hysteresis up to a wind speed of about 35 m/s.

3.4.6 Effects of environment on rubber and the flow sensor

It is necessary to discuss the effect of the environment on rubber since the major application area of the flow sensors developed in this PhD project is environmental fluid flow monitoring. Various changes can occur in a rubber component as a result of the conditions under which it is used or stored. If the conditions are too severe the rubber may rapidly become unserviceable; conversely it could last indefinitely under less arduous conditions. The ways in which different conditions can affect natural rubber are described briefly below; in many cases the effects of the changes can be eliminated, or at least minimised, by suitable compounding. It is emphasised that many of the deleterious conditions referred to are not encountered in general engineering applications and especially not in flow measurement.

The physical properties of rubbers are generally temperature dependent, and are also reversible with temperature provided no chemical changes occur in the rubber. However, like many other organic materials, rubber is prone to degradation by oxygen particularly at *high temperatures*. At service temperatures approaching those used for vulcanisation (about 140^0C), further vulcanisation may occur resulting in increased hardness and decreased mechanical strength. Conventional rubber compounds can be used at the maximum temperatures (60^0C) likely to be encountered in practice, but with special compounding natural rubber can be used for many months up to 100^0C and intermittently even higher. At very high temperatures (350^0C and above) rubber first softens as molecular breakdown occurs then resinifies, becoming hard and brittle. When maintained at *low temperatures* certain rubbers may crystallise, and this results in a progressive stiffening and loss of elasticity. Natural rubber takes many days to crystallise at around -25^0C, and increasingly longer at higher or lower temperatures. Crystallisation disappears rapidly as the temperature is increased. Low temperature crystallisation is not generally a serious practical problem in natural rubber. Since the flow sensor that has been developed is an environmental sensor, such extreme temperatures may not be encountered by it but in applications where this could be a problem, the necessary precautions will be taken.

The effect of oxygen and ozone on rubber have already been considered in Section 3.3.4. Rubbers are protected against this degradation by adding antidegradants.

Light coloured rubbers, when exposed to sunlight, are susceptible to the oxidation initiated by the ultra-violet radiation, and their surfaces are rapidly degraded to give a crazed resinous skin. Although the need for light coloured rubbers is rare in engineering applications, a reasonable measure of protection can be achieved with a ultra-violet absorber and a suitable antioxidant. Carbon black fillers which is incorporated in most engineering rubbers provides additional and effective protection by shutting out the ultra-violet radiation.

Swelling in liquids is another problem which is encountered by rubber. If a rubber absorbs a large volume of liquid it will become weak and useless for almost every conceivable engineering application. There is, however, a limit to the amount of liquid that can be absorbed by different rubbers, and it is this equilibrium swelling which is the conventional measure of swelling resistance. All rubbers are resistant to some liquids, although there is no one rubber which is resistance to swelling by all liquids. Natural rubber is swollen to a negligible extent by water and is swollen very little by acetone, alcohol and vegetable oils such as castor oil. Most rubbers are swollen by degreasing solvents but the 'oil-resistant' rubbers, as the name implies, are only slightly swollen by lubricating oil.

The swelling of rubber by liquids is a diffusion controlled process and, up to the equilibrium swelling ratio, the volume of liquid absorbed is proportional to the square root of the time for which the rubber has been immersed in the liquid. For most organic liquids the rate of penetration depends upon the viscosity of the swelling liquid rather than on its chemical nature. Thus the time to penetrate 5 mm is about four days for a mobile liquid like benzene, one to two years for an engine lubricating oil, and about thirty years for a thick grease such as Vaseline (Figure 3.9). When the need for oil measurement using this flow sensor arises, adequate protection for the rubber sensing beam against oil splashes can normally be obtained by a suitable shield or by coating with an oil resistant paint. Section 3.2.4 gives an account of the different kinds of rubbers available for measuring different fluids.

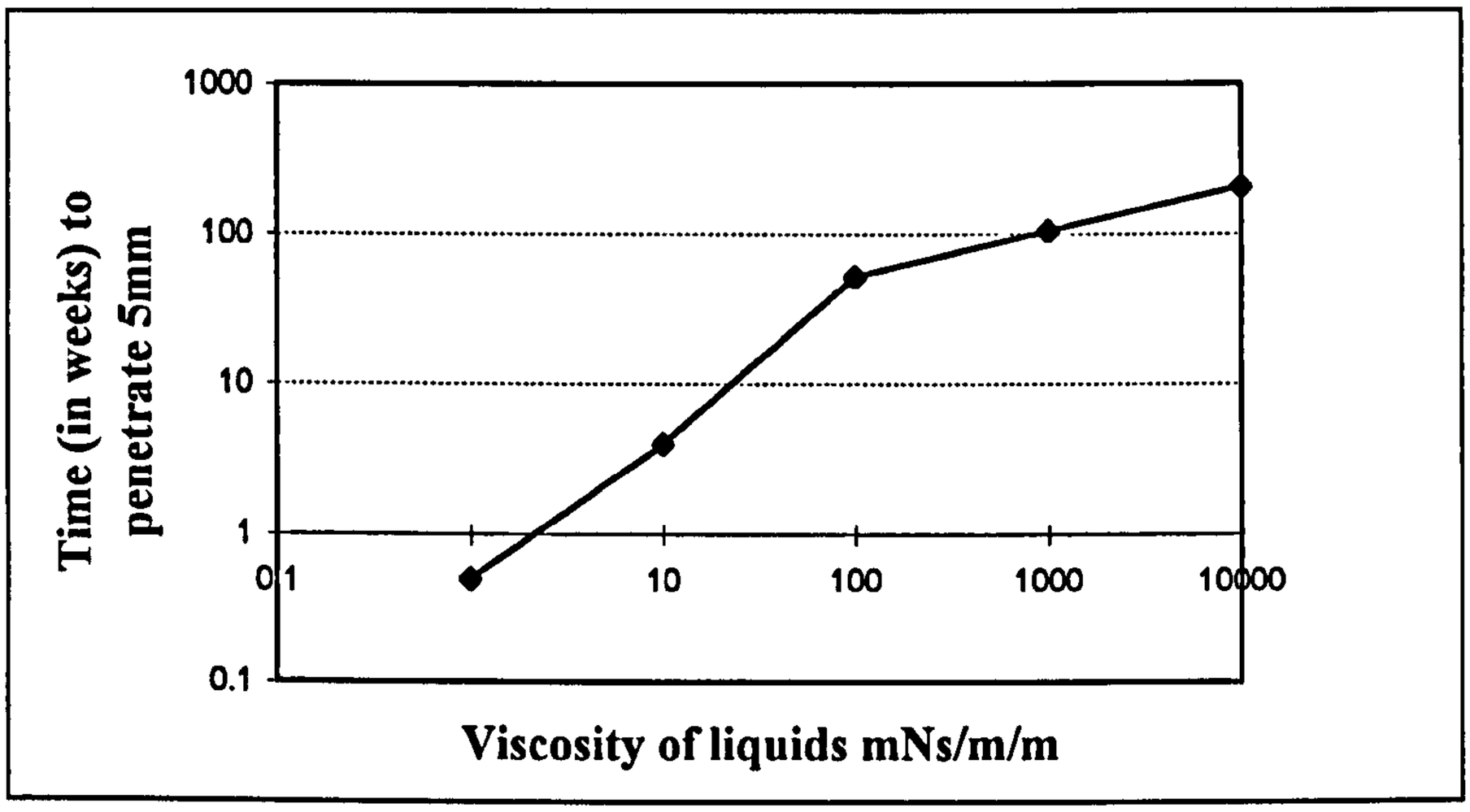

Figure 3.9: The time taken by a liquid to penetrate a given distance into rubber depends on its viscosity. The curve shows the time taken to penetrate 5 mm into natural rubber; it would take four times as long to penetrate 1 cm. (Courtesy Lindley P.B)

Degradation by chemicals other than oxygen and ozone is unlikely to be a serious consideration in most engineering applications of rubber. Rubber is resistant to most inorganic acids, salts and alkalis (with the exception of concentrated sulphuric acid, the halogens and strong oxidising agents such as nitric and chromic acids) and is widely used for the linings of tanks and chemical baths, especially those containing caustic solutions.

3.5 HOW TO ENSURE THE EFFECTIVENESS OF RUBBER AS A SENSING BEAM MATERIAL

Having considered the way rubber is compounded and its physical properties, some of the noteworthy points which was requested and used by the Malaysian Rubber company during the design of the rubber used for the sensing beam were as follows:

- The use of the right type of curing agent and accelerator to ensure proper vulcanisation of the rubber

- Addition of fillers to increase the strength of rubber.

- Use of the appropriate antidegradant to prevent cracking under strain and reducing/eliminating the oxidation of the rubber by heat, ultraviolet light and some metals such as copper, cobalt and manganese. This increases the longevity of elastomers in air. There is evidence that rubber can survive very long periods (14-

year trials of longevity at an outdoor weathering site in Panama [3.8]) in service at ambient temperatures up to at least 30^0C without any measurable deterioration.

- Introduction of liquids between chains. The addition of liquids, termed plasticizers, which fill some of the space between polymer chains makes it easier for the chains to move and increases flexibility.

- Ensuring that the shaping process is completed before the onset of crosslinking, but at the same time ensuring that crosslinking would then proceed as quickly as possible. This is done for the efficient manufacture of the rubber.

- From elasticity theory and incompressible fluid dynamics it has been shown [Chapter 4] that the extension or compression (ε) at the surface of the beam at its longitudinal centre is given by

$$\varepsilon = (3\rho V^2 S C_D L) / 2 a^2 b E \qquad (3.5)$$

where ρ is the fluid density, V is the fluid speed, S is the area of drag element, C_D is the drag coefficient, L is the longitudinal length of beam, E is the Young's modulus, a is the beam thickness, and b is the beam width. Putting in typical figures, for a beam 100 mm x $(10mm)^2$ and modulus of 5×10^6 N/m^2, and a drag element 10 cm^2 with drag coefficient of 1.0, an air flow of 10 m/s would give a strain of 0.04 or 4%, which is about the largest strain which can be used with polymide/nichrome strain gauges. As the best value of the Young's modulus was found to be 5 MN/m^2 a rubber cylinder having a value for Young's modulus close to this value was requested from the Malaysian Rubber Company.

- This flow sensor was used in the wind tunnel to measure air flow. If this sensor is required to measure water and other liquids, the necessary precautions should be taken to protect the rubber beam against their effects and to utilise the appropriate polymer which is chemically resistive to the fluid being measured as discussed earlier in this chapter.

CHAPTER 4

THE ELECTRICAL STRAIN GAUGE TARGET FLOW SENSOR

A novel technique for the measurement of fluid flow velocity is discussed in this chapter. The operation is based on strain measurement of deformation of an elastic rubber cantilever. Strain is measured using the conventional electrical strain gauges which have been in the market for the last five decades. Extensive research have resulted in strain gauges having excellent performance characteristics. This has led to the electrical strain gauge (Chapter 2) becoming the basic sensing element of several load transducers and in this project has been used to sense the deflection of a rubber cantilever due to force exerted by fluid flow.

This chapter describes the design, optimisation and calibration of the original research work undertaken to develop a target flow sensor (reviewed in Chapter 1) to measure one and two dimensional air flow, which in turn enables the determination of the speed and direction of wind velocity. The results of the experiments performed in a wind tunnel and preliminary experiments in a water tank to measure one dimensional water speed are presented here. Rubber has been chosen as the sensing beam material (Chapter 3) as the rubber formulations offer the most useful range of moduli and there are different types available for the various fluids and the different temperature ranges. A major advantage of this flow sensor is that it can be calibrated in a safe and easy-to-handle fluid like water and then be optimised for hazardous applications, where a calibration with the actual fluid may not be possible. Therefore, these design features enable this target flow sensor to handle wide temperature ranges and be compatible with almost any fluid.

4.1 PRINCIPLE OF OPERATION OF THE FLOW SENSOR

4.1.1 Principle of one dimensional fluid flow measurement

The drag equation from incompressible fluid dynamics is:

$$F_D = \frac{C_D \ \rho A V^2}{2} \qquad (4.1)$$

where ρ is the fluid density, V is the fluid's velocity at the point of measurement, A is the projected area of the body normal to the flow, C_D is the overall drag coefficient, a dimensionless factor; its magnitude depends primarily on the physical shape of the object and its orientation relative to the fluid stream.

From the **theory of elasticity** [4.1], for *a cantilever beam of length L with a point load at end,* shown in Figure 4.0, the mass of the beam can be ignored, since the beam in practice will be vertical.

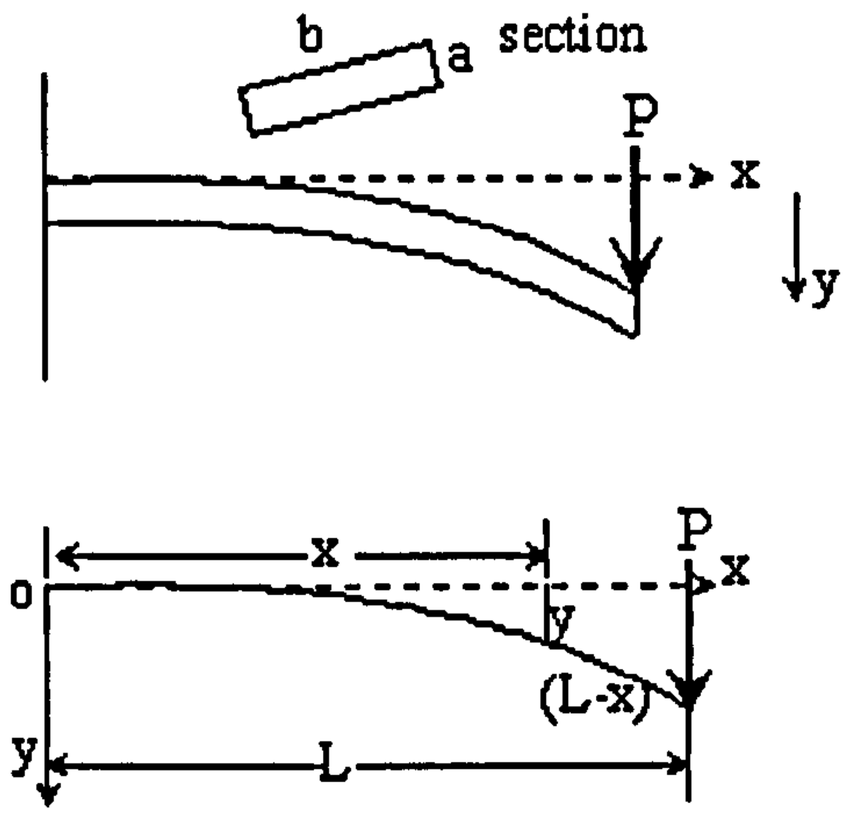

Figure 4.0: The bent cantilever

The shear force (P) will be constant along the beam. The bending moment, M will be P(L-x) so that it varies linearly from PL at x = 0 to 0 at x = L, where x is the linear displacement along the beam.

The distance 'y' is measured from the neutral plane, which for a rectangular section is the mid-plane.

$$\text{The radius of curvature} = \frac{1}{\rho} = \frac{M}{EI} \qquad (4.2)$$

where E is the modulus of elasticity or the Young's modulus and I is the moment of Inertia of the cross section where it is assumed that the force is applied perpendicular to the broad face of width 'b'.

$$I = \frac{b\,a^3}{12} \qquad (4.3)$$

Through the thickness 'a' of the beam, the strain is ε_x.

$$\varepsilon_x = \frac{\sigma_x}{E} = \frac{y}{\rho} \tag{4.4}$$

Substituting Equation (4.2) in Equation (4.4) gives:

$$\varepsilon_x = \frac{y\,M}{E\,I} \tag{4.5}$$

The strain at the surfaces is

$$\varepsilon_x = \frac{a}{2\,\rho} = \frac{a\,M}{2\,E\,I} \tag{4.6}$$

Substituting Equation (4.3) in Equation (4.6) gives:

$$\varepsilon_x = \frac{a\,P\,(L-x)\,12}{2\,E\,b\,a^3}$$

$$\varepsilon_x = \frac{6\,P\,(L-x)}{E\,a^2\,b} \tag{4.7}$$

or the shear force P is

$$P = \frac{\varepsilon\,E\,a^2\,b}{6\ (L-x)} \tag{4.8}$$

From Dimensional analysis[1], we observe that equations (4.1) and (4.8) can be equated.

$$\frac{C_D\ \rho\,A\,V^2}{2} = \frac{\varepsilon\,E\,a^2\,b}{6\ (L-x)}$$

Therefore, the strain

$$\varepsilon = \frac{3C_D\rho\,A\,V^2\,(L-x)}{E\,a^2 b} \tag{4.9}$$

---

[1] Dimensional analysis for Equation (4.1):

$$F_D = \frac{kg}{m_3} * \frac{m^2}{\sec^2} * m^2 = \frac{kg\,m}{\sec^2} = N$$

Dimensional analysis for Equation (4.8):

$$P = \frac{1 * N\,m^{-2}\,m^2\,m}{6\,m} = N$$

From Equation (4.9), it can be seen that the *strain is a square law function of fluid speed.* This was the fundamental equation that was used to relate the fluid speed with the output of the target flow sensor that was developed in this PhD project.

4.1.2. Principle of two dimensional fluid flow measurement

In order to determine the two dimensional fluid flow to measure the magnitude and direction of the fluid velocity, it is necessary to relate fluid speed to strain measured in two orthogonal directions. The fluid speed, U has orthogonal components U_x and U_y which are related to $strain_x$ and $strain_y$ respectively. Since fluid speed is proportional to the square root of strain, according to Equation 4.9, $U_x \alpha \sqrt{strain_x}$ and $U_y \alpha \sqrt{strain_y}$, and hence the magnitude, $|U|$, of fluid velocity is:

$$|U| = \sqrt{U_x^2 + U_y^2}$$

thus $$|U| \alpha \sqrt{Strain_x + Strain_y} \qquad (4.10)$$

Therefore, magnitude of the fluid velocity, $|U|$, is proportional to the square root of the sum of the orthogonal strain components, $strain_x$ and $strain_y$. The fluid velocity direction, θ, is calculated using the relation

$$\theta = Tan^{-1}\left[\frac{\sqrt{Strain_y}}{\sqrt{Strain_x}}\right] \qquad (4.11)$$

4.2. ONE DIMENSIONAL AIRFLOW MEASUREMENT

4.2.1. Sensor design

The sensor was developed by bonding two R-S 308-102 strain gauges on to the opposite sides of a square sectioned elastic rubber beam supplied by the Malaysian Rubber company using the strain gauge techniques described in Chapter 2. Initial experimental work used a digital strain indicator to measure the strain. It was a ten input unit which could be used for quarter, half, or full bridge inputs. Reading is given directly in microstrain (which is a strain of 1 part in 10^6 i.e. an elongation of 1 μm in 1 m). The front panel gauge factor dial had values to cover the range of gauge factors likely to be encountered in use, but gauge factors outside this range could easily be accommodated

by setting the gauge factor to 2.00 and calculating the strain. A precision two stage zero adjustment was provided for each channel ensuring ease of zero setting together with ease of re-setting for subsequent tests. An analogue output was provided on the rear panel for connection to a C.R.O. The bridge circuits were energised from an internal source supplying 2 volts, 5 volts or 10 volts DC. The internal circuit of the strain meter is shown in Figure 4.1a.

The strain gauge was connected at the rear of the instrument in the half bridge configuration with an external dummy arm. The connections were as follows: supply positive to P1, supply negative to P2, gauge junction to S1, link P1 to P3 and P2 to P4 and gauge factor set to 2.00. The active gauge was connected between terminal P1 and S1 and the external dummy arm between S1 and P2. P1 was linked to P3 and P2 to P4 on the rear panel (Figure 4.1b) The bridge voltage was set to 2 volts.

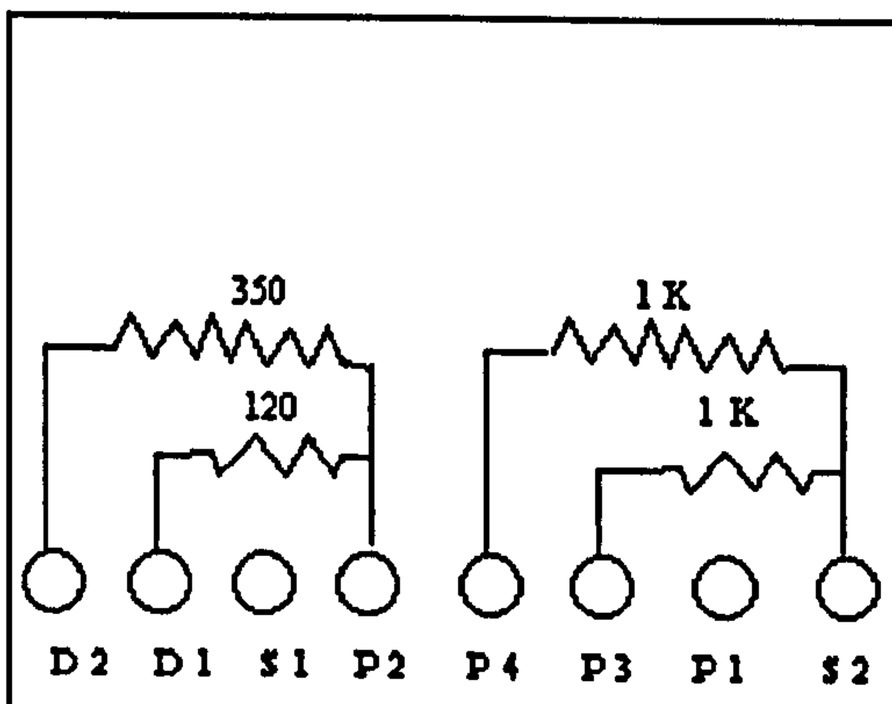

Figure 4.1a: Internal circuit: Digital strain meter

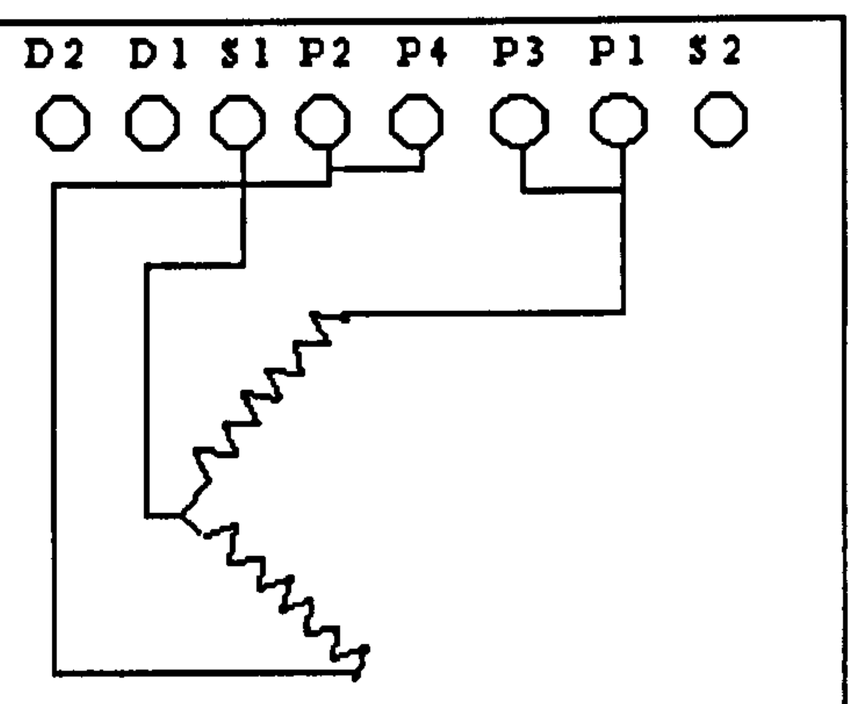

Figure 4.1b: Half Bridge: Digital strain meter

4.2.2. Experiments in the wind tunnel

The sensor was mounted in a 460 x 460 mm closed circuit wind tunnel, with a maximum fan speed of 1700 revolutions per minute (rpm). The airflow was calibrated in m/s, as a function of fan speed in rpm using an anemometer and stop watch. The flow sensor was mounted in such a way that one gauge underwent compression and the other gauge underwent an expansion as shown in Figure 4.3. The wind speed was set at different values and the corresponding microstrain readings from the digital strain indicator were noted.

Table 4.1: Strain meter readings for one dimensional air flow measurement

Fan speed (rpm)	**Wind speed (m/s)**	**microstrain**	**$\sqrt{\text{microstrain}}$ root strain**
0	0	0000	0
100	1	0012	0.0035
200	4	0049	0.007
300	7	0140	0.0118
400	11	0262	0.0161
500	14	0402	0.02
600	17	0580	0.024
700	20	0865	0.029
800	23	1099	0.033
900	26	1291	0.035
1000	29	1535	0.039
1100	32	1843	0.042
1200	35	2159	0.046
1300	38	2448	0.049
1400	41	2700	0.051
1500	44	2990	0.054
1600	47	3200	0.056
1700	50	3346	0.057

Table 4.1 gives the different readings obtained. A graph of wind speed versus square root of the microstrain (referred to as 'root strain') was plotted. (Figure 4.2). 'Root strain', is a dimensionless unit that has been defined in this thesis and it refers to $\sqrt{\text{strain}}$ for one dimensional flow measurement and to $\sqrt{\text{strain}_x + \text{strain}_y}$ for two dimensional flow measurement.

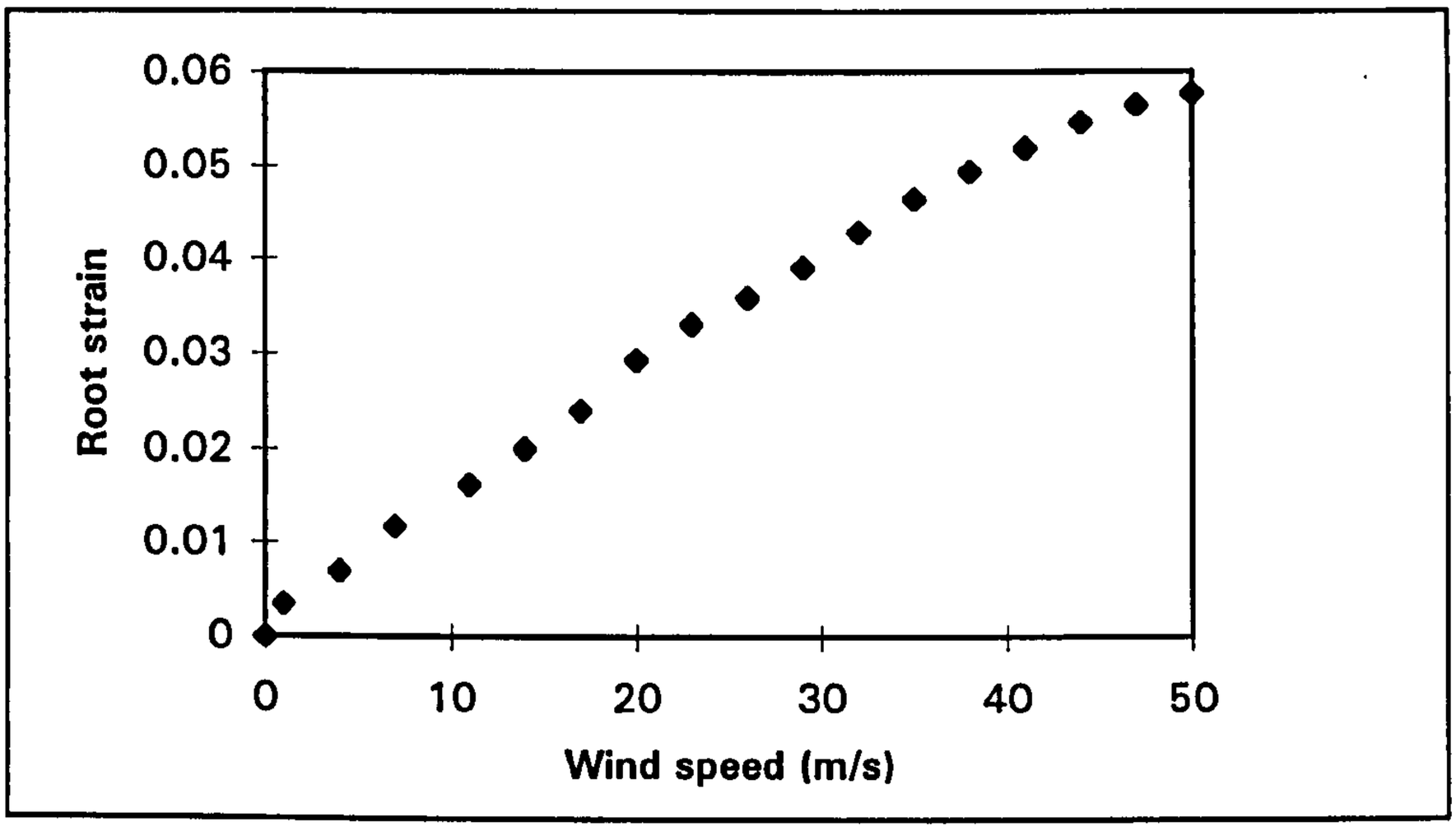

Figure 4.2: Root strain vs. wind speed for one dimensional air flow measurement

The plot was linear with a correlation co-efficient of 0.989, indicating a linearity of 1.1%. [2.4: pp 973]. The linearity indicated that the strain is a square-law function of speed. The sensor had a sensitivity of 0.0012 root strain / (m /s). The output voltage signal of approximately 2 volts available at the rear BNC socket of the strain meter was connected to a storage oscilloscope and the available dynamic response of this output was stored as waveforms which was then plotted on a X-Y plotter.

4.3. TWO DIMENSIONAL AIR FLOW MEASUREMENT

4.3.1. Design of the Elastic beam

The critical portion of this flowmeter is the elastic rubber beam. There are several relevant facts pertaining to the elastic beam. First, if the strain gauge bridge is positioned on the rubber beam to take advantage of the principal strains, one gauge on the compression side and one on the tension side, an electrical signal is generated that is sensitive only to the general fluid motion down the conduit. Any stresses and strains induced in other directions such as by flow turbulence are not sensed. Second, by nature of the dimensions of the rubber beam and the strain gauge bridge circuitry, pressure induced strains electrically cancel out. The temperature induced strains also tend to cancel. Third, the drag or force generated by flow can be transferred to the rubber beam as a couple (bending moment and force). These moments produce a stress/strain field in the walls of the sensing rubber beam that is uniform and directly proportional to the applied force.

One of the major features of this flowmeter is the capability to handle high-pressure applications with little effect on the output signal. The thickness of the rubber beam determines the maximum operating pressure and the sensitivity, the electrical output for a given force. Material properties will limit the operating pressure. The stress-induced strains from internal pressure will be the same magnitude and positive throughout the rubber beam. Strain gauge bridge theory states that if all four arms of the bridge experience the same strain, the net effect on the output will be zero. For the same reasons, the thermal effects tend to reduce. A change in temperature changes: (a) the resistance of each gauge of the bridge, (b) the gauge factor or the strain sensitivity of each gauge and (c) Young's modulus of the rubber beam. Ideally, as with the pressure effect, the gauge resistance change with temperature is identical for each gauge and should cancel. The net effect is an offset of the bridge voltage, which is termed the bridge zero temperature coefficient. The other two effects (b and c) are combined in the characteristic termed span temperature coefficient.

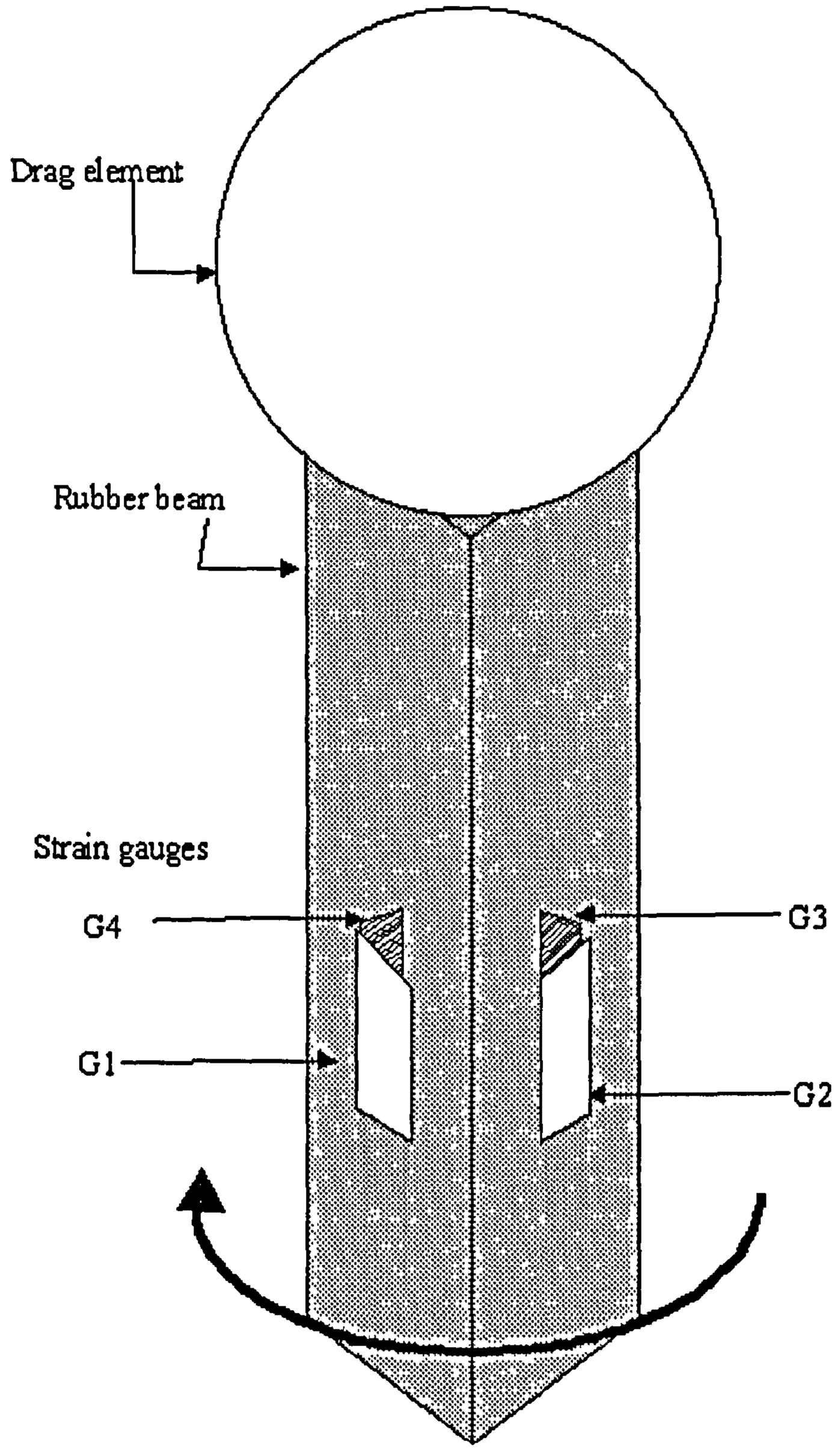

Figure 4.3: Schematic of the electrical strain gauge flow sensor

Ideally, the strain gauge material is chosen so that its gauge factor thermal coefficient is matched to the modulus coefficient.

A square-sectioned rubber beam made of polybutadiene polymer (unfilled vulcanised rubber), 0.165 m long and 0.0135m wide, supplied by the Malaysian rubber company was used as the elastic beam. In the case of the wind speed device, the modulus of the beam will need to be low to achieve good sensitivity. This is why rubber was chosen as the sensing beam material. Further discussion of this was made in Chapter 3. A spherical

drag element of a radius of 0.0202 m was attached to one end of the square section rubber beam. (Figure 4.3).

4.3.2 The force measuring element

Four strain gauges (RS 308-102), whose foil materials are made of copper nickel alloy is attached to the four longitudinal surfaces of the beam. Copper nickel alloy is commonly used in strain gauge construction because the resistance change of the foil is virtually proportional to the applied strain. All gauges have 30mm integral leads to alleviate damage to the gauges due to excessive heat being applied during soldering and installation. The strain gauge is stuck to the rubber beam by a special adhesive layer: the RS 554-850 quick set epoxy.

4.3.2.1 Specifications of the strain gauge used

Measurable strain_____2 to 4% maximum

Thermal output 20 to 160 deg C _____+/-2 microstrain/deg C

160 to 180 deg C_____+/-5 microstrain/deg C

Gauge factor change with temperature_____+/-0.015%/deg C

Gauge resistance_____120 ohms

Temperature change_____-30 deg C to +80 deg C

Gauge length_____8 mm

Gauge width_____2 mm

Gauge factor_____2.1

Base length_____13 mm

Base width_____4 mm

4.3.2.2 Signal conditioning and amplification

The Wheatstone bridge is the sensing circuit utilised to measure the resistance changes produced when active gauges are exposed to strain. The bridge, in effect a dual voltage divider, is powered by a constant voltage source of a few volts dc. It converts very small resistance changes in the gauge into millivolt electrical signals. The half bridge circuit of the Wheatstone bridge is utilised to which the two gauges G1 and G3 (mounted on opposite sides of the rubber beam) are connected on the two arms. Two wire wound resistors R1 and R2 are connected to the other two arms as shown in Figure 4.4. $V_{out} = e$

× V × k / 2 where e is the strain in microstrain, V is the bridge voltage, k is the gauge factor, G1,G2,G3,G4 are the active gauges and R1,R2,R3,R4 are 1kohm 0.1% wirewound resistors. The voltage signal from the Wheatstone bridge is sent to a strain gauge amplifier [RS 308-815] which is a purpose designed hybrid, low noise, low drift, linear dc amplifier in a 24 pin package, specifically configured for resistive bridge measurement. This amplifier overcomes the problem of common mode by removing the common mode voltages.

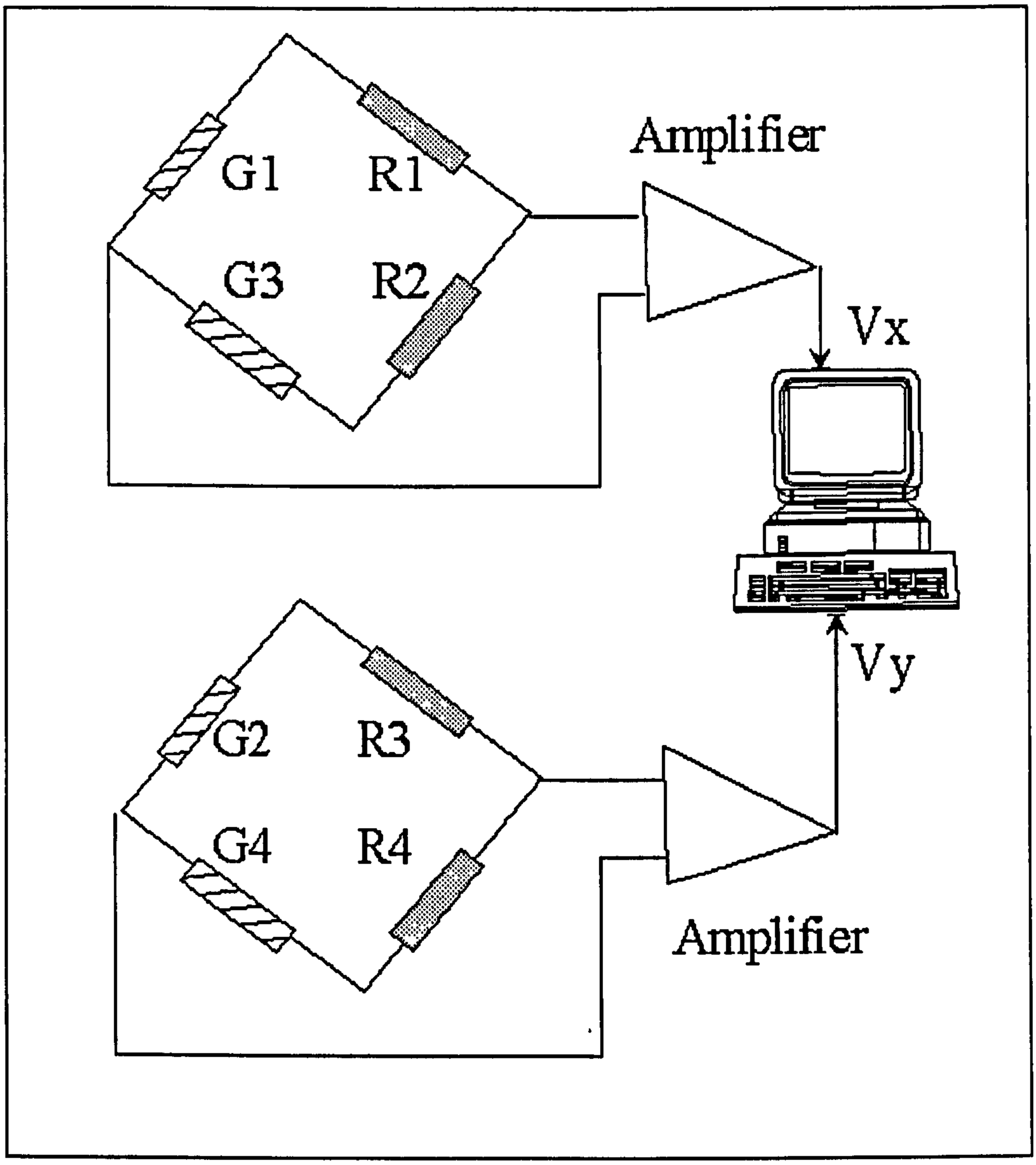

Figure 4.4: Signal conditioning and amplification

This is achieved by controlling the negative bridge supply voltage in such a manner that the voltage at the negative input terminal is always zero. Thus for a symmetrical bridge, a negative bridge supply is generated equal and opposite to the positive bridge supply,

hence zero common mode voltage. The other two gauges G2 and G4 are likewise connected in the half bridge mode of the Wheatstone bridge circuit and to the amplifier.

4.3.3 Data acquisition and analysis

The x and y voltage signals from the two amplifiers are sent to the two channels of a 12 bit data acquisition board Lab PC+ of a 486 DX PC. The acquisition and analysis of data are performed using a general purpose programming system with extensive libraries of functions and subroutines called Labview supplied by National Instruments Corporation.

4.3.3.1 Labview

Labview programs [4.2] are called virtual instruments (VIs) because their appearance and operation imitate actual instruments. However, they are identical to functions from conventional language programs. The VIs have three features which are discussed below:

- The interactive user interface of a VI is called the front panel, because it simulates the panel of a physical instrument. The front panel can contain knobs, push buttons, graphs, and other controls and indicators.
- The VI receives instructions from a block diagram, which is constructed in a graphical programming language called G.
- VIs are hierarchical and modular. They can be used as top level programs, or as subprograms within other programs or subprograms.

4.3.3.2 *Data acquisition*

Two VIs are used to acquire and process the signals from the two channels. The first VI called collect.vi (Figure 4.5) writes the voltage data to a file named *.SCL as it is acquired. This VI uses the double-buffered technique of data acquisition whereby data is continuously acquired into a circular acquisition buffer at the same time that data retrieved from the buffer in each loop iteration is written to file. A file is opened or created, the acquisition initialised, and the number of channels being acquired from is written to the file. The acquisition is then started, and "# of scans to write at a time" scans are read from the acquisition buffer and written to the file in SGL format on each

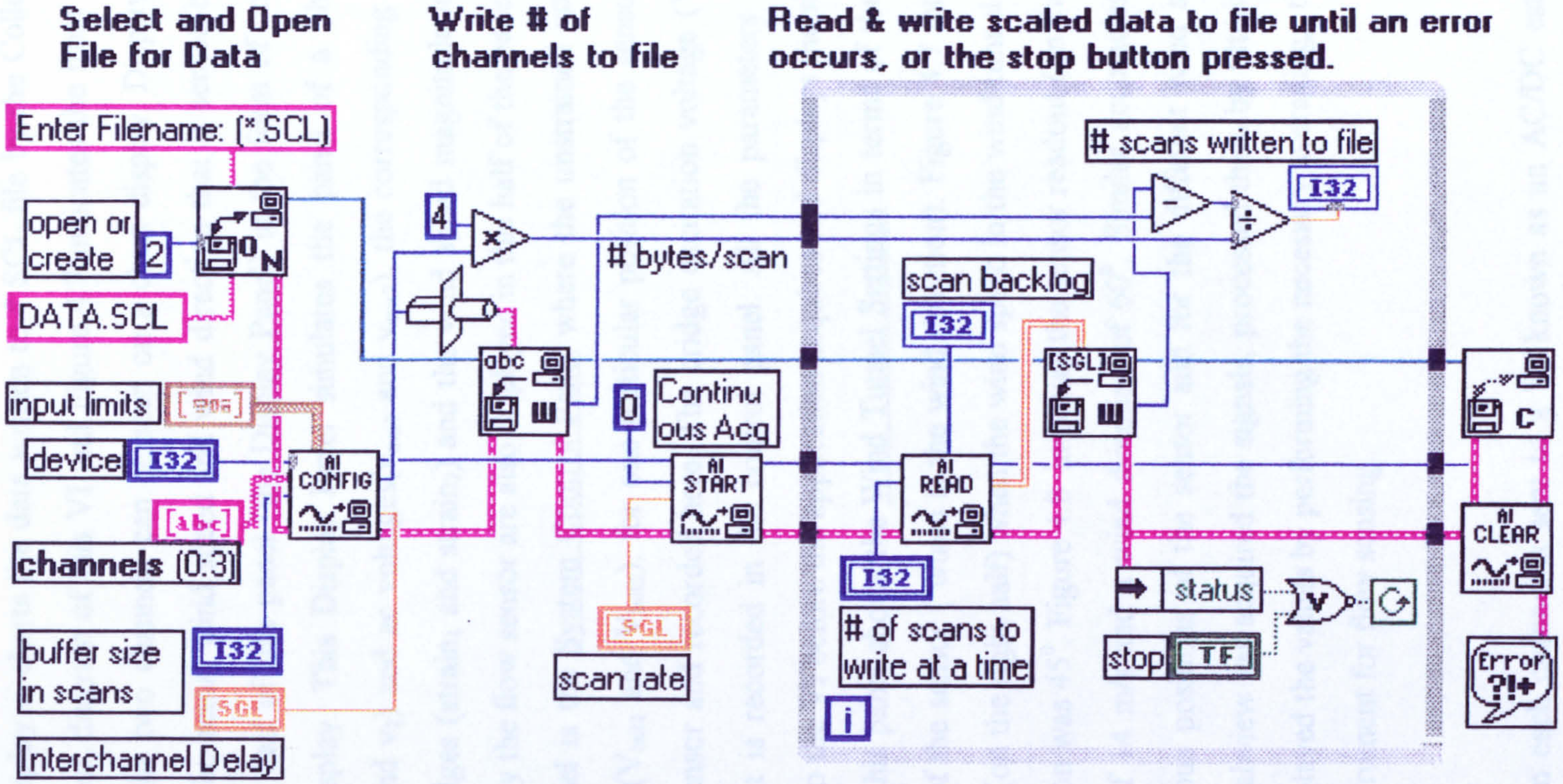

Figure 4.5: Block diagram of the virtual instrument program created with Labview to acquire and store the strain gauge signals.

loop iteration. When the stop button is pressed, the acquisition is stopped and the file closed.

The second VI called Display.vi charts the data written to *.SCL file by the Collect.vi. Figure 4.6 shows the block diagram of this VI and Figure 4.7 indicates the front panel where the signals from the two channels can be seen on a chart display. Display.vi is programmed to display the actual wind speed and wind direction that is sensed by the flow sensor on the right half of this panel (the Display Panel) in the form of both an anologue and digital display. This Display Panel simulates the panel of a physical instrument. The dc (v_1 and v_2) and ac voltages(v_{rms1} and v_{rms2}), the corresponding strain values from the two bridges ($strain_1$ and $strain_2$) and the wind speed magnitude in root strain which are sensed by the flow sensor are also displayed in this half of the panel. The top, left half of this panel is the System Control Panel where the unstrained voltages from both the channels (V_{init1} and V_{init2}), for one particular position of the sensor, are initially read from the sensor and recorded here. The bridge excitation voltage (V_{ex}) is the other parameter that is recorded in the control panel. All the parameters in the control panel are fed into the VI before the application acquires and displays the signals. The bottom left half of this panel shows the Wind Tunnel Settings in terms of the wind speed and the position of the sensor (which is the wind direction). Figure 4.7 indicates the flow sensor readout (on the right half) when the wind speed in the wind tunnel was 4 m/s and the wind direction was 45^0. Figure 4.8 indicates the sensor readout (on the right half) at a wind speed of 14 m/s and a wind direction of 60^0. Similar accuracies were obtained at all the various positions of the sensor and for the different wind speeds. Hence the program in Labview has acquired the signals, processed them by filtering out the unwanted noise, displayed the values by performing the necessary averaging, thereby acting as a complete instrument for flow sensing.

4.3.3.3 *Data processing*

The Voltage signal from each channel is sent to a VI known as an AC/DC estimator which gives the values of both V_{ac} and V_{dc}. V_{dc} is sent to a VI called Strain Converter (Figure 4.9) which converts the voltage read from the strain gauge to root strain using the formula:

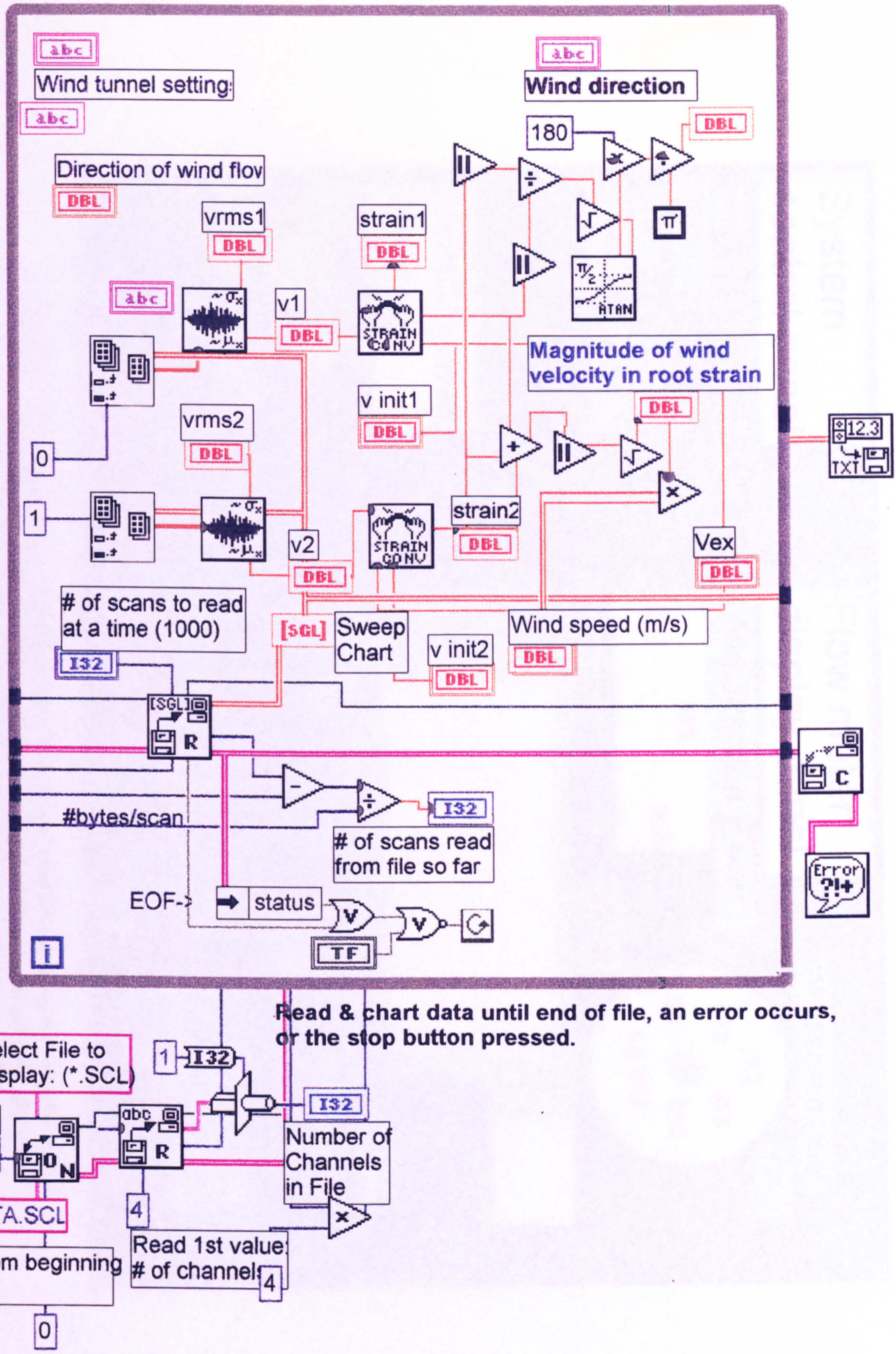

Figure 4.6: The Block diagram of the VI used to display and process the stored strain gauge signals

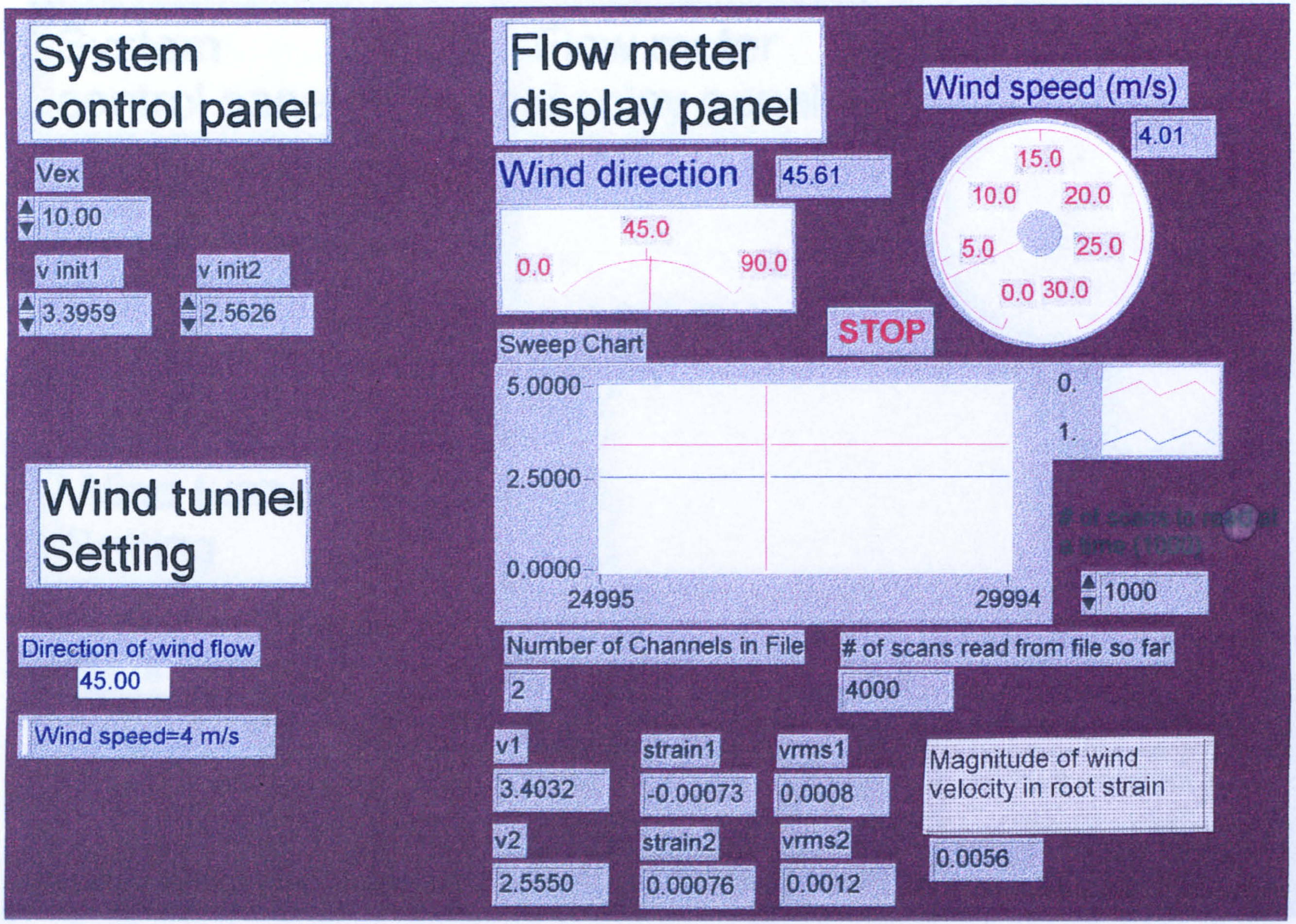

Figure 4.7: The automated configuration of the virtual instrument program created with Labview to display the wind speed and direction generated by the flow sensor when the wind speed was 4 m/s and the wind direction was 45°.

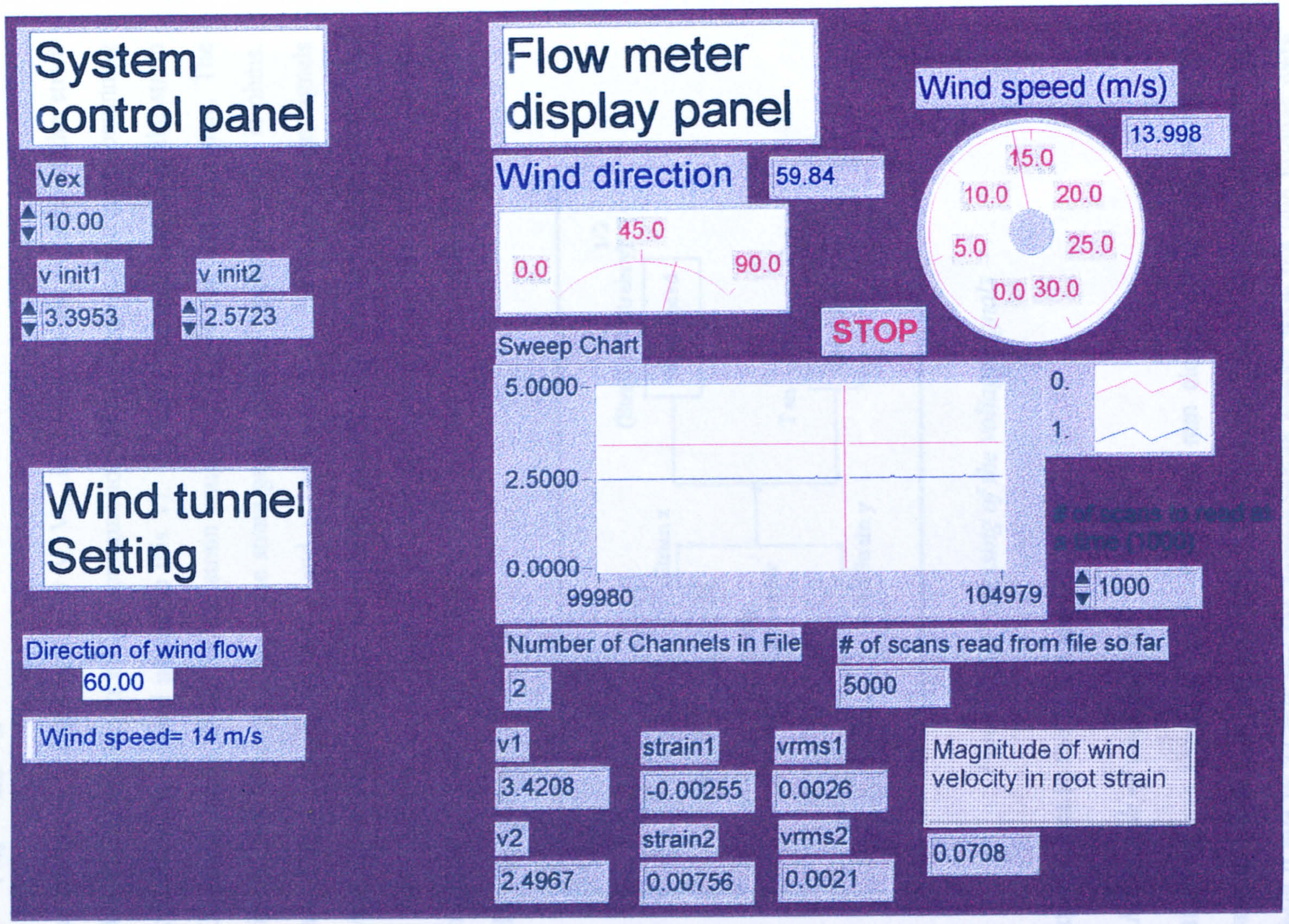

Figure 4.8: The automated configuration of the virtual instrument program created with Labview to display the wind speed and direction generated by the flow sensor when the wind speed was 14 m/s and the wind direction was 60°.

$$\text{Strain} = \frac{-2V_r}{GF}.\left(1+\frac{R_L}{R_g}\right) \qquad (4.12)$$

where $Vr = (V_{sg} - V_{init})/V_{ex}$ (4.13)

V_{ex} is the excitation voltage used =10 V, V_{init} is the unstrained voltage of the strain gauge after it is mounted in its bridge configuration. This voltage is read at the beginning of the application, saved and passed to this VI. V_{sg} is the voltage read from the strain gauge. GF is the gauge factor of the strain gauge = 2. R_L is the lead resistance. The default in Labview is set to 0. R_g is the strain gauge nominal resistance value in ohms. $Strain_x$ and $Strain_y$, which are the x and y components of the strain gauge signals respectively, from both the channels are added together and then the square root of the absolute value of this sum is calculated to obtain the magnitude of strain which is related to the magnitude of wind speed (Equation 4.10). The wind direction is calculated as indicated by Equation 4.11.

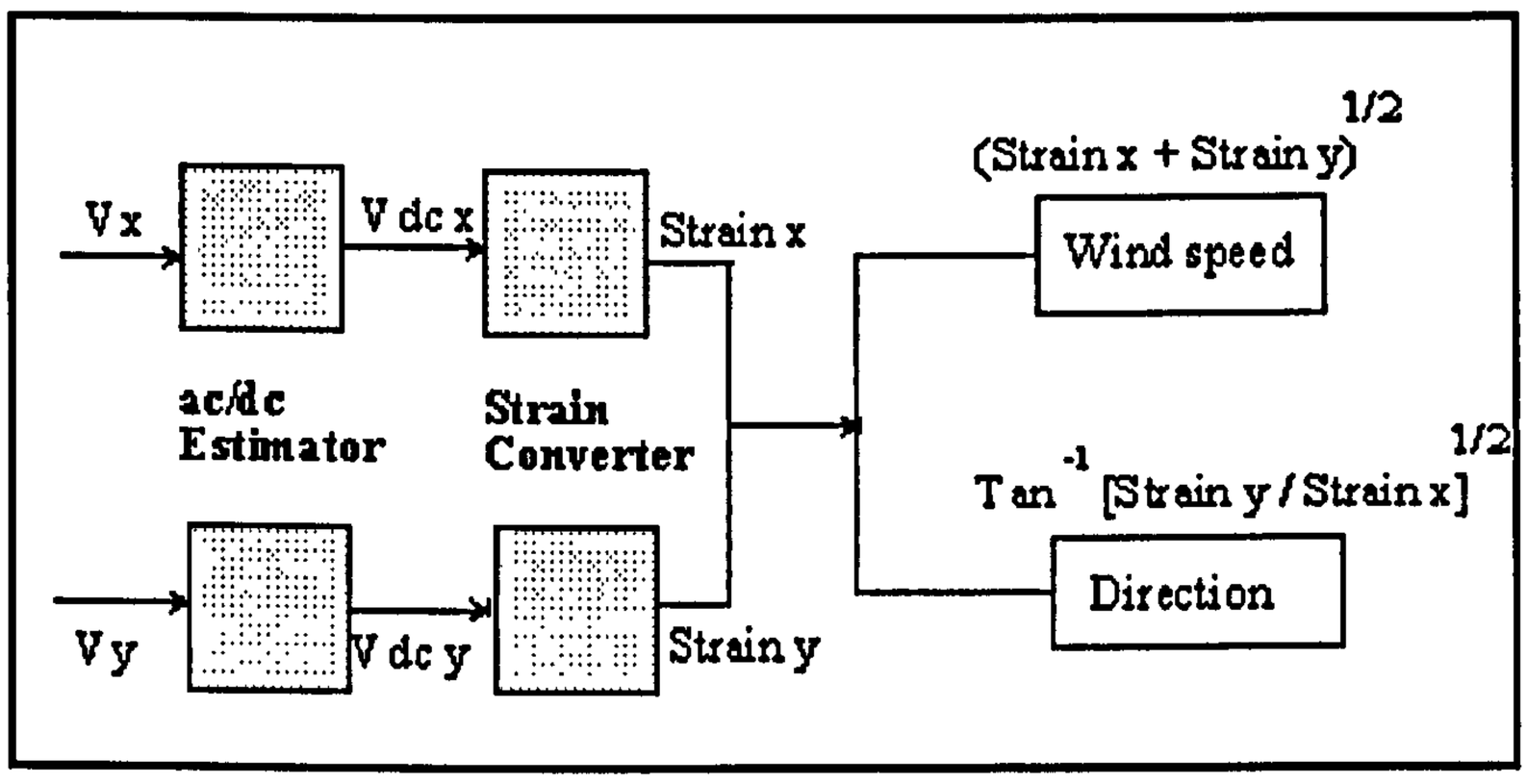

Figure 4.9: Processing of the voltage signals

4.3.4 Experiments in the Wind tunnel

4.3.4.1 Magnitude of wind velocity

The instrument was mounted in the 460 x 460 mm closed circuit wind tunnel, the photograph of which is shown in Figure 4.10. The wind speed in the wind tunnel was varied from 0 m/s to 23 m/s and the corresponding signals from the two bridges were acquired and analysed.

Figure 4.10: Photograph of the closed circuit wind tunnel

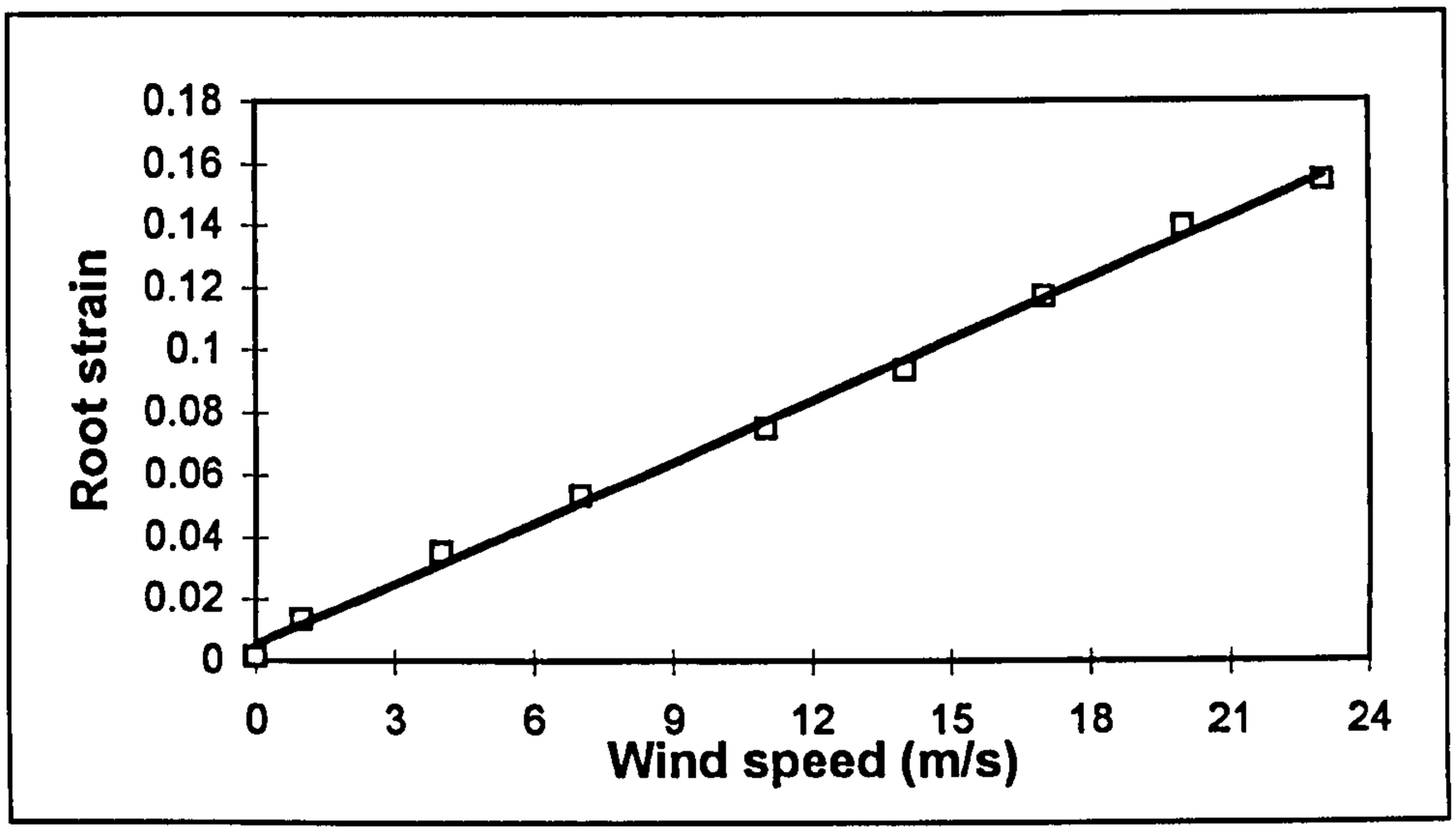

Figure 4.11: Root strain plotted against wind speed when the flowmeter is oriented at 45 degrees to wind flow.

The Table A-1 in the Appendix shows the results of this calculation for different values of wind speed. Wind speed was plotted versus $(strain_x+strain_y)^{1/2}$ as shown in Figure 4.11. The graph shown in Figure 4.11 has a linear gradient, having a linearity within 3%, indicating that wind speed is indeed proportional to square root of strain, thus verifying Equations 4.9 and 4.10. A linear regression analysis indicates a sensitivity of 0.0065 ± 0.0001 root strain s/m, and a resolution of 0.43 m/s. In this first prototype of the sensor, the range was limited by noise signals due to beam oscillations at speeds greater than 23m/s, causing the strain gauge wires to touch each other, and causing spurious signals. In principle, greater speeds up to 50 m/s can be monitored by this sensor, if the strain gauges are mounted effectively. Consideration of Equation 4.9 indicates that the gradient of the graph in Figure 4.11, is dependent on fluid density, the area of the drag element, and the dimensions and material properties of the beam. Therefore, by matching the beam material and dimensions to the fluid, the sensor can be optimised for particular applications.

The device was clamped on a turn table and this was rotated about its longitudinal axis from 0^0 to 90^0 at 15^0 intervals. This was done for two reasons. First, it was necessary to show that the sensor output was independent of the angle of orientation of the sensor to the direction of wind flow. Secondly, this experiment was performed to monitor if the sensor could measure the wind direction. At each angle V_x and V_y were recorded as a function of wind velocity, over a range from 0 to 23 m/s (Table A-2 in the Appendix).

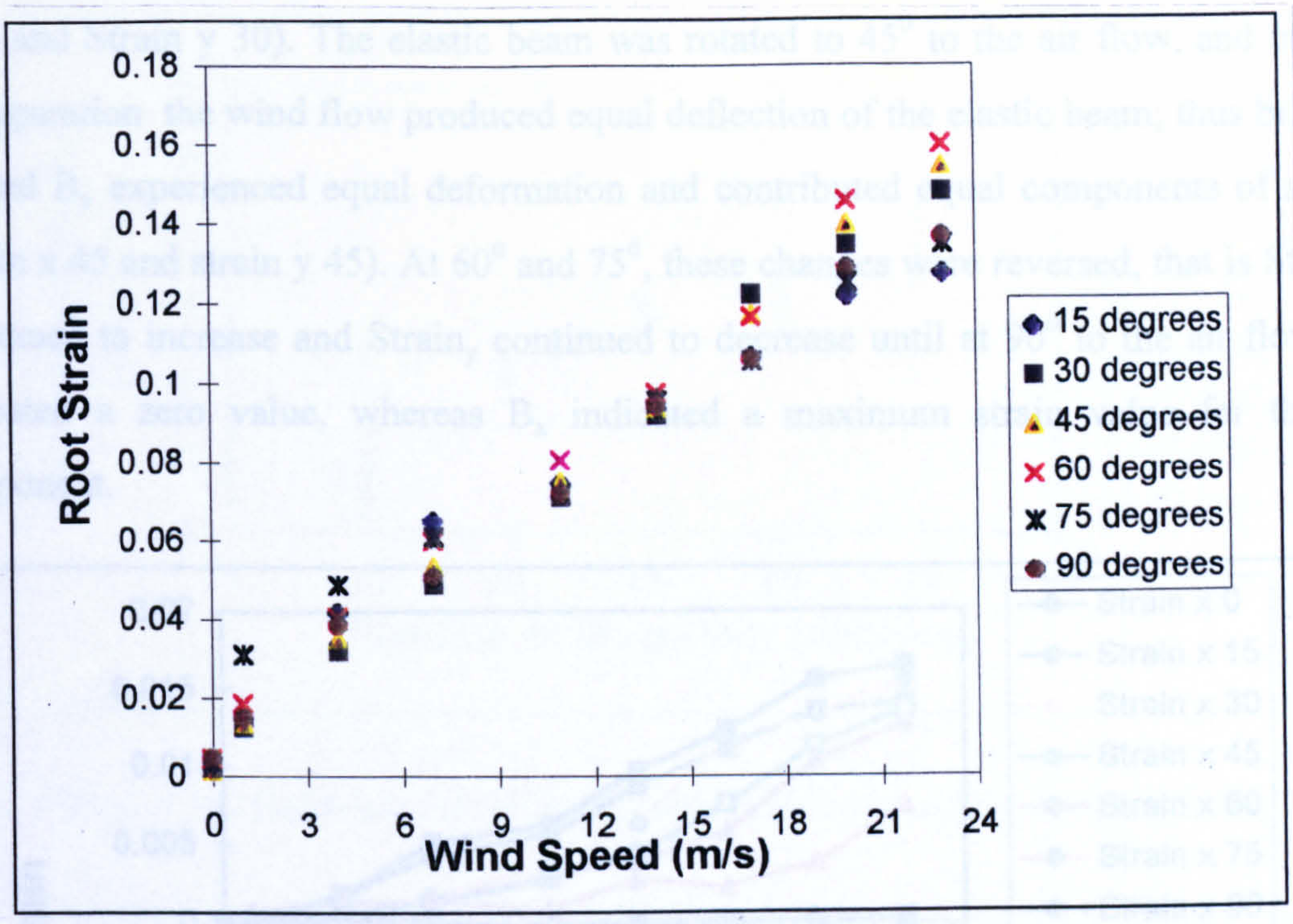

Figure 4.12: Root strain plotted against wind speed with the flowmeter oriented at various angles to wind flow.

The graph plotted between wind speed and $(strain_x+strain_y)^{1/2}$ for different angles is shown in Figure 4.12. Consideration of the 95% confidence limits (Appendix A-4) for each plot indicate that the plots are coincident, and that the sensor output is independent of angle of orientation of the elastic beam to the direction of wind flow. Therefore, all the data presented in Figure 4.12 can be used to obtain a calibration curve for the sensor, which will be valid for multi-directional airflow. When a linear regression was performed on all the data, the sensitivity was found to be 0.0062 ± 0.0001 root strain s/m and the resolution to be 0.64 m/s.

Figure 4.13 shows how the x and y components of strain vary with wind speed, for different orientations of the sensor to the airflow. When the elastic beam was positioned at 0^o to the air flow, the bridge(B_y) giving the y component of strain, $Strain_y$ was perpendicular to the air flow, and experienced maximum deflection (indicated as 'Strain y 0' in Figure 4.13). Bridge(B_x) experienced zero deflection, being parallel to the air flow, and contributed the x component of strain, $Strain_x$. This was indicated as 'Strain x 0' in Figure 4.13. As the sensor position was rotated by 15^o, bridge B_y moved 15^o away from the wind flow and experienced slightly reduced deflection than at 0^o (Strain y 15) while bridge B_x moved 15^o towards the wind flow and underwent increased deflection than at 0^o (Strain x 15). These changes were enhanced at 30^o (Strain

x 30 and Strain y 30). The elastic beam was rotated to 45° to the air flow, and in this configuration the wind flow produced equal deflection of the elastic beam; thus bridges B_x and B_y experienced equal deformation and contributed equal components of strain (strain x 45 and strain y 45). At 60° and 75°, these changes were reversed, that is $Strain_x$ continued to increase and $Strain_y$ continued to decrease until at 90° to the air flow B_y indicated a zero value, whereas B_x indicated a maximum strain value for the x-component.

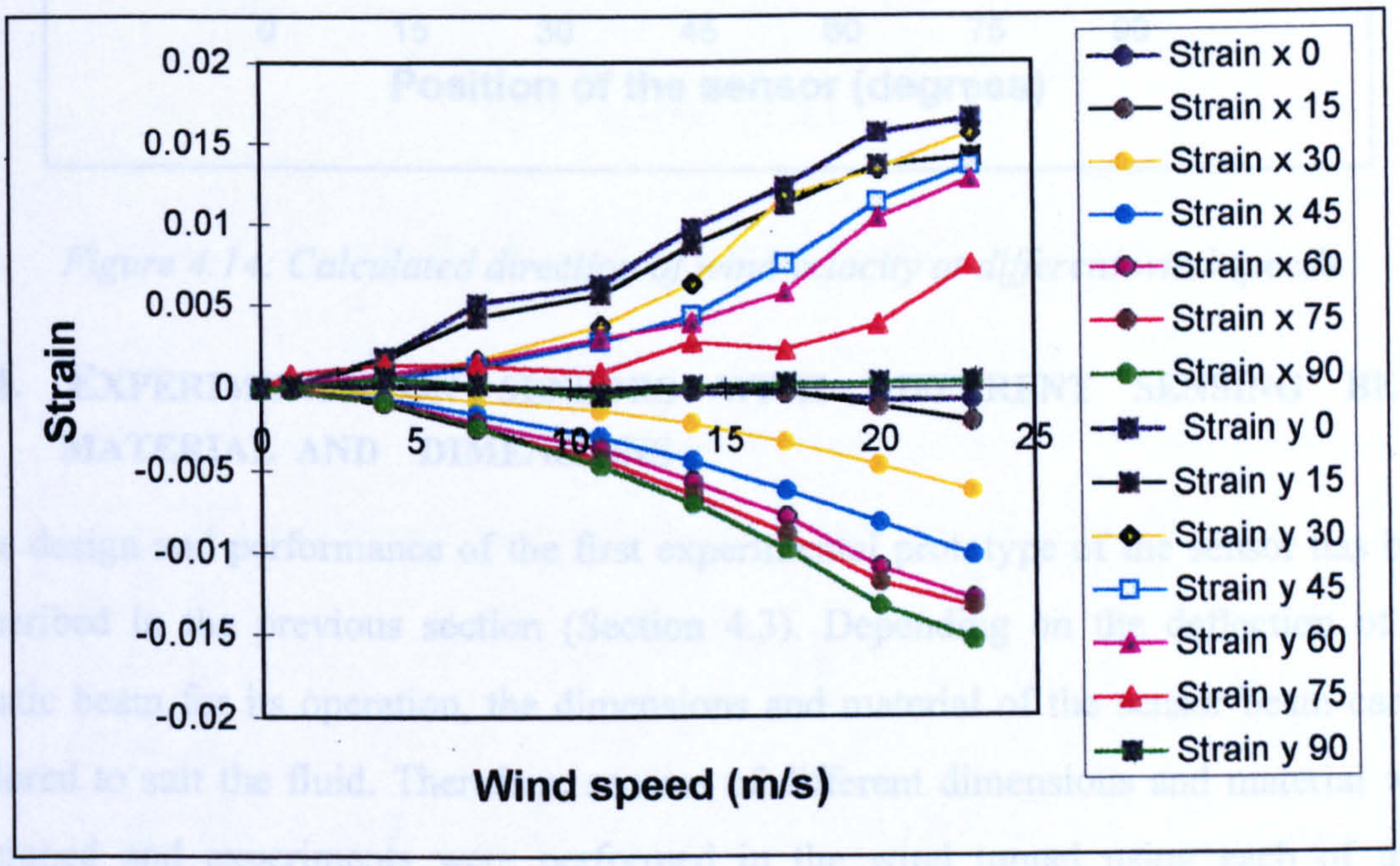

Figure 4.13: Wind Speed plotted against $Strain_x$ and $Strain_y$ for different orientations of the sensor

4.3.4.2 Direction of wind velocity

The direction of wind velocity was calculated according to Equation 4.11 for the different wind speeds. Figure 4.14 shows the plots of the wind flow direction at different wind speeds for various sensor positions. Several authors [4.3, 4.4] have discussed the inability of calculating the wind direction accurately at low wind speeds. The situation is similar in this case and the readings get more accurate as the wind speed increases especially beyond 11 m/s as obvious from the plots of Figure 4.14. These plots are co-incident from the consideration of the 95% confidence limits (Appendix A-4). From the plots, the directional sensitivity of the sensor is 0.76 ± 0.03 degrees and the resolution is 3.6°.

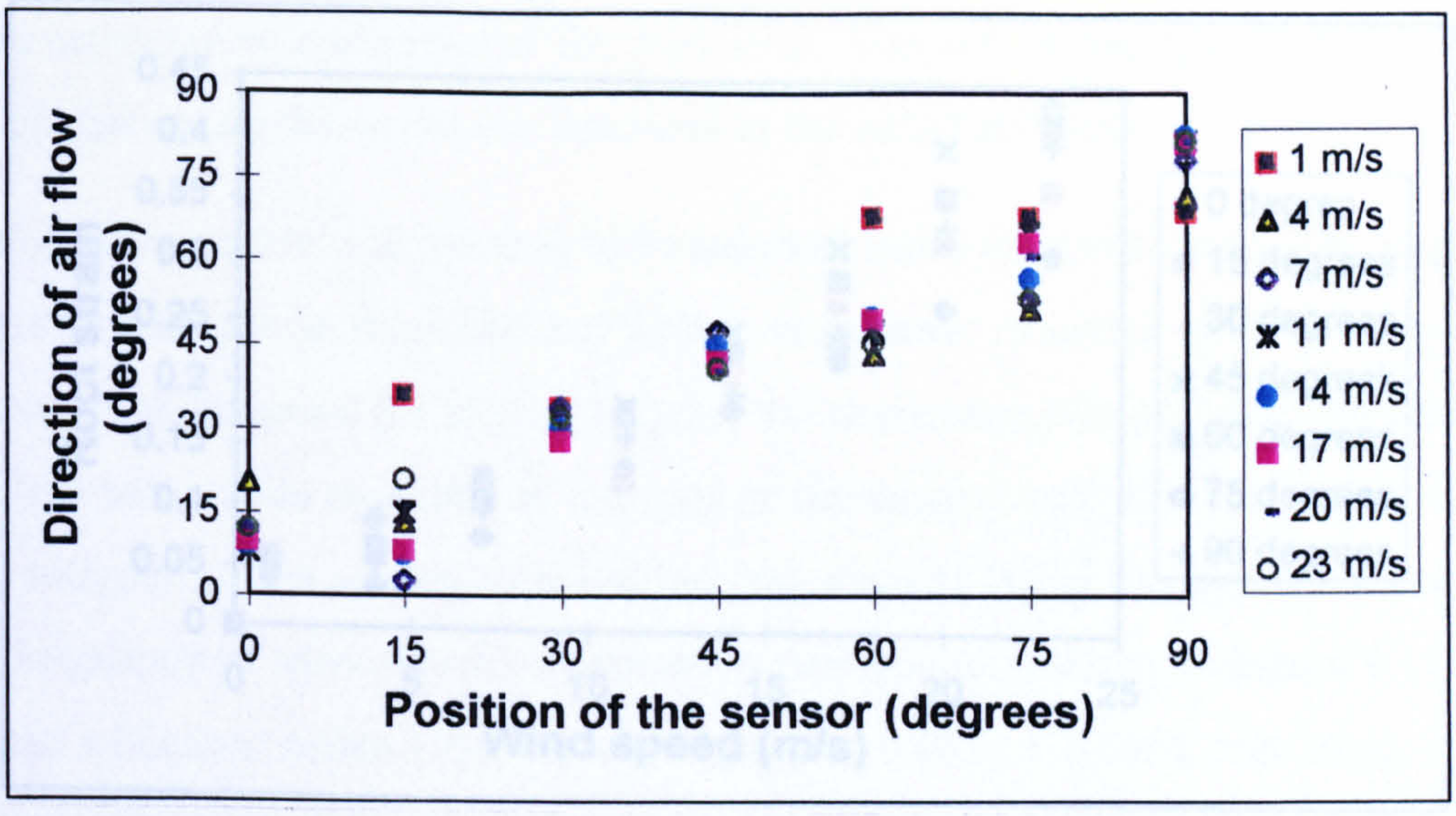

Figure 4.14: Calculated direction of wind velocity at different wind speeds.

4.4. EXPERIMENTS ON SENSORS WITH DIFFERENT SENSING BEAM MATERIAL AND DIMENSIONS

The design and performance of the first experimental prototype of the sensor has been described in the previous section (Section 4.3). Depending on the deflection of the elastic beam for its operation, the dimensions and material of the sensor beam can be tailored to suit the fluid. Therefore, sensors of different dimensions and material were designed and experiments were performed in the wind tunnel using each of these sensors, a few of which are reported in this section.

4.4.1. Experimental Prototype 2: Hollow plastic beam.

The elastic rubber beam was replaced with a hollow plastic beam (used for hot water pipe insulation), 0.195 m long and 0.018 m inner width and 0.035 m outer width with a spherical sphere attached to one end and the other end clamped. The voltage signals generated from the two Wheatstone bridges were detected by a multimeter due to the non-availability of a PC at that time. Magnitude and direction of wind velocity were deduced and the plots are shown in Figures 4.15 and 4.16 respectively.

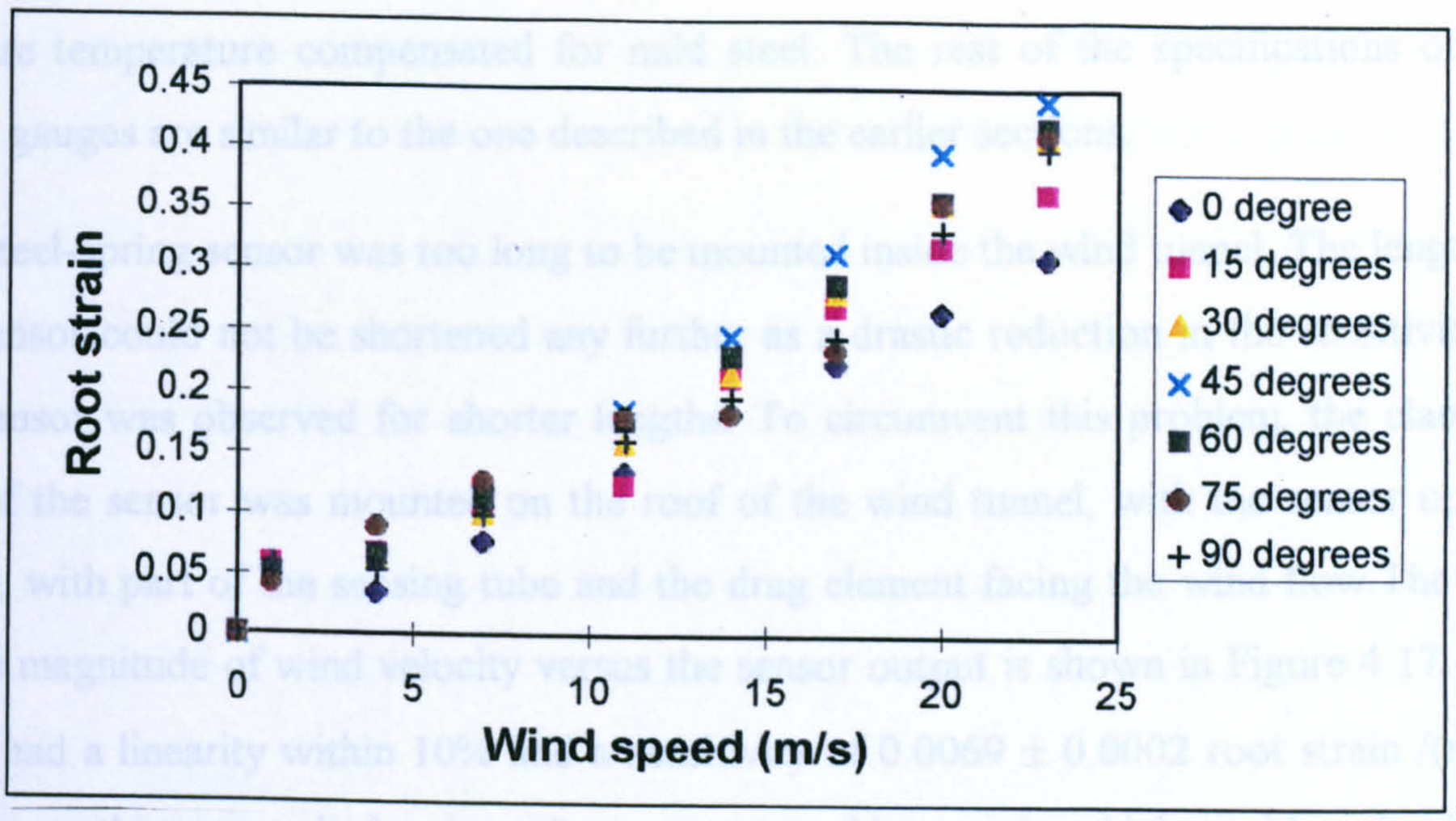

Figure 4.15 : Magnitude of wind speed for the second prototype of the sensor

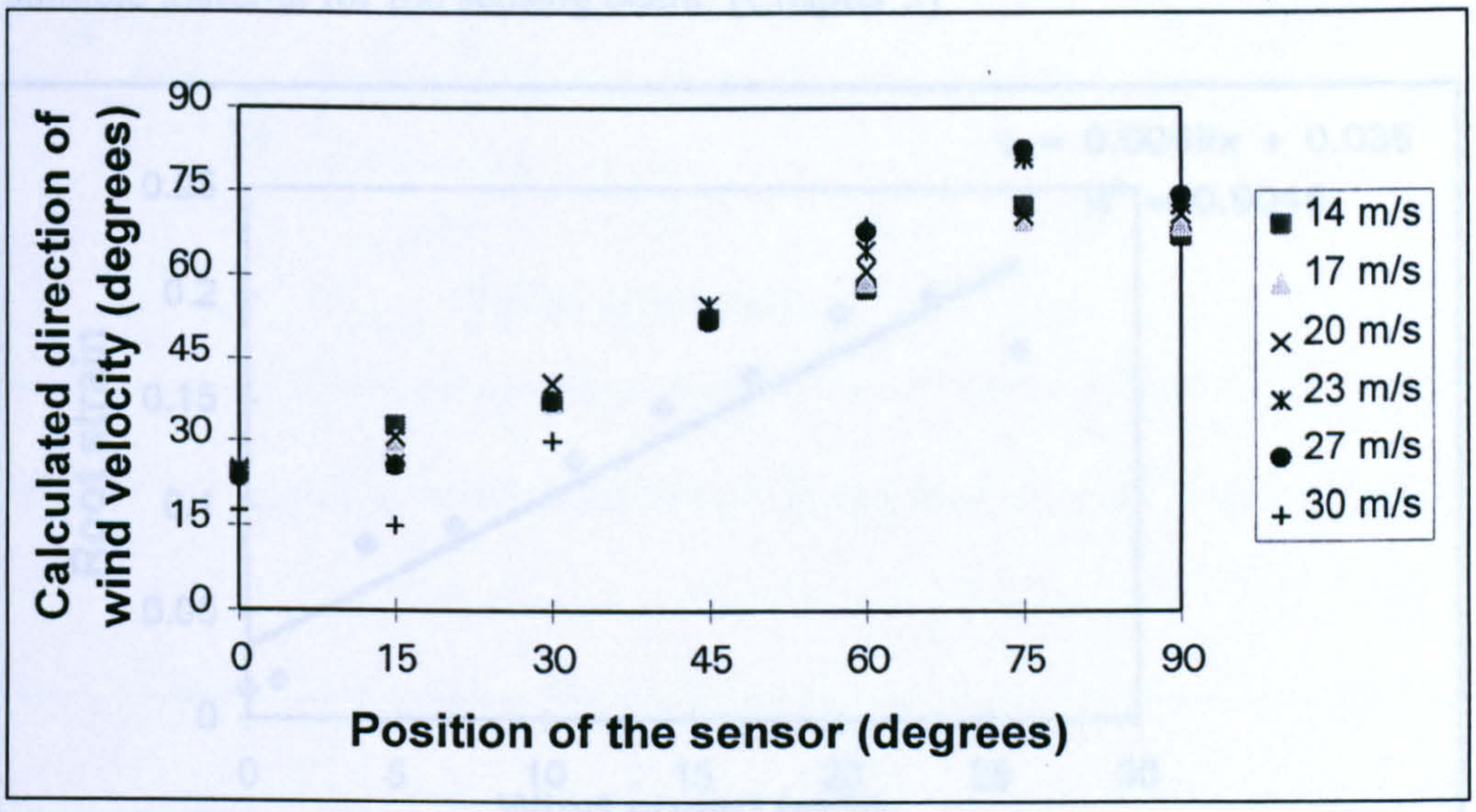

Figure 4.16: Direction of wind velocity for different wind speeds.

4.4.2. Experimental Prototype 3: A steel-spring sensing tube

Since certain applications need a more rugged instrument, it was thought that replacing the sensing beam with a steel rod might be a good option. Since a flexible rod was required, a spring element made of steel, 0.335 m long and 0.015 m thick was chosen to be the sensing rod. A heavy, spherical ball, having a diameter of 0.0728 m was attached to the free end. The strain gauges used this time were the 5 mm long gauges [RS 632-168]. These gauges are made of copper-nickel alloy with polyimide as the base material

and are temperature compensated for mild steel. The rest of the specifications of the strain gauges are similar to the one described in the earlier sections.

The steel-spring sensor was too long to be mounted inside the wind tunnel. The length of the sensor could not be shortened any further as a drastic reduction in the sensitivity of the sensor was observed for shorter lengths. To circumvent this problem, the clamped end of the sensor was mounted on the roof of the wind tunnel, with the sensor upside down, with part of the sensing tube and the drag element facing the wind flow.The plot of the magnitude of wind velocity versus the sensor output is shown in Figure 4.17. The plots had a linearity within 10% and a sensitivity of 0.0069 ± 0.0002 root strain /(m/s). However, this sensor had quite a large amount of hysteresis which could probably be reduced by using a suitable form of steel as the sensing tube. But the very presence of hysteresis when using steel as the sensing beam material has indicated that rubber is a more suitable material for the sensing beam. [Chapter 3]

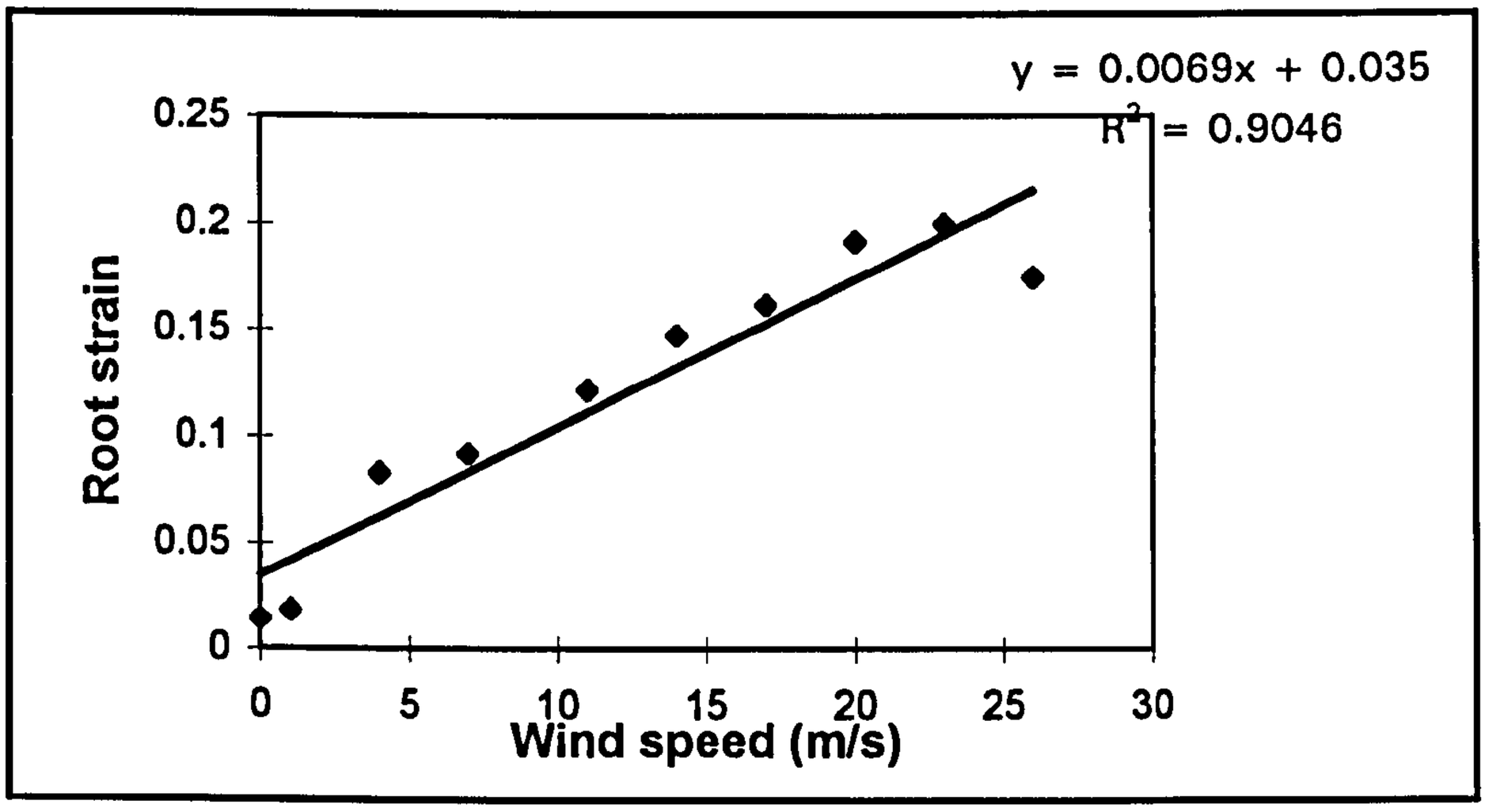

Figure 4.17: Magnitude of wind velocity for the steel-spring sensor

4.4.3. Experimental Prototype 4: A rubber cylinder of circular cross-section

This version of the sensor consisted of a rubber cylinder of circular cross-section, made of polybutadiene polymer, 0.162 m long and 0.024 m thick supplied by the Malaysian Rubber Products Research Association with a spherical ball of radius 0.0202 m attached to its free end. The modulus of Elasticity of this rubber was found (as discussed in Chapter 3) to be 1.2×10^6 N/m^2. The four strain gauges were attached to the longitudinal surfaces of the rubber strip, 90^0 apart from each other. The signals were

acquired and processed as described in Section 4.3.3 using a 486 - DX laptop computer via a 12-bit data acquisition board DAQ-card 1200 supplied by National Instruments.

The sensor was oriented at different positions from 0-360^0 at 22.5^0 intervals in the wind tunnel and the x and y components of strain were measured and processed to give strain magnitude and direction, which were related to the magnitude and direction of the wind velocity.

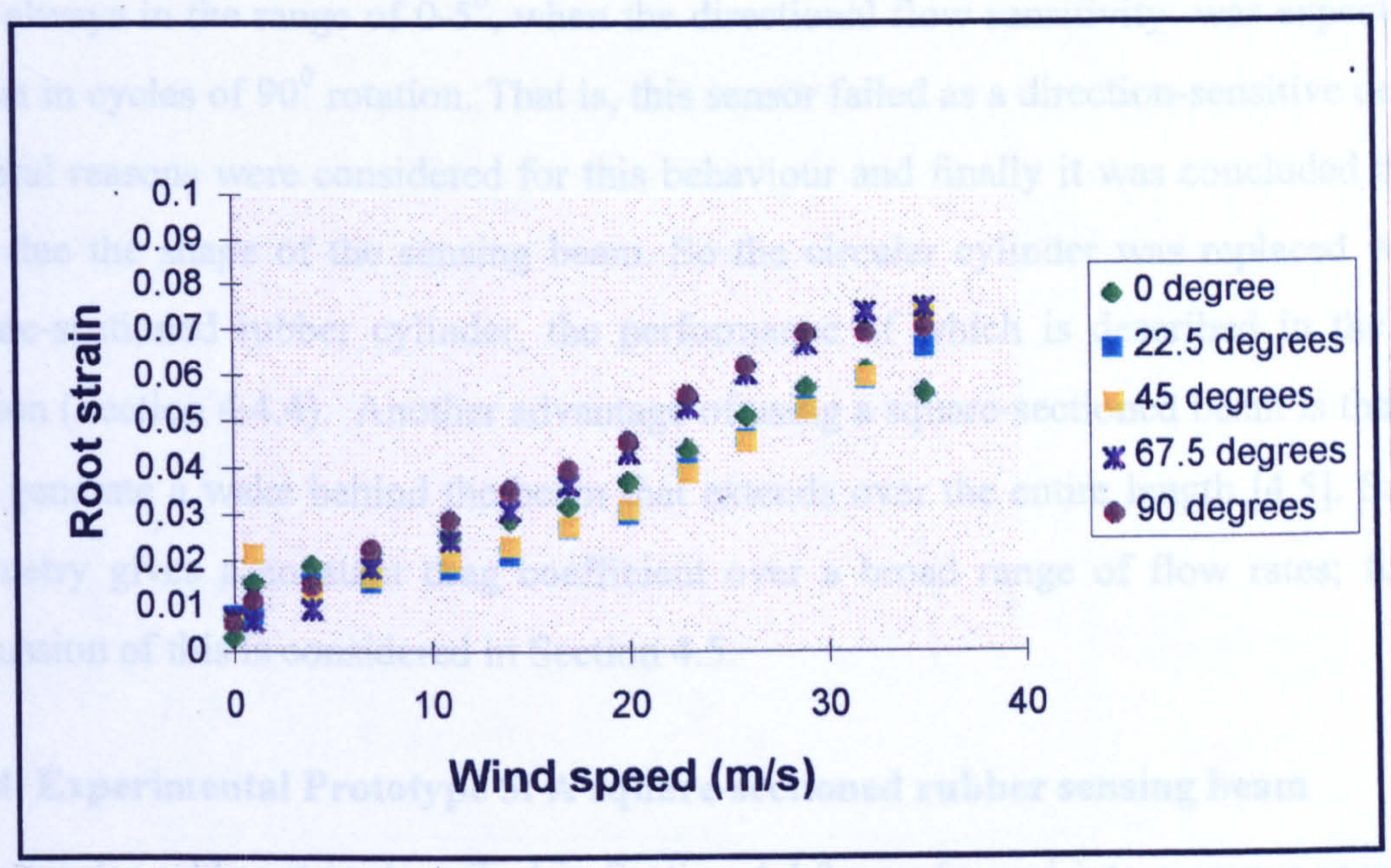

Figure 4.18: Magnitude of wind speed in root strain from 0^0 to 90^0 sensor positions.

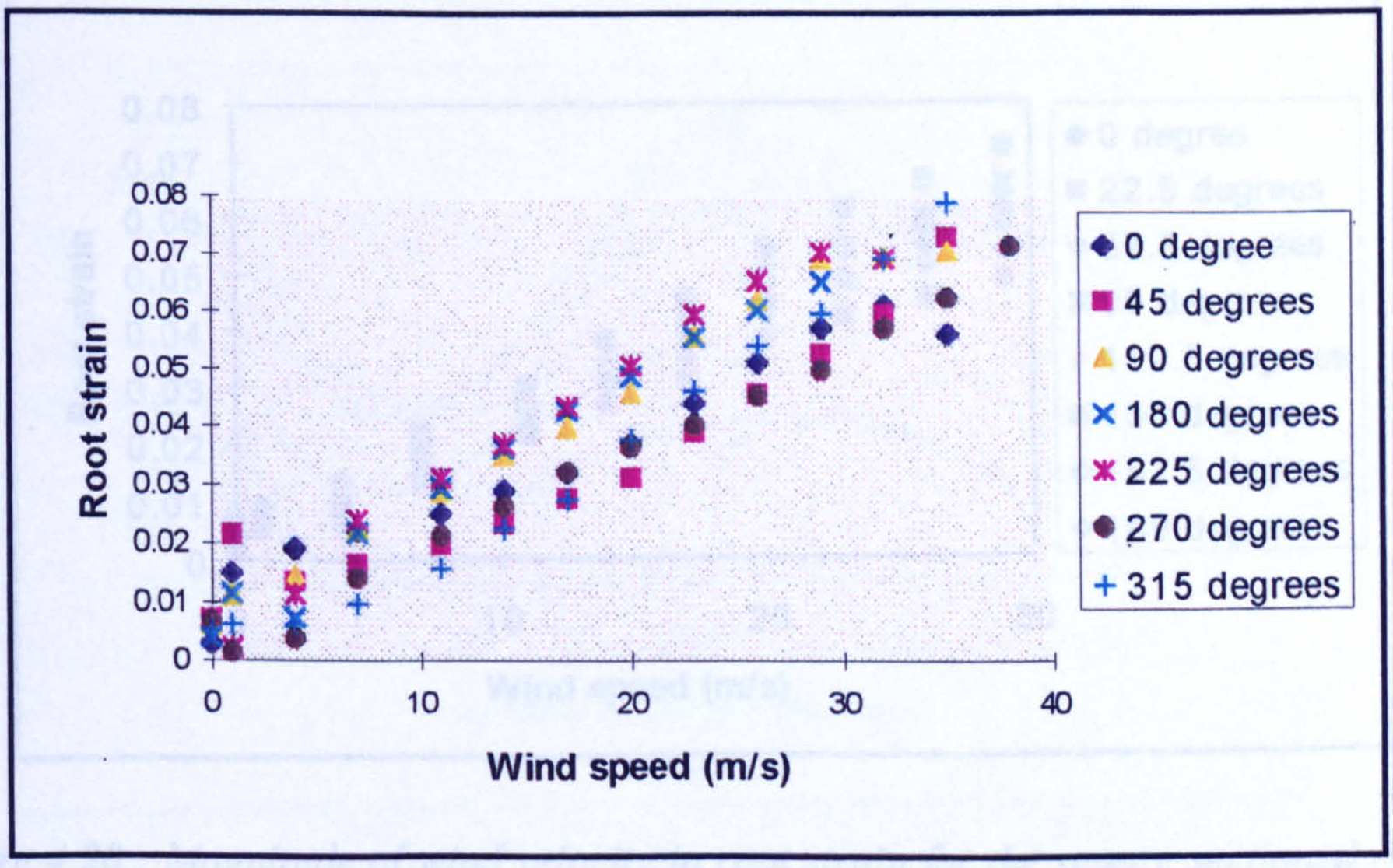

Figure 4.19: Magnitude of wind speed in root strain from 0 to 360^0 sensor positions

Figure 4.18 shows the plots for the magnitude of wind velocity versus strain magnitude for the orientation of the sensor in the first quadrant with its longitudinal axis normal to the direction of wind flow and Figure 4.19 shows the plots for the sensor orientation in all the four quadrants ($0\text{-}360^0$).

While attempting to deduce the direction of wind velocity, an unexpected observation was made. At every position of the sensor from 0 to 360^0, the direction of wind velocity was always in the range of $0\text{-}5^0$, when the directional flow sensitivity was expected to repeat in cycles of 90^0 rotation. That is, this sensor failed as a direction-sensitive device. Several reasons were considered for this behaviour and finally it was concluded that it was due the shape of the sensing beam. So the circular cylinder was replaced with a square-sectioned rubber cylinder, the performance of which is described in the next section (Section 4.4.4). Another advantage of using a square-sectioned beam is that this will generate a wake behind the beam that extends over the entire length [4.5]. Such a geometry gives a constant drag coefficient over a broad range of flow rates; further discussion of this is considered in Section 4.5.

4.4.4. Experimental Prototype 5: A square-sectioned rubber sensing beam

The circular rubber strip described in Section 4.4.3 was formed into a square-sectioned beam by immersing the rubber beam in liquid nitrogen and slicing the beam on all four

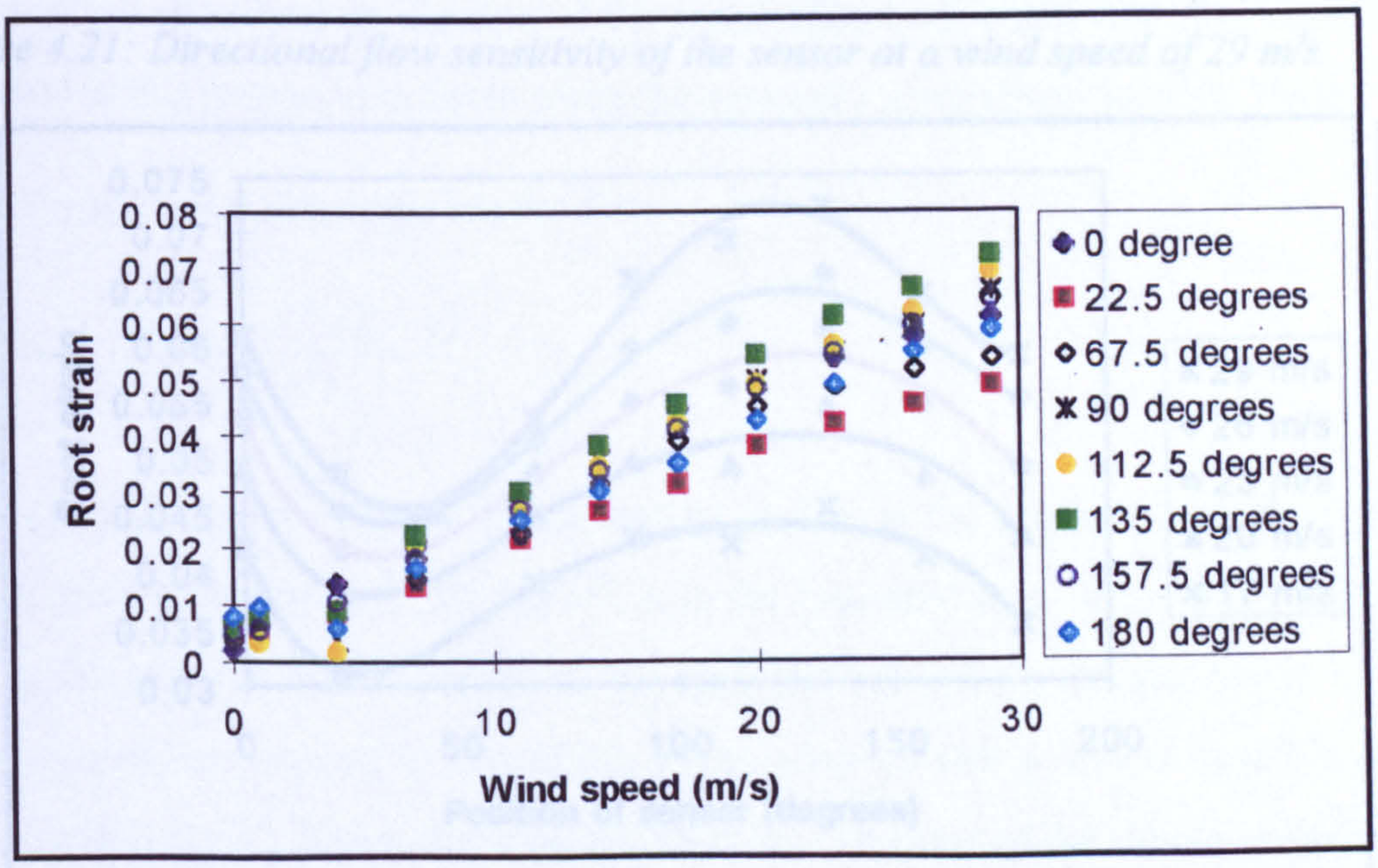

Figure 4.20 : Magnitude of wind velocity in root strain for the square sectioned rubber sensing device.

sides, parallel to its longitudinal axis. Some amount of surface roughness was induced by this method. The sensor length was the same as the previous one (0.165 m) and each of the four sides was 0.015 m wide. During the experiments in the wind tunnel, the sensor position was rotated from 0 to 180^0 at 22.5^0 intervals. Figure 4.20 shows the plots for the magnitude of wind velocity versus root strain at all the positions.

The next part in the experimental stage was the most crucial one: could the same rubber beam be direction-sensitive sensor just by virtue of the fact that the strip had a different shape? Figure 4.21 shows the plot for the direction of wind velocity in root strain as the sensor was rotated from 0-180^0 at a wind speed of 29 m/s. The plot is an indication that the sensor is directional flow sensitive, repeating in cycles of 90^0 rotation.

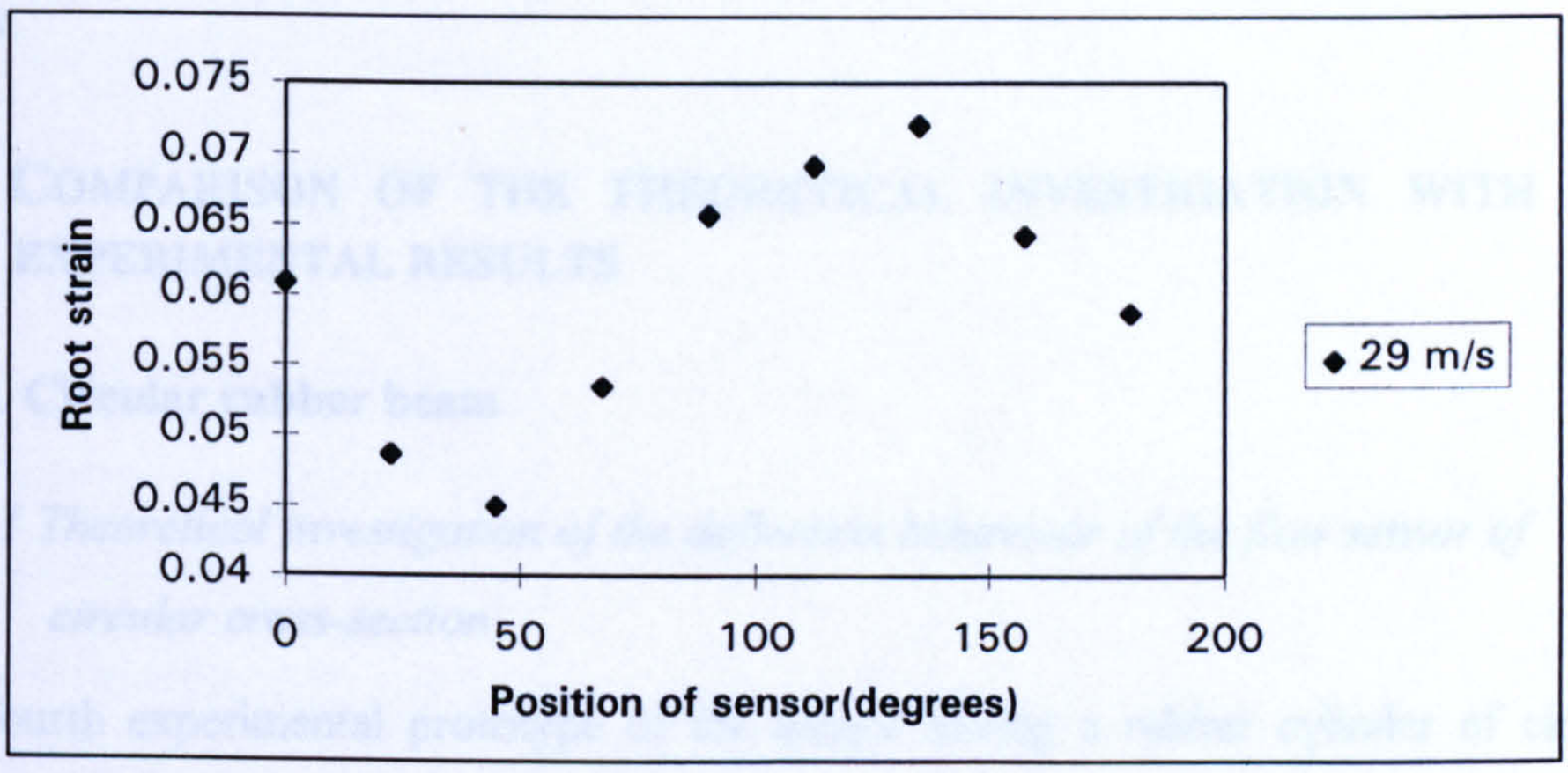

Figure 4.21: Directional flow sensitivity of the sensor at a wind speed of 29 m/s

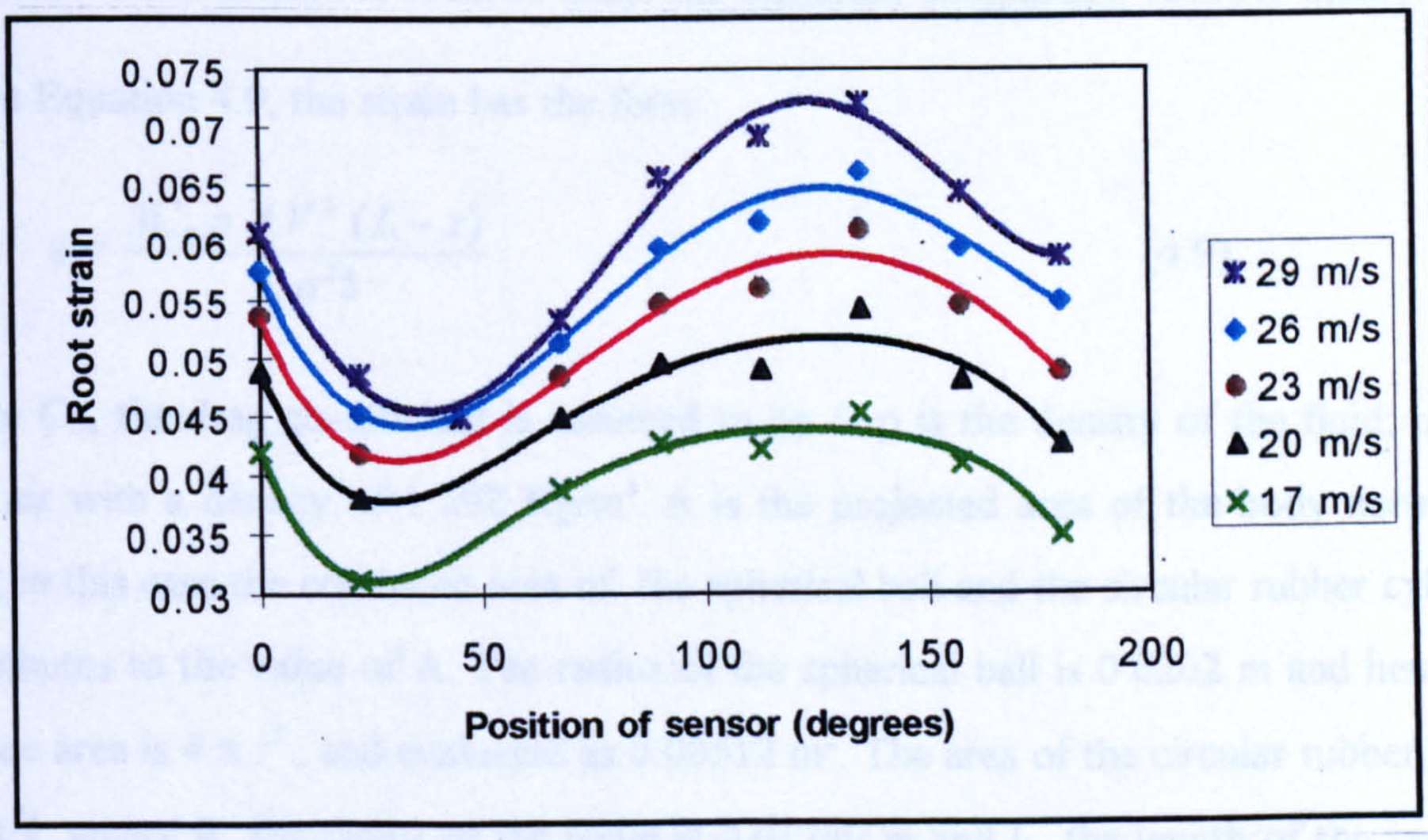

Figure 4.22 : Measurement of flow direction at varying wind speeds.

Figure 4.22 shows the plots for direction of wind velocity versus root strain at different wind speeds. As explained in an earlier section, measurement of flow direction is not very accurate at very low wind speeds (in this case, below 10 m/s).

4.4.5 Comparison of the different prototypes

After conducting experiments on the different experimental prototypes (discussed in sections 4.4.1 to 4.4.4), two conclusions were made. The first is that rubber seems to be a better choice for the sensing beam material when compared to steel, as the latter had a large amount of hysteresis. The second is that a square-sectioned rubber beam is preferred to a cylindrical rubber beam as the former is directional sensitive and provides a constant C_D over a wider flow range, thereby increasing the dynamic range of the sensor.

4.5. COMPARISON OF THE THEORETICAL INVESTIGATION WITH THE EXPERIMENTAL RESULTS

4.5.1. Circular rubber beam

4.5.1.1 Theoretical investigation of the deflection behaviour of the flow sensor of circular cross-section

The fourth experimental prototype of the sensor having a rubber cylinder of circular cross-section described in Section 4.4.3 was utilised to carry out the experiments described in this section in order to make the necessary comparison with the theory.

From Equation 4.9, the strain has the form:

$$\varepsilon = \frac{3C_D \rho A V^2 (L-x)}{E a^2 b} \qquad (4.9)$$

where C_D, the drag co-efficient is assumed to be 1. ρ is the density of the fluid; in this case air with a density of 1.292 Kg/m^3. A is the projected area of the body normal to flow; in this case the combined area of the spherical ball and the circular rubber cylinder contributes to the value of A. The radius of the spherical ball is 0.0202 m and hence its surface area is $4\pi r^2$, and evaluated as 0.00512 m^2. The area of the circular rubber beam is $\pi R^2 L$ where R, the radius of the beam is 0.01289 m and L, the length of the beam is 0.162 m. Therefore, the area of the rubber beam is found to be 8.5×10^{-5} m^2. Hence the

combined area (A) of the drag element is 0.00521 m^2. The symbol x, in Equation 4.9, denotes the distance between the gauge location and the clamped end of the beam which should ideally be 1/2 to 1 'b' to reduce the influence of the clamping force on the strain distribution in the gauge area.[4.5]. For this sensor, the value of 'x' is 0.02 m. The beam width 'a' and the beam thickness 'b' has the value 0.024 m. The modulus of elasticity (Y) has been deduced already in Chapter 3 to have a value of 1.2 $\times 10^6$ N/m^2. Substituting all these values in Equation (4.9), the theoretical values of strain for different wind speeds are obtained as shown in Table 4.2.

Table 4.2 : Theoretical strain at different wind speeds.

Wind speed (m/s)	**Theoretical strain**
0	0
1	0.0002
4	0.003
7	0.009
11	0.021
14	0.034
17	0.050
20	0.069
23	0.092
26	0.117
29	0.146
32	0.178
35	0.214
38	0.251
41	0.293
44	0.337
47	0.385
50	0.435

4.5.1.2 Determination of the drag co-efficient and Reynolds number

C_D is the overall drag coefficient which is determined by empirical data. The sensor output: $\sqrt{\text{Strain}_x + \text{Strain}_y}$ in root strain has been found experimentally at varying wind speeds and at different sensor positions. Considering the experimental strain at one particular position of the sensor, the actual value of C_D for this particular sensor and at that particular sensor position can be obtained according to Equation (4.14):

$$C_D = \frac{Experimental\ strain}{Theoretical\ strain} \tag{4.14}$$

Table 4.3 depicts the values of C_D obtained at different wind speeds.

Table 4.3 : Determination of C_D

Wind speed (m/s)	**Theoretical strain**	**Experimental strain**	**Drag co-efficient**
0	0	0	DIV/0
1	0.0002	1.93E-06	0.011
4	0.003	1.35E-05	0.004
7	0.009	0.0002	0.0229
11	0.021	0.0005	0.0213
14	0.034	0.0007	0.0202
17	0.050	0.001	0.0204
20	0.069	0.0013	0.0190
23	0.092	0.0015	0.0173
26	0.117	0.002	0.01725
29	0.146	0.0025	0.0167
32	0.178	0.003	0.0181
35	0.214	0.0038	0.0181
38	0.251	0.005	0.0201

The Reynolds number is determined using Equation 4.15;

$$\text{Re} = \frac{\rho V D}{\eta} \tag{4.15}$$

where ρ is the density of the fluid, V is the velocity of fluid, D is the pipe diameter and η is the absolute viscosity of the fluid.

But the kinematic viscosity of a fluid (ν) is related to the absolute viscosity according to Equation 4.16;

$$\nu = \frac{\eta}{\rho} \qquad (4.16)$$

In the case of air, the kinematic viscosity at 15°C and 101.3 kPa is 14.5 X 10^{-6} m^2/sec and the pipe diameter is 0.46 m. Thus, the Reynolds numbers obtained for the wind speeds encountered in the described experiments are plotted in Figure 4.23 indicating a Reynolds number range from 0 to 1.5 ×10^6.

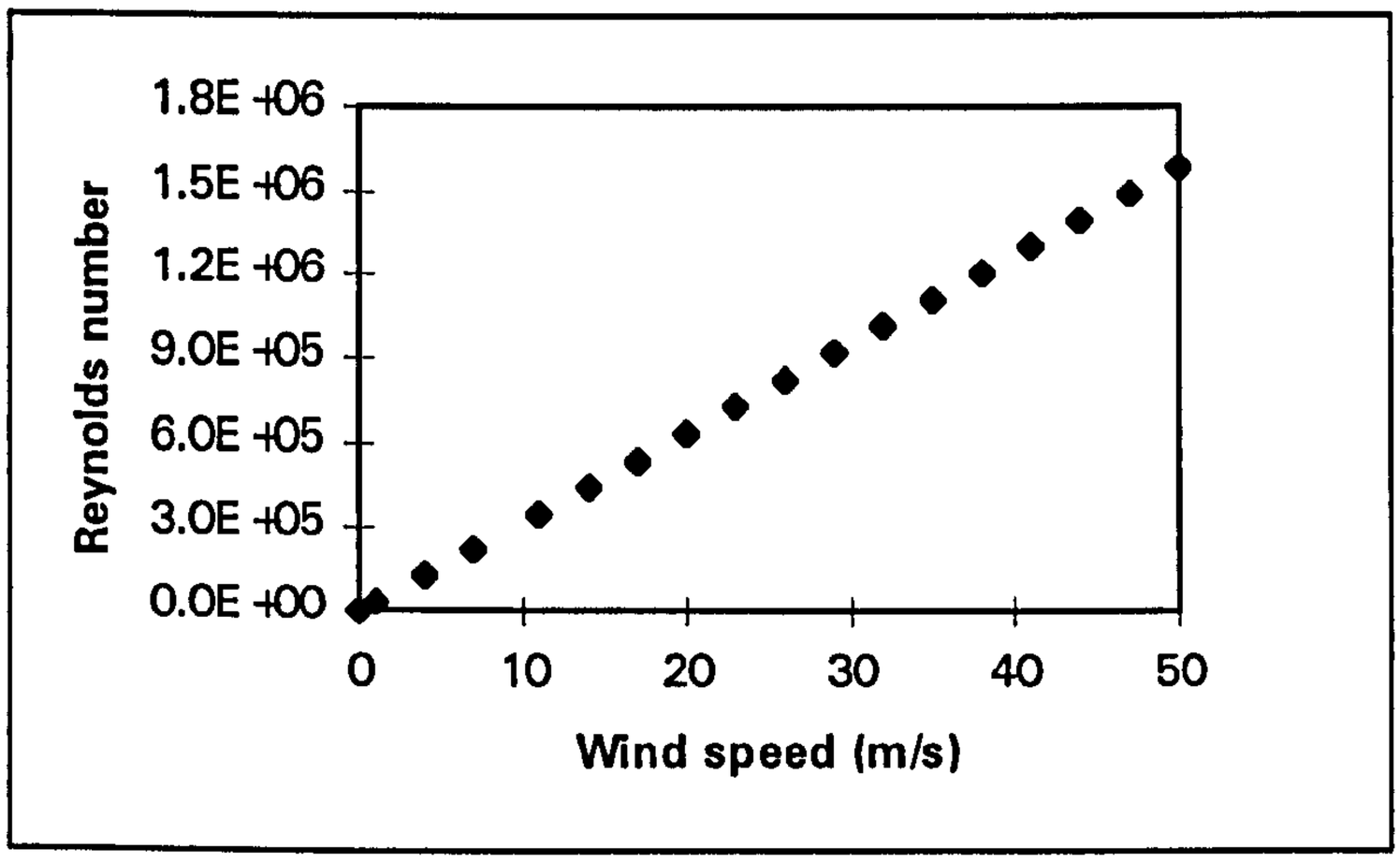

Figure 4.23: Reynolds number versus Wind speed for a pipe diameter of 0.46 m.

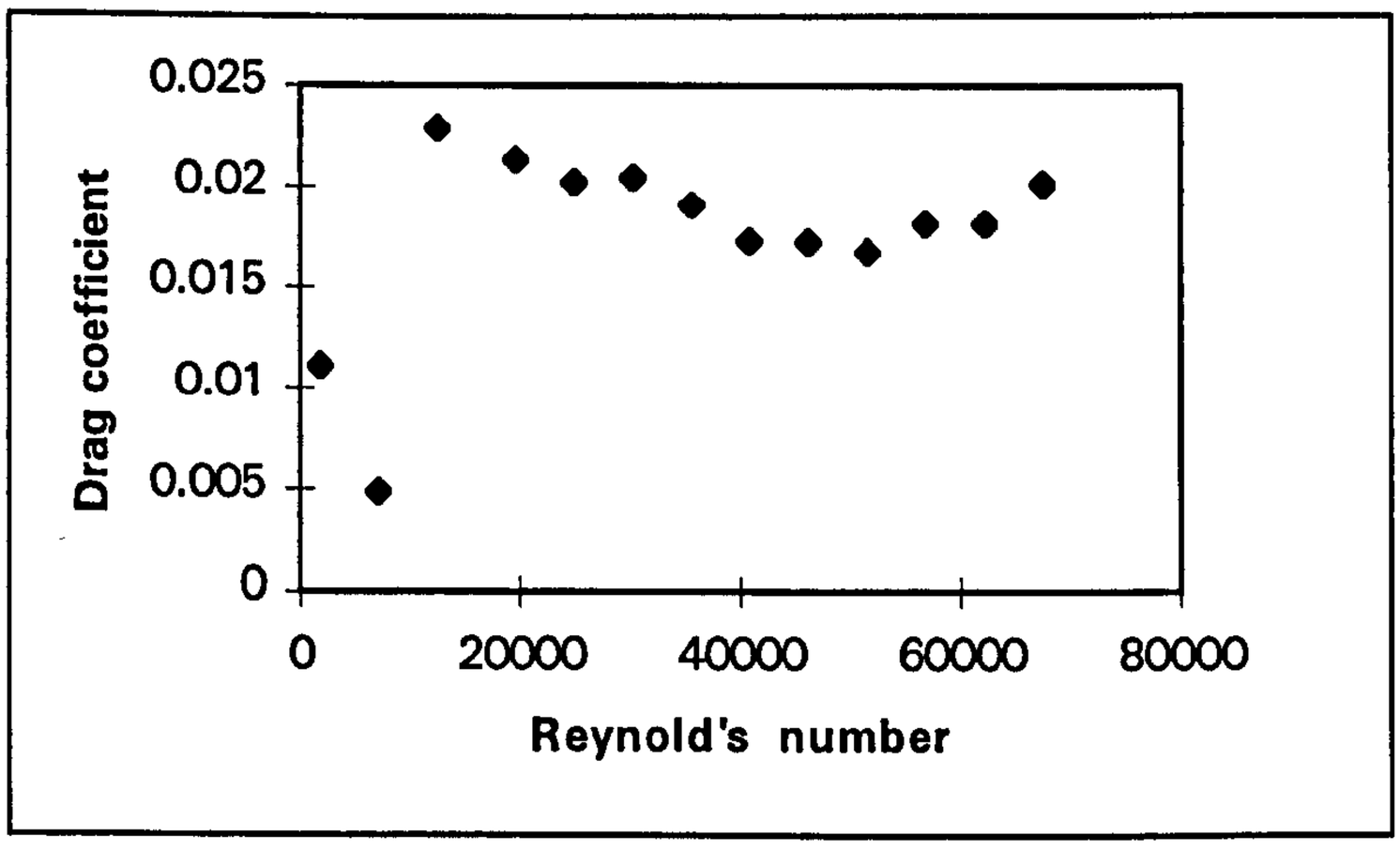

Figure 4.24: Drag co-efficient at different Reynolds numbers for the circular sensor

Figure 4.24 shows the plot between the Reynolds number and C_D. The value of C_D is found to vary for laminar, transitional and turbulent flow. The different ranges of Re for each of these flow regions is indicated in Chapter 1.

4.5.1.3 Comparison with the experimental results

From Table 4.3, it can be observed that C_D varies for laminar, transitional and turbulent flows. For simplification of the calculations, the optimum value of C_D for this particular sensor is found to be 0.0175, by calculating the mean from the different values of C_D obtained. Substituting this value back into Equation 4.9, the actual values for the theoretical strain is obtained. Table A-3 in the Appendix shows these values tabulated against the experimental strain for the different wind speeds. Figure 4.25 shows the experimental and theoretical values of strain plotted versus wind speed showing excellent conformity between the theory and experiments.

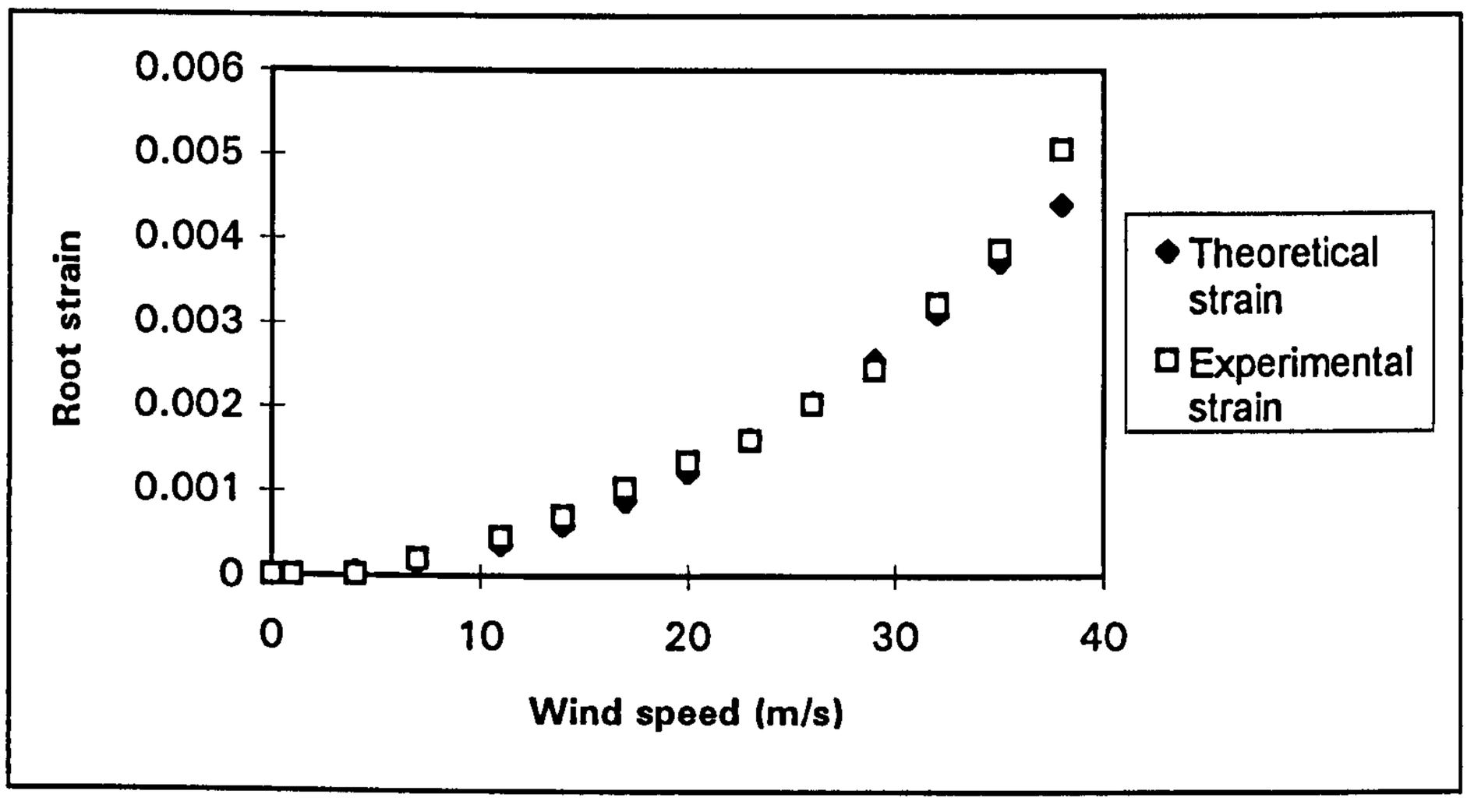

Figure 4.25: Comparison between the theoretical and experimental strain

4.5.2 Square-sectioned rubber beam

The drag coefficient for the square sectioned rubber sensor is deduced in a manner similar to the previous section. C_D is found to have a constant value over a broad range of flow rates.(Figure 4.26). This graph has the same form as those published for C_D's as found in several published sources [4.6].

The differences in the constancy of C_D between Figures 4.24 and 4.26 is because the square-sectioned rubber sensor is a sharp-edged body. The term sharp-edged body is

applied to those bluff objects having an angularity of some sort that disrupts the flow [4.7]. A consequence of this is that such bodies show, in general, little or no Reynolds number effects, as shown in the experiments conducted by the author (Figure 4.26). This result substantiates earlier investigations by other authors. Mott [1.15] has confirmed this discussion and has attributed this to the fact that the bodies with sharp edges always

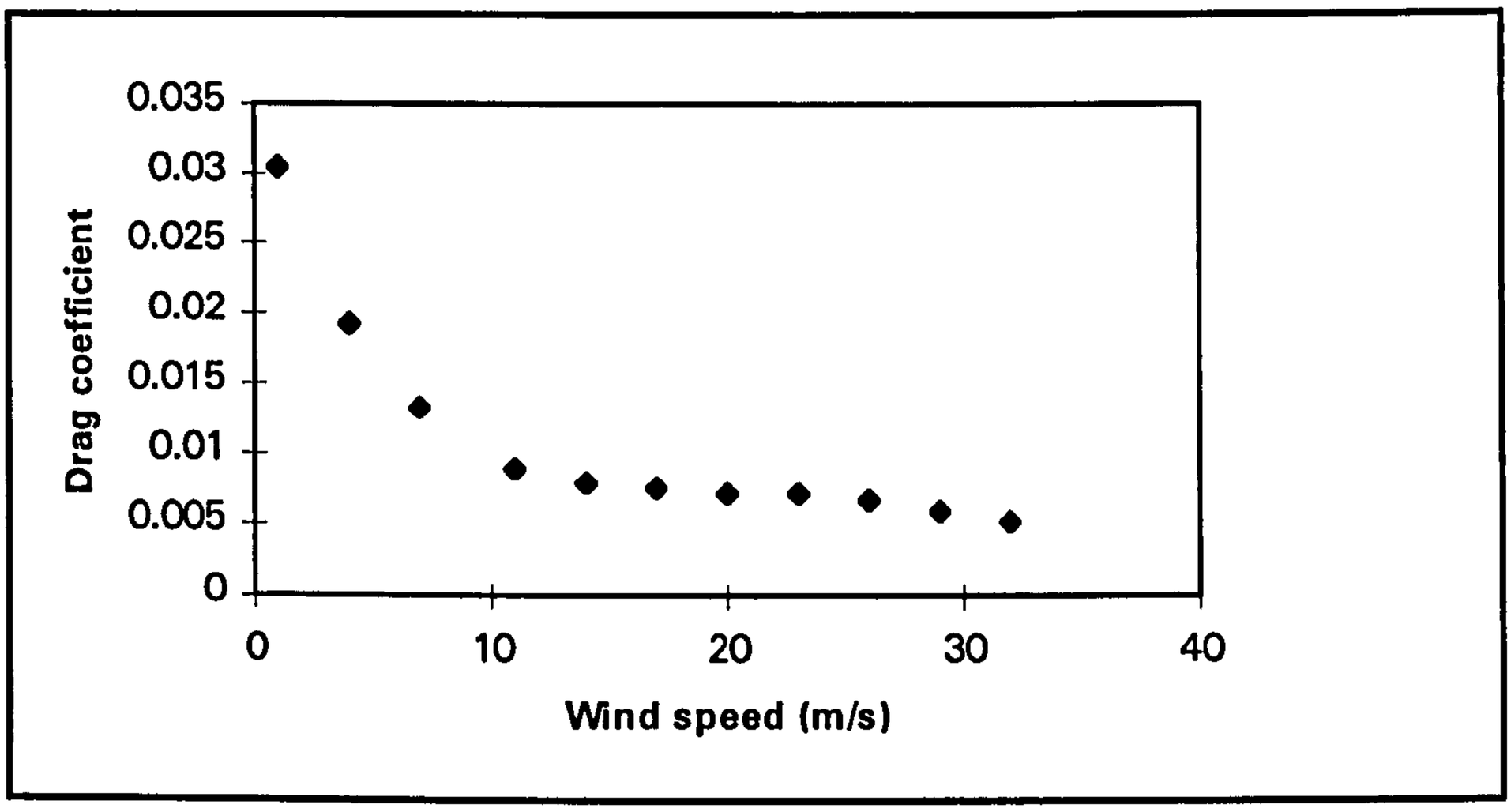

Figure 4.26: Plot of drag coefficient versus wind speed for the square sectioned sensor

cause the boundary layer to separate at the same place. Therefore, the drag coefficient for such sharp-edged bodies are nearly independent of the Reynolds number. On the contrary, the cylindrical sensor is a bluff body. With a non-streamlined or bluff body, the rate of pressure rise from shoulder to tail is so strong that the boundary layer becomes stalled very rapidly, right near the shoulder itself. A broad eddying wake forms downstream of the separation. Therefore, a net pressure drag appears since the average pressure on the forward half of the body exceeds the average pressure on the rearward half. This wake varies with the separation point which is a function of the fluid's velocity. The result is a varying drag coefficient (Figure 4.24) that greatly limits the dynamic flow range of the flowmeter.

4.5.3 Optimisation of the shape and dimensions of the sensing element

With reference to the experimental results described in Section 4.5.2, it can be deduced that a square-sectioned sensing beam is the best choice in terms of a constant C_D for wider flow ranges and directional sensitivity. Ideally, the spherical ball (the drag element) should also be replaced with a flat, circular disk especially in applications where the flow

is directed only on the drag element. This is not so much of a necessity here as the entire sensor is immersed in the air in the wind tunnel, and the principal area of the sensor normal to the flow is both the sensing tube and the spherical ball.

The optimisation of the length (L) and thickness (a) of the beam is derived by referring to the equations which describe the sensitivity and natural frequency of the beam. The sensitivity of the sensor is obtained from Equation 4.9 where the strain, ε, is:

$$\varepsilon \alpha \frac{\rho A V^2 (L-x)}{E a^2 b} \tag{4.17}$$

where L is the length of the beam and (L-x) is the unsupported length of the beam and a is the beam thickness. The target flow sensor is a simple plane beam, supported at one end and free at the other. Its motion can be described by the wave equation for thin beams derived by Sommerfield [4.8] where it has been derived that the natural frequency of the beam is:

$$f_n \alpha \frac{a}{L^2} \sqrt{\frac{E}{\rho}} \tag{4.18}$$

So for high sensitivity, a long, thin beam is required (Equation 4.17) and a short, thick beam (Equation 4.18) is required for high frequency response (high f_n). Therefore, depending on the application, the sensitivity and frequency response can be defined, from which the length and thickness of the beam can be derived and used in the design of the flow sensor.

4.6 ONE DIMENSIONAL WATER FLOW MEASUREMENT

Preliminary measurements to measure the speed of water were made using the same sensor that was used for the one dimensional air flow measurement, described in Section 4.2. Water was pumped into a water tank through a triangular weir. The sensor was positioned so that the water exerted a force on the drag element which caused the sensing beam to deflect. The compression and extension resulting from the deflection was measured by strain gauges attached to the opposite sides of the longitudinal surfaces of the rubber beam. The flow sensor used for this project was calibrated against a current meter having conical cups. The current meter was calibrated against a known standard

which is traceable to the National Bureau of Standards (NBS) and two basic equations were derived for two flow ranges which are:

$$V = 0.2357n + 0.015 \quad \text{for } n < 0.59 \tag{4.19}$$

$$V = 0.2545n + 0.004 \quad \text{for } n \geq 0.59 \tag{4.20}$$

where V is the velocity of the fluid and n is the number of revolutions/second which is displayed by a counter on the meter.

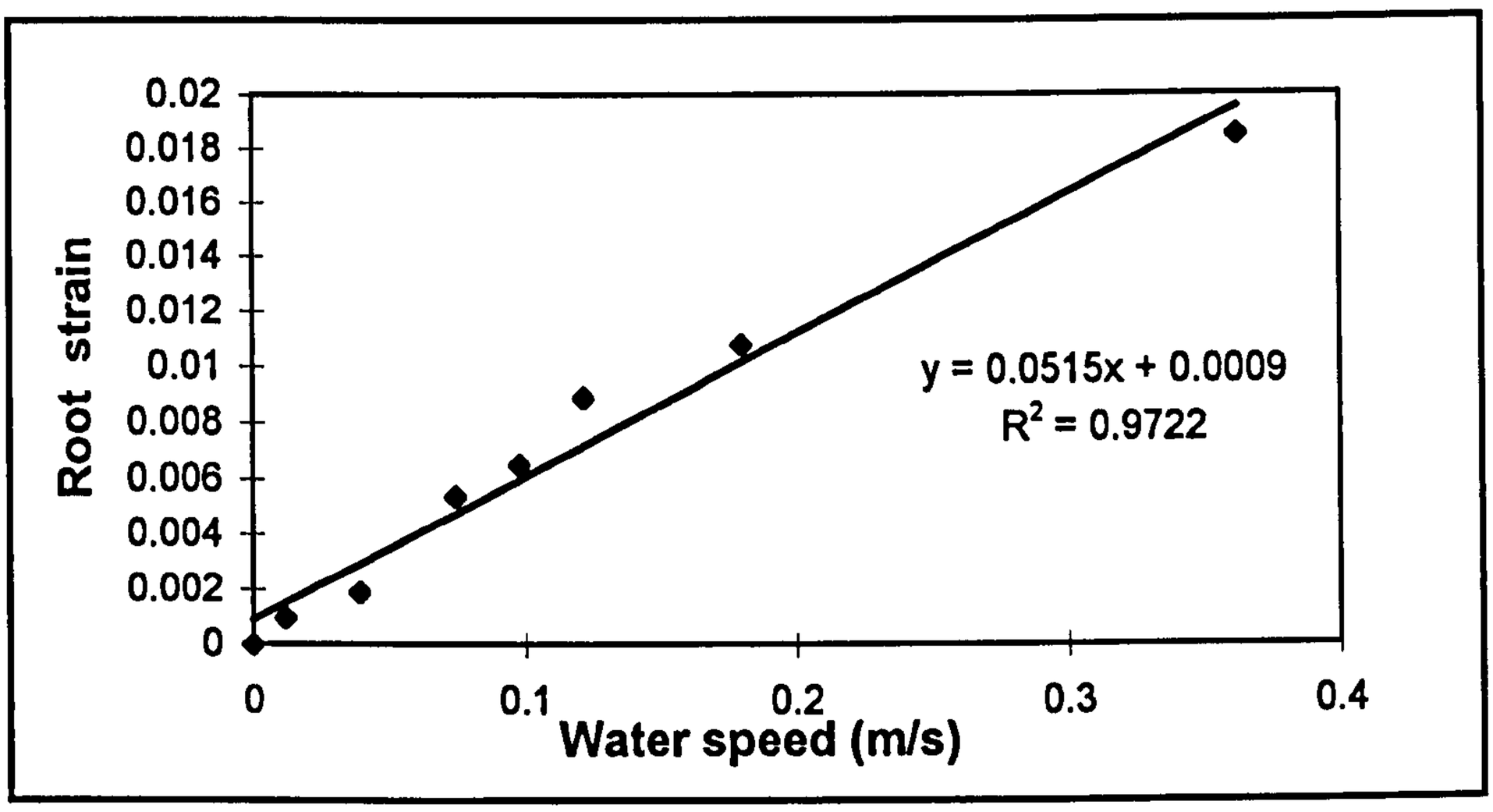

Figure 4.27: One dimensional measurement of water speed

Figure 4.27 shows the calibration curve that was obtained by measuring the strain gauge signals from the target flow sensor and the water speed as indicated by the current meter at different water speeds pumped through the V-notch. Experiments were conducted up to a speed of 0.4 m/s. The sensor had a resolution of 0.017 m/s, sensitivity of 0.0515 ± 0.003 root strain /(m/s) and a linearity of 2.8%. Further experiments could not be performed on this calibration as the current meter that was loaned for this work was reclaimed by the owner.

However, having performed the experiments in the wind tunnel to measure air flow (Figure 4.2) using the same sensor, the author was able to predict the possible range of the flow sensor to measure water flow. Figure 4.28 indicates that for the measured range of air flow, which is 50 m/s (right Y-axis), the corresponding range for water flow would be 1.2 m/s (left Y-axis). Hence, this sensor could measure water speed up to 1.2 m/s and probably even higher, giving a turn-down ratio of 23:1 or higher.

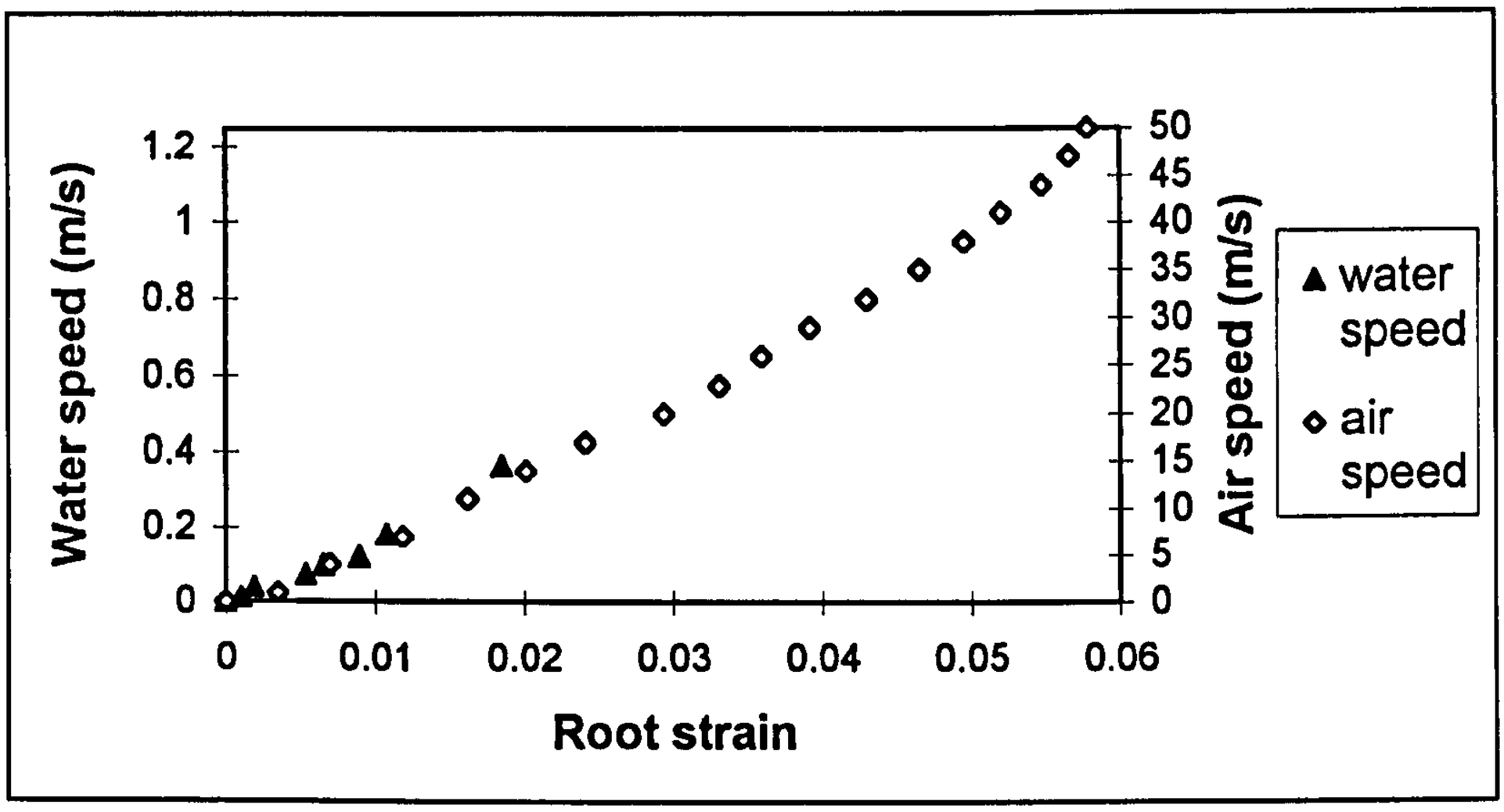

Figure 4.28: Air and Water speed measurements in one dimension

4.7 EXTENDING THE TARGET FLOW SENSOR TO OTHER FLUIDS

The target flow sensor has been calibrated to measure flow of air and preliminary experiments have been performed to measure water speed. One of the major advantages of the target flowmeter is that it can provide a solution with high accuracy for difficult and dangerous fluids, where a calibration with the actual fluid may not be possible. The general formula to measure the unknown fluid, after calibration has been performed on a known fluid, is derived in this section.

As expressed in Equation 4.1, the drag equation is:

$$F = \frac{C_D \rho A V^2}{2} \qquad (4.1)$$

where F is the force exerted on the drag element, C_D is the drag coefficient, A is the characteristic area of the sensor normal to the flow, ρ is the density of the fluid, and V is the velocity of the fluid. For a given flowmeter, the drag coefficient (C_D) and 'A' are constant when correcting to another fluid. What is to be determined is the velocity of the new fluid. Let subscript 'o' refer to the fluid on which the calibration has been performed and subscript 'n' refer to the new fluid.

$$F_o = k_o \rho_o V_o^2 \qquad (4.21)$$

where $k_o = \frac{C_D A}{2}$

$$F_n = k_n \rho_n V_n^2 \qquad (4.22)$$

where $k_n = \frac{C_D A}{2}$

Since $k_o = k_n$ and $F_o = F_n$, Equations 4.21 and 4.22 can be equated.

$$\rho_o V_o^2 = \rho_n V_n^2$$

Solving for V_n yields,

$$V_n = V_o \left[\frac{\rho_o}{\rho_n}\right]^{1/2} \qquad (4.23)$$

Equation 4.23 enables the calibration of the flow sensor in the new fluid after calibrating it in an easy-to-handle fluid by having a knowledge of the densities of the two fluids.

An illustration of this is shown below based on the work done on the electrical target flow sensor. The electrical strain gauge target flow sensor has been used to measure the air flow and the calibration results from that has been used to derive the velocity of water after substituting the values for the density of air (≈ 1 kg/m^3) and that of water (1000 kg/m^3) in Equation 4.23. Substituting the densities of air and water in equation 4.23,

$$V_{water} = V_{air} \times \sqrt{\frac{1}{1000}} = 0.031623 \times V_{air} \qquad (4.24)$$

The calibration values obtained for the velocity of air from the experiments conducted in a wind tunnel are given in Table 4.1. These are substituted in Equation 4.24, along with the densities of the two fluids to obtain the velocity of water. The readings are given in Table A-4 in the Appendix.

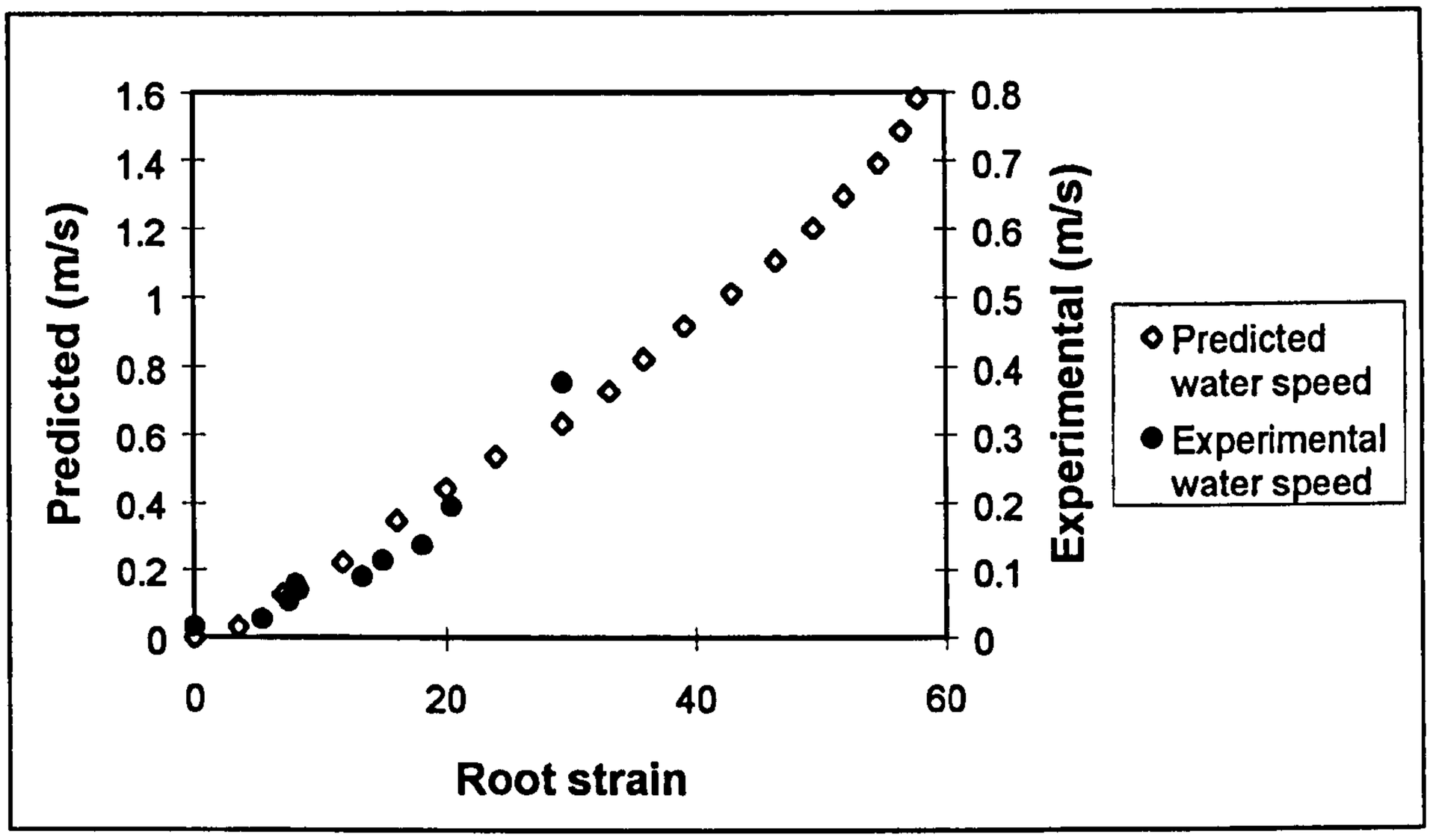

Figure 4.29: Plot showing the observed water speed (experimental) and predicted water speed (from Equation 4.24) versus flow sensor output.

The plots of the observed water speed (experimental) and the predicted water speed (generated from Equation 4.24) versus the sensor output (square root of the microstrain) is shown in Figure 4.29. The correlation between the two plots obtained confirms that Equation 4.23 is valid and it can be used to extend to any other fluid as long as the density of the fluid is known or can be measured using a hydrometer.

4.8 DISCUSSION

The design, optimisation and calibration of a resistive strain gauge target flow sensor to measure one and two dimensional fluid flow has been discussed. The results of the experiments performed in a wind tunnel which enabled the flow sensor to generate wind speed and wind direction irrespective of each other has also been presented. A brief account has been given of the preliminary measurements in a water tank to measure one dimensional water speed. The ability of the flow sensor to provide a solution with high accuracy where a calibration with the actual fluid may not be possible after being calibrated in a safe and easy-to-handle fluid has been investigated. Hence the flow sensor has proved itself as an ideal sensor which is simple and of low cost and compatibility with almost any fluid is possible. The next chapter discusses the continuation of the experimental work to determine the performance characteristics of the flow sensor, thereby making the sensor suitable for commercial exploitation.

CHAPTER 5

PERFORMANCE CHARACTERISTICS OF THE ELECTRICAL STRAIN GAUGE FLOW SENSOR

5.1 INTRODUCTION

The purpose of a measuring instrument is to obtain the true value of the measured variable. The ideal measuring instrument would do this exactly, but in practice, this ideal is never achieved. There is always some uncertainty in the measurement of a variable. There is even some uncertainty in the standards used to calibrate a measuring instrument. For this reason this chapter commences with a brief review of statistics, the subject that deals with uncertainty, from point of view of the experiments on the flow sensor.

The next three sections divide the characteristics of the flow sensor into three categories: operating characteristics, static characteristics, and dynamic characteristics. Operating characteristics include measurement details, operational details, and environmental effects. Static characteristics deal with accuracy when the value of the measured variable is constant or changing very slowly. In contrast, dynamic characteristics deal with the measurement of a variable whose value is changing rather quickly.

Knowledge of the type of data expected is the utmost importance in the selection of test equipment and in the determination of test methods. Extreme errors are possible if the nature of the data and the abilities of the measurement equipment are not properly matched. There are two general classes of data: static and dynamic. In addition, dynamic data can be further subclassified into transient, periodic and random studies. Instrument choice is a compromise between performance characteristics, ruggedness and durability, maintenance requirements and purchase cost. The results from the present work on the electrical strain gauge flow sensor are presented in each section to determine its performance characteristics.

5.2 STATISTICS FROM THE FLOW SENSOR EXPERIMENTS

5.2.1 Brief introduction

The statistics most commonly used to represent the properties of a distribution are the mean, median, mode, standard deviation and standard error. This section summarises the discussions of Davies and Goldsmith (1972). [5.1] There is an uncertainty when we measure the value of a variable. This uncertainty occurs when repeated measurements under identical conditions give different results. The individual measurements of a variable are called *observations*, and the entire collection of observations is called a *sample*. The simplest statistical measure of the sample is the arithmetic average or mean. The sample mean is an estimate of the expected value of the next observation. The mean is computed by summing the observations and dividing by the number of observations. The mean of a sample of n observations is given by the following equation:

$$\text{Sample mean} = \bar{x} = \frac{x_1 + x_2 + x_3 + \ldots\ldots x_n}{n} \qquad (5.1)$$

Median is the central number of the series if the data are arranged in order of magnitude. If n is an odd number, this definition is complete. If n is even it is ambiguous, and in this case it is usual to take the mean of the two central values as the median. Mode is the value of the variate which occurs most frequently.

The mean gives us an estimate of the expected value of an observation, but it gives no idea of the dispersion or variability of the observations. For a measure of variability, we begin by computing the deviation between each observation and the mean.

$$\text{Deviation of observation } x_i = d_i = x_i - \bar{x} \qquad (5.2)$$

The standard deviation is, S_x is a measure of variability.

$$S_x = \sqrt{\frac{d_1^2 + d_2^2 + d_3^2 + \ldots + d_n^2}{n-1}} \qquad (5.3)$$

The standard deviation gives us an idea of the variability of the observations in the sample. If the errors in measurement are truly random and we take a large number of observations, 68% of all observations will be within 1 standard deviation of the mean.

Over 95% of all observations will be within 2 standard deviations of the mean, and almost all samples will be within 3 standard deviations of the mean.

The variance of a population is the mean squared deviation of the individual values from the population mean.

The range is the simplest of all measures of dispersion. It is the difference between the highest and lowest values of the variate in a sample.

Standard error is the error in the mean of a finite data set of measurements.

5.2.2 Results from the present work on the flow sensor

In order to analyse the stability of the response of the flow sensor, Labview was used to acquire and record the voltage signals from the sensor. Figure 5.1 shows the block diagram of the VI used in this analysis. This VI was also able to write to a spreadsheet file for storage and analysis of the data. The VI was programmed to acquire one data point every second and hence 1800 data points in 30 minutes. The wind speed was set at 14 m/s for about 30 minutes and the data was acquired and written to a spreadsheet file.

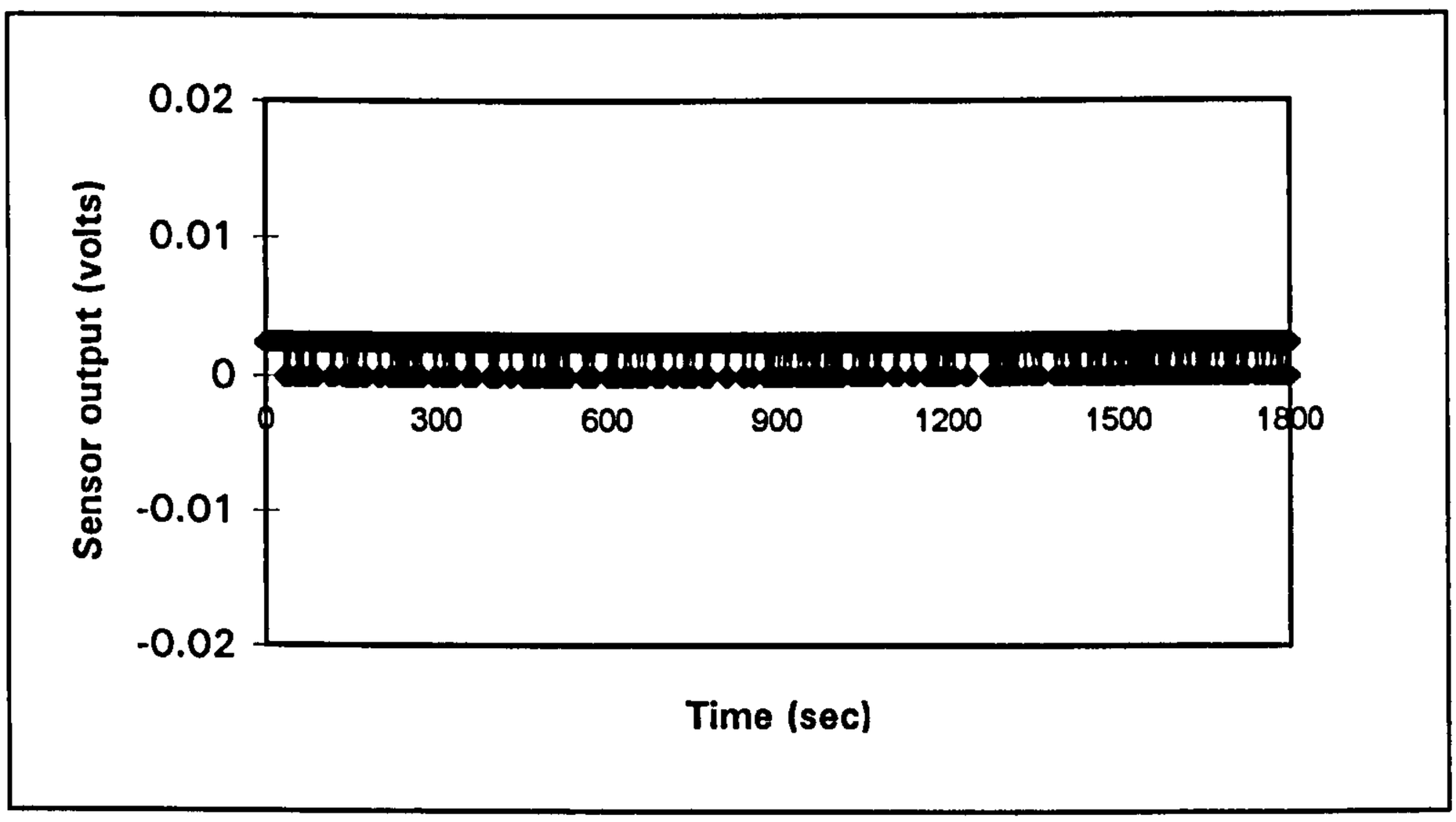

Figure 5.2: Data acquired in 30 minutes

Figure 5.2 shows the plots of the data in root strain for the period of 30 minutes. The summary of the statistics performed on this set of readings is given in Table 5.1. Figure 5.3 shows the histogram obtained for this experiment.

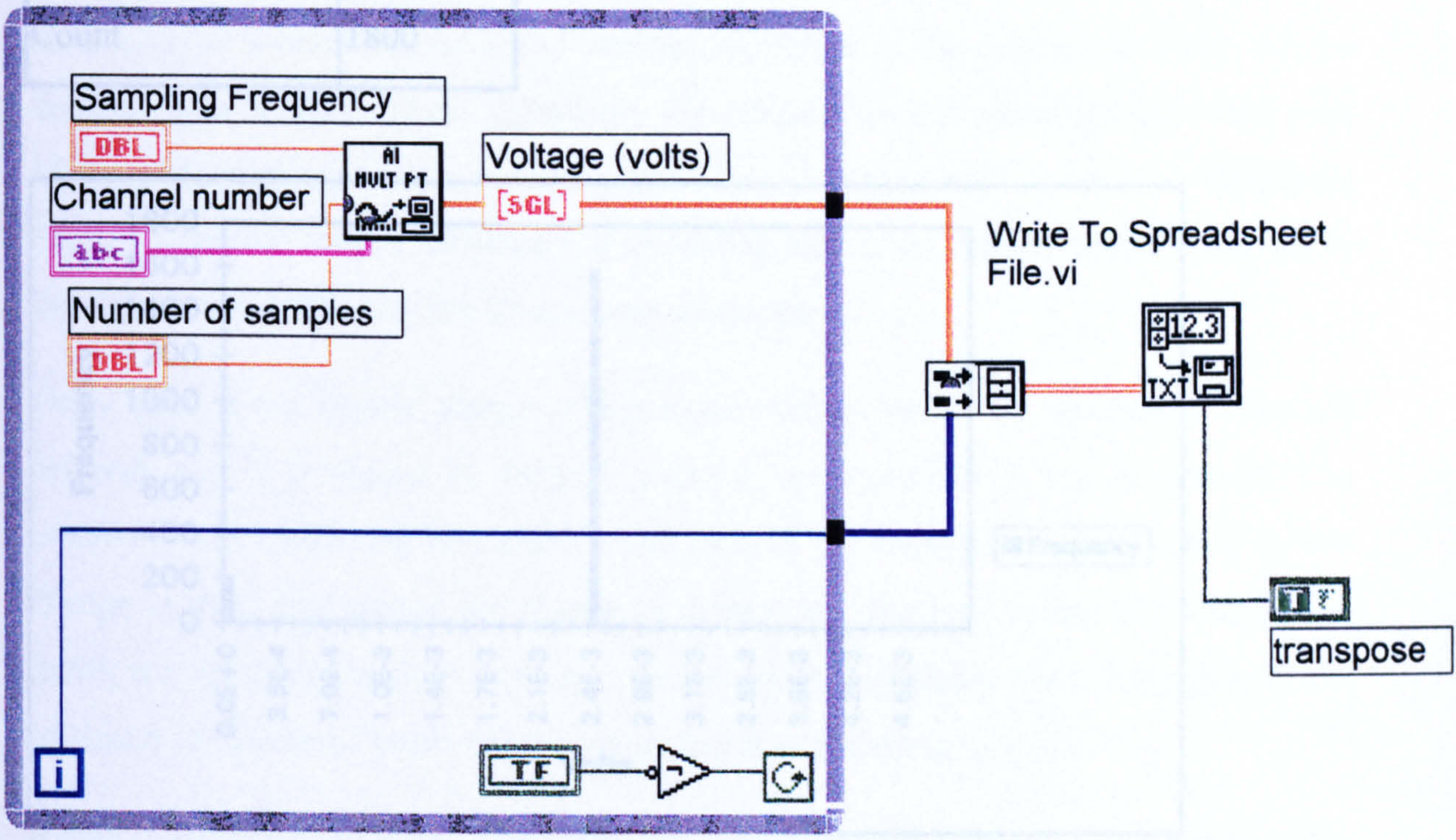

Figure 5.1: Block diagram of the virtual instrument program created with Labview used for the statistical analysis of the flow sensor

Table 5.1: Statistical analysis of the sensor

Mean	0.002168
Standard Error	1.82E-05
Median	0.002441
Mode	0.002441
Standard Deviation	0.000773
Count	1800

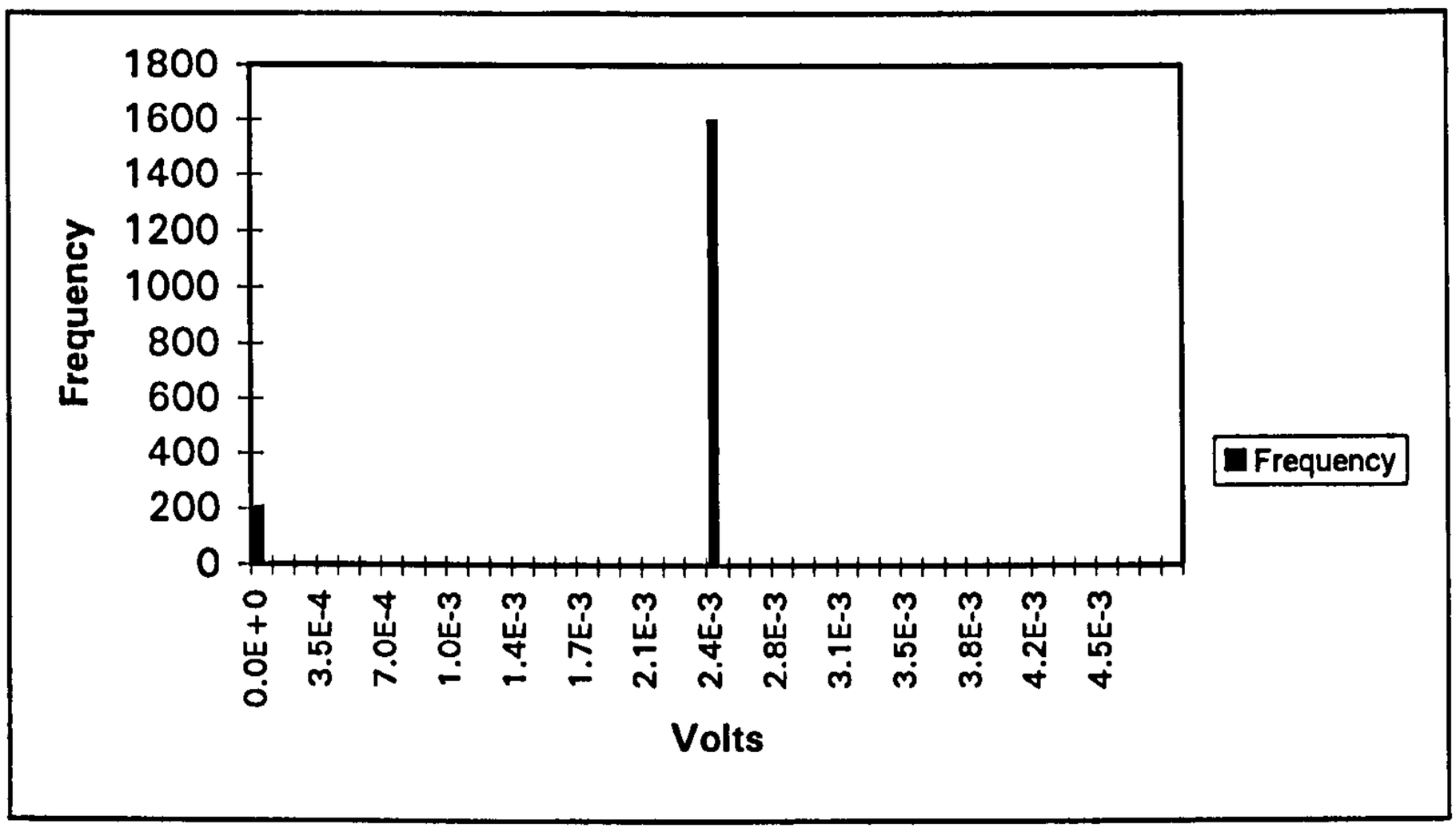

Figure 5.3 : Histogram of Figure 5.1

From the histogram and the table, it can be observed that the mean value is 0.002 volts with a standard error of 1.8E-05. These readings have indicated that the sensor has a very stable response, within the limits of quantization error. The value of 0.0024 occurs most frequently (1597 times of the 1800 measurements taken), and hence that is the value of the median and mode. This experiment was repeated for different wind speeds and each time the sensor indicated a stable response.

5.3 OPERATING CHARACTERISTICS OF THE FLOW SENSOR

Operating characteristics include details about the measurement by, operation of, and environmental effects on the measuring instrument.

5.3.1 Measurement

A measuring instrument can measure any value of a variable within its range of measurement. The range is defined by the lower range limit and the upper range limit. The *range* consists of all values between the lower range limit and the upper range limit. The *span* is the difference between the upper range limit and the lower range limit.

Span = upper range limit - lower range limit

Resolution or *discrimination* is the smallest increment of the measurand which can be detected with certainty by the instrument. *Threshold* of an instrument is a particular case of discrimination and is the minimum input which is necessary to cause a detectable change from zero output. Obviously, a measuring instrument cannot measure changes in the measured variable that are smaller than its threshold.

Dead band is the largest change of the measurand to which the instrument does not respond, and is produced by friction, backlash, or hysteresis in the instrument. The *sensitivity* of a measuring instrument is the ratio of the change in output divided by the change in input that caused the change in output. For the flow sensor reported in this thesis, the sensitivity is given as root strain per (m/s). The sensitivity is a function of the thickness of the elastic beam and the gauge factor of the strain gauges.

Range, resolution, threshold, dead band and sensitivity are different characteristics that relate in different ways to an increment of measurement.

5.3.2 Operation

The *reliability* of a measuring instrument is the probability that it will do its job for a specified period of time under a specified set of conditions. The conditions include limits on the operating environment, the amount of overrange, and the amount of drift of the output. Strain gauge force sensors such as load cells and pressure transducers have been manufactured for many decades. The technology used for these sensors is the same as that for the strain gauge target flowmeter. Shapiro [5.2], in his paper has spelt out the excellent long term stability and reliability of such sensors. "Over the 33 month period that the unit was out in the field, all performance parameters showed outstanding stability. The full scale sensitivity showed an average change of -0.055% in 6 months. The combined error (linearity, hysteresis, and repeatability), zero balance and non-return

to zero showed no measurable changes over the $2\frac{3}{4}$ year time span." This clearly demonstrates the outstanding stability and accuracy achievable by the bonded strain gauge sensor.

Overrange is any excess in the value of the measured variable above the upper range limit or below the lower range limit. When an instrument is subjected to an overrange, it does not immediately return to operation within specifications when the overload is removed. A period of time called the recovery time is required to overcome the saturation effect of the overload. The overrange limit is the maximum overrange that can be applied to a measuring instrument without causing damage or permanent change in the performance of the device. Thus one reliability condition is that the measured variable does not exceed the overrange limit.

Drift is an unspecified change over a specified period of time. Zero drift is the variation in an instrument output which is not caused by any change of input, when the measured variable is held constant at its lower limit; it may be caused by internal temperature changes and component instability. Sensitivity drift is a change in the sensitivity of the instrument over the specified period. Zero drift raises or lowers the entire calibration curve of the instrument. Sensitivity drift changes the slope of the calibration curve. The reliability conditions specify an allowable amount of zero drift and sensitivity drift.

5.3.3 Environmental effects

The environment of a measuring instrument includes ambient temperature, ambient pressure, fluid temperature, fluid pressure, electromagnetic fields, acceleration, vibration and mounting position. The operating conditions define the environment to which a measuring instrument is subjected. The operative limits are the range of operating conditions that will not cause permanent impairment of an instrument.

5.3.4 Operating characteristics of the flow sensor:

Table 5.2 gives the operating characteristics of the electrical strain gauge flow sensor described in Chapter 4 with particular references to the experimental prototypes 1,4 and 5.

Table 5.2 : Operating characteristics of the resistive strain gauge flow sensor

Characteristics	Experimental prototype 1	Experimental prototype 4	Experimental prototype 5
Lower Range limit	0.8 m/s	1 m/s	1m/s
Upper range limit	23 m/s	40 m/s	30 m/s
Span	22.2 m/s	39 m/s	29 m/s
Resolution	0.4 m/s	1.9 m/s	0.8 m/s
Sensitivity	0.0065 ± 0.0001 root strain/(m/s)	0.0016 ± 0.0001 root strain/(m/s)	0.0024 ± 6 E-05 root strain/(m/s)
Overrange	50 m/s	50 m/s	50 m/s

5.4 STATIC CHARACTERISTICS OF THE FLOW SENSOR

Accuracy of measurement is one consideration in the choice of instrument for a particular application. Other parameters such as sensitivity, linearity, hysteresis are further considerations. These attributes are collectively known as the static characteristics of instruments. The various static characteristics of the flow sensor are defined in the following subsections. [5.3, 5.4].

5.4.1 Accuracy

Accuracy is the degree of conformity of the output of a measuring instrument to the true value of the measured variable as determined by some type of standard. A statement of accuracy may be expressed in terms of uncertainty and a confidence level. The interval within which the true value of a measured quantity is expected to lie, with a stated probability, is called uncertainty. The confidence level associated with the uncertainty indicates the probability that the interval quoted will include the true value of the quantity being measured. The rated accuracy of the strain gauge flow sensor is determined by the statistical summation of all random and systematic errors.

Random errors, sometimes called precision or experimental errors, are those which cause a variation in repeated measurements even when the value of the quantity being measured does not change. Examples of random errors are repeatability, hysteresis and linearity. Systematic errors, sometimes called bias errors, are temperature and pressure effects and the calibration of the flowmeter itself. These errors can generally be numerically corrected. That is, if the temperature and pressure effect data are recorded for the flowmeter, the data can be used to correct the electrical output. With today's technology, these characteristics can be programmed into a real-time computer and the output corrected immediately. There is a third form of error during a measurement called a spurious error. *Spurious errors* are clearly mistakes or blunders which invalidate a result, such as transposing numbers when recording the data. There is no way of dealing with spurious errors except to discard the results associated with them, but random and systematic errors give rise to corresponding kinds of uncertainty in the result. These concepts are illustrated in Figure 5.4.

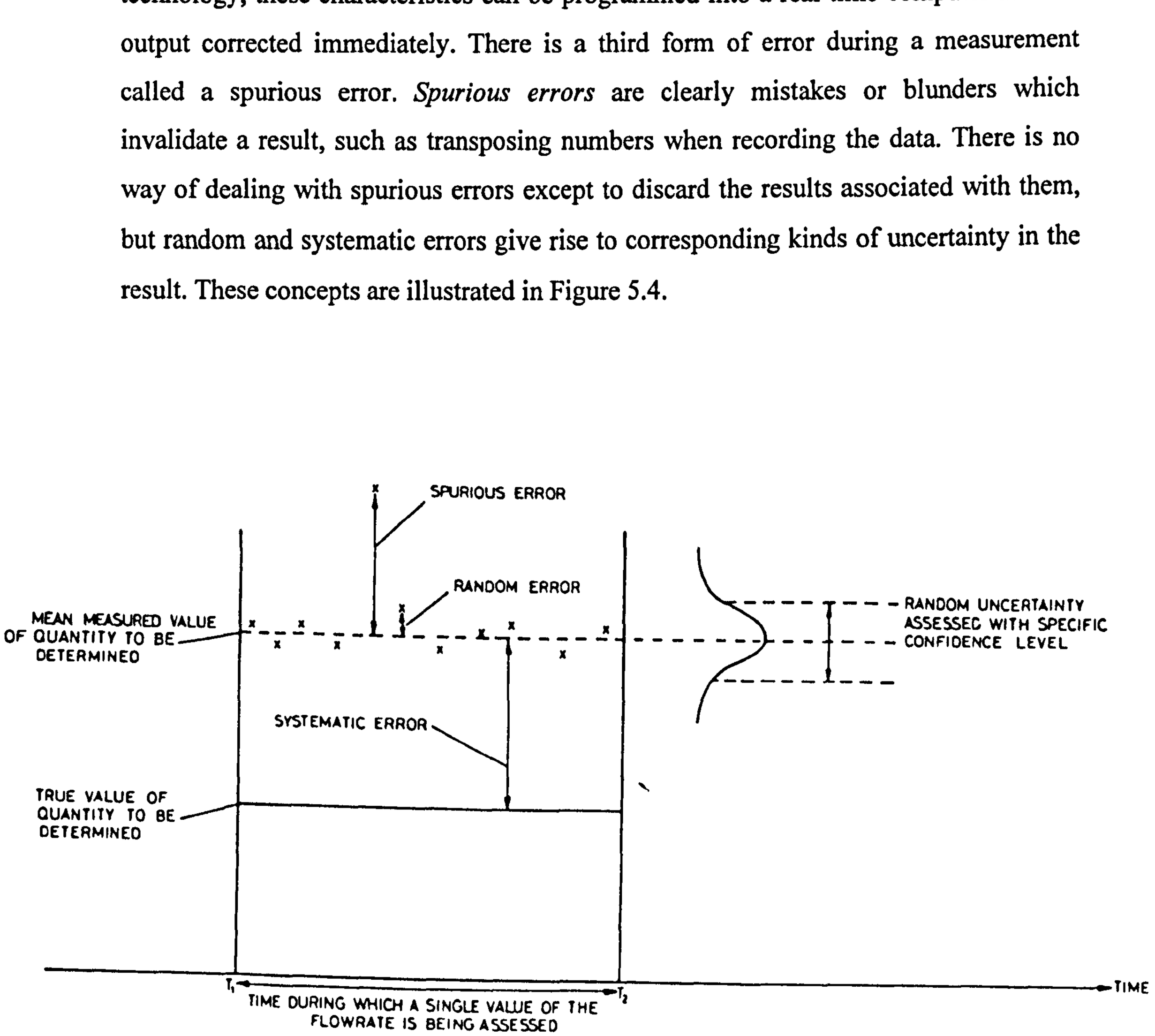

Figure 5.4: Illustrating error and uncertainty

One way of reducing the uncertainty in the flow rate measurement is by repeating the measurement and reporting the average value as the result. The test is repeated a number of times, and the accuracy is given as the maximum positive and negative error (deviation from the ideal value).[5.5]

5.4.2 Repeatability/Reproducibility

The terms repeatability and reproducibility mean approximately the same but are applied in different contexts. Repeatability describes the closeness of output readings when the same input is applied repetitively over a short period of time, with the same measurement conditions, same instrument and observer, same location and the same conditions of use maintained throughout. Repeatability(r) has been defined as[5.6]:

$$r = 2.83\ \sigma_r \qquad (5.4)$$

where σ_r is the standard deviation of the measurement results. For the flow sensor, the standard deviation is 0.00077 (from Table 5.1) and hence its repeatability is 0.022.

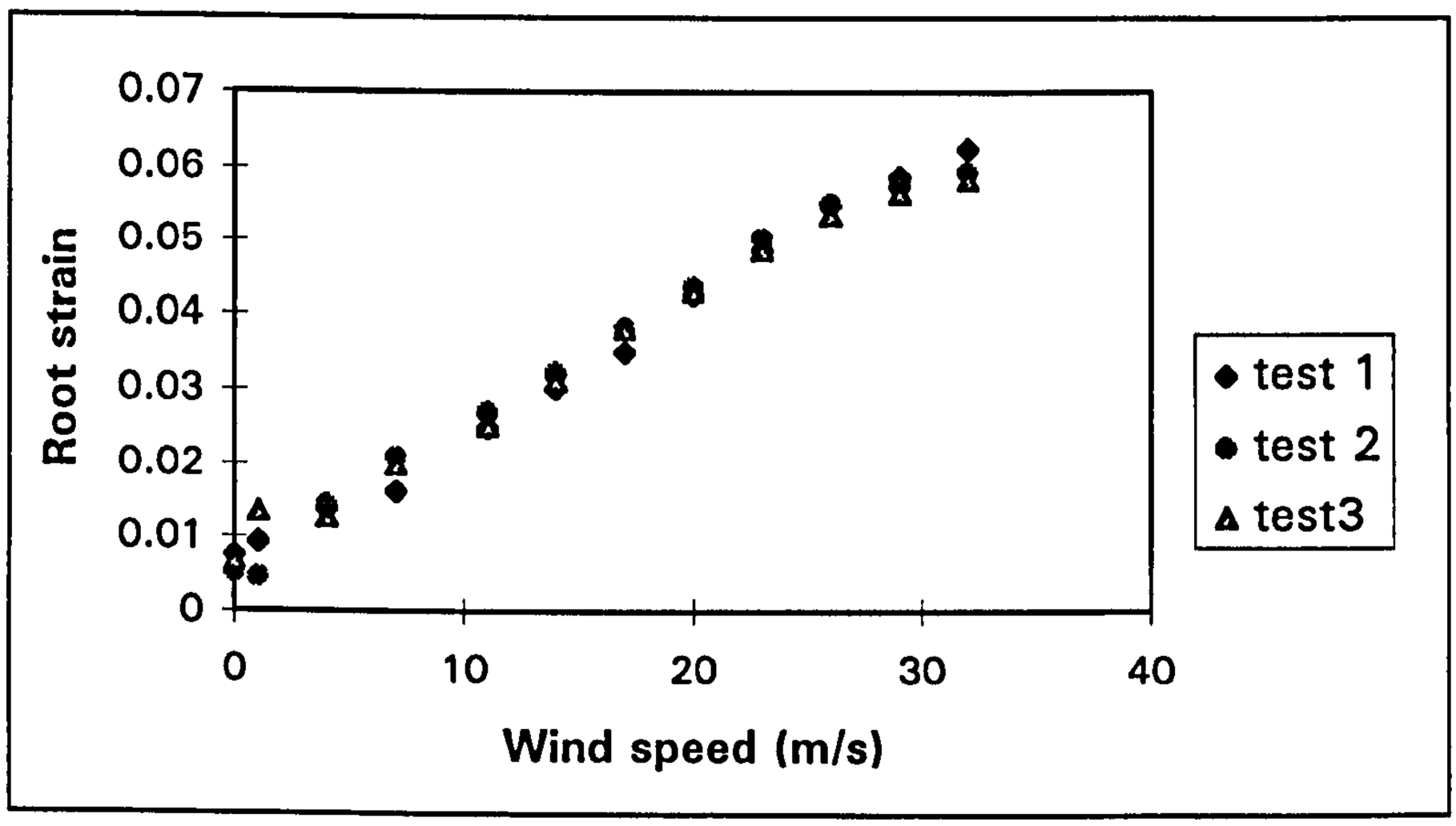

Figure 5.5: Reproducibility tests for the experimental prototype sensor 5

Reproducibility describes the closeness of output readings for the same input when there are changes in the method of measurement, observer, measuring instrument, location, conditions of use and time of measurement. Both terms thus describe the spread of output readings for the same input. Figure 5.5 shows the results of the experiments performed on the sensor described in Section 4.4.4. This sensor has a very good reproducibility of 0.4%.

5.4.3 Hysteresis

This is the algebraic difference between the average errors at corresponding points of measurement when approached from opposite directions (that is, increasing as opposed to decreasing values of the input.) It may be caused by backlash, friction or the characteristics of magnetic materials[5.7]. For the sensor described in Section 4.4.4, the wind speed was steadily increased from 0 to 35 m/s and then steadily reduced to 0 m/s. The co-incidence between the loading and unloading curves of Figure 5.6 indicates a very stable sensor with negligible hysteresis at higher values of wind speeds.

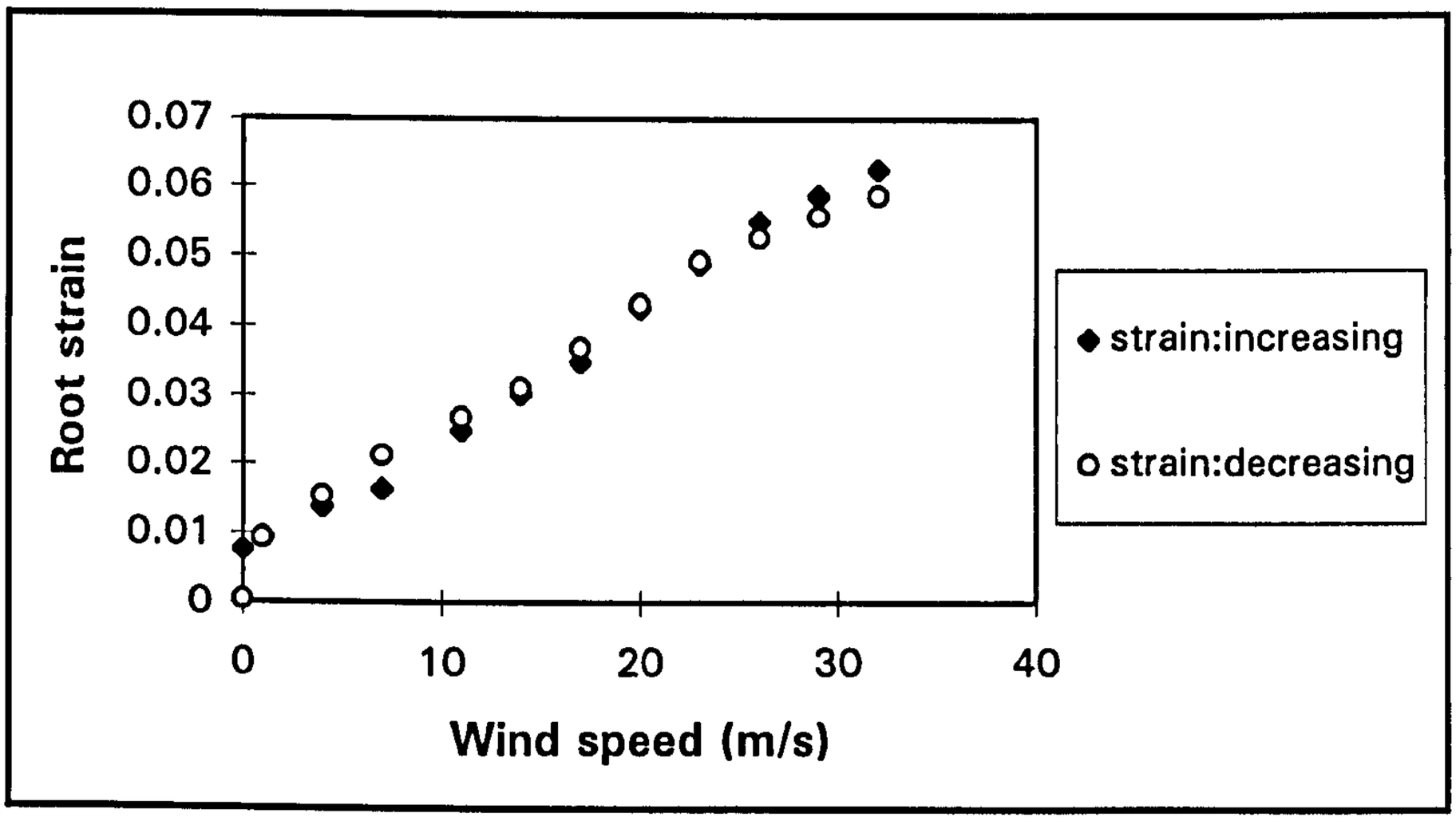

Figure 5.6: Test for hysteresis for the experimental prototype sensor 5

5.4.4 Linearity

The ideal measuring instrument would produce a perfectly straight calibration curve. On a graph of percent input versus percent output, the ideal straight line would pass through the points (0,0) and (100,100). The ideal never actually occurs, and the closeness of the calibration data to a straight line is called the linearity of the measuring instrument. The most common types of linearity are independent linearity, terminal-based linearity, zero-based linearity, and least-squares linearity. [5.8] The linearity of the target flowmeter is usually expressed as the maximum percent deviation of the calibration data from a zero-based straight line.

5.5 DYNAMIC CHARACTERISTICS OF THE FLOW SENSOR

Dynamic characteristics describe the performance of a measuring instrument when the measured variable is changing rapidly. Most sensors do not give an immediate, complete response to a sudden change in the measured variable. A measuring instrument requires a certain amount of time before the complete response is indicated by the output. The amount of time required depends on the resistance, capacitance, mass or inertance, and dead time of the measuring instrument. Dynamic characteristics are stated in terms of the step response, ramp response, and frequency response of the measuring instrument.

5.5.1.Step response

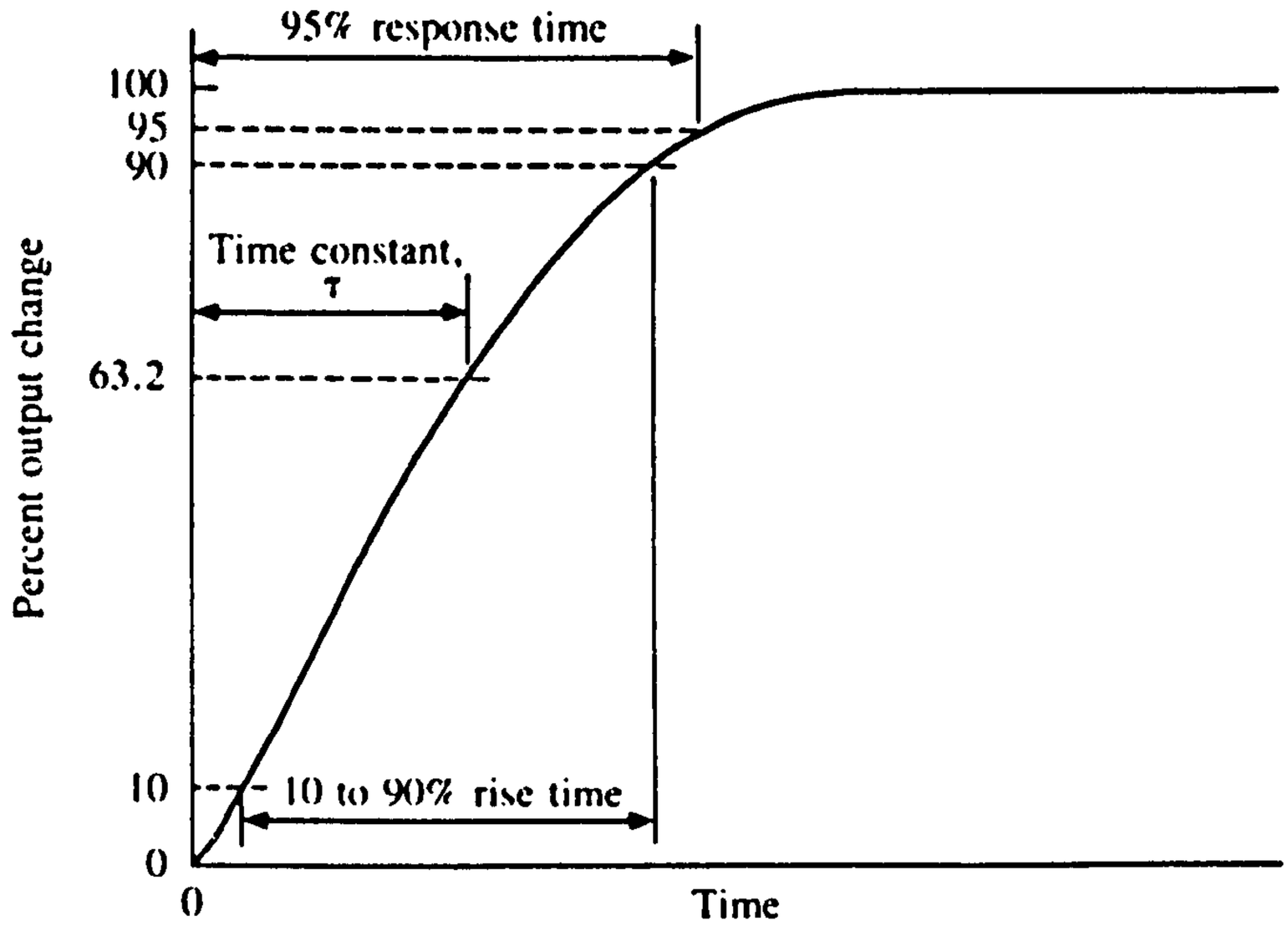

Figure 5.7: Typical step response curve for an overdamped or critically damped measuring instrument. The response is stated in terms of the response time and the rise time.

The response of a measuring instrument to a step change in the measured variable is often used to define its dynamic characteristics. The step response of an instrument can be classified as overdamped, critically damped, or underdamped. The step response of over or critically damped instruments is stated in terms of response time and rise time.

The step response of underdamped instruments is stated in terms of rise time, overshoot and settling time.

A typical over or critically damped step response curve is shown in Figure 5.7. In the graph, the output is normalised by using the percent of output change instead of actual output values. Terminology applied in terms of the percent of output change can easily be applied to step changes of any given size. The *response time* is the time required for the output to reach a designated percentage of the total change. The percentage is stated as a prefix. The 95% response time is the time required for the output to reach 95% of the total change. The 63.2% response time is given the special name time constant and symbol `τ`. *Rise time* is the time required for the output to go from a small percent change to a large percent change. The two percentages are stated as a prefix. Thus a 10 to 90% rise time is the time required for the output to go from 10% to 90% of the total change. A 5 to 95% rise time is the time required for the output to go from 5% to 95% of the total change. If the percentages are omitted, they are assumed to be 10% and 90%. The rise time is a function of the speed of the response as well as the natural frequency of the system.[5.9]

A typical underdamped step response curve is shown in Figure 5.8. The rise time is the same as it was for the over or critically damped response. *Overshoot* is the maximum height of the curve measured above the 100% change line. This is a function of the damping of the system, and for unstable systems excessive overshoot is an immediate indication of an underdamped and potentially unstable situation. Should the damping be so great as to prevent overshoot completely, the system will be sluggish and contain excessive lag in the range of its normal response. Transient measurements permit the complete understanding of the system response, and make possible the design of systems with critical damping, which is the proper compromise between zero overshoot with its attendant lag and the damped oscillations associated with excessive overshoot. The *settling time* is the time it takes for the response to remain within a small band above and below the 100% change line. The 2% settling time is shown in Figure 5.8.

Underdamped responses are also stated in terms of the natural frequency and the damping ratio. The natural frequency is the reciprocal of the period of the oscillation (shown in Figure 5.8). The *damping ratio* (ζ) is related to the rate at which the

oscillations diminish. It is a number that determines the type of damping of a second-order system. The response is underdamped if $\zeta < 1$, critically damped if $\zeta = 1$, and overdamped if $\zeta > 1$.

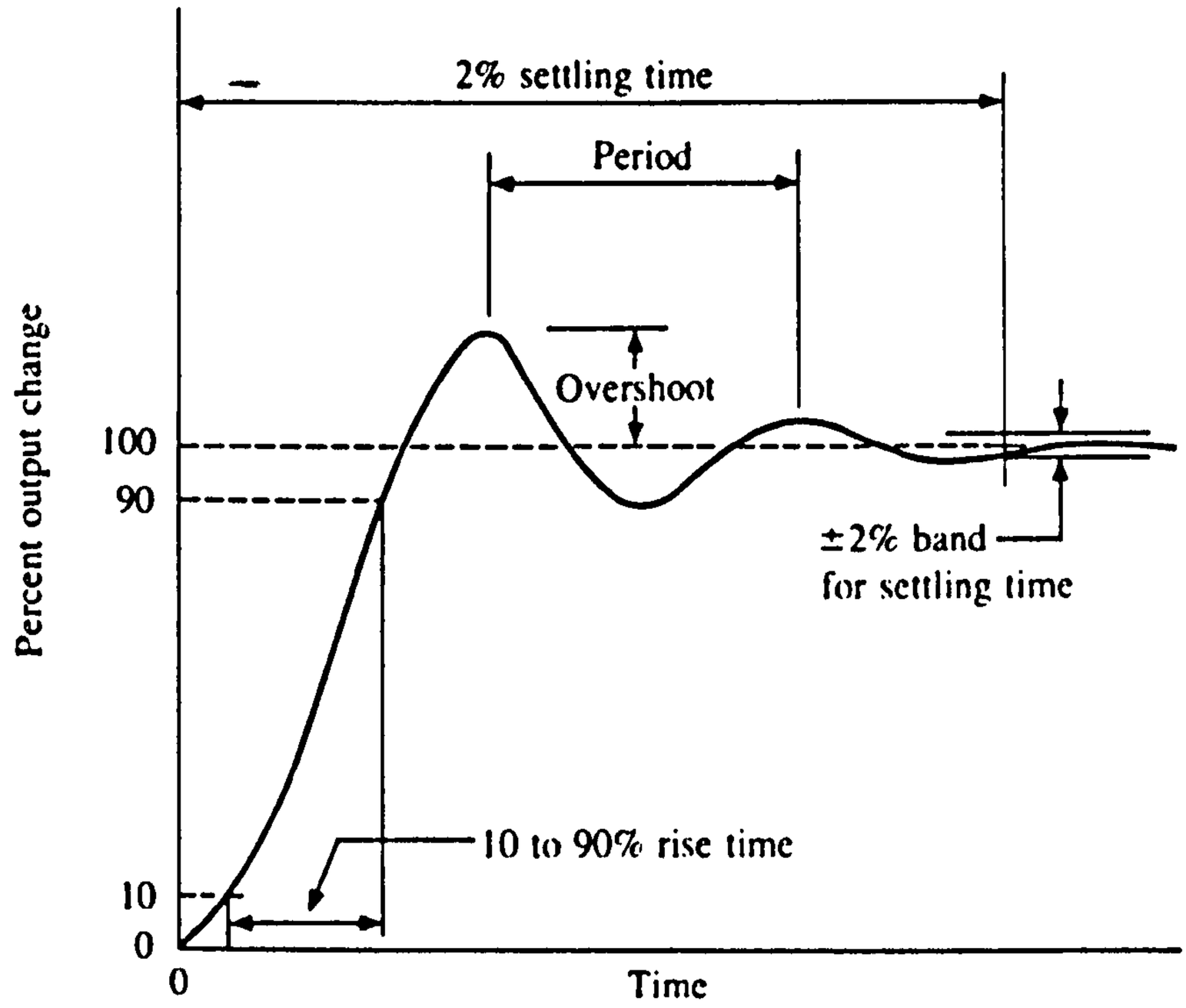

Figure 5.8: Typical step response curve for an underdamped measuring instrument. The response is stated in terms of the rise time, overshoot and settling time.

The standard equation for a second order system is given by:

$$\frac{q_o}{q_i} = \frac{K}{D^2/\omega^2 + 2\zeta D/\omega + 1} \qquad (5.5)$$

where q_o is the output reading, q_i is the measured quantity, D is an operator and replaces d/dt, K is the static sensitivity, ω is the undamped natural frequency and ζ is the damping ratio. Any instrument whose response can be described by Equation 5.5 is known as a second order instrument. If Equation 5.5 is solved analytically, the shape of the step response obtained depends on the value of the damping ratio parameter ζ. The

output responses of a second-order instrument for various values of ζ are shown in Figure 5.9.

For case A where $\zeta = 0$, there is no damping and the instrument output exhibits constant amplitude oscillations when disturbed by any change in the physical quantity measured. For light damping of $\zeta = 0.2$, represented by case B, the response to a step change in input is still oscillatory but the oscillations gradually die down. A further increase in the value of ζ reduces oscillations and overshoot still more, as shown by curves C and D, and finally the response becomes very overdamped as shown by curve E where the

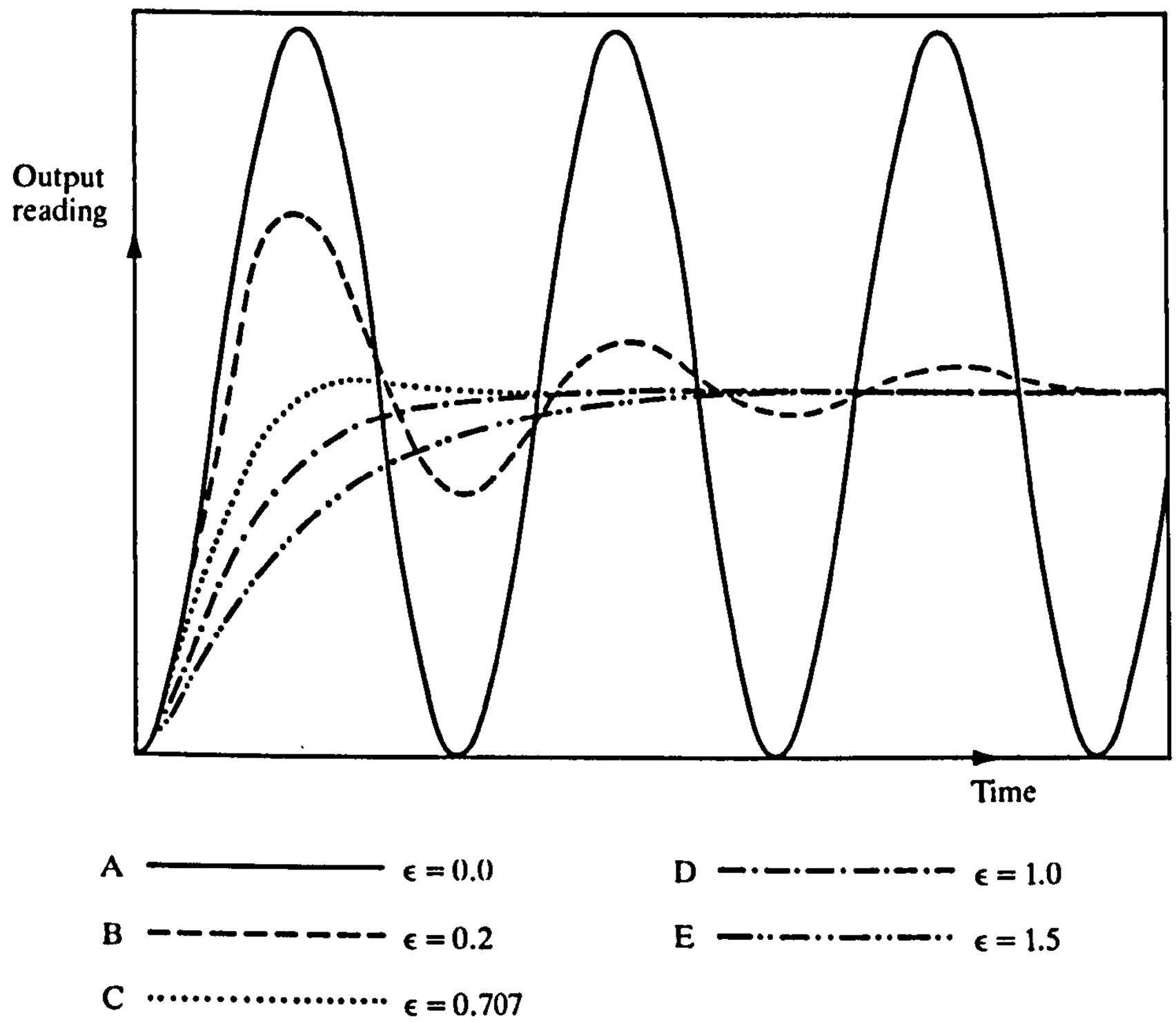

Figure 5.9 : Responses of second order instruments. (Courtesy: Morris A S, 1993)

output reading creeps up slowly towards the correct reading. The extreme response curves A and E are grossly unsuitable for any measuring instrument. If an instrument

were to be only ever subjected to step inputs, then the design strategy would be to aim towards a damping ratio of 0.707, which gives the critically damped response C. Unfortunately, most of the physical quantities which instruments are required to measure do not change in the mathematically convenient form of steps, but rather in the form of ramps of varying slopes. As the form of the input variable changes, so the best values of ζ varies, and the choice of ζ becomes a compromise between those that are best for each type of input variable behaviour anticipated. Commercial second-order instruments are generally designed to have a damping ratio somewhere in the range 0.6-0.8.

5.5.2 Wind tunnel experiments

An open ended wind tunnel with a maximum wind speed of 33 m/s using a specially designed shutter arrangement was used for investigating the transient response of the sensor. The working section of this wind tunnel discharges direct to the atmosphere. Labview was used to acquire the response and transfer to a spreadsheet file. Figure 5.10 shows the block diagram of the VI used for this analysis. F_h is the high cut-off frequency which was set to 5 Hz. The sample rate (sampling frequency,f_S) was set at 100 and the number of samples, $N_S = 1000$, so that the actual sample period was $1/f_S = 0.01$ seconds i.e. data is acquired every 0.01 seconds for a period of $N_S/f_S = 10$ seconds. The sensor was mounted in the wind tunnel and with the shutter closed, the wind tunnel was set at a particular wind speed. Since the shutter was closed, the sensor did not undergo any deflection. When the shutter was opened, the deflection of the sensor was detected and analysed using the VI.

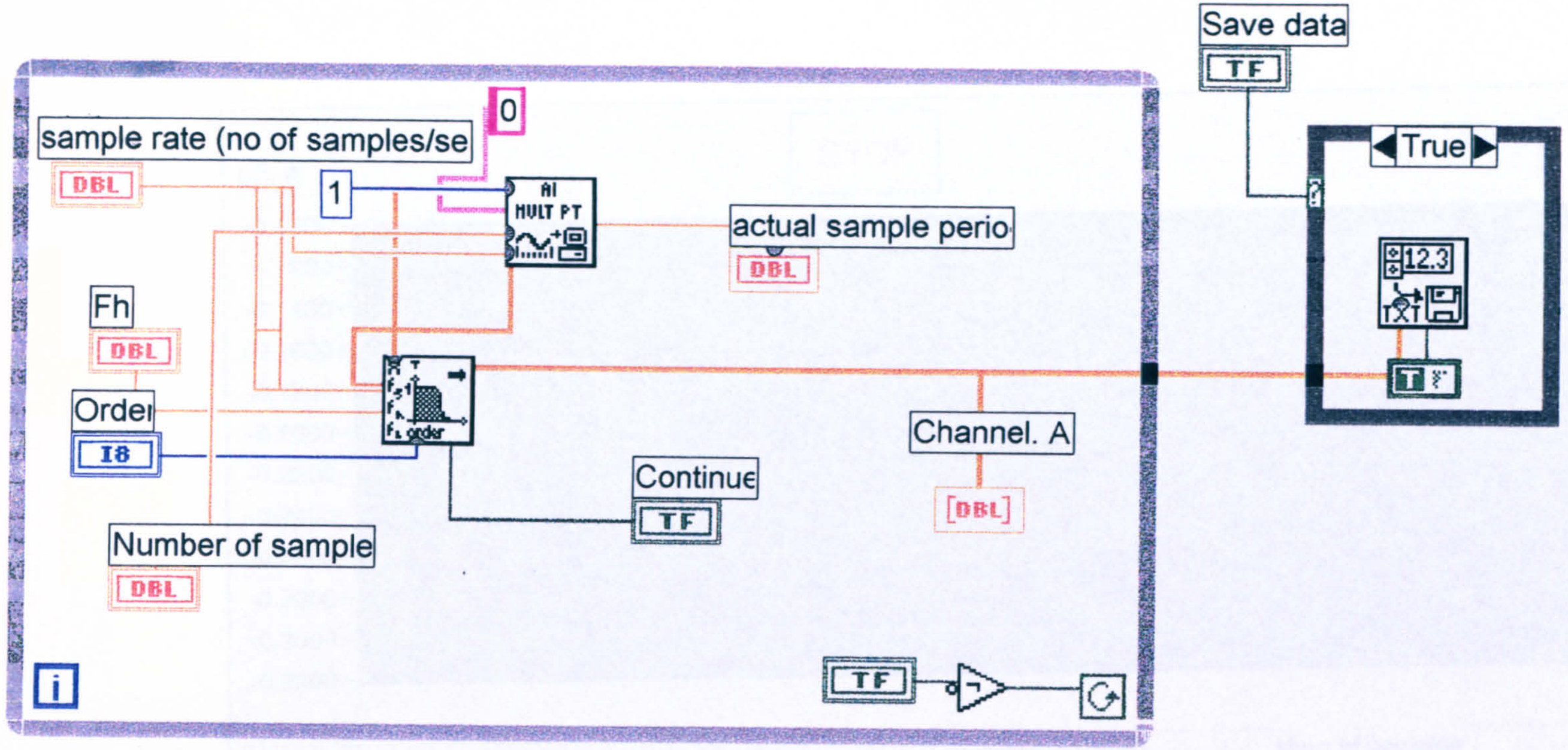

Figure 5.10: Block diagram of the virtual instrument program created to obtain the transient response of the sensor

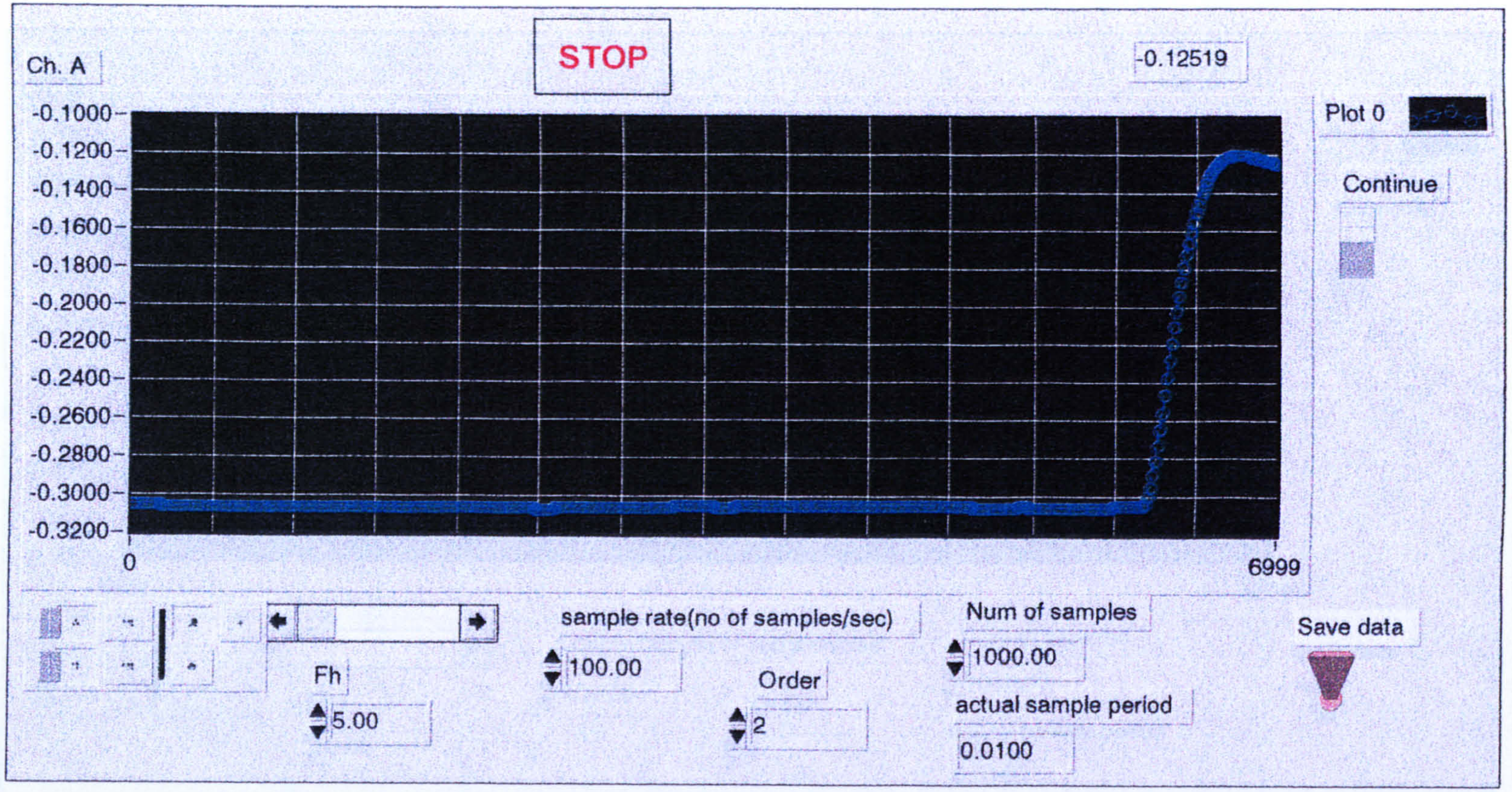

Figure 5.11a: Front panel of the virtual instrument program indicating the response of the electrical strain gauge flow sensor to a step input in an open ended wind tunnel.

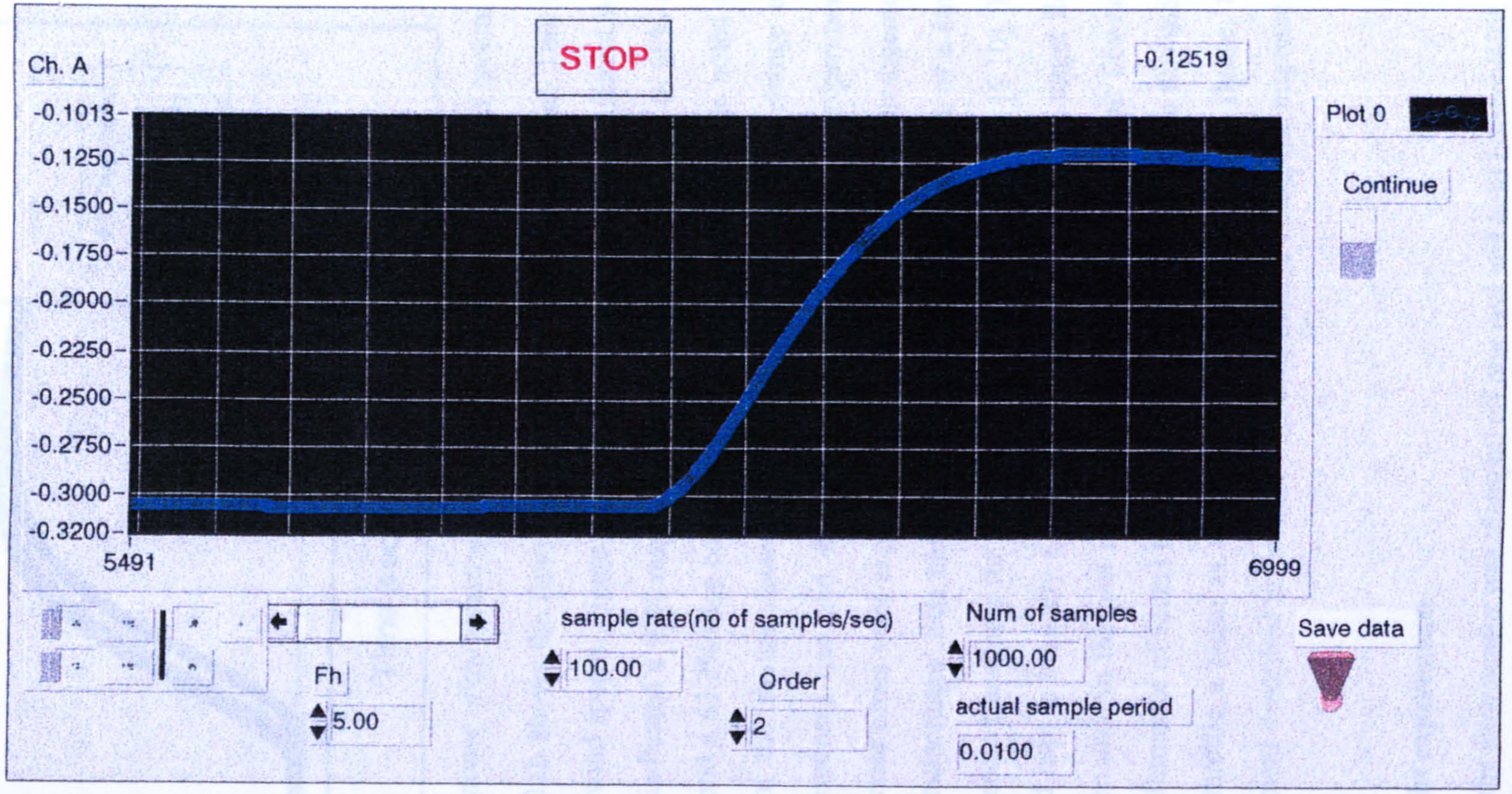

Figure 5.11b: The sensor response, from the wind tunnel experiment, by zooming into the area of interest of Figure5.11a.

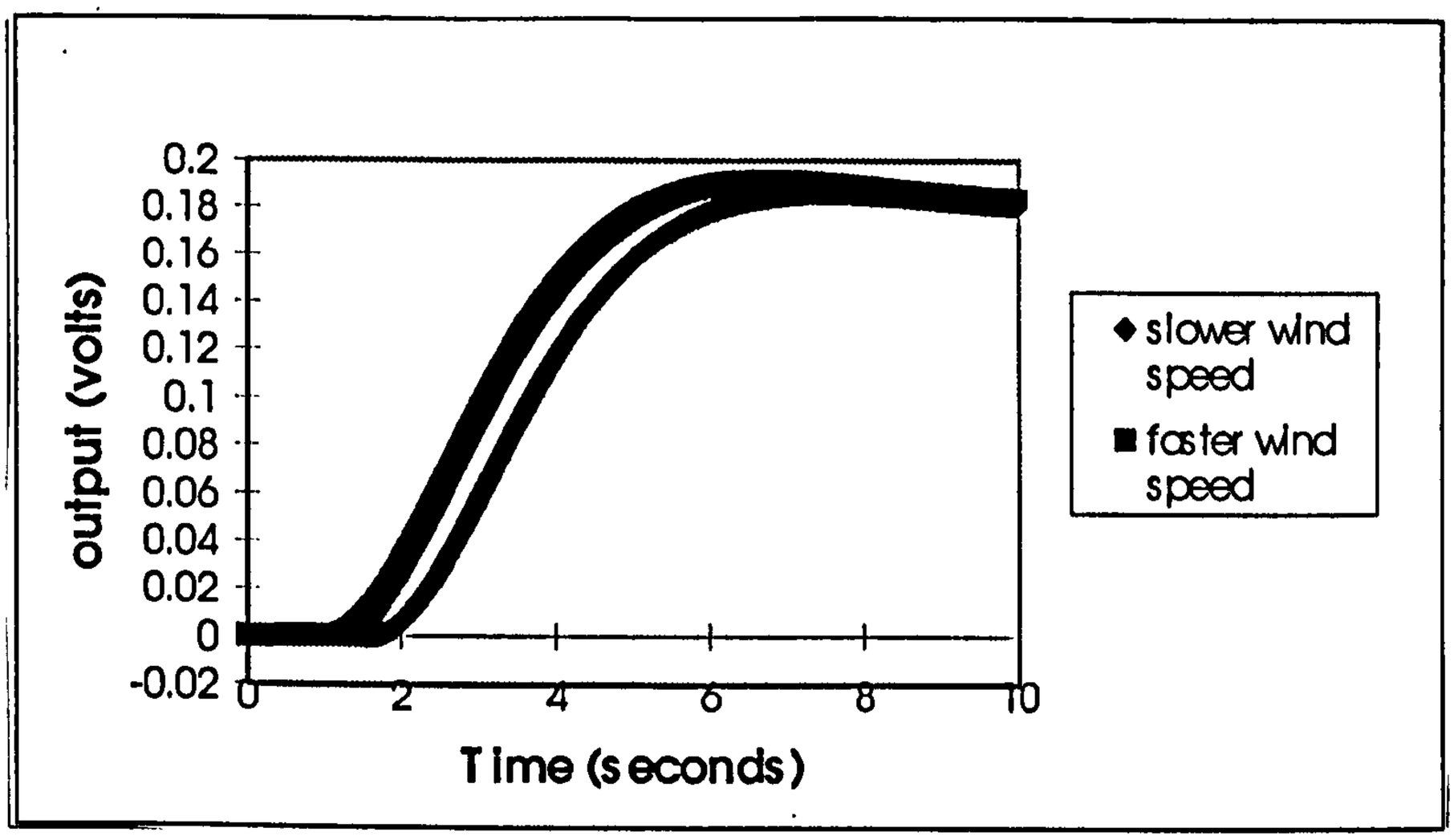

Figure 5.12: Response of the resistive strain gauge flow sensor at 2 wind speeds.

Figure 5.11a and 5.11b shows the front panel of the VI with the response. This was repeated at different wind speeds. Figure 5.12 shows the response at two different wind speeds. The sensor indicated a 95% response time of 4.9 seconds, a 10% to 90% rise time of 2.8 seconds and a 63.2% time constant of 3.4 seconds. It should be noted that the operating time of the shutter device and the time for the flow to change also contribute to the response, rise and fall times procured from these experiments. However, faster response times were expected with a better experimental arrangement. The strain gauge manufacturers' data have indicated that the response time of a strain gauge bridge in a pressure transducer for the range 20-25000 kN/m^2 is 1 ms [5.10]. The flow sensor presented here is basically a pressure transducer. Furthermore, target flow sensors have also been used in the past to measure the thrust and propellant flowrates for evaluating the performance of rocket thrusters. The quick response of the flowmeter made it possible to throttle a pulse as small as 10 milliseconds. [5.11]. Hence, the experimental arrangement described in Section 5.5.3 was used to detect the response of the sensor.

5.5.3 Dropping weight experiments

In this configuration, the flow sensor was clamped on one end and held horizontally. A weight of 50 g was held directly above the free end of the sensor. Labview was once again used to acquire the response, using the virtual instrument program shown in Figure 5.10. The sample rate was set at 100 and the number of samples at 500, so that

data was acquired every 0.01 second for a period of 5 seconds. Once the acquisition started, the weight was dropped so that it made contact with the edge of the rubber beam of the sensor, before falling into a holder below it, and the deflection of the sensor was detected and analysed using the VI. The deflection that the sensor underwent was sufficiently high as indicated by the sensor output of 1.6 V. Figure 5.13 shows the front panel of the VI with the response and Figure 5.14 shows the same response plotted by the spreadsheet file, Excel. The sensor indicated a 95% response time of 50 milliseconds and a time constant of 30 milliseconds. This experiment was repeated eleven times and similar values were obtained for the response time.

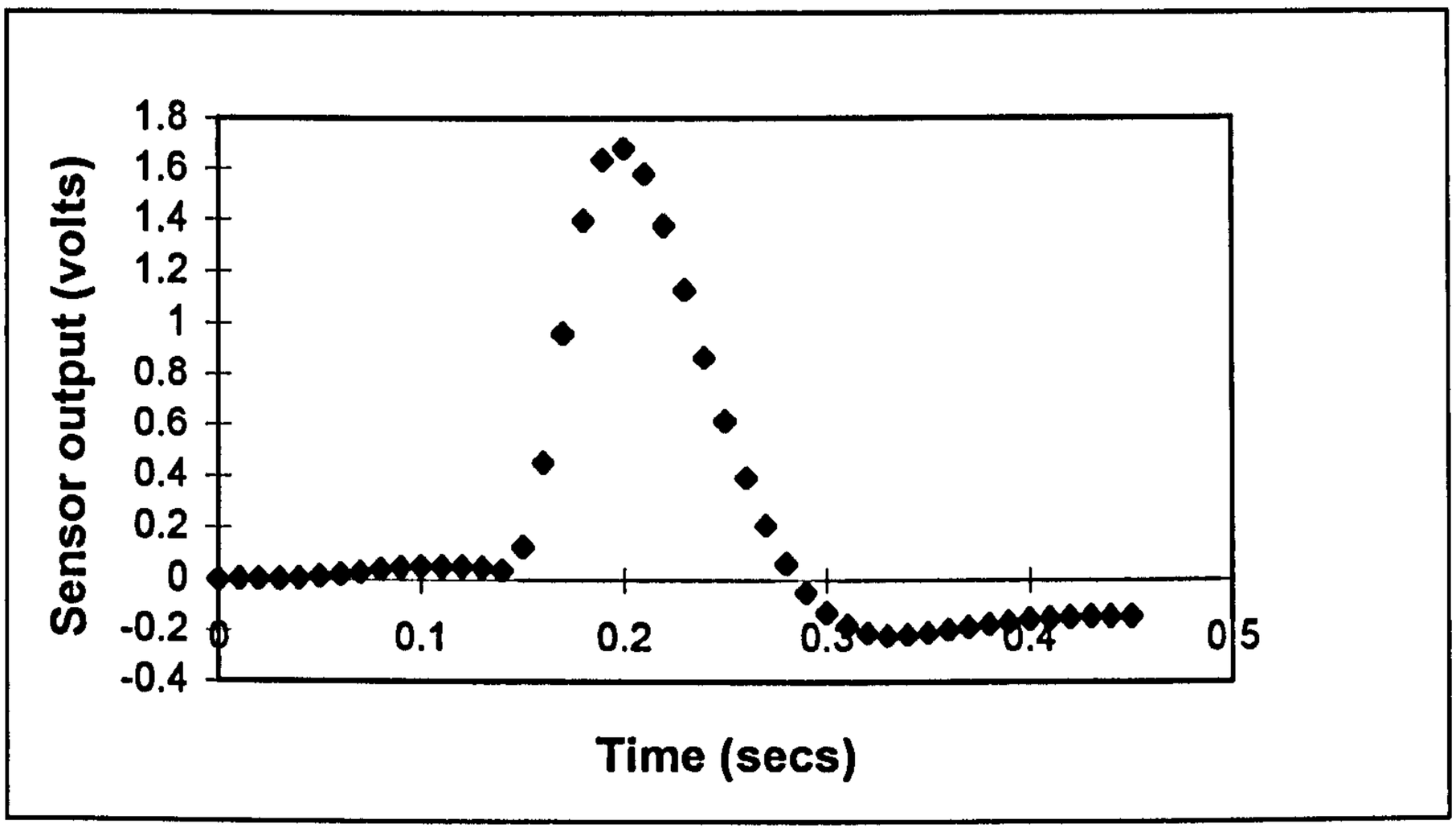

Figure 5.14: Response time determination by weight-dropping experiment

However, during three out of these eleven experiments, the response was obtained as indicated in Figure 5.15. This happened when the weight was made to fall directly on the longitudinal face of the rubber beam of the sensor, instead of falling on its edge. The response time was again 50 milliseconds. But the output was oscillating about its final value with decreasing amplitudes until the oscillations came to rest. This was the response due to both the sensor and the weight and hence inertia was present and energy was being dissipated. However, the purpose of the experiment was to obtain the response time of the flow sensor. A 95% response time of 50 milliseconds indicates a flow sensor with a very fast response time.

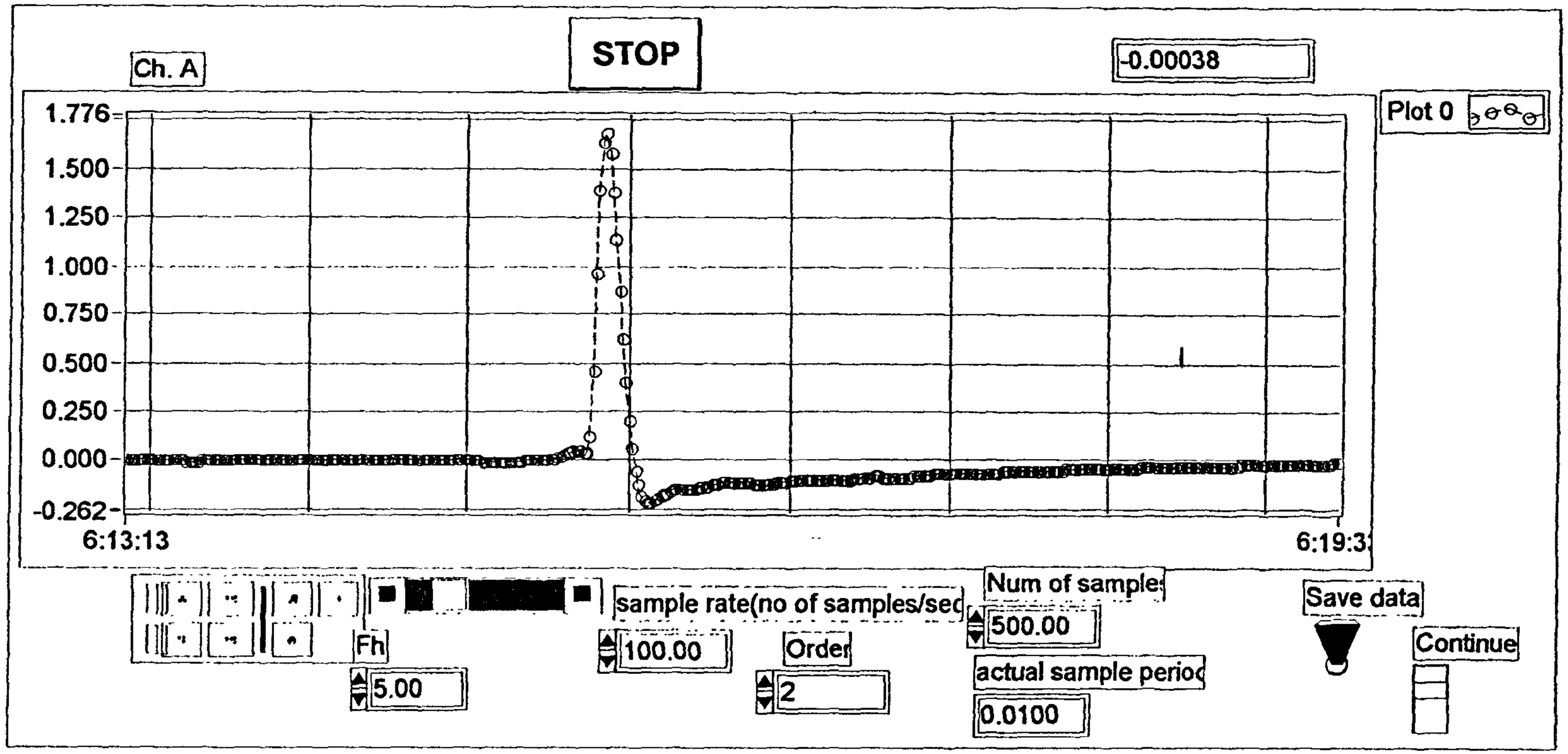

Figure 5.13: Front panel of the VI with the sensor response obtained by dropping weight on the longitudinal edge of the flow sensor.

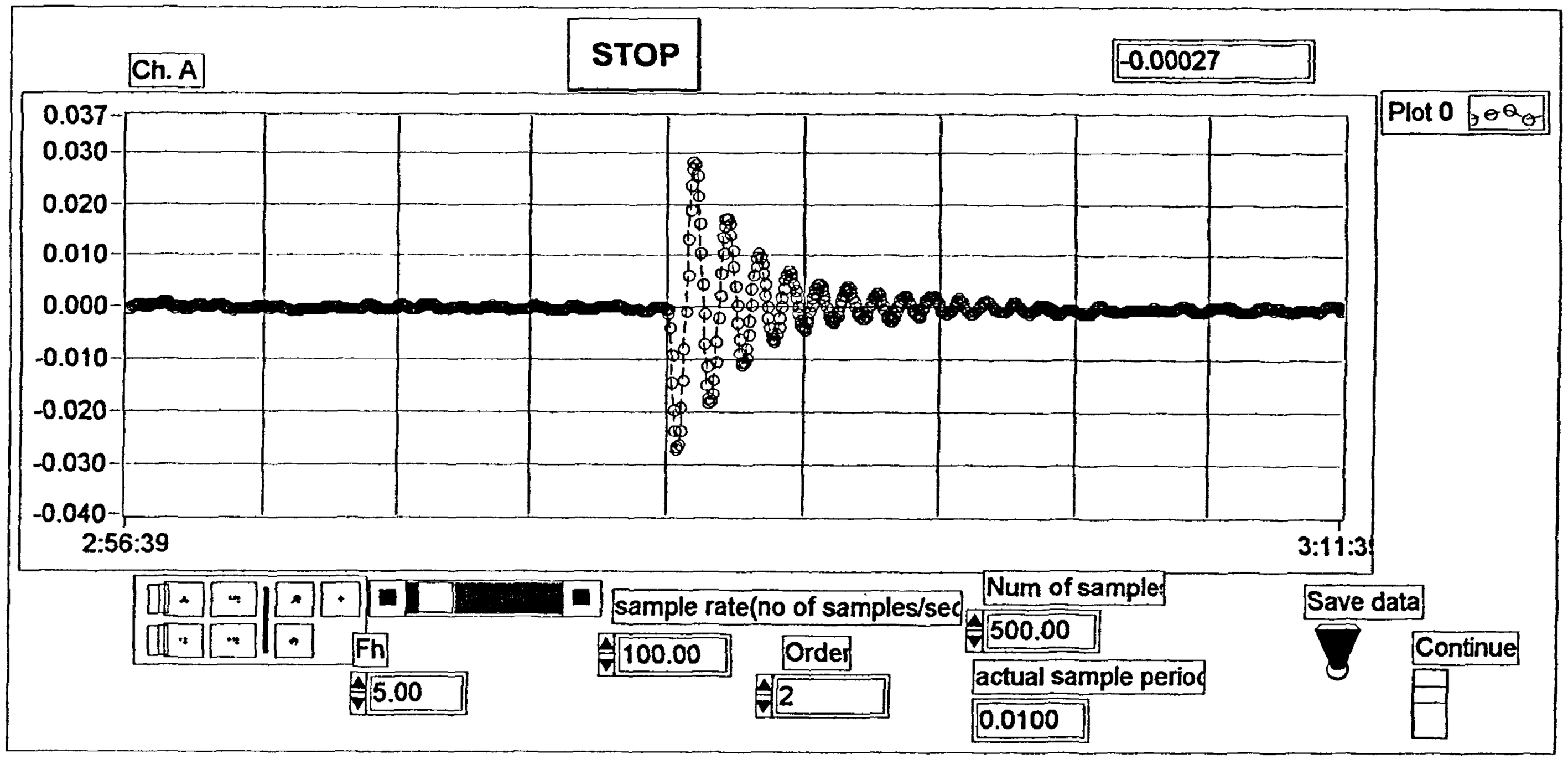

Figure 5.15: Front panel of the VI with the sensor response obtained by dropping weight on the longitudinal face of the flow sensor.

5.6 DISCUSSION

This chapter has reviewed the experiments conducted to determine the performance characteristics of the electrical strain gauge flow sensor. From the tests conducted to analyse the static characteristics of the flow sensor, it has been shown that the sensor has a linear and stable response, negligible hysteresis and a repeatability of 0.022%. The experiments that were conducted to determine the response time indicated that the sensor has a very fast response time of 50 milliseconds. These performance characteristics of the flow sensor have indicated that the sensor has the potentiality for commercial exploitation as discussed in Chapter 9.

CHAPTER 6

A REVIEW OF OPTICAL FIBRE SENSORS

6.1 INTRODUCTION TO OPTICAL FIBRE SENSORS

The basis of operation of fibre optic sensors is the translation of the measurand, into a change in one or more parameters of a light beam. The physical quantity being measured can be physical, chemical, biological or biomedical. The light parameters that can be modulated, include one or more of the following: Intensity, Phase, Polarisation, Wavelength and Transmission time.

Fibre optic sensors usually incorporate either glass/glass, glass/plastic fibres or all-plastic fibres. Plastic fibres have particular advantages for sensor applications because they are inexpensive and have a relatively large diameter of 0.5-1.0 mm, making connection to the source and detector easy. However, plastic fibres cannot be used in certain hostile environments where they may be severely damaged. [6.1] Another disadvantage of this fibre is that it has a large attenuation which may be a problem when remote measurement over large distances are required.

Optical methods for sensing applications were well established before the 1970s. These sensors exploited a range of mechanisms from simple optical switches based upon interrupting an optical beam, to sophisticated interferometry. A common feature of most optical instrumentation is that it is delicate, in the sense that if the optical alignment is disturbed, the performance will rapidly be degraded. Despite the high performance offered by conventional optical sensors, very few had emerged from the optical bench laboratory. Although it was apparent that existing optical sensors could be 'fiberised' very few components had been developed specifically for optical fibre based sensors. In 1976 and 1977 respectively, two papers were published which may be regarded as milestones in the field of fibre optic sensors. Vali and Shorthill [6.2] introduced a Sagnac Interferometer with a reciprocal optical path implemented with an optical fibre and Rogers [6.3] demonstrated the remote measurement of current based upon Faraday rotation in a coil of very low birefringence single mode fibre. These experiments showed that optical fibres had the potential to be exploited in different ways in many sensing

applications. Subsequent to these initial experiments, the range of measurands detected by fibre optic sensors has increased rapidly, as has the number of transduction mechanisms which have been exploited.

The main advantages of fibre optic sensors [6.4, 6.5] over conventional electronic sensors include:

- Immunity to electromagnetic interference, which renders fibre optic sensors ideal for applications such as in switch gear and power stations.
- High reliability and capability of working in many kinds of hostile environment.
- Fibre optic sensors characteristically enjoy long life. For example, the life expectancy of reflective fibre optic switches is quoted at 10 million operations [6.1].
- Development of electrically isolated devices compatible with intrinsic safety requirements. This enables optical fibre sensors to be used for high voltage and medical applications.
- Passive operation (all dielectric) ensuring that no power or electrical circuits are required at the sensing point.
- Long transmission distances allowing use for remote or distributed sensing due to low losses achievable in optical fibres
- Chemical immunity to corrosion, enabling use in hostile environments like the chemical plant applications and invasive sensors in the human body.
- Small size, low cost and light weight particularly with the advent of integrated optical techniques.
- Large bandwidth due to inherent high bandwidth of optical fibres.
- Capability of electrical and optical multiplexing.
- High temperature performance.
- Component costs driven by large commercial telecommunication and optoelectronic market.

  Optical fibres are used to sense the changes in a measurand in two distinct ways which gives rise to two major classes of fibre optic sensor, intrinsic sensors and extrinsic sensors, illustrated in Figure 6.1.

1. In the case of intrinsic sensors, the measurand directly modulates some physical property of the fibre. The fibre sensor relies on the properties of the optical fibre

itself to convert the action of the measurand into a modulation of the light beam passing through it.

2. Extrinsic sensors are sensors in which the light leaves the fibre and enters a physically separate modulator, where the characteristics of the light are changed by the measurand. The light then enters the same or a different return fibre. The advantage of extrinsic sensors is that modulators can be specially designed to maximise the modulation depth, making available a wider range of modulation mechanisms than for intrinsic modulators. The disadvantage is that the number of optical interfaces is increased, with a resultant loss of optical power and the danger of contamination of optical surfaces.

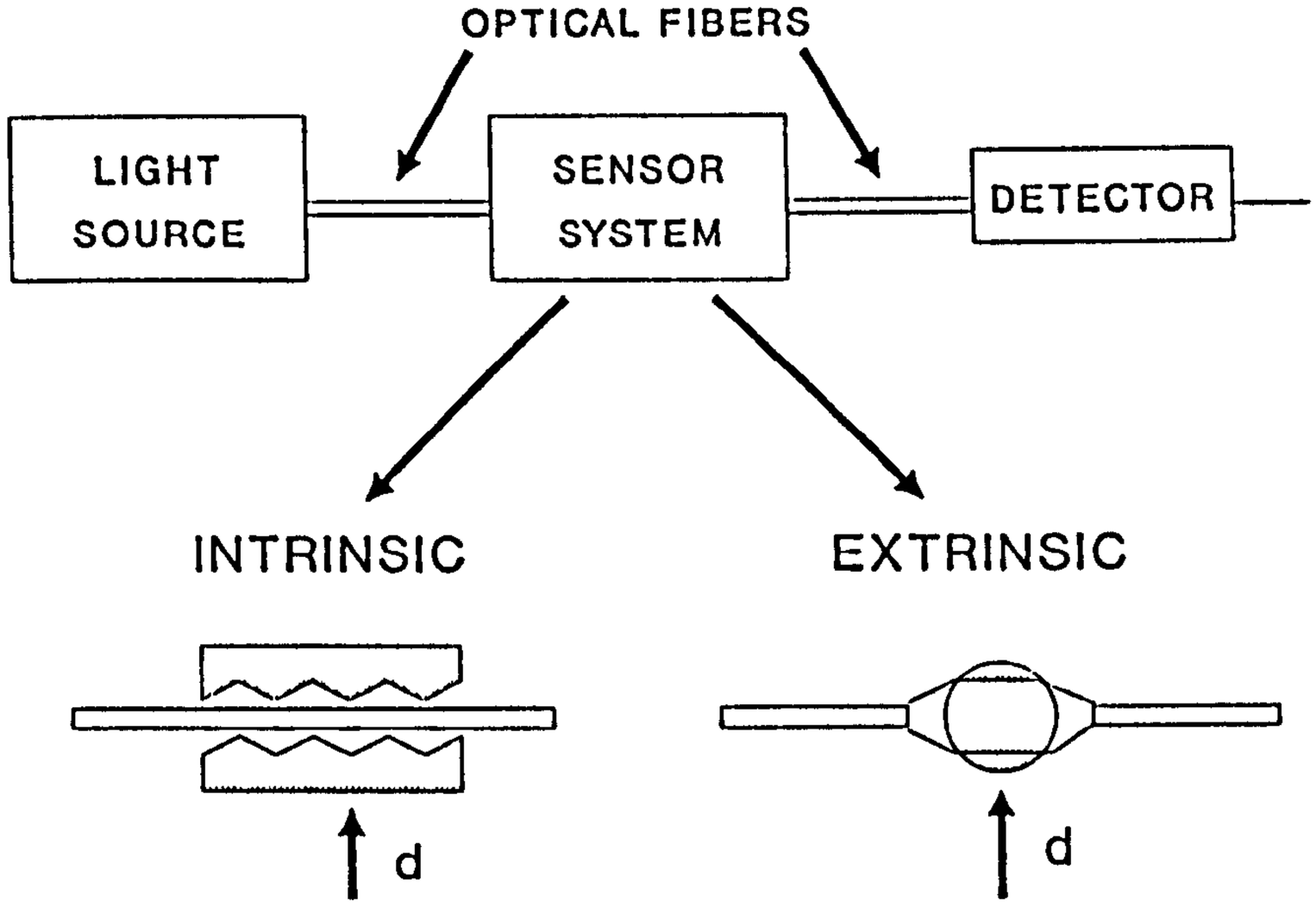

Figure 6.1: Extrinsic and intrinsic fibre optic sensors.(E. Udd, 1991)

The next section summarises the different transduction mechanisms employed in optical fibre sensors. This chapter then reviews the various optical fibre flow sensors and discusses their working principle.

6.2 TRANSDUCTION MECHANISMS

Fibre optic sensors may also be subdivided by transduction mechanisms and classified as intensity modulated, polarisation modulated, wavelength modulated, or phase modulated. Intensity sensors tend to be based on multimode fibre, whereas only monomode fibres are used to modulate the other light parameters. In general, the performance offered by an interferometric or phase sensor for physical measurements, is much greater in terms of range to resolution, than an intensity sensor for the same measurand. A summary of the transduction mechanisms which can be exploited is given in Table 6.1. Some of these mechanisms are described in the sections that follow.

Table 6.1: Summary of fibre sensing mechanisms which can be exploited in fibre optic sensors.

Intensity changes via	Polarisation changes via	Wavelength and frequency changes via	Interferometric changes
Microbending loss Breakage Transmission-Reflection Refractive index Evanescent fields Absorption Molecular scattering Modified cladding	Faraday rotation Kerr effect Pockels effect Photoelastic effect	Fluorescence Phosphorescence	Dual beam interferometers Multiple beam interferometers

6.2.1 Intensity modulated Sensors

The sensor developed in this project uses the intensity modulation mechanism; therefore it is appropriate to describe Intensity modulated sensors and their working principle in detail. Of the many individual fibre sensor types demonstrated in the lab, fibre intensity sensors are most advanced from an engineering and commercial standpoint. Fibre optic intensity sensors predominate in industrial applications for several reasons which include:

- Simple to implement.
- Simple, manufacturable sensor assemblies.
- Simple, low cost signal processors, such as photodiodes to convert intensity to electrical signal which can then be processed.
- Ability to maximise the power through the sensor as opposed to wavelength modulation where one wavelength or waveband is isolated using filters, diffraction gratings, etc which reduces the overall power budget.
- Ability to provide an absolute measurement and being particularly well adapted for digital measurements.

These advantages of the Intensity modulated sensors gave the author enough reasons to choose this form of modulation over the others.

6.2.1.1 Microbending Sensors

Microbending sensors causes a loss of light from a multimode fibre due to bending of the fibre. Figure 6.2 shows the basic idea of a microbending sensor. A fibre is mounted between a pair of plates containing parallel grooves. When pressure pushes the plates together, it causes microbends in the fibre, which let some light leak out, reducing optical power transmitted by the fibre. Microbending sensors exploit this phenomenon by bending the fibre on a scale comparable with its diameter. Light is coupled from propagation modes to radiation modes, causing it to be transferred from the core into the cladding, instead of being internally reflected. The more severe the mechanical perturbation or bending, the more light is coupled to radiation modes and is lost. Thus the important characteristics of a microbend sensor are that it uses a multimode optical fibre, it is a light intensity sensor and the light intensity decreases with mechanical bending. Microbending sensors can therefore be used to measure force, pressure or displacement and other parameters which can be mechanically related to force [6.7].

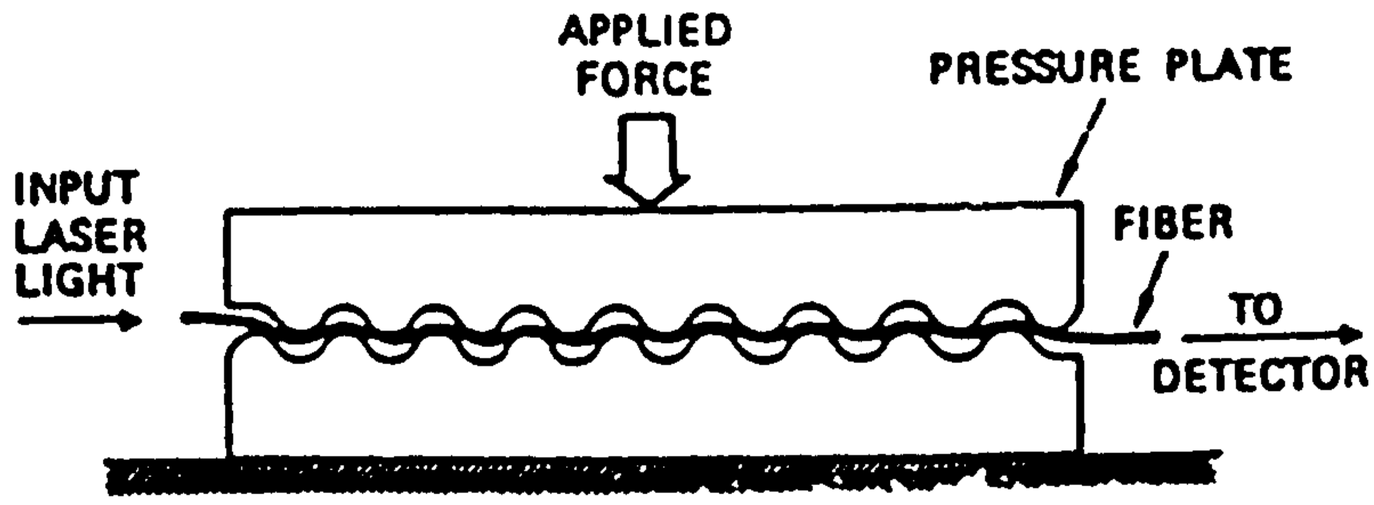

Figure 6.2: Microbending Sensors (J.Hecht: 1993)

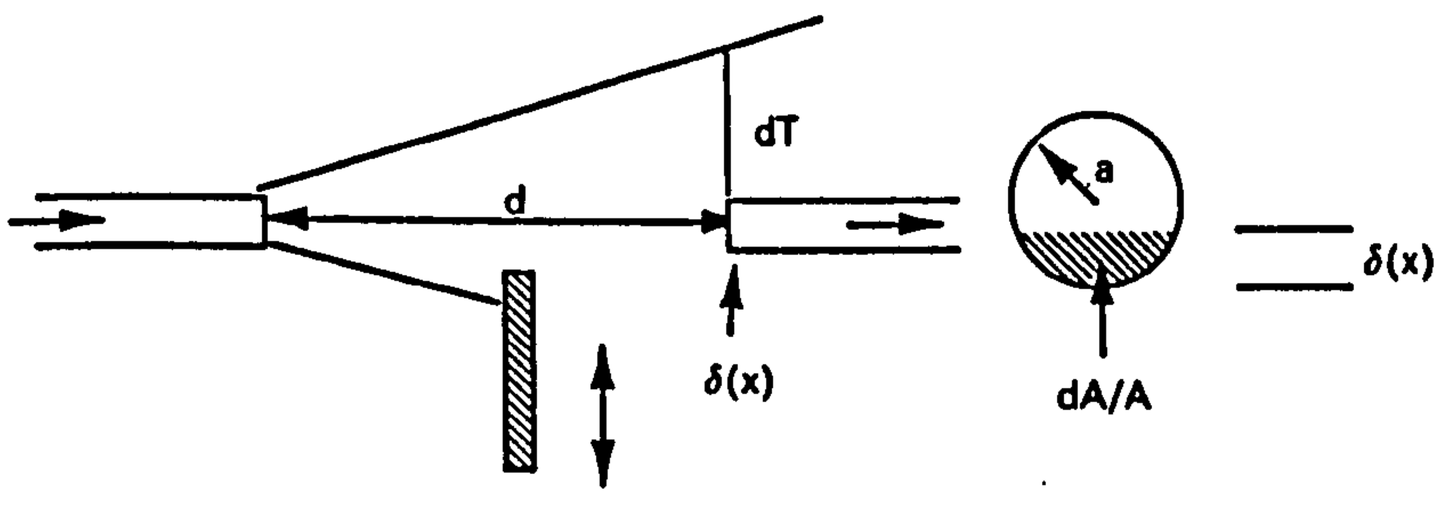

Figure 6.3: Transmission-Reflection modulation sensors- basic shutter modulator

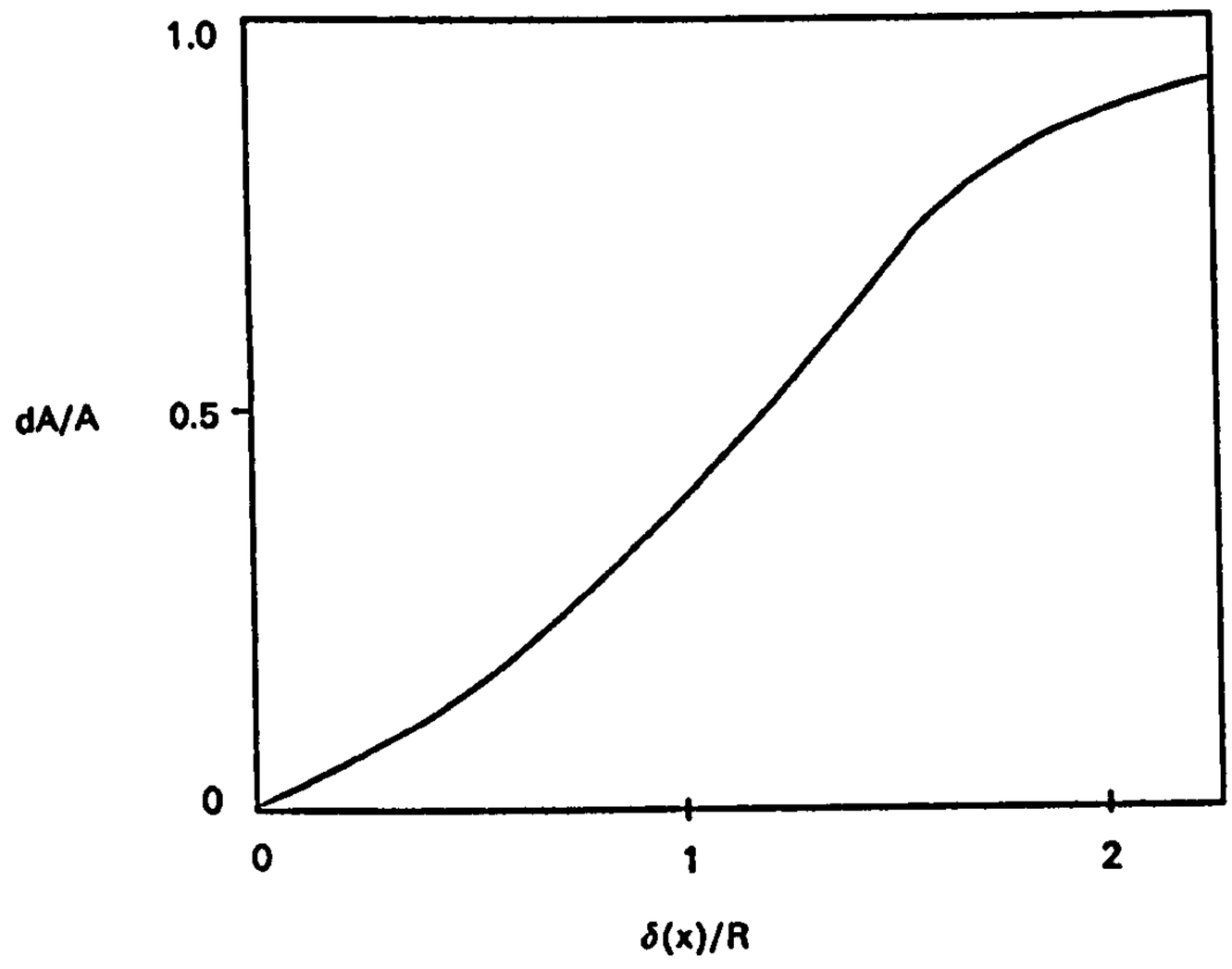

Figure 6.4: Characteristic of the shutter modulator (Grattan K T V: 1995)

6.2.1.2 Breakage or crack sensors

Microbend sensors are not supposed to strain fibres to the breaking point. However, severe strains can break fibres, and in some cases that can be useful for sensing, for example to verify the structural integrity of a dam [6.8]. The optical fibres are embedded in a concrete matrix and the intensity of light transmitted is monitored for sudden changes. If internal stresses caused the concrete to crack inside the dam, it could snap the embedded fibre, causing the light intensity to drop. This could be a vital early warning of structural problems.

6.2.1.3 Transmission-Reflection modulation sensors

The generic form of modulator which represents this family of sensors is the planar shutter moving across the optical channel transversely, to reduce the channel cross-section and hence its transmission. (Figure 6.3). The light intensity transmitted is governed by a reduction in the area of the optical aperture, and hence the spatial displacement of the shutter. [6.6]. Although the modulation is not rigorously linear (Figure 6.4), there is an extended midrange over which approximate linearity and hence resolution is maintained.

A similar analysis applies to a modulator in which the light beam from the addressing fibre, is expanded by a lens into a larger cross-section parallel beam before being focused for collection by the receiving fibre.

The analysis may also be applied to two overlapping gratings (one stationary and the other movable) consisting of alternate transparent and opaque regions of equal width. Movement of one grating with respective to the other produces transmission changes from 50% of the noninterrupted beam value (when the opaque fringes overlap) to zero (when the opaque and transparent fringes overlap). The resulting light modulation becomes periodic as a function of movable grating position. (Figure 6.5).

An important subset of this class of sensors involves a reflecting element whose position determines the light intensity diverted onto a receiving fibre. (Figure 6.6)

Although the reflective and transmissive modulators primarily detect displacement they may be used in combination with other primary transduction means for monitoring

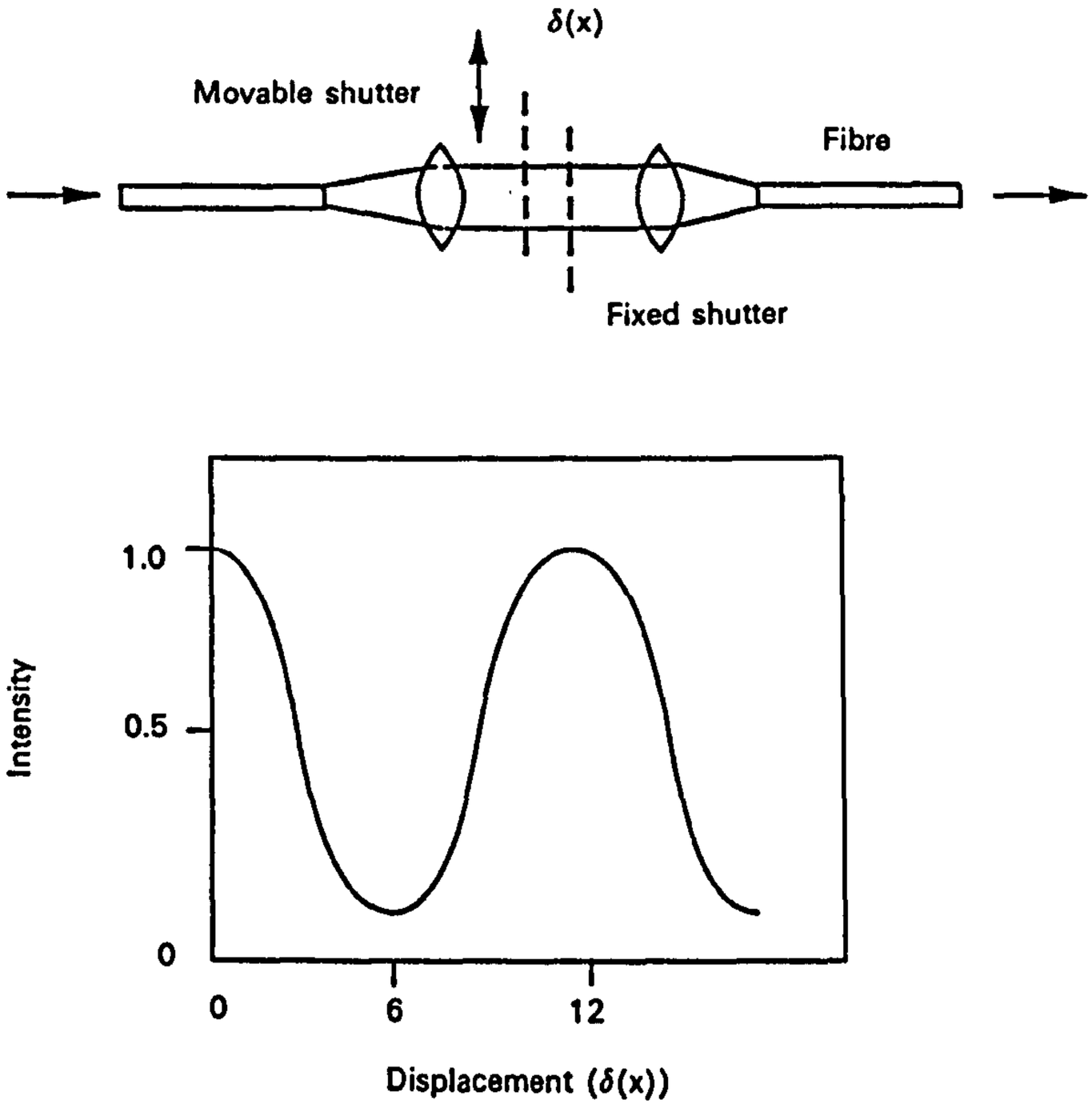

Figure 6.5: Overlapping fringe modulator: Principle and characteristic (Grattan K T V: 1995)

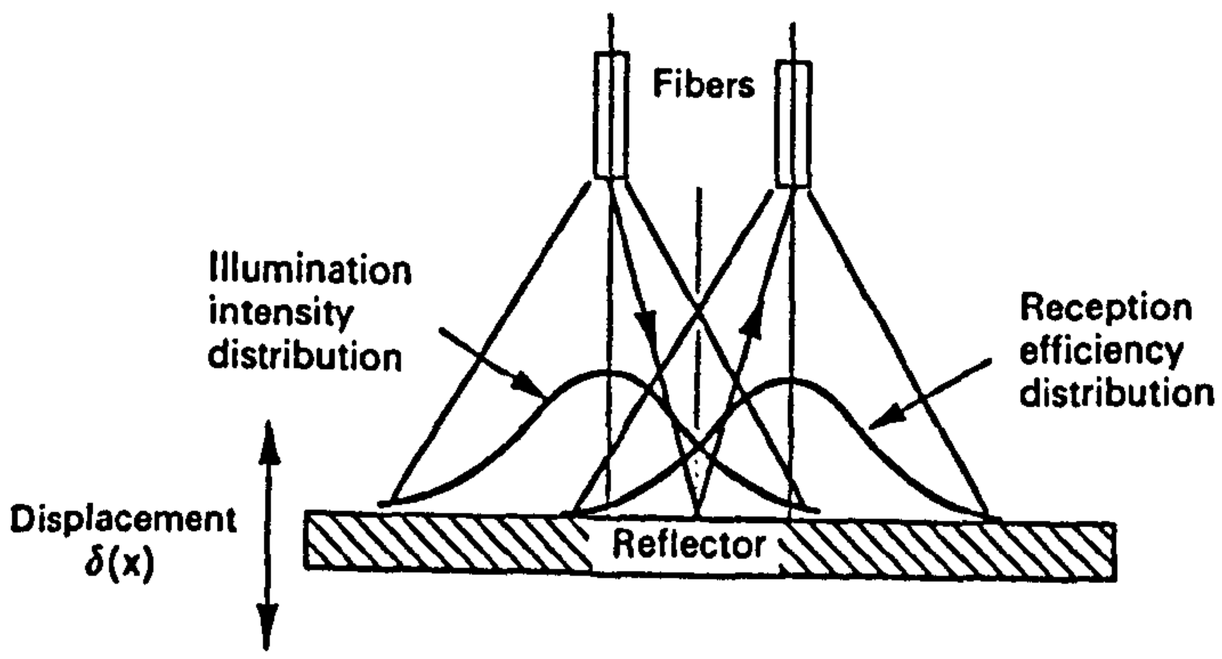

Figure 6.6: Moving reflector monitor (Grattan K T V: 1995)

other parameters such as pressure (via membrane displacement) and electric current (via electromagnetic displacement).

6.2.1.4 Sensors based on refractive index changes

Intrinsic attenuation modulation is due to changes in the light intensity propagating through a fibre when the normal process of total internal reflection, which assists the transmission, is perturbed. In terms of geometric optics, the condition for modulation is

$$\theta_m < \sin^{-1}(n_2 / n_1) \qquad (6.1)$$

This may be achieved by varying the refractive indices of the core or cladding (n_1, n_2 respectively), or geometry of the fibre core governed, so that the ray propagation angle (θ_m) is affected. Changes in the refractive index of the cladding may be induced in a number of ways, each corresponding to the potential for sensing a different parameter. The cladding may be made from electro-optic, or magneto-optic or photoelastic (e.g. [6.9]) material to form electric field, magnetic field or pressure sensitive modulators. Liquid level detectors (e.g. [6.10]) have been demonstrated, whereby the presence of the liquid adjacent to the fibre causes the necessary refractive index change to reduce the signal intensity in the fibre core. (Figure 6.7).

6.2.1.5 Modulation by evanescent wave coupling

Refractive index changes can also be induced simply by the microdisplacement of two fibres, so that a thin layer of the surrounding medium with its different refractive index is introduced. This phenomenon of total internal reflection called frustrated total internal reflection (FTIR) or attenuated total internal reflection (ATR) involves the penetration of the electromagnetic wave into the adjoining medium to a depth d (evanescent field) which is of the order of the optical wavelength. Thus, displacement of the two fibres relative to each other (Figure 6.8) over distances of this order, changes the condition for internal reflection by perturbing the evanescent field associated with the wave and so modulates the light flux in the fibre. Figure 6.9 shows another form of sensor where two fibres are placed side by side and evanescent coupling takes place depending on the separation of the fibres. Displacements of less than the wavelength of light used, may be resolved. [6.11].

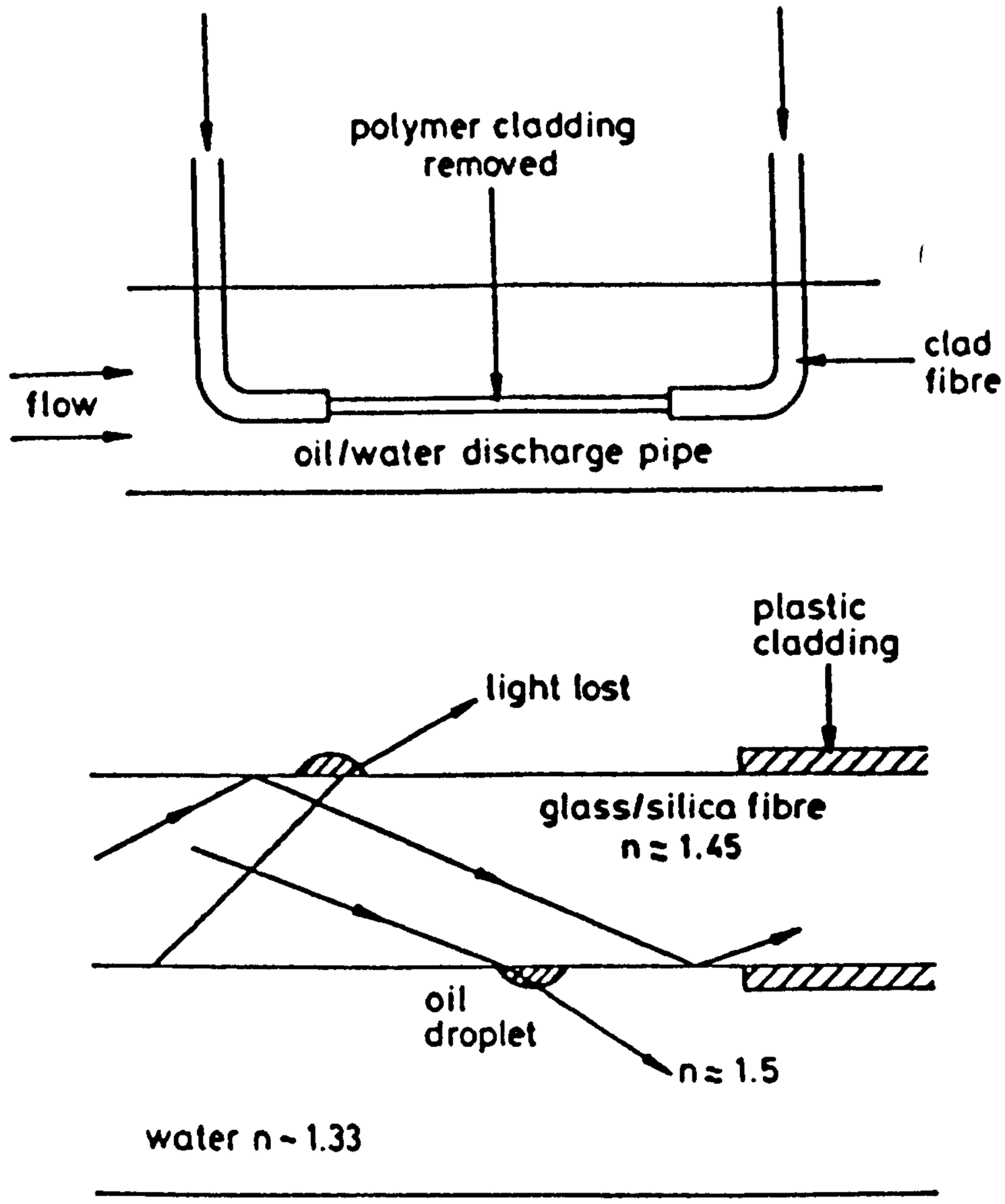

Figure 6.7: Sensor based on change in cladding refractive index (Pitt.G.D et al: 1984)

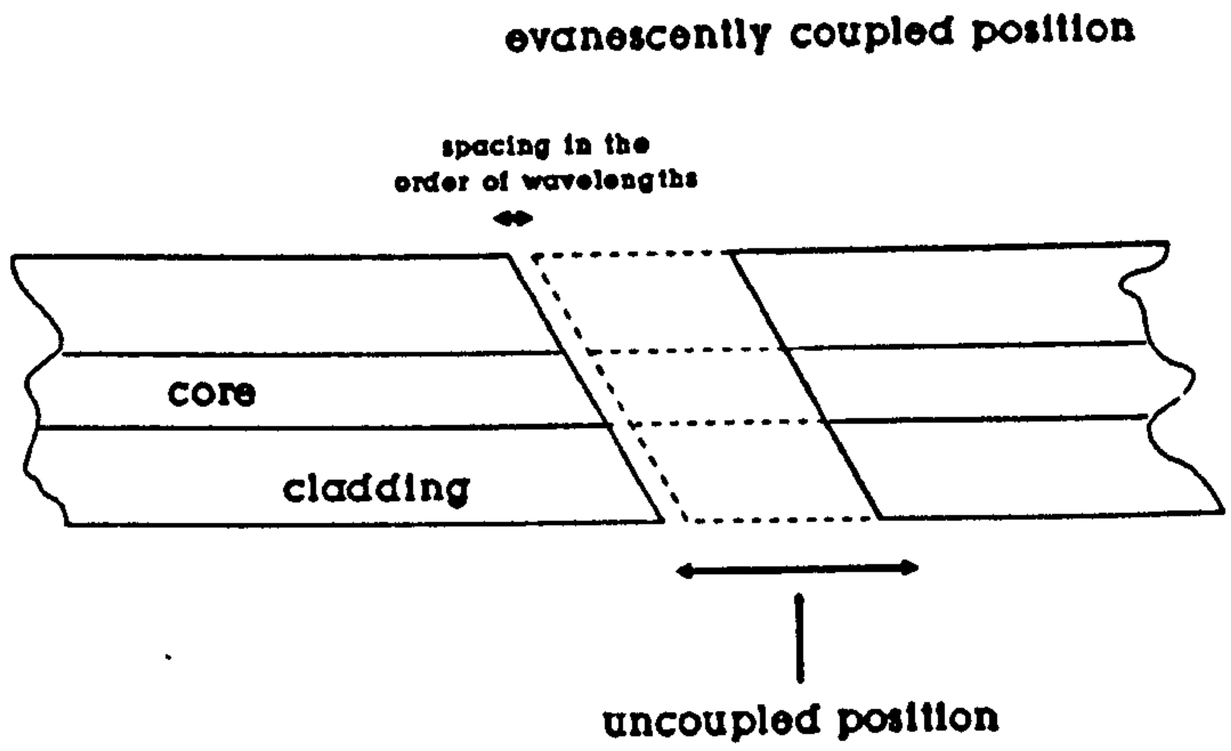

Figure 6.8: Sensor based on modulation by evanescent wave coupling (Scully P : 1991)

6.2.1.6 Absorption and light scattering sensors

Intensity modulation by absorption bands in chemicals has been used for some types of sensors for both physical and chemical parameters. [6.12] One of the early developments measured the absorption of an equilibrium mixture of N_2O_4 and NO_2 sealed in a capsule at the end of a fibre bundle (Figure 6.10). Absorption of light in the gas is strongly temperature-dependent. This device was intended for temperature measurement of high voltage transformer windings.

Scatter loss arises principally because of random fluctuations in the composition and density of the core of a fibre. In a well-made high-silica fibre, the main contribution to the scatter loss is due to Rayleigh scattering, where the material fluctuations occur over a scale which is short compared to the wavelength, λ. Rayleigh scattering characteristically varies as λ^{-4}, so short wavelengths are scattered much more strongly than long wavelengths. In fibres with doped silica cores, the magnitude of the scattering increases with the doping level. Sensors based on light scattering are used for turbidity measurement (i.e. measurement of the loss in transmission due to scattering). The direct measurement of the scattered light level is also possible. The presence of oil in water can be measured by monitoring the transmitted light and the level of light scattered from oil droplets in the sample.

6.2.1.7 Modified cladding

The attenuation in a fibre can be modified by removing the normal cladding of the fibre and replacing by either a liquid or another solid cladding material, either of which has a refractive index with a high positive or negative temperature coefficient. The most sensitive fibres are those in which the indices of the core and cladding are nearly equal, yet have different temperature coefficients. If the temperature rises, the indices may approach unity, giving rise to a significant loss of light from the core.

A commercially available silicone-resin coated type of silica fibre can act as a detector for low temperatures, because the coefficient of refractive index with temperature is greater for the initially lower index silicone cladding than it is for silica. However, at a temperature below -25^0C, the cladding increases in refractive index to a value above that of the core, with a resulting loss of guidance, and hence high losses. Such a fibre can be used for the distributed detection of cryogenic liquid leaks.

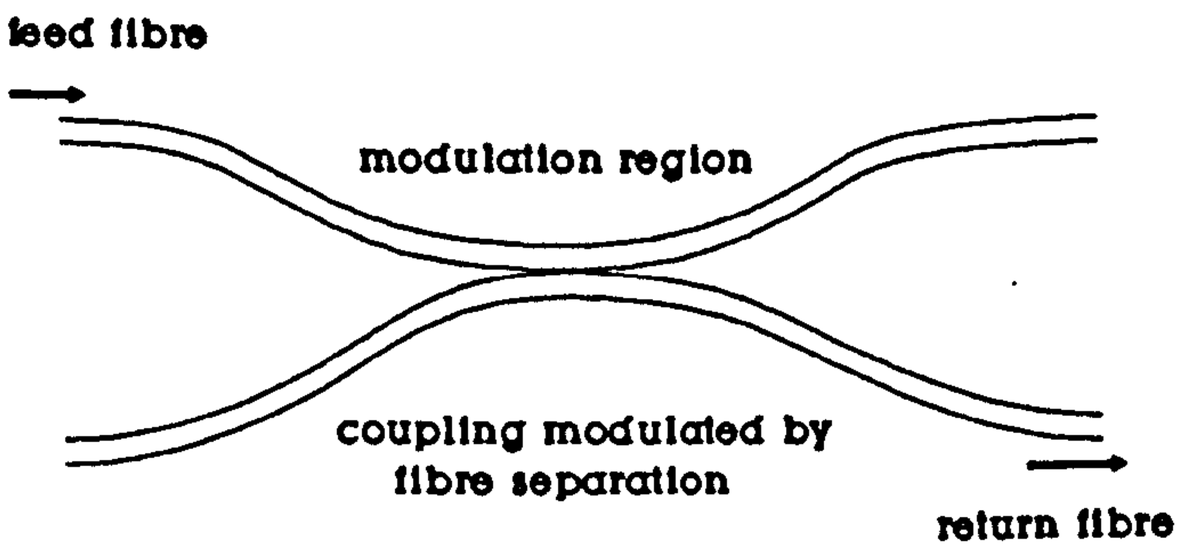

Figure 6.9: Optical fibre based displacement sensor (Scully P J: 1991)

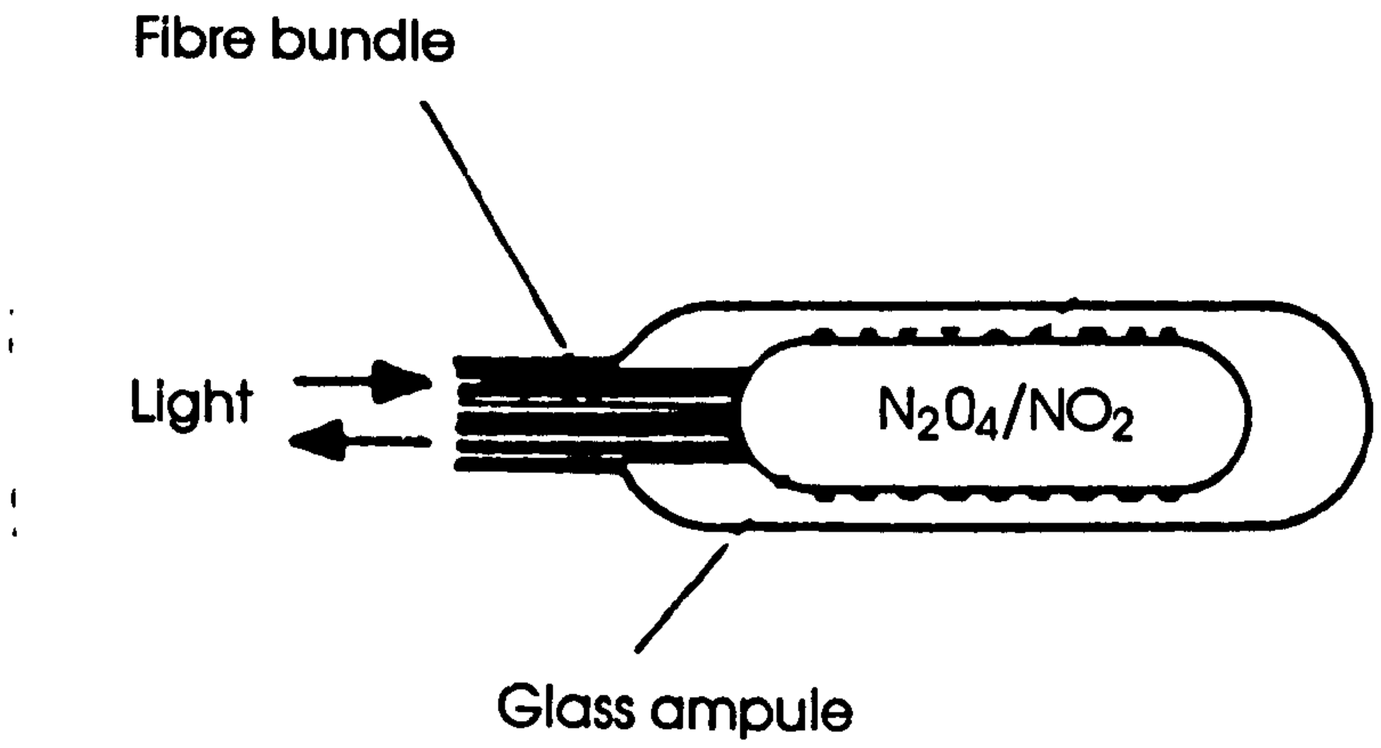

Figure 6.10: Absorption sensor (Culshaw B and Dakin J: 1989)

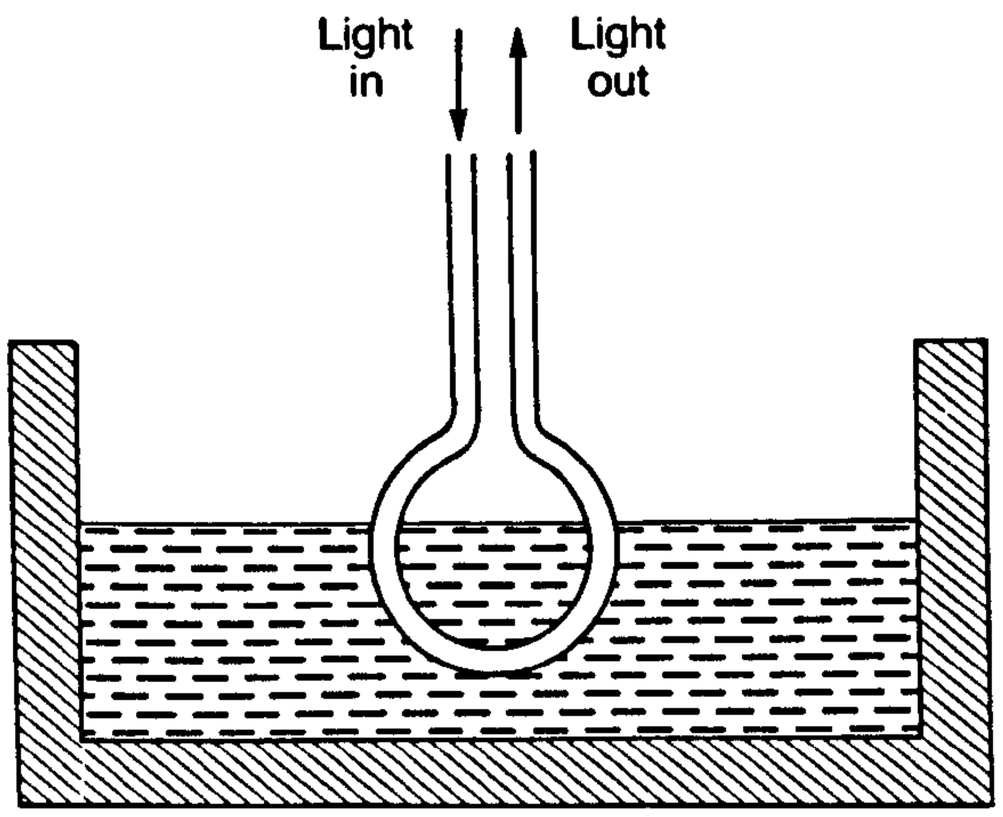

Figure 6.11: Fibre loss sensor - Level detector (Morris A: 1993)

A simple level detector can be made from a loop of unclad fibre as shown in figure 6.11. When a liquid covers the loop, the higher-order guided light modes are lost from the fibre into the liquid. [6.13]

6.2.2 Polarisation modulated sensors

A number of materials, when exposed to electric or magnetic fields, exhibit effects which can alter the state of polarisation of a transmitted beam of light. The main physical interaction mechanisms are the Faraday, Pockels and Kerr effects and photoelastic effect. These effects can be used for a direct optical measurement of electric or magnetic fields, or for an indirect measurement of voltage and current which are produced by the fields. Fibre optic sensors have been developed using electro-optic and magneto-optic materials. Such polarisation modulation sensors are called polarimetric sensors. The polarisation characteristics of a light signal may also be altered by propagation through a birefringent medium.

One of the best known intrinsic sensors based on polarisation modulation is the Faraday effect current sensor [6.14]. In this device (Figure 6.12) plane-polarised helium-neon laser light is launched into a specially designed single-mode fibre having very low intrinsic birefringence. Birefringence describes a material which is optically anisotropic, possessing two axes of refraction. The fibre is coiled around a current carrying bus-bar. The associated magnetic field rotates the plane of polarisation of the incident light and the polarisation change is related to the magnitude of the current by measuring the output of the fibre using a simple polarisation analyser consisting of a Wollaston prism and two optical detectors. Currents of typically 10,000 amperes have been measured, with a resolution of 30 amperes. Such large currents are typical of the electricity supply industry.

Another family of polarisation modulation sensors is that based on photo-elasticity (i.e. stress-induced birefringence in normally isotropic optical materials when subjected to anisotropic strain). The photoelastic sensor works on an optical principle where the anisotropic strain is the perturbing influence (rather than electrical voltage).

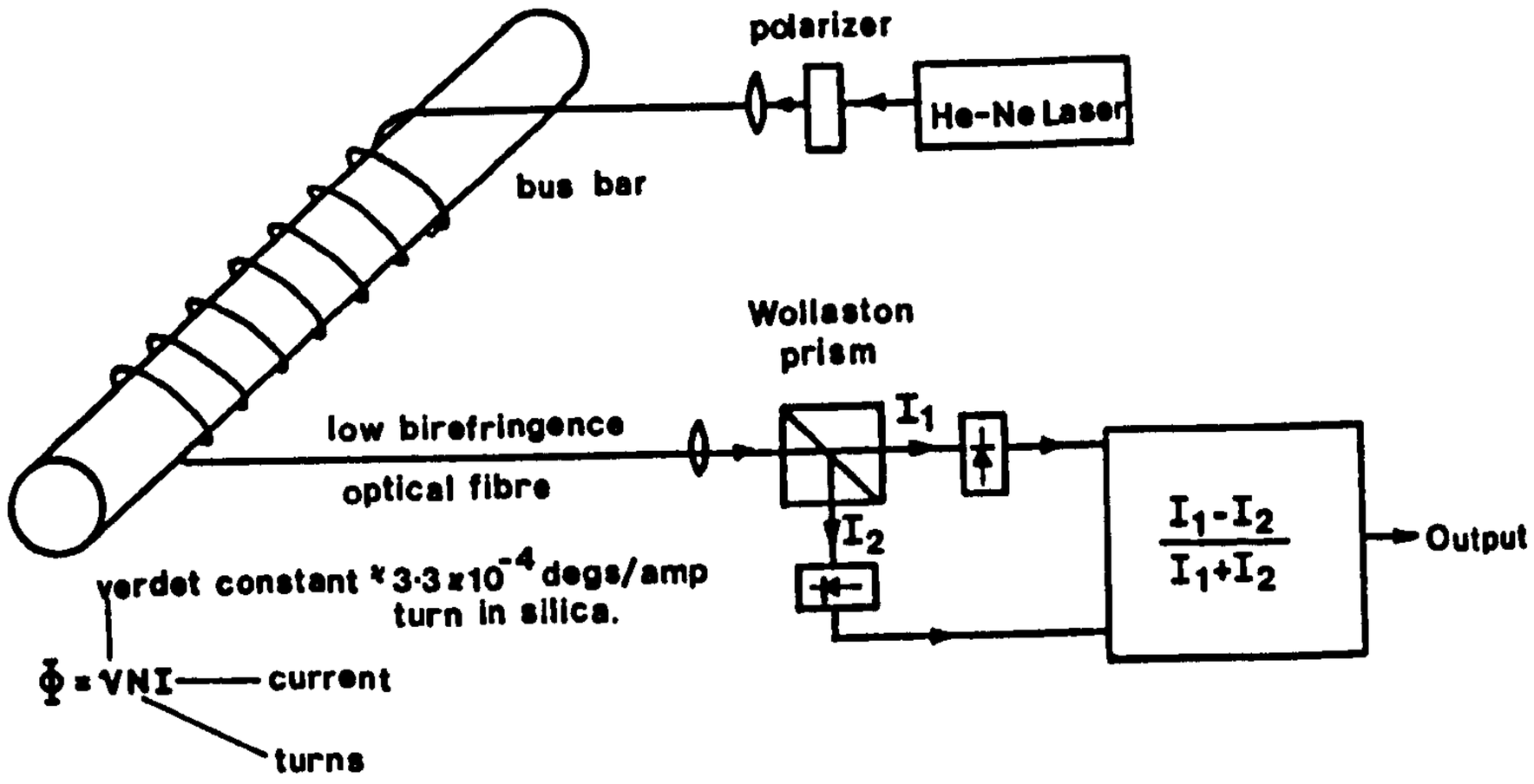

Figure 6.12: An optical fibre based current sensor using Faraday rotation. (Rodgers A J, 1987)

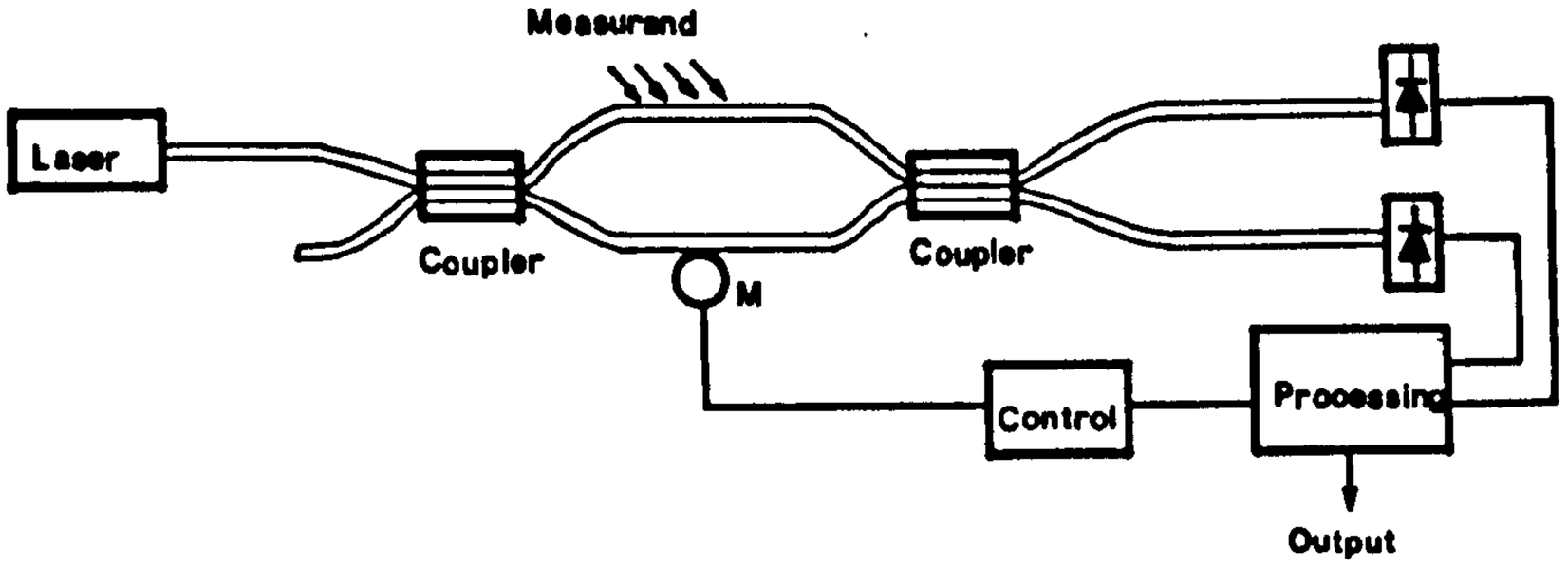

Figure 6.13 a : Mach Zender Interferometer (Andonovic I et al: 1989)

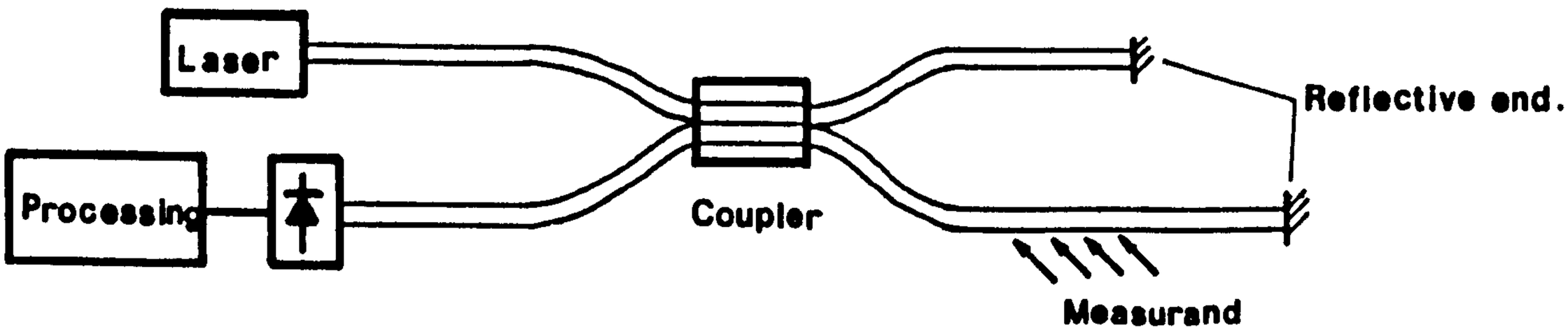

Figure 6.13 b : Michelson Interferometer (Andonovic I et al: 1989)

6.2.3 Wavelength and frequency modulated sensors

The next category of sensors are those based on modulation of optical wavelength or frequency. A modulation of optical frequency inevitably involves equivalent changes in optical wavelength. Wavelength modulation sensors operate by measuring changes in the spectrum, the wavelength distribution of light arriving at the optical receiver. To achieve this in a readily detectable manner, relatively large changes in transmitted, fluorescent or reflected spectra are desirable. Such modulation may be achieved by the use of specially designed sensing heads incorporating spectral filters. Alternatively, the use of materials, such as fluorescent species or indicator dyes, which have characteristic change in their optical emission or transmission spectra brought about by interaction with the measurand may be used. (e.g. the absorption spectra of various gases may be used to determine their concentration). In wavelength-modulation sensor systems, optical receivers generally tend to be slightly more complex than for simple intensity types. Prior to detection, some form of wavelength analysis or filtering is required, and this involves the utilisation of more specialised optical components, such as dichroic beam splitters, optical filters, diffraction gratings or other dispersive elements, and even complete miniaturised solid state spectrophotometers. The main advantage of spectral-filtering sensors over simpler intensity-based sensors is that , in the former , the required information does not lie in the measurement of the absolute intensity, but rather in the distribution of intensity at a number of selected wavelengths. Therefore these sensors tend to be less sensitive to overall changes in the attenuation characteristics of components such as fibres, connectors, cables and optical sources. A range of sensors for measuring physical, chemical and biomedical parameters have been designed under this category of transduction. [6.15]

Fluorescence and phosphorescence are modulation mechanisms in which the spectral content of emitted light is altered. The modulating material emits light at different wavelength to the incident light under certain conditions brought about by the measurand. For example, Luxtron Co. (USA) has developed a medical thermometer, based on the temperature variation with fluorescence quenching, of a rare earth phosphor mixture at the end of an optical fibre probe. [6.16]

Under the frequency modulated sensors the most widely implemented sensors are those based on laser Doppler velocimetry. Laser light reflected off a moving object undergoes

a doppler frequency shift. In the simplest case, where the frequency shifted light is mixed on a photodetector with a reference beam derived directly from the optical source, an intermediate frequency signal is equal to the doppler frequency shift. A typical set-up of the laser Doppler anemometer is shown in Figure 1.18 in Chapter 1. Laser light is passed through a polarising beam splitter into a multimode optical fibre immersed in the medium whose velocity is to be measured. Some light is backscattered into the fibre by the medium and transmitted to the detection circuitry via the beam splitter. Optical fibre Doppler probes have been developed to measure particle flow in fluids and invasive blood flow. [6.15]

6.2.4 Phase Modulated sensors

The final modulation mechanism, which applies to fibre optic sensors, utilises the measurand-induced phase modulation of light guided in optical fibres. Phase modulated optical fibre sensors use fibres as the two arms of an optical interferometer. Use of optical fibres enable long optical paths to be assembled without alignment problems. A fibre based optical interferometer enables interferometry to be performed in the field in a compact and rugged instrument. When monochromatic light is travelling along a single-mode optical fibre waveguide, a phase change (φ_1) occurs due to the delay characteristics of the optical fibre. The value of φ_1 can undergo large changes when the single-mode fibre waveguide is subject to temperature or pressure changes [6.17] or tensile strain [6.18].

6.2.4.1 Principle of interferometry

In order to detect a change in optical phase, some form of optical interferometer is required. In this arrangement, part of the light from the optical source is split off into a different optical path of length L_2, to serve as an optical phase reference when later recombined. Assuming that the path L_2 is in a similar single-mode fibre, then φ_2 is the phase of the light as it emerges from the reference fibre. It is arranged that, ideally, this fibre will not be subjected to the effect of the measurand and therefore, φ_2 remains constant. The interference of the light emerging from the reference and sensor fibres can be treated in the same way as that from a two-beam interferometer. The output intensity, I_{out}, is therefore of the form:

$$I_{out} = I_1 + I_2 + 2\sqrt{I_1 I_2}\cos\{\varphi_1 + \Delta\varphi_1 - \varphi_2\} \quad (6.2)$$

Here I_1 and I_2 are the individual intensities from each path. The sensitivity of this function to small changes becomes a maximum when $\varphi_1 - \varphi_2$ takes on values equal to $\pi/2$, $3\pi/2$, $5\pi/2$..... At these points (termed the "quadrature points"), a maximum change occurs in the output intensity for a given $\Delta\varphi$.

There are several common arrangements for fibre interferometers. In general, fibre interferometers can be classified as two beam and multiple beam interferometers.

6.2.4.2 Two beam interferometers

The simplest interferometers divide the light from a source into two beams which follow separate paths before they are recombined. These are called two-beam interferometers. The configuration of two types of two-beam interferometers implemented in fibre-optic form (i.e. the Michelson and Mach Zender) are shown schematically in Figure 6.13a an 6.13b respectively. By suitably coating the sensing fibre, the interferometer can be made particularly sensitive to a wide range of measurands. There has been considerable interest shown in the use of fibre optic Mach Zender interferometer for the measurement of magnetic fields. [6.19] In this method, one arm of the interferometer is either coated with or bonded to a magnetorestrictive material. Under the influence of a magnetic field, the magnetorestrictive materials apply a longitudinal strain on the fibre, this causing the required optical phase change of the light in the fibre. Very low magnetic field can be detected this way. The final two-beam interferometer to be considered is the optical fibre Sagnac interferometer which forms the basis of the optical fibre gyroscope. In this configuration, the beams travel through the same closed path, but in opposite directions as shown in Figure 6.14. Phase differences between the counter-propagating beams are created by nonreciprocity in the optical path. The main application of this interferometer is to detect rotation, which is one source of such nonreciprocity.

Such interferometric devices are extremely sensitive and are capable of very high resolution measurements. They are intrinsic sensors as the measurand acts upon the optical properties of the fibre.

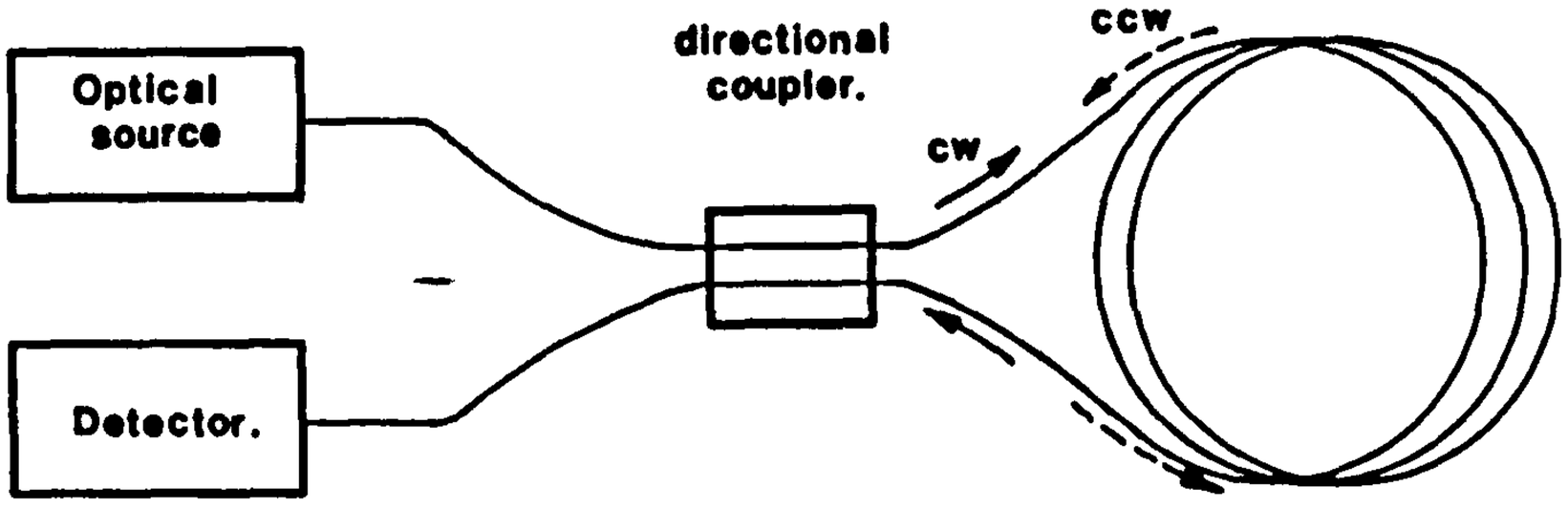

Figure 6.14: Sagnac Interferometer (Grattan K T V: 1995)

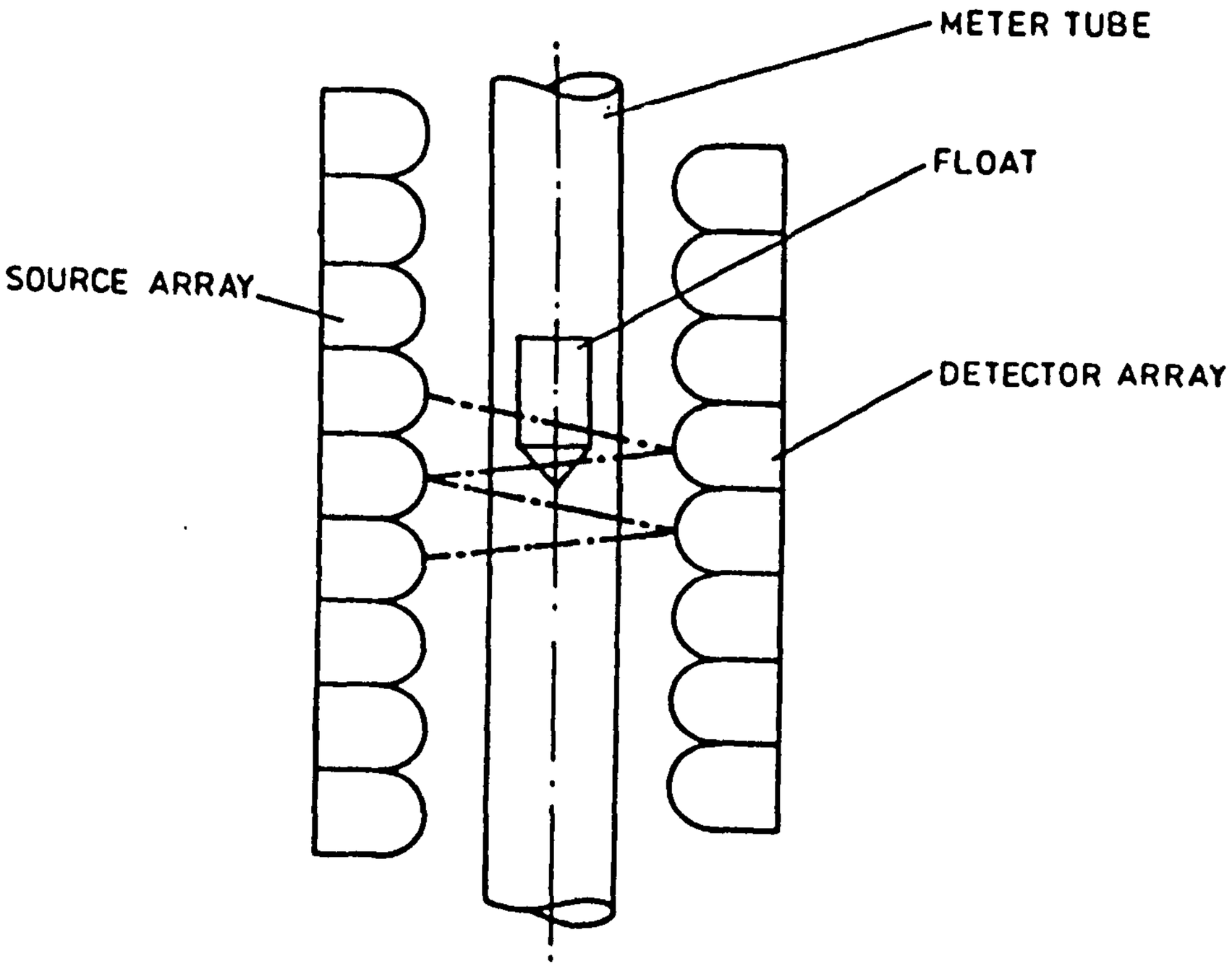

Figure 6.15: Smart's variable area flowmeter (1985)

6.2.4.3 Multiple beam interferometers.

Multiple beam interferometers divide the light into many separate paths before mixing. One way to achieve this is to construct an optical cavity which possesses a single path, which is traversed many times by an input beam. If the sensing region is within the cavity, the measurand acts on the light on every pass, potentially greatly multiplying the effect on the pathlength. The resulting interference between the many progressively delayed waves produces a transmission characteristics which has a resonant behaviour. One form of this type of interferometer is the Fabry-Perot interferometer which has been used to measure temperature, mechanical vibration, magnetic fields, voltage and strain. T. Liu et al have demonstrated the use of a multimode extrinsic Fabry-Perot interferometric sensor to measure quasi-static and dynamic strain in composites.[6.20]

6.3 REVIEW OF OPTICAL FIBRE FLOW SENSORS

Flow sensing is of particular interest in this thesis; therefore there is a need for a review on the different optical fibre flow sensors used in industry. In recent years, considerable interest has been shown in the possibility of using optical sensing techniques for the measurement of flow. Several optical flowmeters have been proposed in the last few years, which have been reviewed by Baker and Morris [6.21] and Dickinson [6.22]. One of the conclusions drawn by Baker and Morris is that *the most successful optical flowmeter design are likely to be those which are based on existing flowmeter constructions.* The optical fibre flow sensor developed in this project is based on an existing flowmeter - the target flowmeter reviewed in Chapters 1 and 4. As the different types of flow meters in general have already been discussed in Chapter 1, the following section assesses the suitability of optical sensing techniques for the various types of flowmeters reviewed in that chapter.

6.3.1 Variable area optical flowmeters

Rotameter - type variable area meters have traditionally been used to give a visual indication of flowrate [Chapter 1.3.1.1]. This limits their use to areas to which the operator has a direct line of sight to the meter. The application of a suitable means for sensing the float position would allow them to be interrogated remotely. Several such devices have been proposed which are based on optical sensing mechanisms. The majority of these devices require that the light should pass through the fluid. However, in

many cases, this does not provide any great obstacle since 'rotameters' are often made from glass or clear plastic and are used to monitor clear liquid and gas flows.

In the device described by Smart [6. 23], which is now commercially available, arrays of semiconductor sources and detectors are located vertically on opposite sides of a rotameter-type variable area meter. Nine equally spaced sources are used with eight detectors, which are similarly equally spaced, but are shifted by half a pitch with respect to the source array, as shown schematically in Figure 6.15. A coarse estimate of the position of the float is obtained, by sequentially activating the sources and scanning the detectors electronically. This indicates which pair of detectors are closest to a prescribed edge of the float. The analog outputs from these detectors are then simply processed in order to yield an accurate measurement of float position.

In another design proposed by Norgate [6.24], an electro-optic technique is used, in which the resistance of a wedge-shaped photoconductive film varies as the shadow of the rotameter float moves along its length.

6.3.2 Fibre optic Impeller devices

Turbine meters are often used for highly accurate flow measurement in the smaller pipe diameters and for relatively clean fluids. [Chapter 1.3.3.3]. It is relatively simple to pass light across the pipe from a fibre-optic emitter such that the exposed light beam is 'chopped' by the impeller blades. At present the read-out is often via magnetic linkage from a coded disc attached to the impeller shaft. There are obvious advantages to a purely optical passive detection system, and the use of a coded disc is not novel. Different approaches are found in the mode of detection from the coded disc, i.e. reflective and transmissive. The former has the advantage of having only one fibre lead to the sensor. In the device proposed by Place and Maurer [6.25], the optical sensor is in the form of a reflective device in which the reflector is attached to a spring. On the underside of the spring is a small magnet. As shown in Figure 6.16, in operation, this magnet is attracted to the passing turbine blades, which are also magnetised. Hence, each blade passage results in a slight tilting of the reflector and hence a decrease in the amount of light collected by the return fibre. Since the intensity variations thus produced can be readily resolved at a remote detection point (several hundred meters),

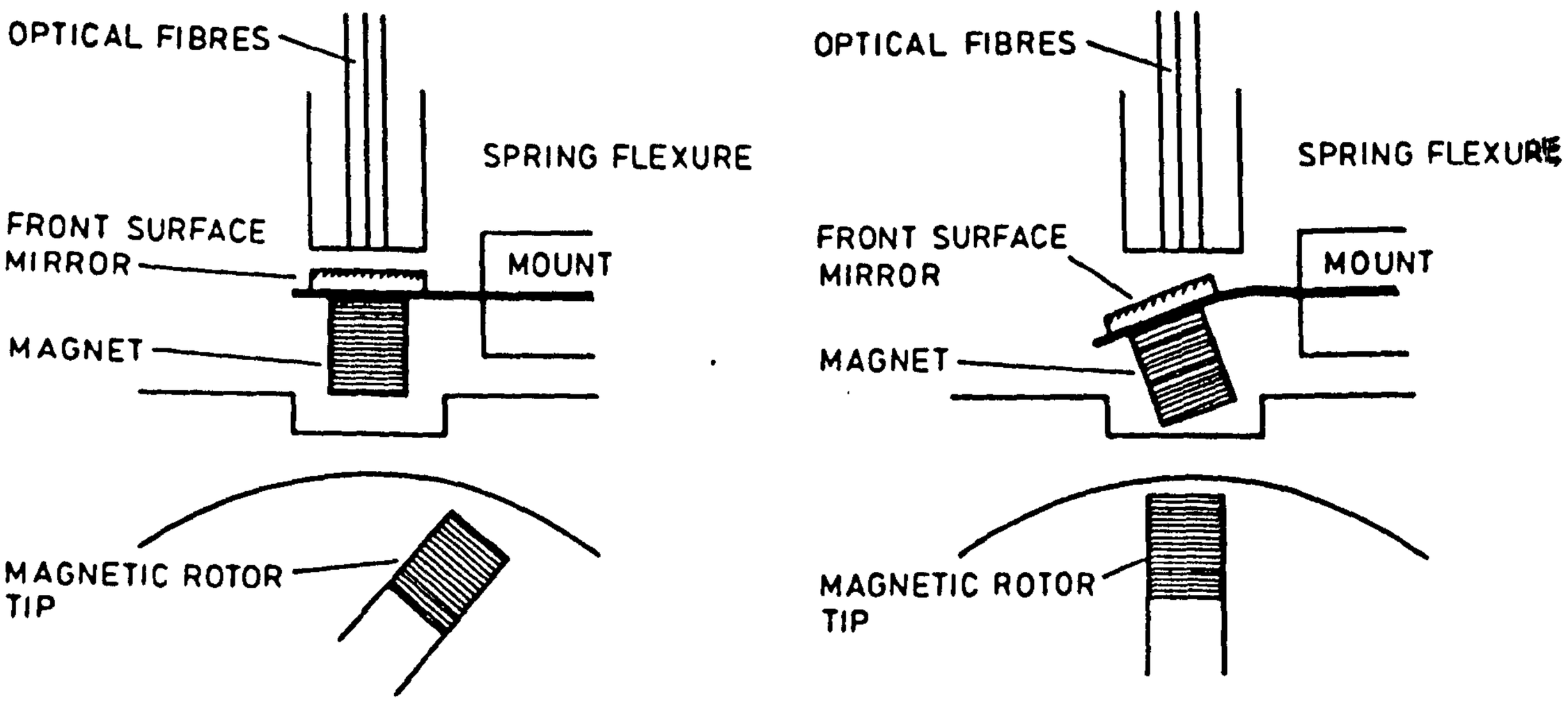

Figure 6.16: Turbine meter pick-up described by Place and Maurer (1986)

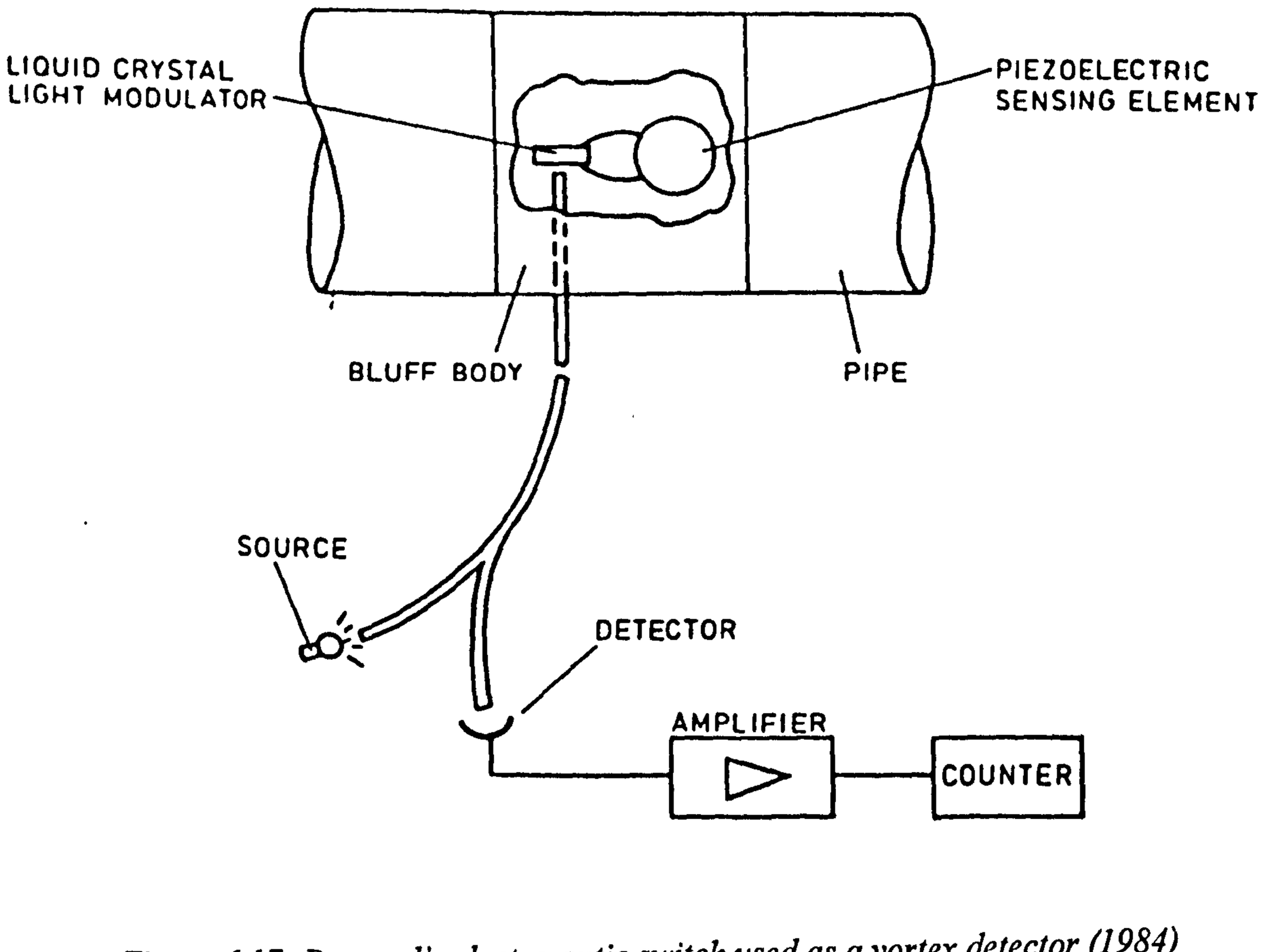

Figure 6.17: Barnard's electro-optic switch used as a vortex detector (1984)

the authors claim that this type of pick-up is particularly suited for use in the hazardous and difficult environments encountered in the oil and gas industry both on and off-shore. This form of detection has several disadvantages. These include the drag produced by the detector, the setting up of eddy currents in the pipe walls by the motion of the magnetised blades and the strict alignment tolerances imposed on the sensor mechanism.

6.3.3 Vortex shedding optical flow sensors

Vortex shedding flowmeters [Chapter 1.3.3.4] rely on the regular generation of a series of vortices downstream of a bluff-body inserted in the flow line. Vortex sensing techniques used in commercially available instruments include capacitive and piezoelectric pressure sensor and strain dependent vortex sensors. One of the main problems with present designs is the difficulty in detecting vortices at low flowrates. Several optical techniques have been proposed which are claimed to overcome this problem. These include the monitoring of variations in pressure and straining of the bluff body which are described in the following sections.

6.3.3.1 Pressure based vortex sensors

The sensor described by Barnard [6.26] is a hybrid electro-optic vortex detector based on a piezoelectric pressure sensing diaphragm and a liquid crystal light modulator. The arrangement is shown schematically in Figure 6.17. The modulator consists of a layer of a liquid crystal on a reflective base. When a voltage is applied across the modulator, the liquid crystal becomes opaque. In Barnard's device, this modulator forms the reflector in a fibre optic reflective sensor housed in the bluff body of a vortex meter. When vortices are shed, the oscillatory differential pressure across the bluff body causes the piezoelectric element to flex and relax. With the output voltage from the piezoelectric element connected across the modulator, the intensity of the reflected light is modulated at the vortex shedding frequency. The advantages of this sensor is that it has a built-in power supply which responds readily to the desired measurand and that the flowmeter is electrically isolated from both the process fluid and the outside world. The major problems are likely to be the temperature stability of the device and the ageing of the liquid crystal. A sensor design which has the advantage that the optical sensing is

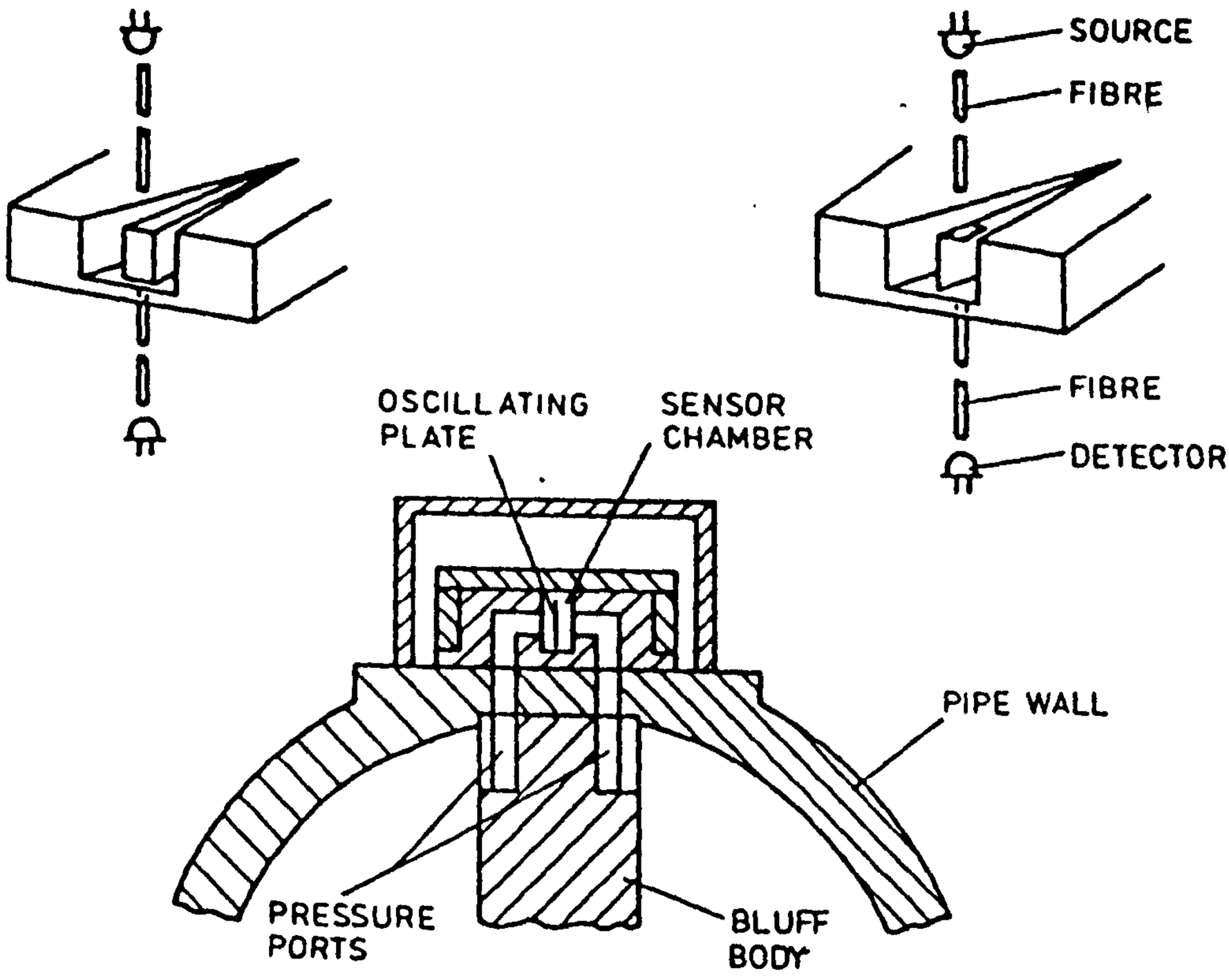

Figure 6.18: Vortex detector described by Tsuruoka and Miyoshi (1986)

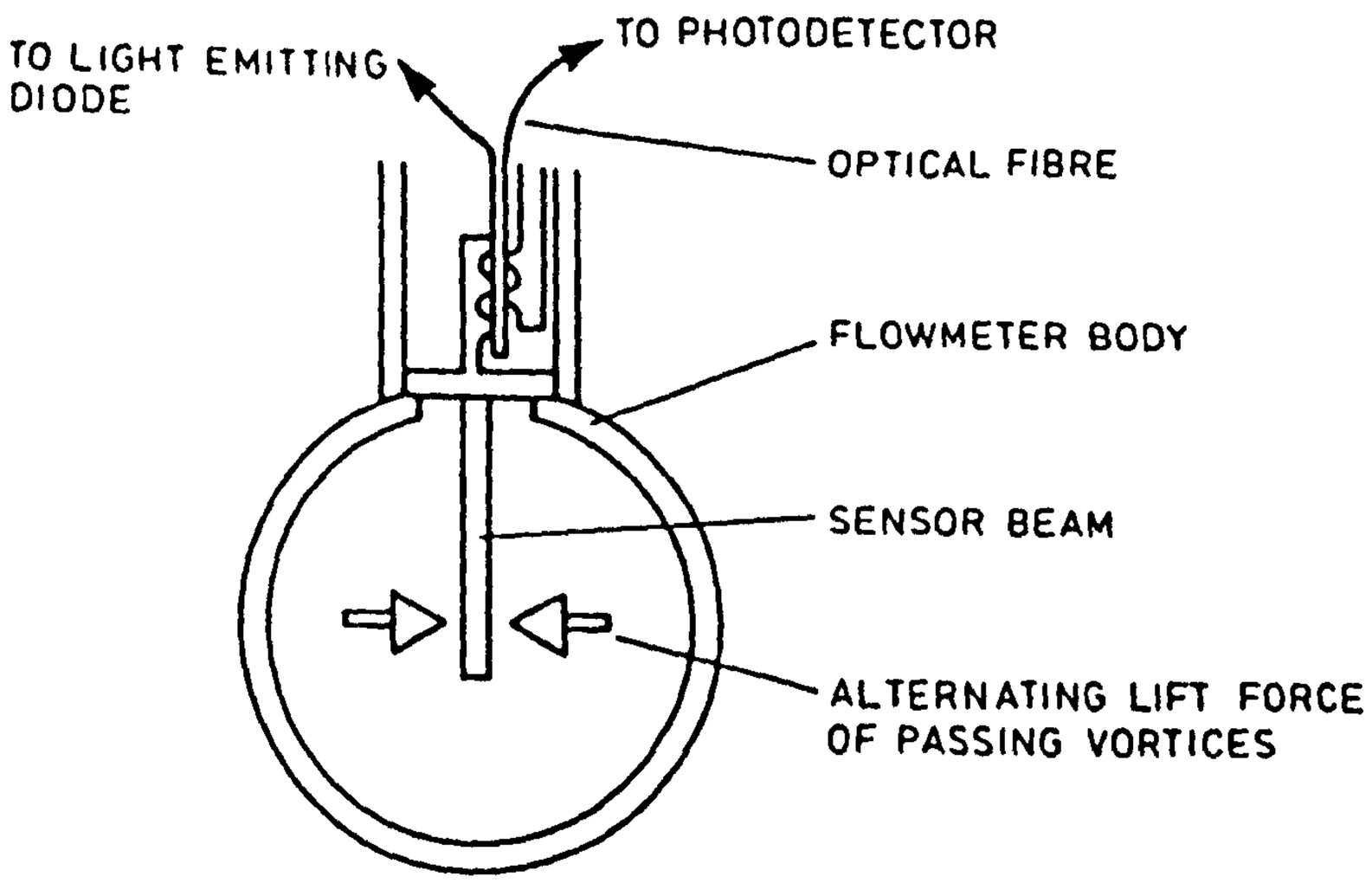

Figure 6.19: Microbend vortex sensor described by Sovik (1985)

performed outside the pipe has been proposed by Tsuruoka and Miyoshi [6.27]. In their design, a pair of pressure ports within the bluff body transmit the pressure from either side of the bluff body to the sensing mechanism which is external to the pipe as shown in Figure 6.18. The sensing mechanism consists of a thin plate which is caused to flap in response to the oscillatory differential pressure across the body. This plate is centred magnetically. The fact that the sensor is located outside the confines of the pipe implies that it may be possible to replace the sensor without having to shut down the process. The remoteness of the sensor from the process fluid also implies that such a construction could be used in the metering of high temperature fluids.

6.3.3.2 Strain based vortex sensors

In the design described by Sovik [6.28], the flowmeter is of a dual body construction. The first bluff body is fixed and acts merely as a vortex generator while the second, which is only fixed at one end, acts as a transducing element. The transducing element forms one arm of a lever whose pivot is a seal in the wall of the pipe. The other arm of the lever is connected to a pinch plate as shown in Figure 6.19. This pinch plate forms half of a fibre optic microbend sensor. The pinch plate which forms the other half of the sensor is fixed to the flowmeter housing. The shedding of vortices by the first body causes the transducing element to oscillate transversely to the flow direction. This oscillatory straining is transmitted via the levering action to the microbend sensor. Hence, the intensity of the detected light from the sensor is modulated at the vortex shedding frequency. This is the configuration used in the only currently available optically sensed vortex flowmeter.

6.3.4 Thermal flowmeters

The principle of the two major thermal flow sensors - the hot wire and hot film anemometers have been reviewed in Chapter 1.3.4.1. Optical sensing techniques are presently more expensive to implement than electronic methods and it is therefore envisaged that they will not be developed to any great extent in this area. The only possible exception is the development of an accurate, low-cost optical temperature sensor for use in some thermal flowmeters as proposed by Theoderescu et al [6.29]. In their device, a short section of a metal pipe is electrically heated at constant power as

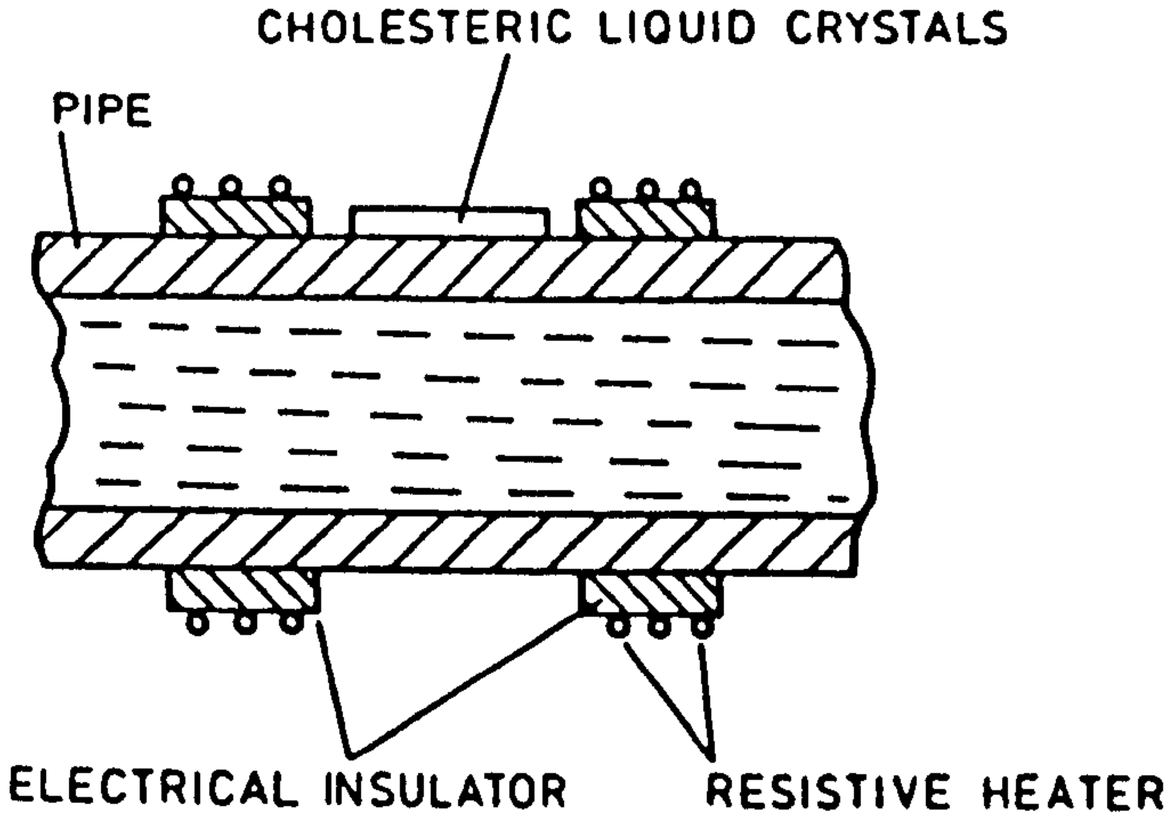

Figure 6.20: Thermal meter described by Theoderescu et al (1981)

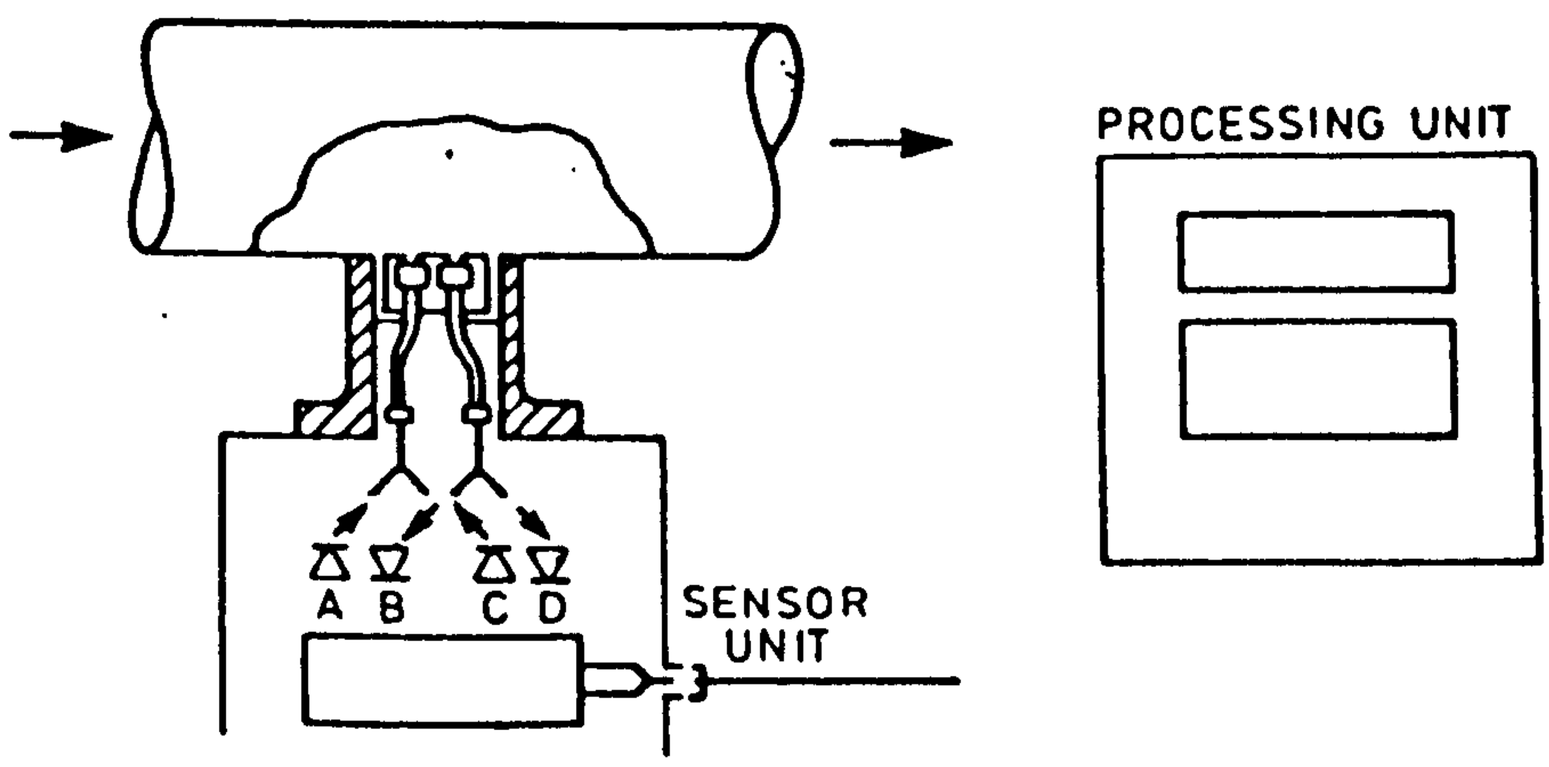

Figure 6.21: Nord's cross-correlation meter (1981)

shown in Figure 6.20. The fluid passes through the section and convects heat away with it. The amount by which the section is cooled is dependent on the fluid flowrate. A layer of cholesteric liquid crystal, in good thermal contact with the pipe section, is used to indicate its temperature. The temperature of the section is derived from the colour of the liquid crystal. Hence, after calibration, the colour of the liquid crystal may be used to infer the fluid flowrate.

This design has the advantage that no obstruction is presented to the flow. In addition, by using fibre optic transmission, it is possible to interrogate it remotely. However, it has several disadvantages. In common with all thermal flowmeters, it is sensitive to changes in thermal conductivity and specific heat capacity which may result from variations in the fluid composition. Also, in addition to its dependence on flowrate, the amount by which the pipe section is cooled depends on the temperature of the fluid itself. The technique used by the authors to minimise this effect is to operate the heater at a very high temperature. This can reduce the effect but may result in overheating of the equipment.

6.3.5 Ultrasonic optical flowmeters

Of the devices included under the category of the ultrasonic flowmeters [Chapter 1.3.3.5], only the cross-correlation and related transit time techniques are likely to undergo further development from the point of view of optical sensing. Cross-correlation flowmeters operate by measuring the transit time of a tagging signal (from turbulence, particles, etc.) in the flow between to axially separated sensors. The signals produced by the detectors both vary randomly as a function of time. However, the transit time may be readily obtained as the value at which their temporal cross-correlation is a maximum. The flowrate is inversely proportional to this transit time.

The optical cross-correlation flowmeter described by Nord [6.30] is used in the metering of paper pulp stock. In this device, which is now commercially available, reflection of light from particles in the fluid is used. In the currently available model, shown in Figure 6.21, short fibres are used to connect the sources and detectors in the body of the flowmeter to windows in the pipe wall. The correlation is performed within the flowmeter itself and the transit time between the two sensors is thus obtained.

6.4 DISCUSSION

This chapter has reviewed the different modulating mechanisms using optical fibres showing that optical fibres have the potential to be exploited in different ways in many sensing applications. Intensity modulated sensors have been reviewed in greater detail than the other mechanisms as the sensor that was developed in this project has used this principle. Last but not the least, the different flow measuring techniques using optical fibres have been discussed in order to have an overall understanding of the different ways in which fibre optics has influenced this important part of the industry - fluid flow measurement.

CHAPTER 7

THE FIBRE OPTIC STRAIN GAUGE

Although attenuation in optical fibres is a disadvantage in communications, it has proven itself useful as a transduction mechanism in fibre optic intensity sensors. For applications where the sensitivity is the primary consideration, optical interferometric sensors have no equal. On the other hand, multimode fibre sensors are preferred in applications where simplicity and robustness are of paramount importance. Many existing multimode fibre strain sensors require the use of external structures to induce perturbations on fibres.[7.1-7.3]. Presented in this chapter is a new class of optical fibre strain sensor that do not require the use of external structures to impose perturbations on fibres. Instead, grooves are formed directly into the fibre cladding and extending into the core. Such grooved fibre sensing elements have been fabricated and tested as strain sensors. These grooved fibre sensing elements may be used as the basis for simple and reasonably sensitive sensors, one application of which is the optical fibre flow sensor described in Chapter 8.

7.1 THE POLYMER FIBRE STRAIN SENSOR FABRICATION

The strain sensor comprises a single 1 mm diameter multimode plastic optical fibre. The fibre has a core diameter of 0.980 mm and is formed from pure Poly-Methyl-Methacrylate (PMMA), and this is surrounded by a thin cladding layer (approximately 20 μm) of fluorinated PMMA. Good fibre end face termination was achieved using a wet (water) polish technique.

Optical fibres can be categorised into two main groups: multimode and single mode fibres. There are a large variety of optical fibres available today. They have different characteristics which usually depend upon the material and the technique used in the fabrication process. Then why was multimode plastic fibres chosen for this project?

7.1.1 Why Plastic Fibres?

All-plastic fibres have some important attractions. The large core diameter, and large NA, typically 0.47, of plastic optical fibres (POF) make connection particularly easy and

reliable. There is no need for connectors with tight mechanical tolerances as with glass fibres and most connection techniques utilise simple and cheap plastic moulded connectors. Plastic fibres do not require expensive equipment such as cleavers and mechanical polishing jig to achieve a good coupling with some other elements of the sensor like photodetectors or the light source. Due to the mechanical properties of the plastic, the fibre is not as brittle as silica fibres giving it a better flexibility and ease of handling. Furthermore, POF are less susceptible to transmission variations due to vibrations which is important in industrial environments. Plastic fibres are very cheap (£0.50 / m) and its low cost is an advantage when considering the cost of the sensor for commercial exploitation. Silica fibres, on the other hand, tend to be stiff and expensive.

Since commercial fibres are manufactured as defect-free as possible, construction of this strain gauge requires the introduction of grooves in a separate process. For this, the fibre must be heated to its softening point (described in Section 7.1.2) and then cooled. Because of the high softening point of glass fibres (on the order of 1000^0C, depending on their impurity content) and their brittle character, it was found that plastic fibres were vastly simpler to work with. In addition to their ductility and low softening point, plastic fibres have the advantage of low rigidity, with a Young's modulus more than twenty times smaller than that of glass. Thus the POF are more sensitive when used in transducers and hence more closely approach the ideal strain gauge. On the negative side, all-plastic fibres have much higher attenuation compared to their glass counterparts, which may be a problem when remote measurement over large distances are required. But for the envisaged application of this flow sensor, this should not be a problem as their transmission is completely adequate in the visible and near infrared over the short length required for the gauge and its leads, typically less than 3 m. The other disadvantage of plastic fibres are that they have less resistance to high temperatures than glass types. Low glass transition temperatures limit most plastics to temperatures below about 85^0C. New types can operate up to 125^0C but have higher losses [6.8]. These temperature limits have been an important problem in automobile applications but for the measurement of fluid flow in this project below these temperatures, this should again not be a problem. Table 7.1 gives the specifications of the fibre used in this project.

Table 7.1: The characteristics of the plastic fibre (Supplier: Toray manufacturers)

core material	polymethyl methacrylate (PMMA)
cladding material	fluorinated polymer
core/cladding diameter	1 mm
Optical construction	step index
Attenuation at 665 nm	200 dB/km
Core refractive index	1.492
Cladding refractive index	1.417
Numerical Aperture	0.47
Acceptance angle	56^0
Minimum bend radius	15 mm
Tensile strength	5 kg
Operating temperature range	-30^0 to 85^0 C
Maximum temperature	100^0 C

7.1.2 The Fibre Groove

The optical fibre strain sensor uses 1mm diameter PMMA fibre as the sensing element. This is sensitised to deformation by building multiple grooves extending to the centre of the fibre. The grooves were formed using a hot scalpel, and a V-groove template designed by the author and manufactured in the department workshop to ensure uniformity of grooves. This was then allowed to cool for a few minutes before being put to the test. The dimensions of the groove were measured in situ using a microscope which allowed the groove apex angle to be determined. These dimensions are discussed in Section 7.3.

7.2 PRINCIPLE OF OPERATION OF THE OPTICAL FIBRE STRAIN GAUGE

As the optical fibre with the grooves is bent as in a cantilever, the angle of the grooves vary. These changes of angle cause light to be attenuated at each groove. The intensity variation can be related to the change of the angle of the groove, caused by the bending of the cantilever. In order to derive a mathematical model of the performance of this

sensor, it is first assumed that the sensor has only one groove, and afterwards the relation derived is extended to different number of grooves.

Figure 7.1 a shows a schematic of the groove before the sensor is subjected to any strain. The depth of the groove has been denoted by 'a' . For this sensor, the depth is 0.5 mm as the V-groove template has been manufactured with a depth of 0.5 mm. So for all our calculations, it shall be assumed that 'a' is 0.5 mm. The width of the groove is assumed to be $2z_0$ and the apex angle of the groove is assumed to be $2\theta_0$. Figure 7.1 b shows the schematic of the same groove when subjected to strain. Here, the apex angle of the groove has increased to $2\theta_x$ and the width of the groove has increased to a value of 2z by a factor $2z_1$.

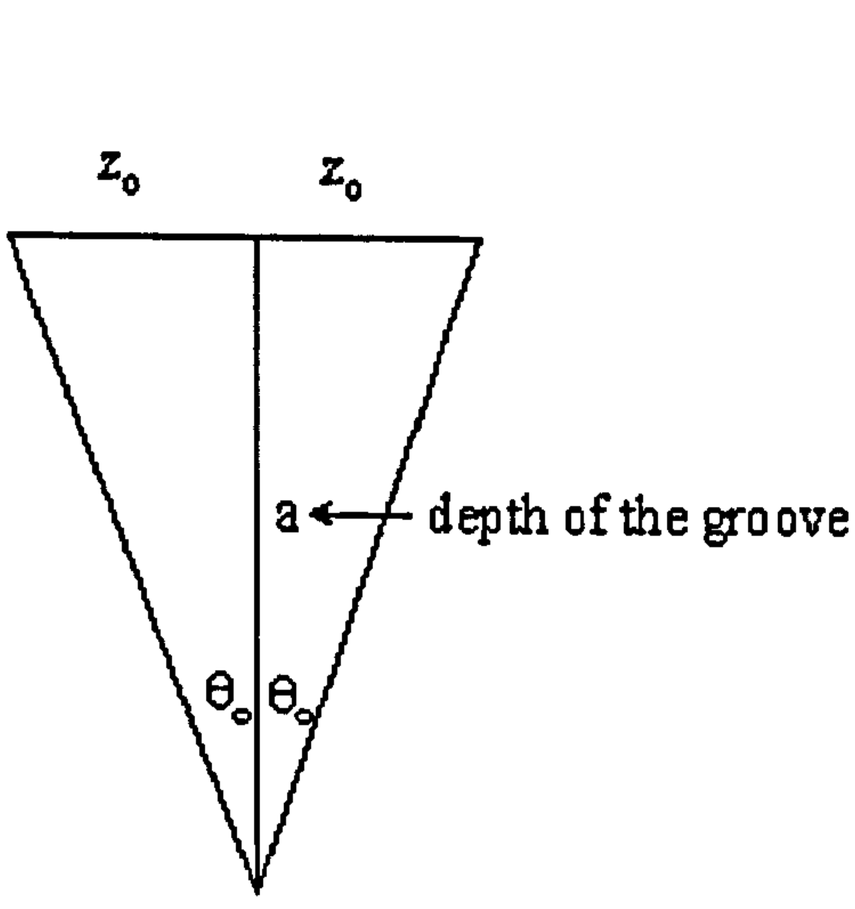

Figure 7.1a: Groove at zero strain

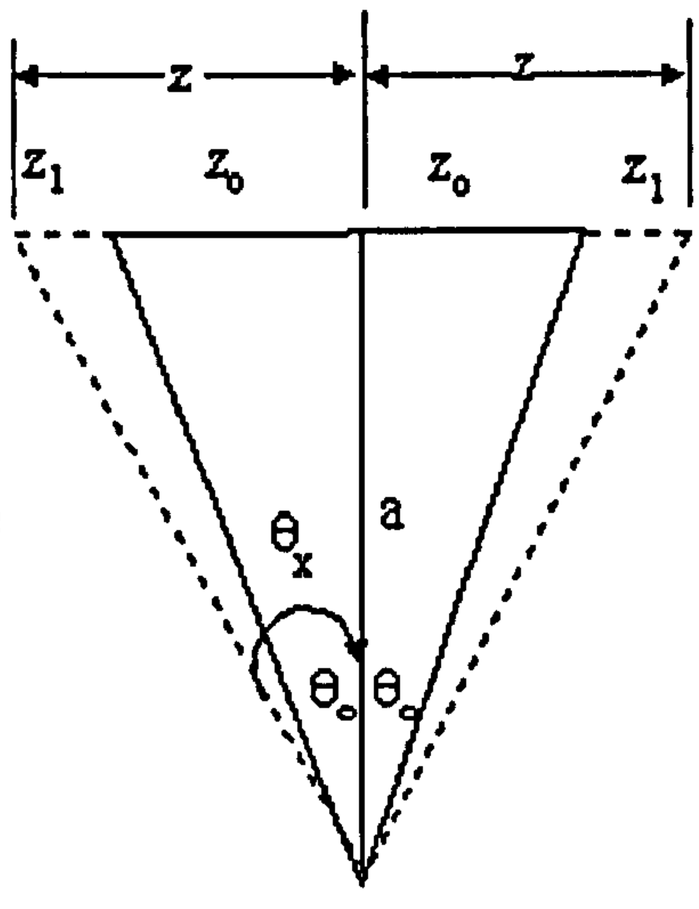

Figure 7.1b: Groove after strain

The very presence of the groove induces a loss of light (P_{L0}) in the fibre which is characterised by the area πz_0^2. After the application of the force, the fibre groove undergoes an extension and therefore more light is attenuated. This light lost due to the strain (P_{Lx}) is given by the area $\pi[z_0 + z_1]^2$. Experimental observation showed that the light emerging from the groove formed a solid cone perpendicular to the axis of the fibre.

From trigonometric equations of Figure 7.1 a and 7.1 b:

$$z_0 = a\ \mathrm{Tan}(\theta_0) \qquad (7.1)$$

$$z = a\ \mathrm{Tan}(\theta_x) \qquad (7.2)$$

$$z_1 = z - z_0 = a\ [\mathrm{Tan}(\theta_x) - \mathrm{Tan}(\theta_0)] \qquad (7.3)$$

Hence it can be derived that:

$$P_{L0} = \pi z_0^2 = \pi a^2 [\mathrm{Tan}(\theta_0)]^2 \qquad (7.4)$$

$$P_{Lx} = \pi[z_0+z_1]^2 = \pi z^2 = \pi a^2 [\mathrm{Tan}(\theta_x)]^2 \qquad (7.5)$$

7.2.1 Definition of strain sensitivity

The gauge factor is a measure of the sensor sensitivity. Suppose the gauge output V volts is changed by ΔV volts when a strain $\Delta L/L$ is applied, then the gauge factor of the resistance strain gauge is defined as:

$$G = \frac{\Delta V}{V} \Big/ \frac{\Delta L}{L} \qquad (7.6)$$

For optical fibre strain gauges under consideration, the output signal of the power meter or the photodetector is proportional to the optical power transmitted through the plastic optical fibre (POF). For our application, strain sensitivity (S_0) is defined as :

$$S_0 \equiv \frac{\Delta P}{P_0 \varepsilon} \qquad (7.7)$$

where ΔP is the strain-induced change in optical power in watts transmitted through the gauge undergoing strain, ε is the value of that strain and P_0 is the optical fibre gauge transmission at zero strain. P_0 is the difference between the power transmitted before the groove was cut(P_i) and the light lost due to the groove at zero strain (P_{L0}).The power transmitted after a strain 'x', denoted as P_x, is the difference between P_i and the light lost from the groove due to that strain (P_{Lx}). Hence:

$$P_0 = P_i - P_{L0}; \quad P_x = P_i - P_{Lx} \qquad (7.8)$$

Figures 7.2a, b and c have been included to understand more clearly the theory mentioned in the previous paragraph. Figure 7.2a shows the POF prior to the grooving. P_{in} is the light intensity injected into the POF by the laser. The output power from the POF, detected by the power meter is P_i which was measured experimentally (Section 7.3.3).

Figure 7.2a: POF before grooving

Figure 7.2 b shows the POF after a groove was inserted but before strain was applied. The light lost at the groove is P_{L0} and hence the output power from the POF is $P_i - P_{L0}$.

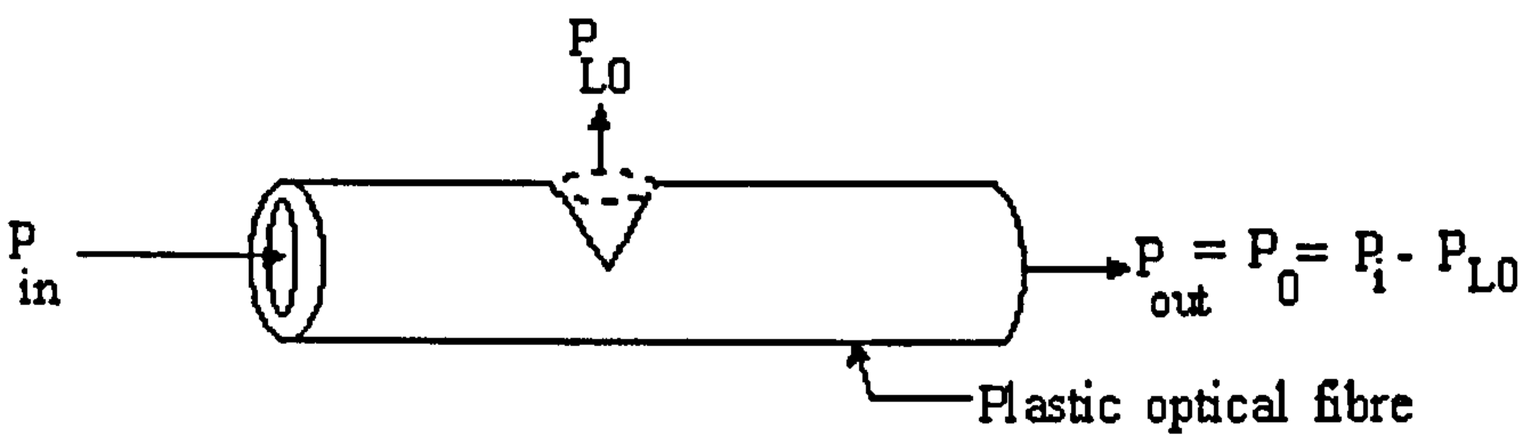

Figure 7.2b: POF after grooving but at zero strain

Figure 7.2c shows the POF after the strain was induced. The light attenuated from the groove in this case is P_{Lx} and hence the output power from the POF is $P_i - P_{Lx}$.

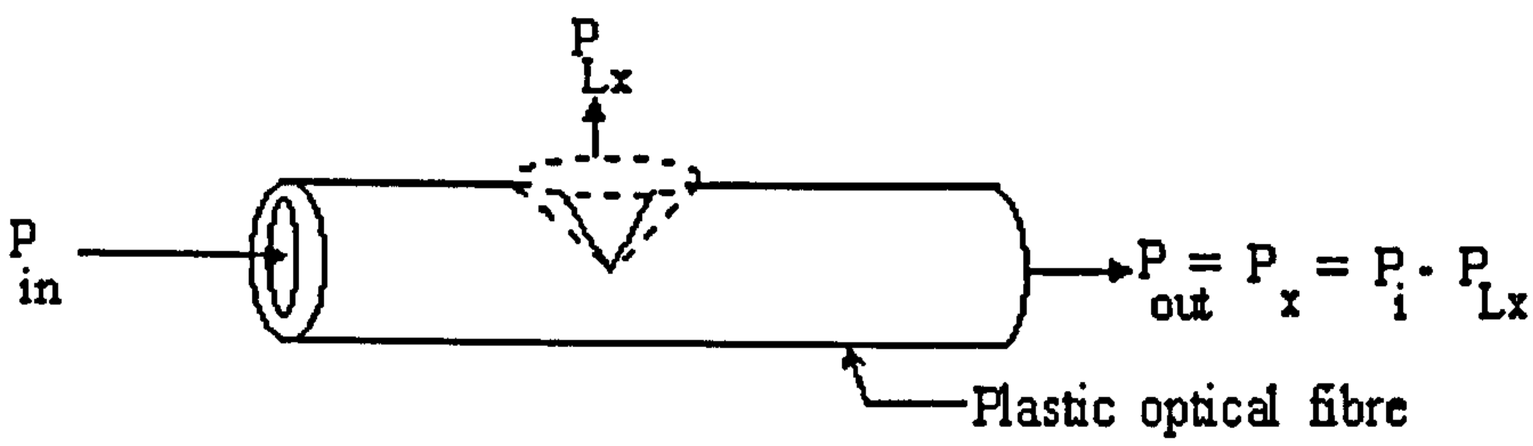

Figure 7.2c: POF after the application of strain

Assuming that the power meter output signal is proportional to the optical power incident on its detector, the change in optical power, ΔP, is proportional to applied strain. Provided that the only optical power loss mechanism that changes when strain is applied is within the gauge itself and not in external connector feed and return fibres, the change in detector output will also be proportional to ΔP. The performance of the sensor is described by the coupling factor (CF) which is defined as the ratio of the change in optical power transmitted by the fibre after a strain is induced, to the power transmitted at zero strain. CF is defined in Equation 7.9, derived from consideration of the trigonometry of Figure 7.1.

$$CF = \frac{\Delta P}{P_0} = \frac{P_0 - P_x}{P_0} = \frac{P_{Lx} - P_{L0}}{P_i - P_{L0}} \qquad (7.9a)$$

Pi has been experimentally determined to have a value of 0.1948 mW (Section 7.3.3). Substituting Equations 7.4 and 7.5 in Equation 7.9a, it is shown that:

$$CF = \frac{(\mathrm{Tan}\theta_x)^2 - (\mathrm{Tan}\theta_0)^2}{k - (\mathrm{Tan}\theta_0)^2} \qquad (7.9b)$$

where $k = \frac{0.1948mW}{\pi a^2} = 248.027\ mW/m^2$. (as $a = 0.5\ X10^{-3}$ m)

Strain (ε) has traditionally been defined as the change in length, ΔL, over the original length, L, and so from Figures 7.1 a and 7.1 b it can be observed that:

$$\varepsilon = \Delta L/L = 2z_1/2z_0 = z_1/z_o \qquad (7.10)$$

Substituting Equations 7.1 and 7.3 in the above equation, it can be shown that:

$$\varepsilon = \frac{(\mathrm{Tan}\theta_x) - (\mathrm{Tan}\theta_0)}{(\mathrm{Tan}\theta_0)} \qquad (7.11)$$

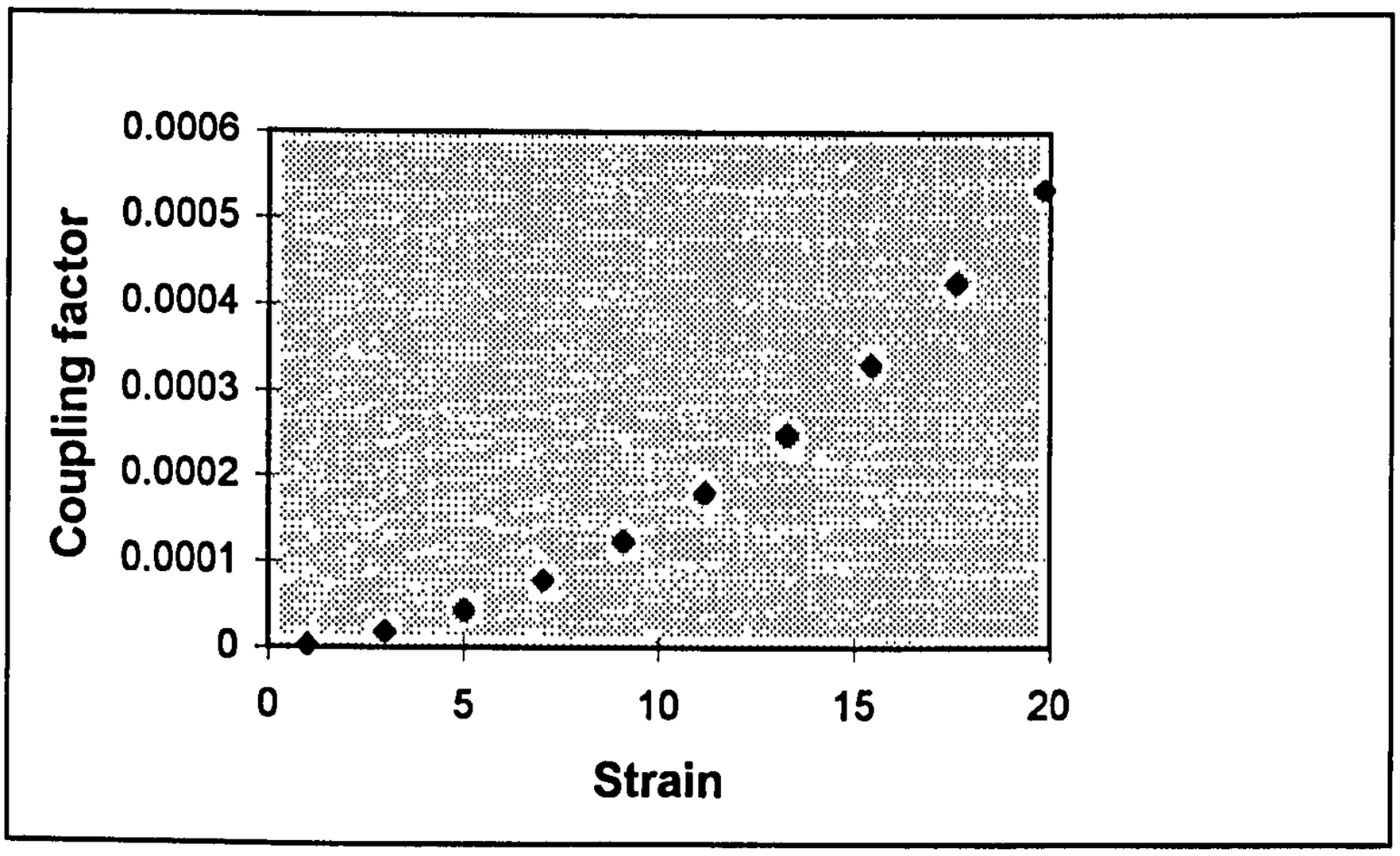

Figure 7.3: Coupling factor versus strain for 1 groove (Mathematical model)

Having theoretically derived the strain and coupling factor (CF) for a single groove, these parameters are plotted in Figure 7.3 for different values of groove angles (θ_x) from 2^0 to 20^0, assuming that the initial groove angle (θ_0), before application of strain is 1^0. From these plots, the strain sensitivity for a single groove, which forms the gauge factor for the optical fibre strain gauge was calculated according to Equation 7.7.

7.2.2 Gauge factor for multiple grooves.

Section 7.2.1 derives expressions for the optical fibre strain sensor with a single groove. However, it was predicted that the strain sensitivity could be increased by increasing the number of grooves. So, in order to mathematically model the effect of increasing the grooves, the coupling factor for 'n' grooves $(CF)_n$ was calculated. The light intensity lost due to the presence of 'n' grooves is $(n\ P_{L0})$ at zero strain and $(n\ P_{Lx})$ after a strain 'x',

assuming that each groove undergoes equal extension. Replacing these terms in Equation 7.9 a the coupling factor for 'n' grooves was obtained:

$$(CF)_n = \frac{nP_{Lx} - nP_{L0}}{P_i - nP_{L0}} \qquad (7.12)$$

Substituting Equations 7.4 and 7.5 in 7.12:

$$(CF)_n = \frac{(\mathrm{Tan}\theta_x)^2 - (\mathrm{Tan}\theta_0)^2}{(k/n) - (\mathrm{Tan}\theta_0)^2} \qquad (7.13)$$

and the strain for 'n' grooves was calculated using the equation:

$$\varepsilon_n = \frac{\left[n(\mathrm{Tan}\theta_x) - n(\mathrm{Tan}\theta_0)\right]}{n(\mathrm{Tan}\theta_0)} = \frac{\left[(\mathrm{Tan}\theta_x) - (\mathrm{Tan}\theta_0)\right]}{(\mathrm{Tan}\theta_0)} \qquad (7.14)$$

From Equations 7.13 and 7.14, the values of the strain sensitivities for different number of grooves varying from 1 to 8 was calculated according to Equation 7.7. As expected there was an increase in the strain sensitivities as the number of grooves increased.

Figure 7.4 shows the values of strain sensitivity plotted against the number of grooves. The strain sensitivity increases by a factor of 2.7 E-05 as the groove number increases for the mathematical model.

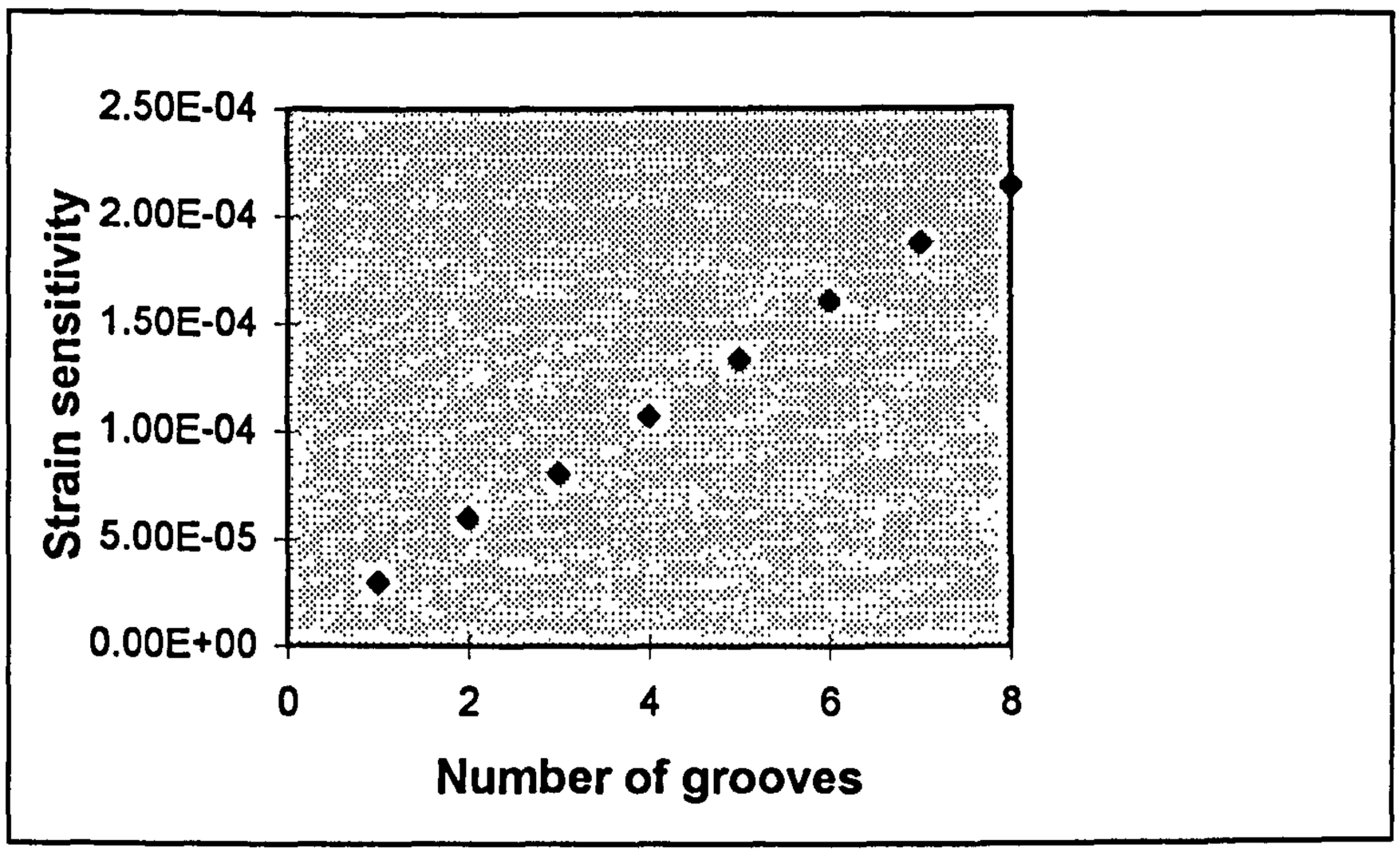

Figure 7.4: Strain sensitivities for different number of grooves

7.2.3 The effect of groove closing

In the mathematical model described in Sections 7.2.1 and 7.2.3, it has been assumed that the strain is applied so that the groove undergoes extension and is opened (Figure 7.1b). It has been shown that the light lost from the groove after a strain 'x', referred to as P_{Lx}, is greater than the light attenuated at zero strain (P_{L0}). However, in actual practise, the applied strain could also result in the closing of the groove (compression). In this case, P_{Lx}, the light attenuated after a strain would be less than P_{L0}. Hence the CF and strain due to the groove closing would be the negative of Equations 7.9 and 7.11, described in Equations 7.15 and 7.16 respectively.

$$CF = \frac{(\mathrm{Tan}\theta_0)^2 - (\mathrm{Tan}\theta_x)^2}{k - (\mathrm{Tan}\theta_0)^2} \tag{7.15}$$

$$\varepsilon = \frac{(\mathrm{Tan}\theta_0) - (\mathrm{Tan}\theta_x)}{(\mathrm{Tan}\theta_0)} \tag{7.16}$$

As the groove closes, the groove angle(θ_x) decreases, and the power transmitted through the POF would increase. However the magnitude of the coupling factor (CF) and the strain increases, just as in the case of the groove opening (that is θ_x increasing). So the effect of the closing of the groove on the CF and strain is the same as for the groove opening. This effect was observed experimentally as well, thereby validating the mathematical model. Therefore, during the experimental observation, it does not matter whether the groove is opening or closing. The change in optical power always causes the magnitude of CF and strain to increase both for the mathematical model and during the experimental process described in Section 7.3.

7.3 EXPERIMENTAL VERIFICATION OF THE THEORY

7.3.1 Experimental arrangement

A specially designed optical arrangement was used to confirm the theoretical model described in the above section. Figure 7.5 illustrates the experimental arrangement that was used to measure the coupling factor and strain for multiple number of grooves.

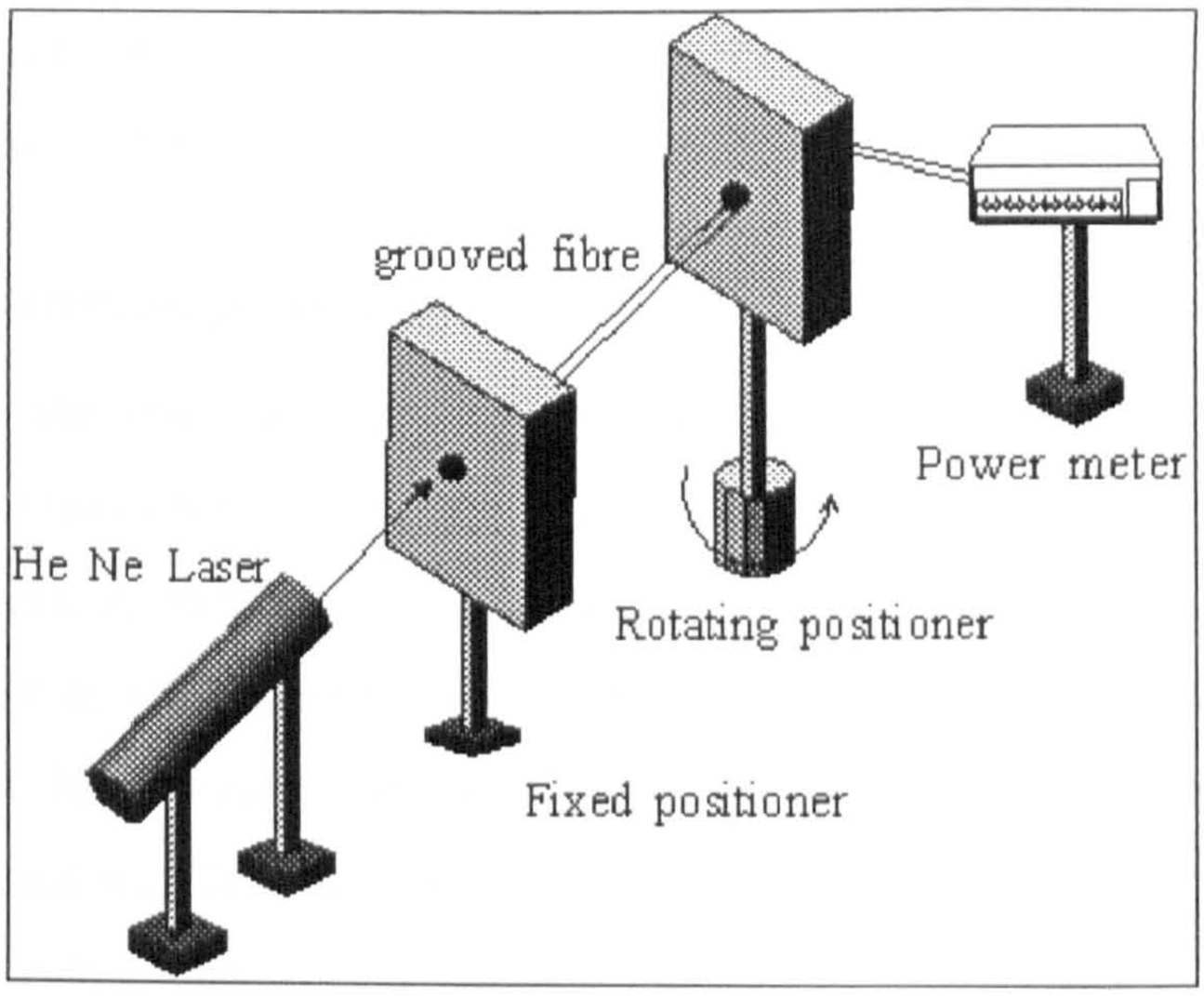

Figure 7.5: Experimental arrangement for measuring the strain sensitivity

Referring to that figure, a straight fibre was connected to the light source (the He-Ne Laser) and the power meter. One end of the fibre was secured onto a fixed positioner and the other end was connected to the power meter. The fibre was threaded through a precision translator equipped with a micrometer which when rotated, would generate tension in the fibre causing the groove angle to change and the strain to increase. The fibre was fixed to the two positioners using a small amount of epoxy. Since the laser and the power meter were also secured to their respective positioners, all fibre strain occurred in the fibre length between the positioner (stationary) and the translator (movable). Thus the fibre connections to the source and detector were undisturbed during the straining process and could, therefore, be eliminated as a contribution to the strain-induced signal.

7.3.2 Thermal effects

Another observed effect during this measurement process, were the negligible changes produced by ambient temperature fluctuations in the fibre's power output when compared to the change in output caused by strain . The stability at room temperature is probably due to the insensitivity of the laser output to temperature and the fact that the numerical aperture of this fibre changes less around 20^0C than it does at certain higher temperatures. [7.4] Furthermore, since the refractive index of PMMA changes less around room temperature than at elevated temperatures[7.4], we can infer that its coefficient of thermal expansion behaves in a similar manner. Thus the errors caused by

the thermal effects on mechanical strain would probably be more severe at elevated temperatures. But no tests were conducted to verify this hypothesis.

7.3.3 The measurement process

Before grooving the fibre, the output of the power meter was noted as 0.1948 mW. This quantity is the optical power entering the fibre optic gauge and is referred to as Pi. The difference between P_i and P_0 is simply the loss introduced by the groove. When the ungrooved fibre was subjected to strain by the translator, the change of the output signal was too small to be observed. On the other hand, if the fibre had grooves, the output signal was reduced significantly. Therefore grooving greatly enhances the sensitivity of this fibre optic strain gauge.

A travelling microscope was positioned perpendicular to the grooved fibre in order to monitor the dimensions of the grooves using the vernier scale in the x and y-axis of the microscope. Initially a groove was inserted into the fibre using a hot scalpel to a depth of 0.5 mm. The power intensity transmitted through the fibre reduced to 0.165 mW (P_o). The width of the groove and hence the initial length of the groove was measured using the travelling microscope. Then the movable positioner was rotated till there was an observable reduction in the power intensity (P_x). Again the dimensions of the groove were measured by the travelling microscope, and the strain was calculated. This was repeated for several rotations of the movable positioner. The experiment was also conducted by moving the micrometer in the opposite direction causing the groove to close and P_x to increase. The coupling factor was calculated as:

$$CF = \frac{\pm(P_x - P_0)}{P_0} \qquad (7.17)$$

In Equation 7.17, the '+' sign was used when the groove closed and the '-' sign was used when the groove opened. For both sets of data taken, the CF and strain increased as predicted by the mathematical model (Section 7.2). Figure 7.6 shows the plot of the experimental coupling factor versus strain after a single groove was built into the fibre.

A second groove was cut into the fibre to a depth of 0.5 mm. The power intensity transmitted through the fibre was further reduced (P_o).

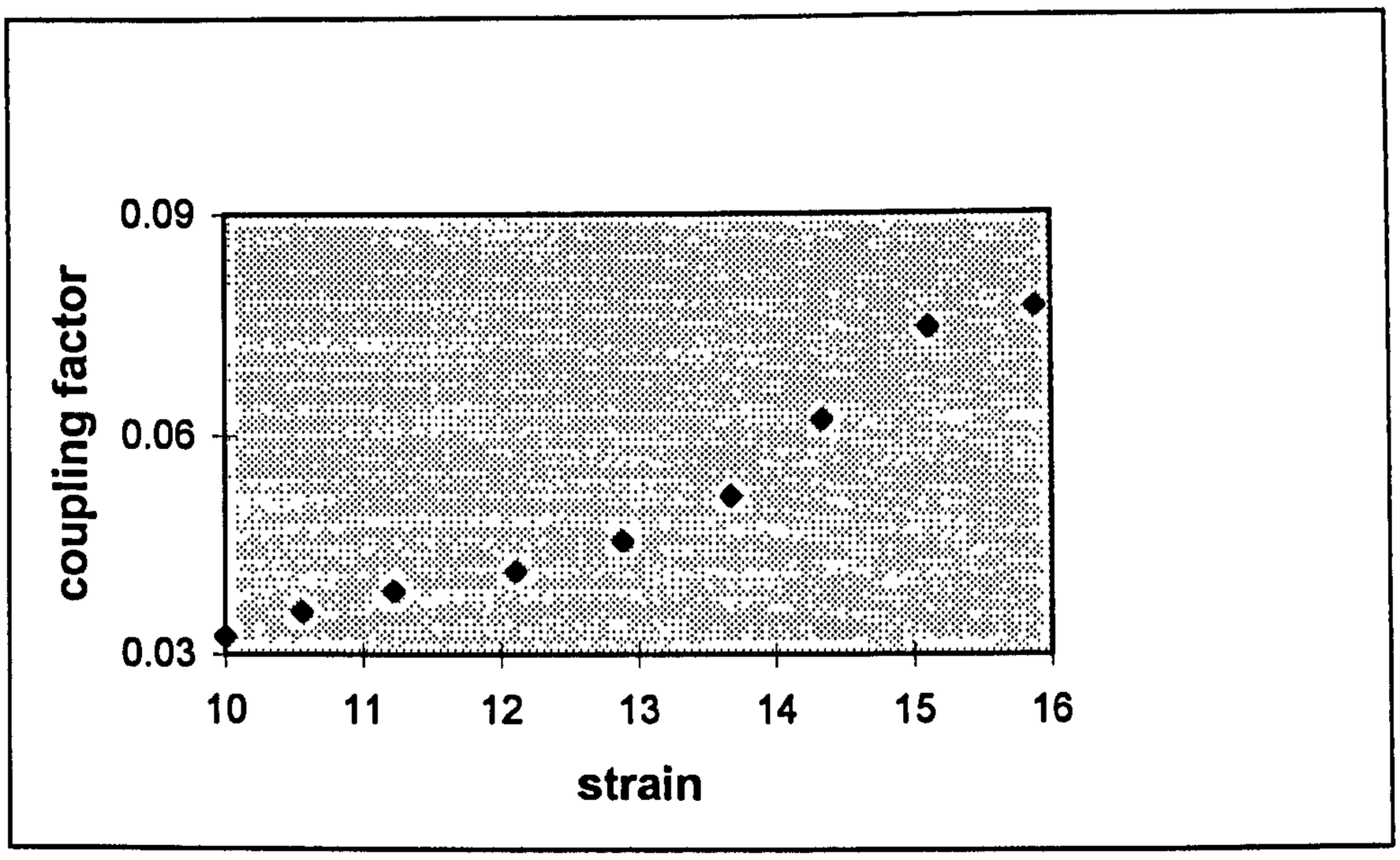

Figure 7.6: Coupling factor versus strain for 1 groove(experimental)

The width of each groove and hence the initial length of each groove was measured using the travelling microscope. Then the movable positioner was rotated till there was an observable reduction in the power intensity (P_x). Again the dimensions of the grooves were measured by the travelling microscope. Strain was measured by finding the ratio between the sum of the change in length of each groove and the sum of the original length of each of the two grooves. The coupling factor was again calculated for two grooves. The coupling factor and the strain were plotted against each other and again the strain sensitivity was observed. This was repeated for up to 8 grooves.

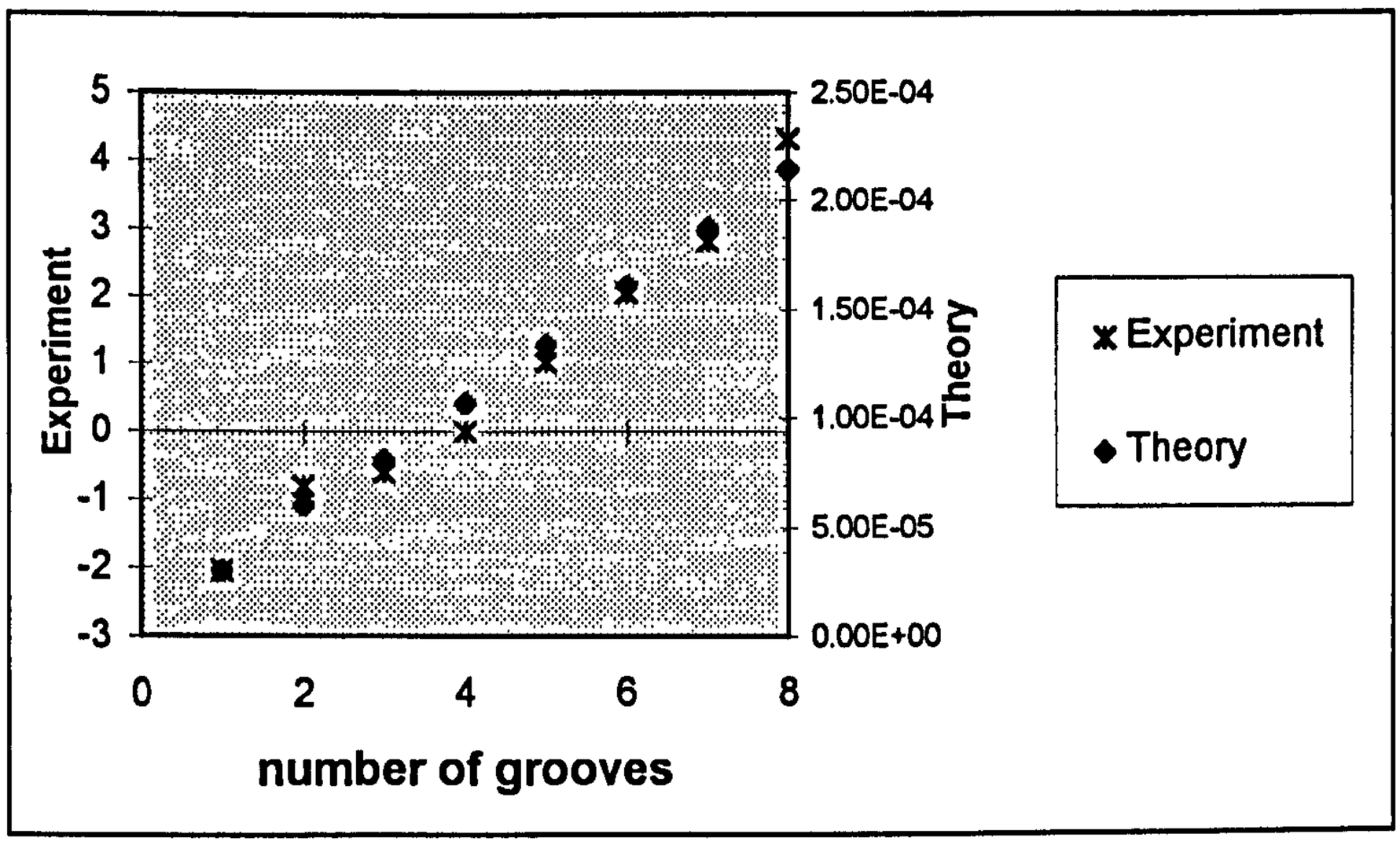

Figure 7.7 : Comparison between the experimental and theoretical strain sensitivities

Figure 7.7 shows the chart obtained by plotting the experimental strain sensitivity and the theoretical strain sensitivity for multiple grooves from 1 to 8. Consideration of the 95% confidence limits showed that the two plots are coincident and that that there exists good correlation between the mathematical theory derived and the experimental observations. The measured strain sensitivities are higher than the values predicted by the simple theoretical considerations. This is probably due to the assumption made earlier on in the theoretical calculation in Section 7.2.1, in which a groove angle of 1^0 was assumed, at zero strain. During the lab tests conducted, the groove angle was 48^0, this accounting for the discrepancies between the theoretical and experimental values. But the fact that the plots do correlate (Figure 7.7) and that the gauge factor, which is the strain sensitivity, increases with the number of grooves, proves the theory associated with the mathematical model. The most important factor limiting the accuracy of the resistance strain gauges is their low gauge factor, typically about 2.0. From Figure 7.7, we observe that there is an increase in the gauge factor of the optical fibre strain sensor with groove number. Experimentally we have obtained gauge factors up to 4.3 for 8 grooves. This is an advantage over the commercially available resistance strain gauge.

7.3.4 The effect of continuous bonding

The optical fibre strain gauge was developed to replace the resistive strain gauges used in the flow sensor described in Chapter 4. Resistive strain gauges are generally bonded over their entire area to the substrate. In order to study the effect of continuous bonding on the optical fibre strain gauge, the fibre was coated with epoxy on the diametrically opposite side of the fibre to where the grooves were present, and bonded to one of the longitudinal faces of the rubber beam, thus bonding the gauge to the beam over its entire length. This imposed restriction on the movement of the fibre optic strain gauge, thereby virtually eliminating the gauge's sensitivity to strain, although power was transmitted through the fibre. Hence an alternate approach was used to attach the fibre to the rubber beam using plastic rings and only bonding the fibre to the beam with the epoxy at the two ends of the fibre optic strain gauge and the rubber beam. [7.5] This is described in detail in Chapter 8. This method retained the strain sensitivity of the fibre optic gauge as the fibre was free to slide within the rings without friction.

7.4 OPTIMISATION OF THE NUMBER OF GROOVES

In order to maximise the sensitivity of the flow sensor, the induced intensity loss as a function of the fibre bending must be optimised. Increasing the number of grooves in the fibre strain sensor increases the strain sensitivity of the sensor (Section 7.3) but this will also increase the insertion loss of the sensitised region of the fibre, which affects the intensity of the light measured at the output of the optical fibre strain gauge. Figure 7.8 shows the measured light intensity transmitted for different numbers of grooves at zero strain. Transmitted power is plotted as a function of groove number 'n'. The plot indicates the reduction in light intensity as the grooves increase.

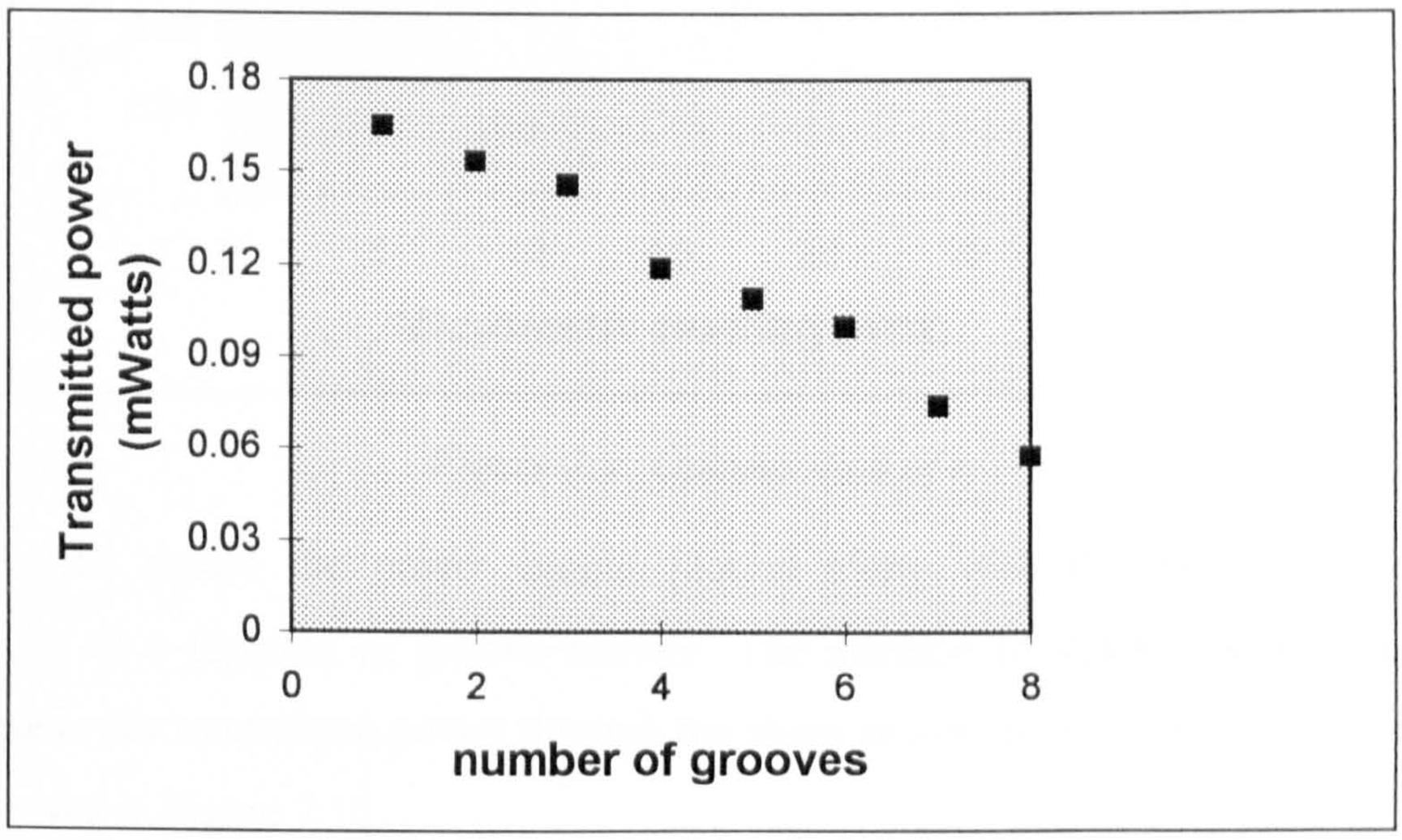

Figure 7.8: Plot showing the reduction in light intensity as the number of grooves increases (experimental)

A compromise must be reached between the number of grooves and the output signal intensity. There must be sufficient grooves to achieve adequate sensitivity, but the number of grooves is limited by the insertion loss and the resultant effect on signal to noise ratio. Figure 7.9 shows a plot of the coupling factor versus displacement of the translator inducing the strain, for different number of grooves. These results were obtained during laboratory experiments. The increase in sensitivity of the fibre optic strain gauge with the number of grooves can be seen in the graph. It can also be observed from the plots that although there is an increase in the sensitivity of the sensor for the tests performed for six, seven and eight grooves, this variation in sensitivity is not very significant. Moreover, from Figure 7.8, the reduction in the light intensity

transmitted through the strain sensor as the number of grooves increases was discussed. Hence the optimum number of grooves was chosen as six where the number of grooves was sufficient to achieve adequate sensitivity for the strain sensor and yet the light intensity transmitted was larger than for seven or eight grooves.

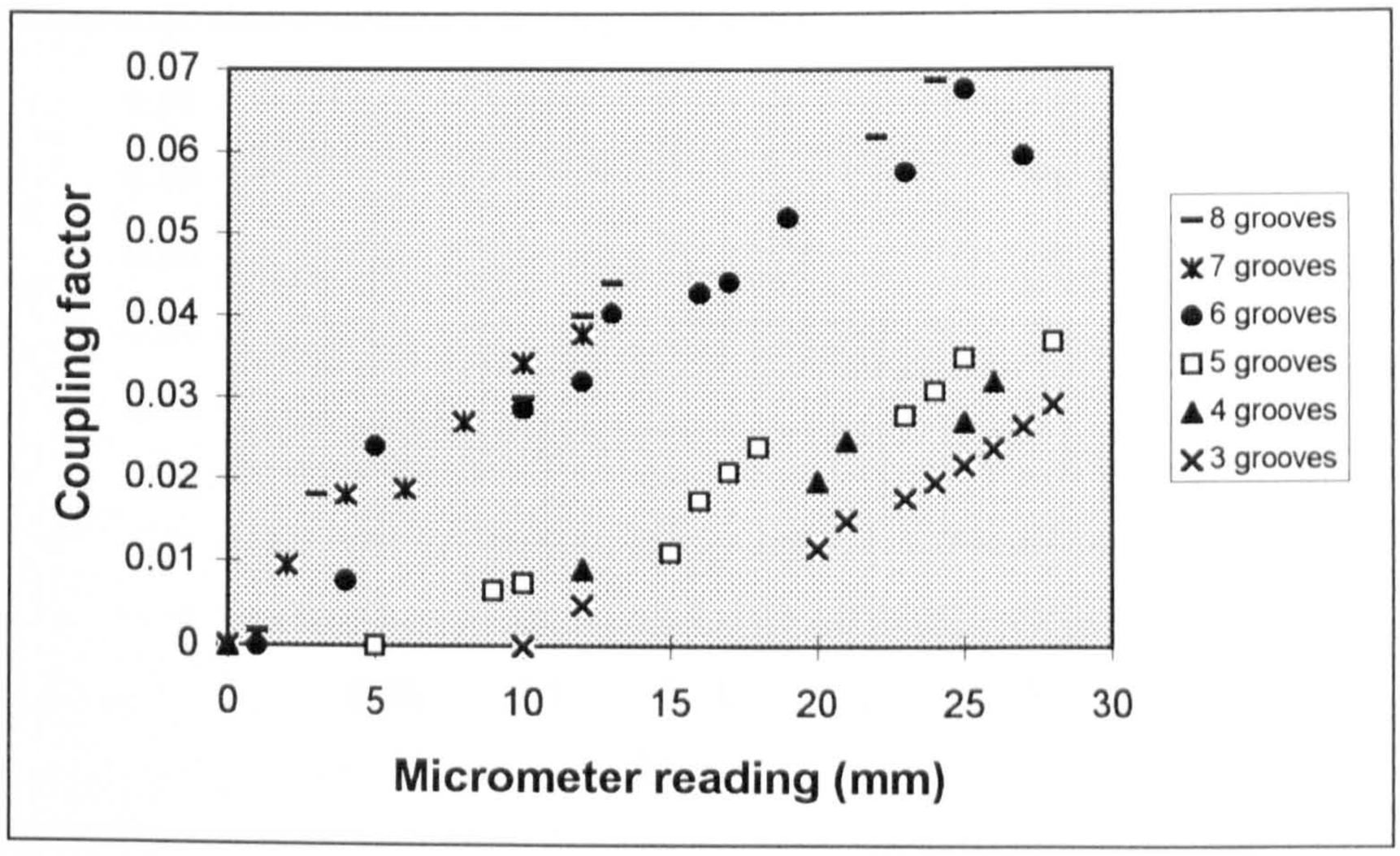

Figure 7.9: Optimisation of n

Figure 7.10 shows the power output plotted along with the experimental strain sensitivity as a function of groove number. The increase in strain sensitivity and the decrease in the transmitted power through the strain sensor, with the groove number can be observed in Figure 7.10.

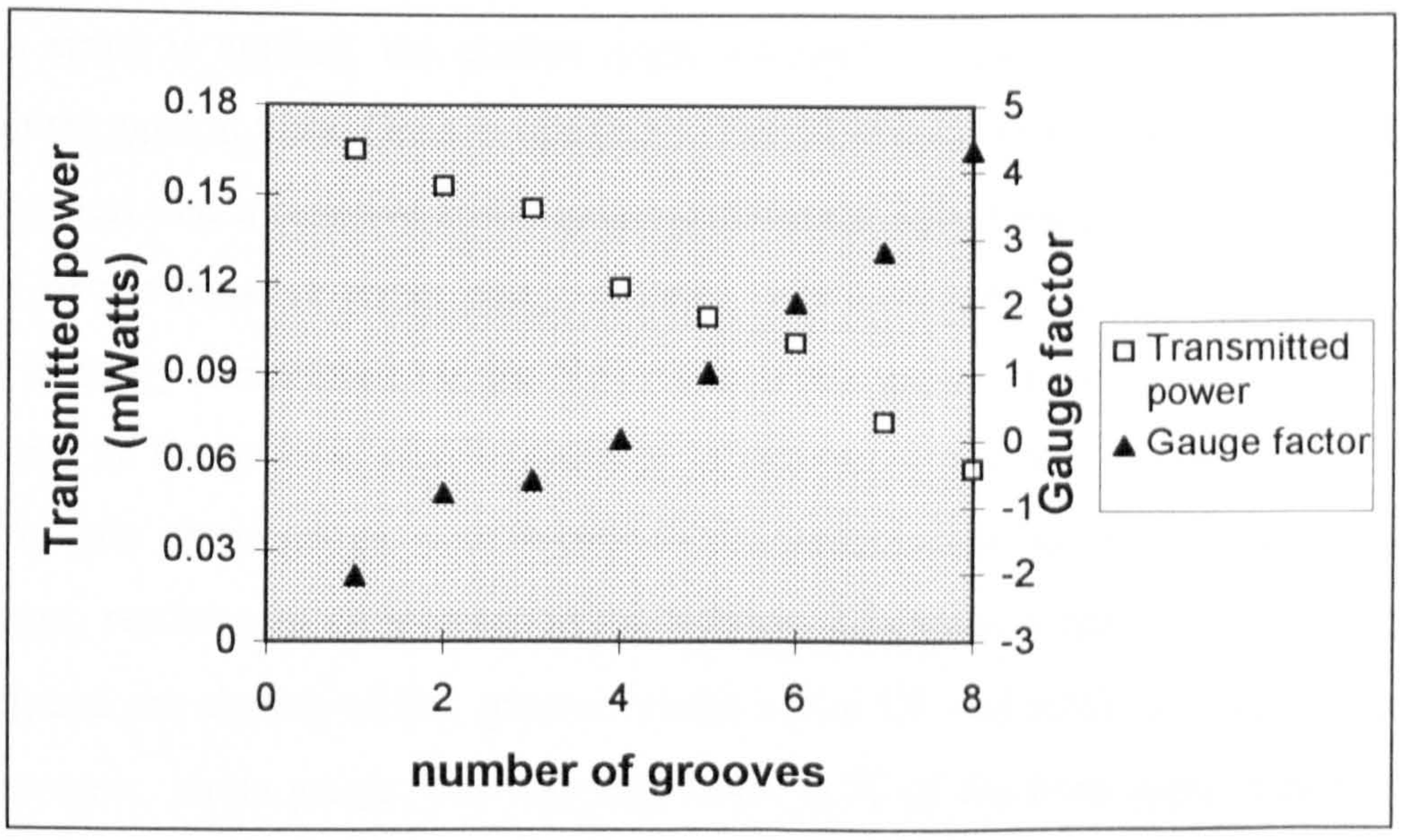

Figure 7.10: Plot showing the effect of the increase in the number of grooves on the transmitted power and gauge factor.

Having observed and confirmed that the optimum groove number is six, further experiments were performed three more times to verify the repeatability of the strain sensor with six grooves. Figure 7.10 shows the plots obtained for each of the four tests conducted indicating fairly good repeatability.

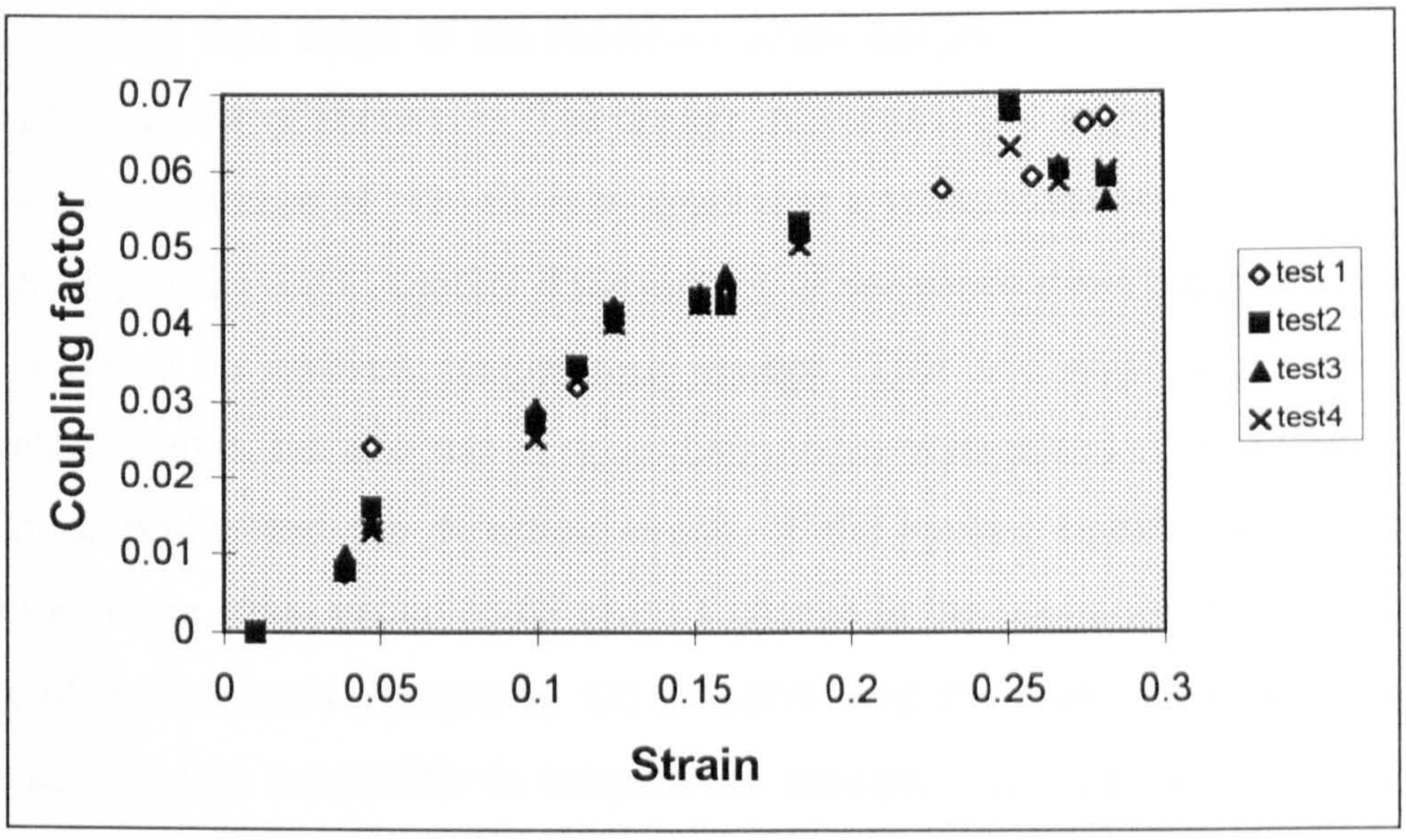

Figure 7.10: Graph to show repeatability of the strain sensor with six grooves

7.5 COMPARISON OF THE OPTICAL FIBRE STRAIN GAUGE WITH THE ELECTRICAL RESISTANCE STRAIN GAUGE

The fibre optic strain gauge reported in this chapter has many similarities with the electrical strain gauge. In Section 7.2.3, it has been shown that as the groove opens when a strain is applied, the groove angle increases, reducing the transmitted power through the optical fibre. Groove opening in the fibre optic strain gauge is analogous to the extension that a resistive strain gauge undergoes. When subjected to extension, the voltage of the resistive strain gauge reduces, which is similar to the reduction in the power intensity transmitted by the fibre optic strain gauge, under extension. Similarly, the closing of the groove, which results in an increase in the transmitted power through the fibre optic strain gauge, is analogous to the compression that a resistive strain gauge undergoes, resulting in an increase in the voltage. Likewise, it has been shown that the opening and the closing of the groove results in the CF and strain always increasing in the fibre optic strain gauge. The coupling factor (CF) of the fibre optic strain gauge is analogous to the ratio of the change in voltage to original voltage of the resistive strain

gauge (Equations 7.6 and 7.7). This ratio always increases whether the resistive strain gauge undergoes compression or extension.

The fibre optic strain gauge has advantages over the resistance or semiconductor strain gauges. The gauge factor of the sensing elements, which is experimentally indicated to be 4.3, is larger than those of the resistance strain gauges. Resistance strain gauges have a gauge factor of about two. The change in resistance of a typical resistance strain gauge with a resistance of 120 Ω, is so small that a Wheatstone bridge followed by an amplifier is typically used. Another disadvantage of resistance strain gauges is their non-linear response to ambient temperature change. This not only limits their useful temperature change, but also sets an upper limit on the voltage and current applied to the Wheatstone bridge and the detecting circuit. If the applied signal is too large, heat dissipation in the strain gauge could cause a change in the gauge resistance even in the absence of applied strain (Chapter 2). On the other hand, the response of the optical fibre strain gauge is less susceptible to temperature changes. Furthermore, the optical fibre does not need an inert atmosphere to be sensitive and their response is not affected by moisture in air. [7.6]. Other noteworthy features, from the laboratory experiments, are their linearity and repeatability. All these advantages make the optical fibre strain gauge ideal for many applications, one of which has been the optical fibre flow sensor (Chapter 8) developed as a continuation of this project.

However, the fibre optic strain gauge has a few disadvantages. The fibre integrity is violated by cutting into the fibre. There is also the possibility of dirt collecting in the fibre groove which might affect the life of the sensor. Furthermore, the changes in the refractive index of the surrounding medium will affect the response of the strain sensor. One method of solving this problem is by sleeving the fibre. This needs further investigation.

7.6 DISCUSSION

This chapter has examined the development of an optical fibre strain gauge by inserting grooves in a plastic optical fibre. A mathematical model has been developed which predicts the effect of the closing and the opening of the grooves on the coupling factor and the gauge factor, which is the strain sensitivity. The theory described in the model has been experimentally verified by conducting lab tests on an optical arrangement. The

number of grooves has been optimised, in order to achieve a compromise between sensitivity and the loss in transmitted power. Finally the similarities between the fibre optic strain gauge and the resistive strain gauge and the advantages and disadvantages of the optical fibre strain gauge were discussed.

CHAPTER 8

THE OPTICAL FIBRE STRAIN GAUGE FLOW SENSOR

Optical fibre sensors previously used for flow measurement, have generally been retrofitted to existing devices such as vortex shedding flowmeters. This means that the fibre often has to be cut with a resulting gap between transmitting and receiving fibre or they are point sensors with a probe like structure at the point of measurement. Light must therefore leave the fibre and be coupled back into the fibre before being detected. Such sensors have high attenuation and therefore are unlikely to be optimised for the measurement application, unlike the sensor presented in this thesis. A few of the various types of optical flowmeters that have been proposed in the last few years were discussed in Chapter 6. It was emphasised that the most successful optical flowmeter designs are likely to be those based on existing flowmeter constructions. Two types of optical fibre flow sensors have been developed which are based on the principle of operation of the resistance strain gauge target flow sensor described in Chapters 4 and 5. This chapter gives an account of the development and results of the original work performed to develop the two optical fibre target flow sensors using the optical fibre strain gauge described in Chapter 7. Both these novel sensors are ideally suited for environmental flow measurement.

8.1 THE OPTICAL FIBRE FLOW SENSOR WITH RUBBER CANTILEVER

8.1.1 Construction of the optical fiber flow sensor in one dimension

The flow sensor comprises a square sectioned rubber cantilever (supplied by the Malaysian Rubber company) which has a drag element attached to its free end. A multimode plastic fibre of 1mm diameter was attached to one of the longitudinal surfaces of the rubber beam. Figure 8.1 shows a schematic of the optical fibre flow sensor. Great care was taken in ensuring good attachment of the optical fibre strain gauge to the beam as is the case with conventional resistance strain gauge bonding. Plastic rings were attached to the surface of the cantilever using epoxy. It was important to ensure that the epoxy used did not affect the material properties of the rubber beam. The rings were slightly larger in diameter ($\varnothing \approx 1.1$ mm) than the polymer fibre, so that the fibre was

free to slide within the rings without friction or snagging. This ensured that no restriction was placed on the deflection of the beam.

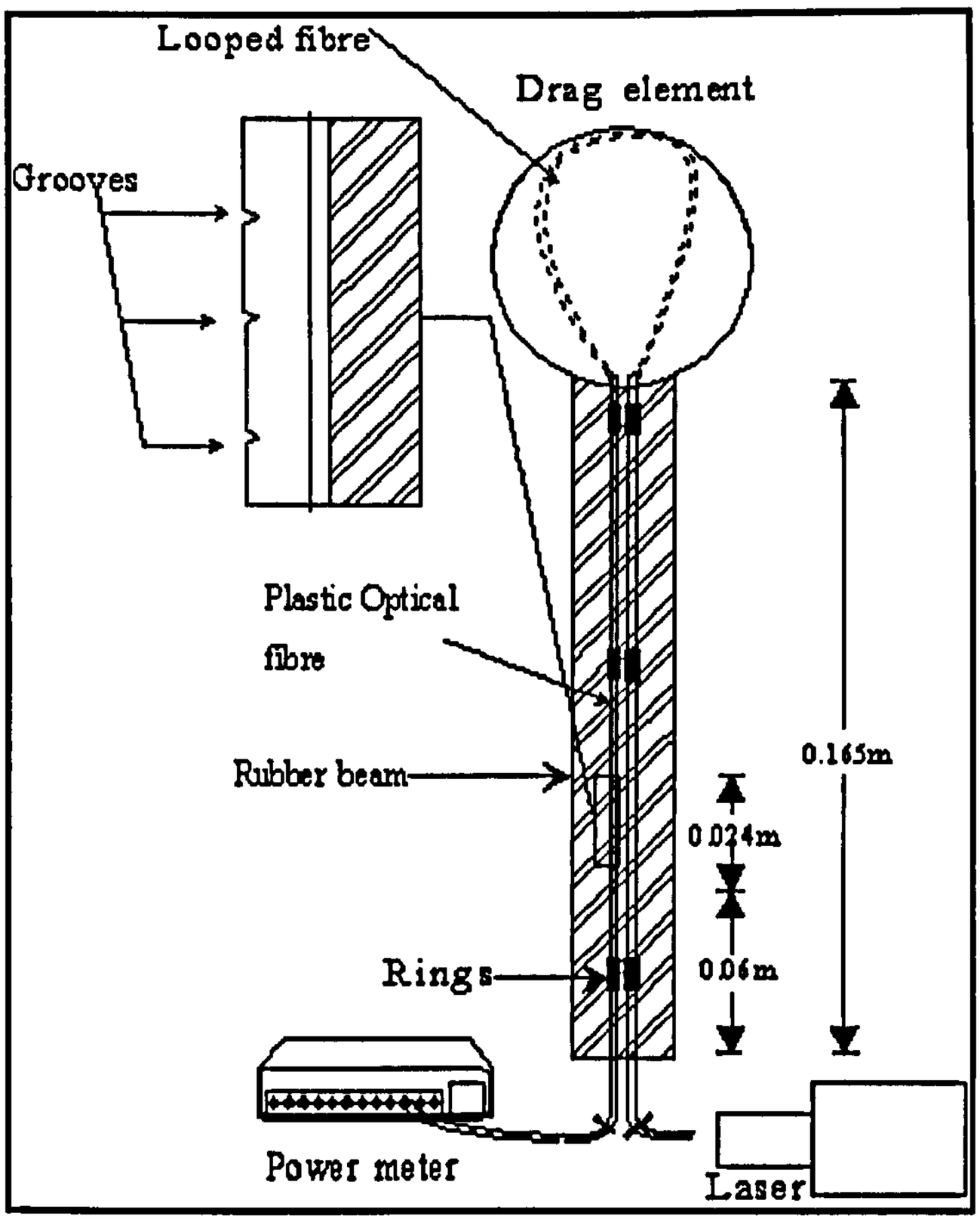

Figure 8.1: Schematic of the optical flow sensor in one dimension (Courtesy:N Schmitt)

However, the rings were small enough to enable the fibre to faithfully track the deflection of the cantilever. The transmitting end of the fibre was connected to a He-Ne Laser and the receiving end to an optical power meter. These could be replaced by a visible LED emitting at peak wavelength of 670 nm and a photodetector respectively to enable portability of the set-up. The fibre was looped at the free end of the cantilever inside the drag element. This enhanced the sensitivity of the device since the force exerted by the fluid flow on the drag element was transferred more effectively to the grooved fibre.

A number of grooves were formed radially into the fibre which extend into the core as shown in Figure 8.1. Six grooves were determined as the optimum number to achieve a compromise between insertion losses and sensitivity as discussed in Chapter 7.4. The depth to which the grooves extend into the core of the fibre is also an important factor in determining the sensitivity of the device, and this depth is also ultimately limited by its

effect on insertion loss and on the inherent strength of the plastic optical fibres (POF). The depth of each groove was 0.5 mm. In order to maximise the fibre sensor sensitivity, the grooves were located where the beam exhibits its maximum deflection, i.e. approximately at one half of the width of the beam from its base, just as in the case of conventional resistance strain gauge location. Table 8.1 gives the dimensions of the square sectioned rubber beam and the drag element with particular reference to the location of the grooves.

Table 8.1: Specifications of the dimensions of the flow sensor

Length of the rubber cantilever	0.165 m
Width of the rubber cantilever	0.0135 m
Diameter of the drag element	0.06 m
Total length occupied by all the grooves on the fibre	0.024 m
Distance of the lowest groove from the base of the cantilever	0.06 m

8.1.2 Principle of operation of the optical fiber flow sensor

As the cantilever bends in the presence of the airflow, the angle of the grooves vary. The groove angle increases when the airflow is facing the sensor and vice versa. These changes of groove angle cause an intensity modulation of the light transmitted through the fibre because light is lost at each groove. Changes in intensity can be related to changes in the angle caused by the force inducing the bending of the cantilever, and therefore to the velocity of the fluid. This effect of the variation of the groove angle on the light transmitted through the fibre was discussed in Chapter 7.2.

8.1.3 Referencing of the optical sensor system

In measurement applications of optical fibre sensors there is the requirement that the output from a system should be related to the measurand alone. In practice, this condition cannot be easily satisfied due to the variable losses within the optical components like the optical fibres, couplers and connectors. Measurement unreliability

can also arise from the instability of the light sources and detectors. It is impossible to eliminate these variations in any optical fibre system design but compensation may be applied by monitoring the undesirable optical signal losses. [8.1]. This is usually done by generating at least one additional (reference) signal which may, along with the measurand signal, be used to make a relative measurement that is free from the so-called common-mode variations. Both signals need to be separately identified, a distinction is normally achieved by employing either spatial separation, temporal separation, wavelength separation or frequency separation.[8.1]

The scheme that was used to generate the reference signal for the optical fibre flow sensor developed in this PhD project is shown in Figure 8.2.

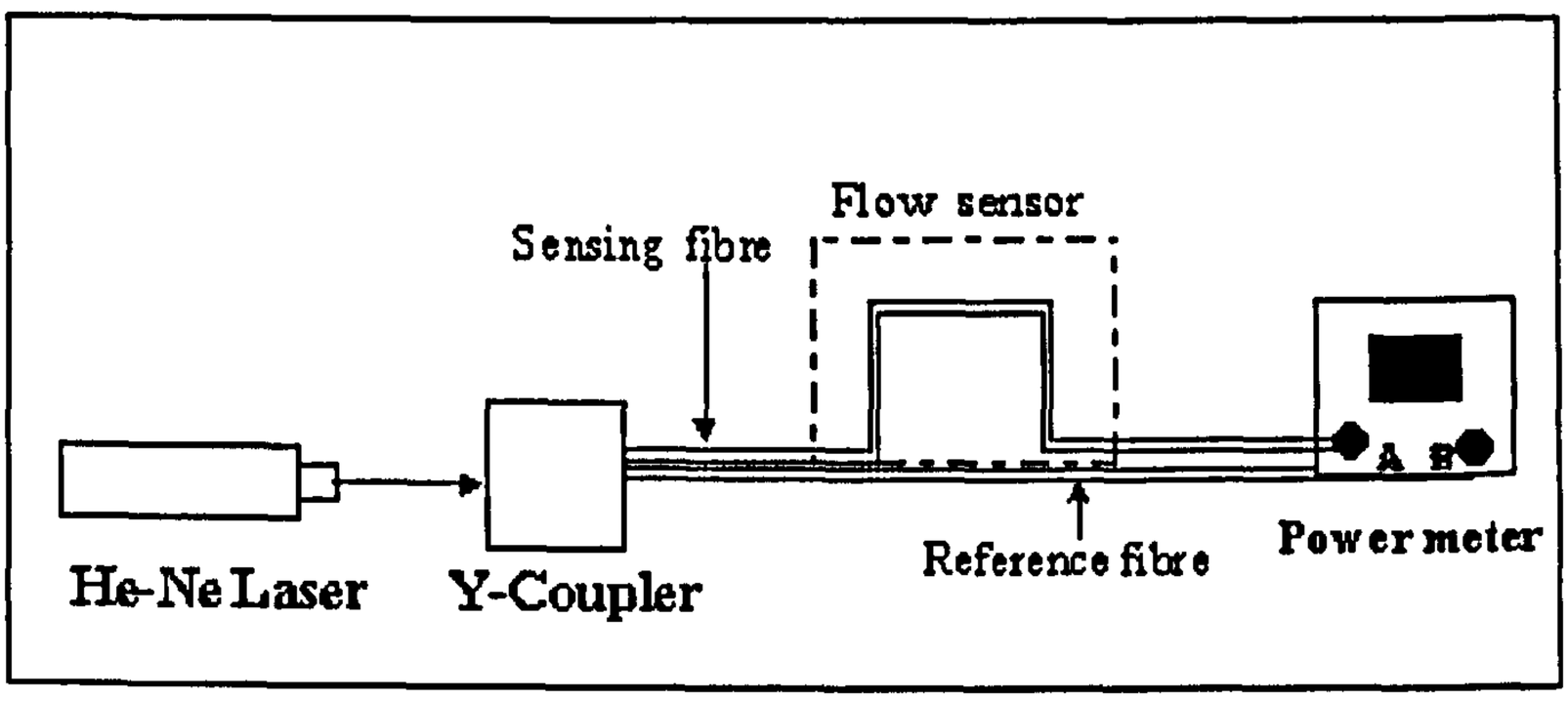

Figure 8.2: Configuration of a spatial referencing scheme used for referencing in the grooved optical fibre flow sensor.

Light from a He-He Laser (S) was passed through a Y-coupler (Y) and transmitted to two optical fibres. The light that was propagated in the first fibre (F_M) with grooves was intensity modulated by the measurand while the reference (F_R) fibre was left unperturbed at this point. The signals from both the fibres were sent to the channels of a power meter (D). The two fibres were sleeved together up to the modulation point. This configuration fulfilled most of the requirements for providing reliable and accurate referencing as discussed by Murtaza and Senior [8.1] which are:

- The sensing and reference fibre were separated just before the modulation point. This ensured that only the sensing fibre was modulated by the fluid flow and both signals were subjected equally to all the remaining environmental effects, the same common mode variations and other constraints acting on the system.

- The single source-based configuration removed the possibility of differential effects likely to arise from source-to-source variations.

- The single photodetector-based configuration eliminated the differential effect that could be significant when two signals are detected by separate photodetectors.

The expressions for the two signals can be written by following their optical path through the system so that

$$I_M = S\ Y\ F_M\ M\ D \tag{8.1}$$

$$I_R = S\ Y\ F_R\ D \tag{8.2}$$

Therefore, the ratiometric output is:

$$V = \frac{I_M}{I_R} = \frac{F_M M}{F_R} \tag{8.3}$$

It can be observed from Equation 8.3 that the source and detector fluctuations and the effect of the Y-coupler were cancelled. But Equation 8.3 shows that the system was sensitive to the loss variation within the optical fibres as separate measurand and reference fibres were used. However, during the measurement process, this loss variation within the optical fibres was insignificant and, therefore, negligible. Hence, this referencing scheme was not adopted during the experiments conducted to measure two dimensional fluid velocity using the optical fibre flow sensor (Section 8.2). Another reason for not using the referencing scheme for the two dimensional flow measurement was that the configuration would require two sources and two power meters if referencing was used. This configuration with an additional light source and power meter would have been too expensive and cumbersome.

8.2 PRINCIPLE OF OPERATION OF THE FLOW SENSOR IN TWO DIMENSIONS

Section 8.1 discussed the construction and principle of the optical fibre flow sensor in one dimension. In order to measure the magnitude and direction of the fluid flow, that is to measure the flow in two dimensions, the principle of operation of the resistive strain gauge flow sensor that was described in Chapter 4, was applied to the optical fibre flow sensor. In that chapter, it was demonstrated that vectorial addition of flow components can be used to measure the magnitude and phase of fluid flow, by sensing the deflection

of an elastic beam in two orthogonal directions. The orthogonal components of strain were measured by placing strain gauges on all four sides of a square cross-sectioned beam. In the case of the optical fibre flow sensor, the orthogonal components of strain were measured by attaching two grooved optical fibres on adjacent sides of the rubber beam, orthogonal to each other, as illustrated in Figure 8.3. These two fibres measured the x and y components of optical strain.

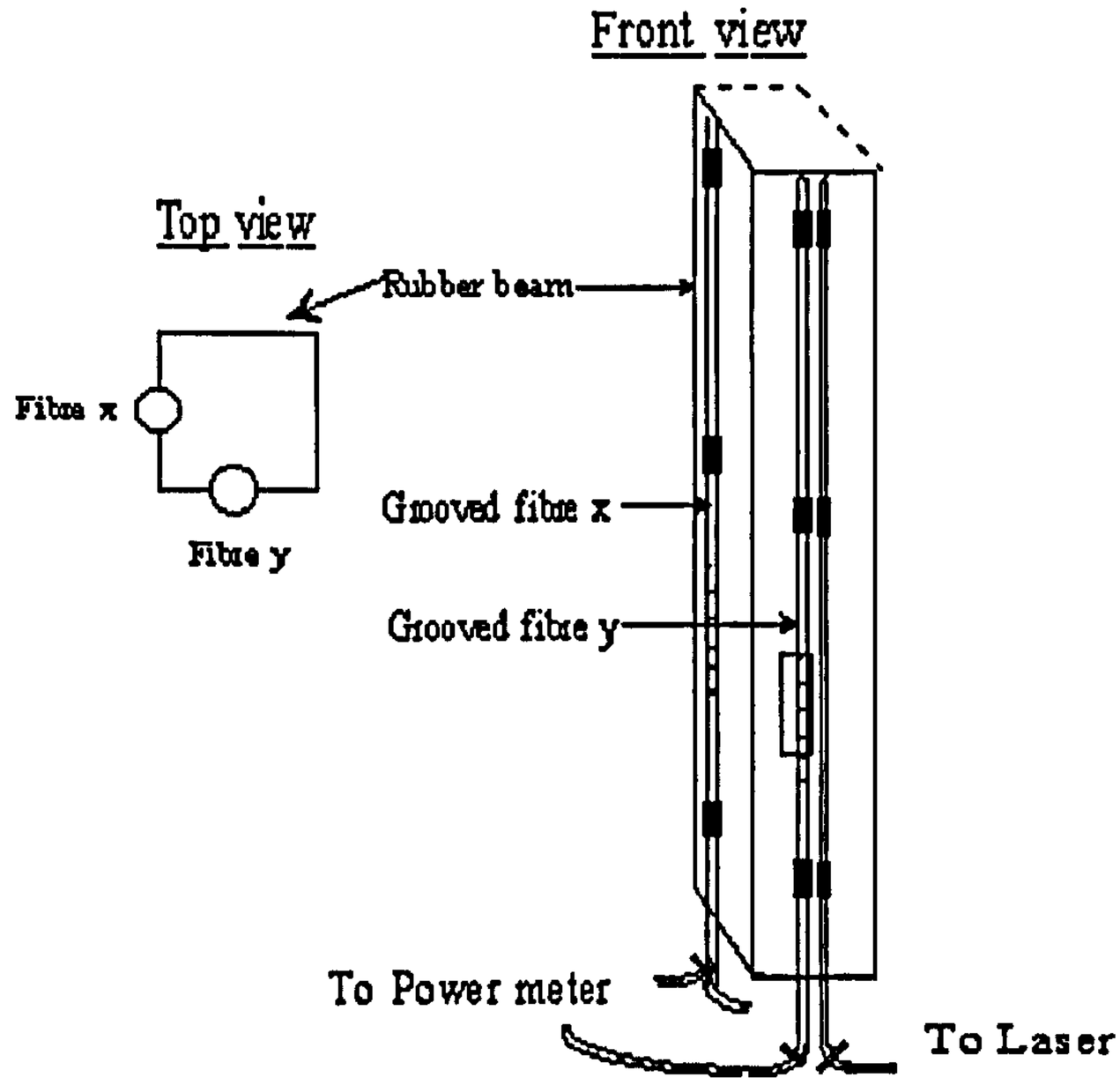

Figure 8.3: Front and top views of a section of the fibre optic flow sensor used to measure the two dimensional fluid flow

Light from a 1 mW helium Neon laser of wavelength 633 nm was split into equal components using a cubic beam splitter, and coupled into each fibre by means of microscope objectives. The transmitted intensity through each of the two fibres was monitored using a power meter. The signals from the power meter were sent to a 486 DX2 laptop computer via a data acquisition card - the DAQ card 1200 to be acquired and processed by Labview, the data acquisition and analysing package supplied by the National Instruments. Figure 8.4 shows the experimental configuration and Figure 8.5 shows a photograph of this configuration near the wind tunnel where the experiments were conducted.

Figure 8.5: Photograph of the optical arrangement comprising of the He-Ne Laser, the beam splitter, the flow sensor in the wind tunnel, the power meter and the PC.

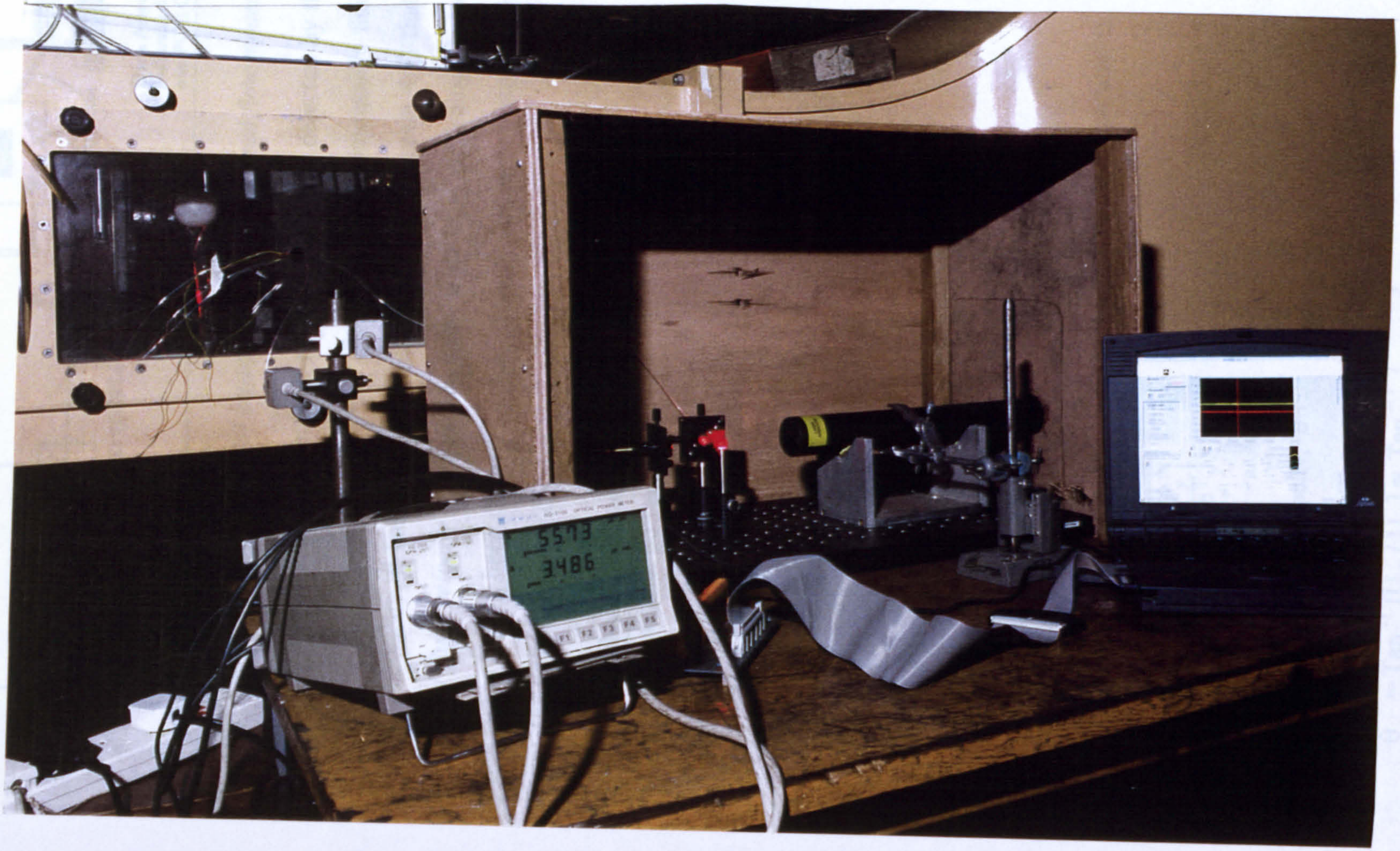

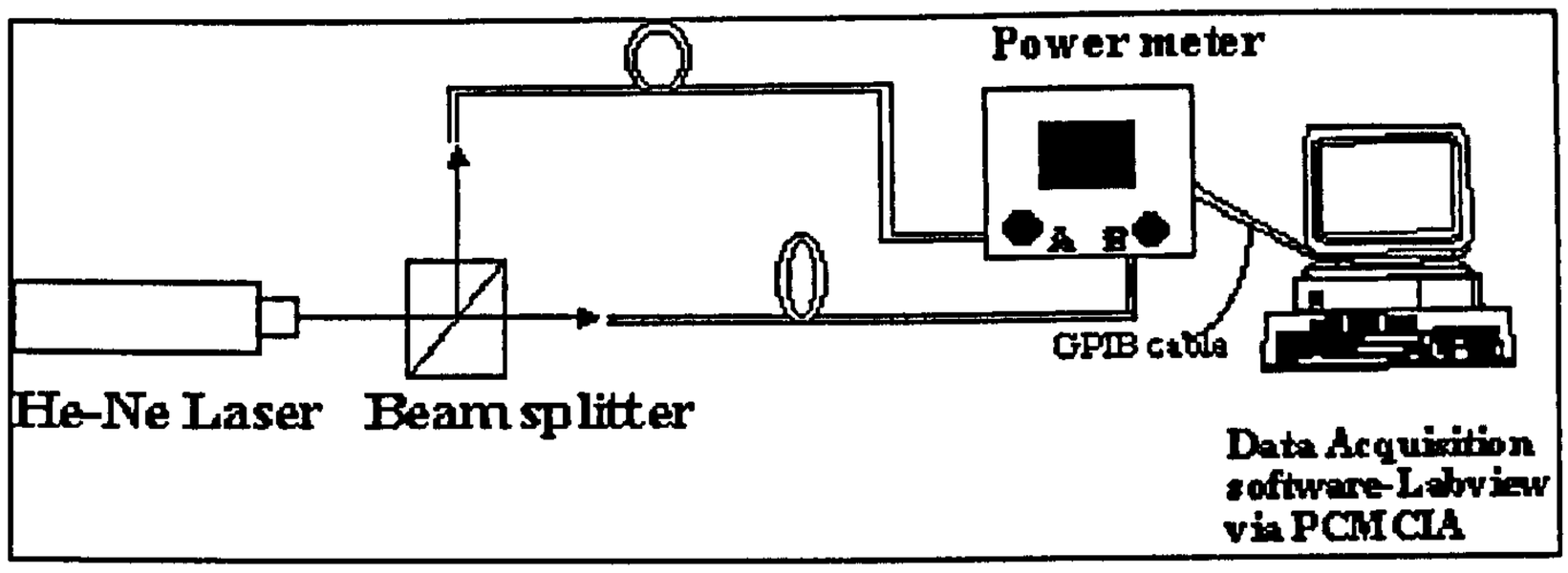

Figure 8.4: Experimental set-up for two dimensional flow measurement

The light intensity transmitted through the two fibres and detected by the two channels of the power meter gave intensities P_x and P_y. From incompressible fluid dynamics and theory of elasticity, it has been shown in Chapter 4 (Equation 4.9) that *the strain is a function of fluid velocity squared.* In order to develop an analogy between the optical strain (units having been defined for this project) and the resistive strain (conventional units), the optical strain was calculated using the formula:

$$\text{Strain}_{opt} = \frac{\text{change in power output}}{\text{original power output}} = \frac{\Delta P}{P}$$

Hence

$$\text{Strain}_x = \frac{\Delta P_x}{P_x} \text{ and } \text{Strain}_y = \frac{\Delta P_y}{P_y} \qquad (8.4)$$

Therefore the magnitude of the wind velocity, $|U|$ is given by

$$|U| = \sqrt{U_x^2 + U_y^2} = \sqrt{\text{Strain}_X + \text{Strain}_Y}$$

Substituting Equation (8.4) in $|U|$, the optical root strain magnitude is:

$$|U| = \sqrt{\left(\frac{\Delta P_x}{P_o} + \frac{\Delta P_y}{P_o}\right)} \qquad (8.5)$$

and the direction of wind velocity, θ

$$\theta = \text{Tan}^{-1}[U_y / U_x] = \text{Tan}^{-1}\sqrt{\frac{\text{Strain}_y}{\text{Strain}_X}}$$

Substituting Equation (8.4) in θ, the optical strain direction is:

$$\theta = Tan^{-1} \frac{\sqrt{\left(\frac{\Delta P_y}{P_o}\right)}}{\sqrt{\left(\frac{\Delta P_x}{P_o}\right)}} \qquad (8.6)$$

The power loss was calculated in optical root strain by measuring the maximum power Po at zero deflection, and $\Delta P = Po - Pv$ where Pv is the power measured at wind velocity, V m/s. Optical strain was therefore calculated for the x and y fibres and combined vectorially to give the magnitude and direction of wind velocity in optical root strain (Equations 8.5 and 8.6)

Figure 8.6 shows a photograph of the optical fibre flow sensor when the sensor was in a working condition. The visibility of the grooves in that photograph indicates that light intensity was lost at the groove region.

8.3 WIND TUNNEL EXPERIMENTS

The sensor was mounted in a 460 x 460 mm closed circuit wind tunnel (Figure 4.10), with a maximum fan speed of 1700 revolutions per minute. The airflow was calibrated in m/s, using an anemometer and stop watch. The beam was equipped with both optical and resistive strain gauges to compare the two responses. The beam with both the optical and resistive strain gauge elements, was clamped on a turn table and rotated round its longitudinal axis from 0 to 90^0. At various angles, P_x and P_y were measured from the optical strain gauges, and V_x and V_y measured from the conventional strain gauges, as a function of wind velocity over a range of 0 to 30 m/s.

8.3.1 Flow sensing and display

Labview was programmed to acquire these signals and to calculate the wind magnitude and direction according to Equations 8.5 and 8.6 respectively. The voltage signals of P_x and P_y from the power meter, along with the calculated values of the magnitude and direction of the wind velocity were sent to a spreadsheet file for storage and further analysis of data again by pre-programming Labview (Figure 8.7).

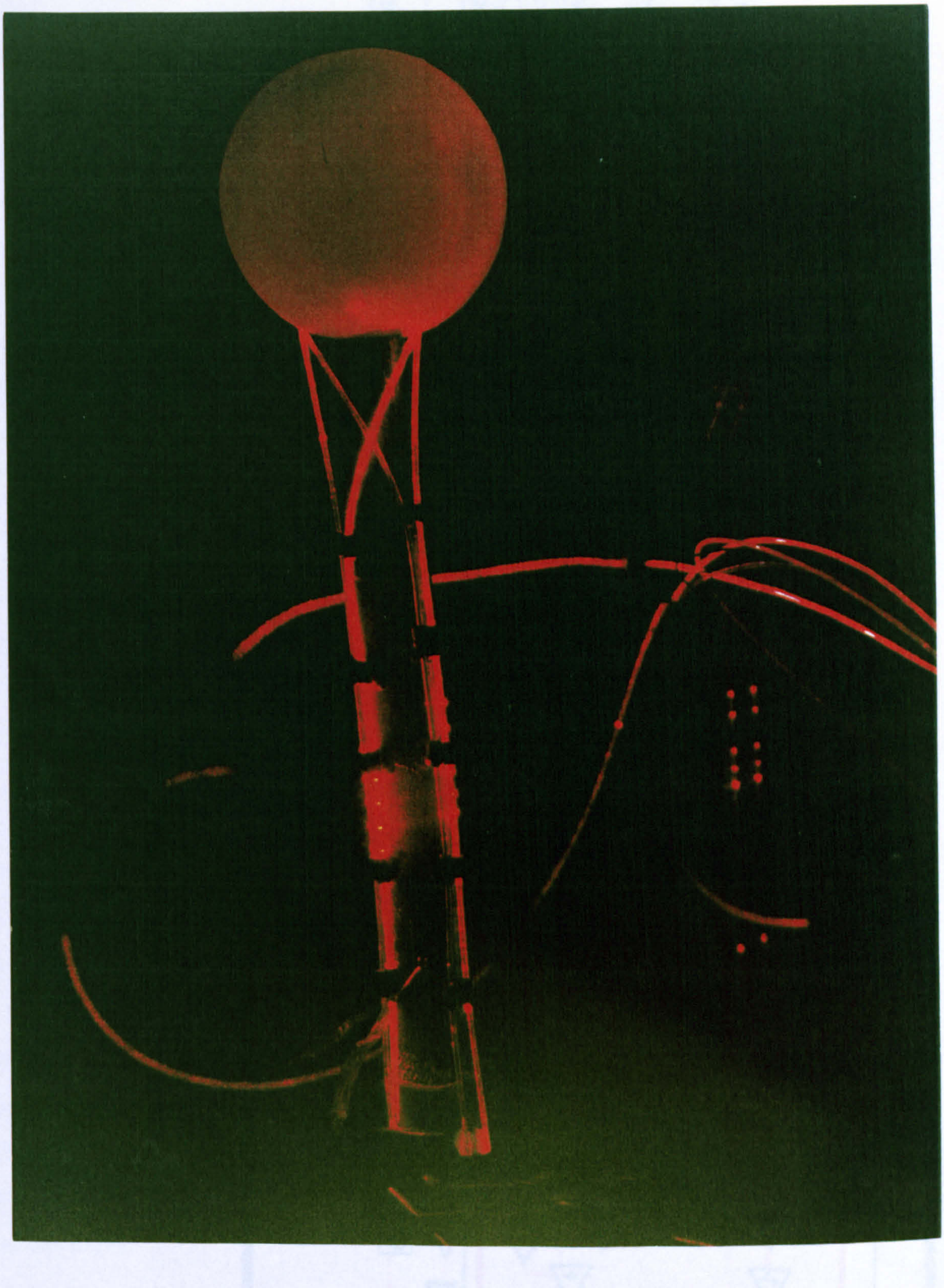

Figure 8.6: Photograph of the optical fibre flow sensor taken during its operation

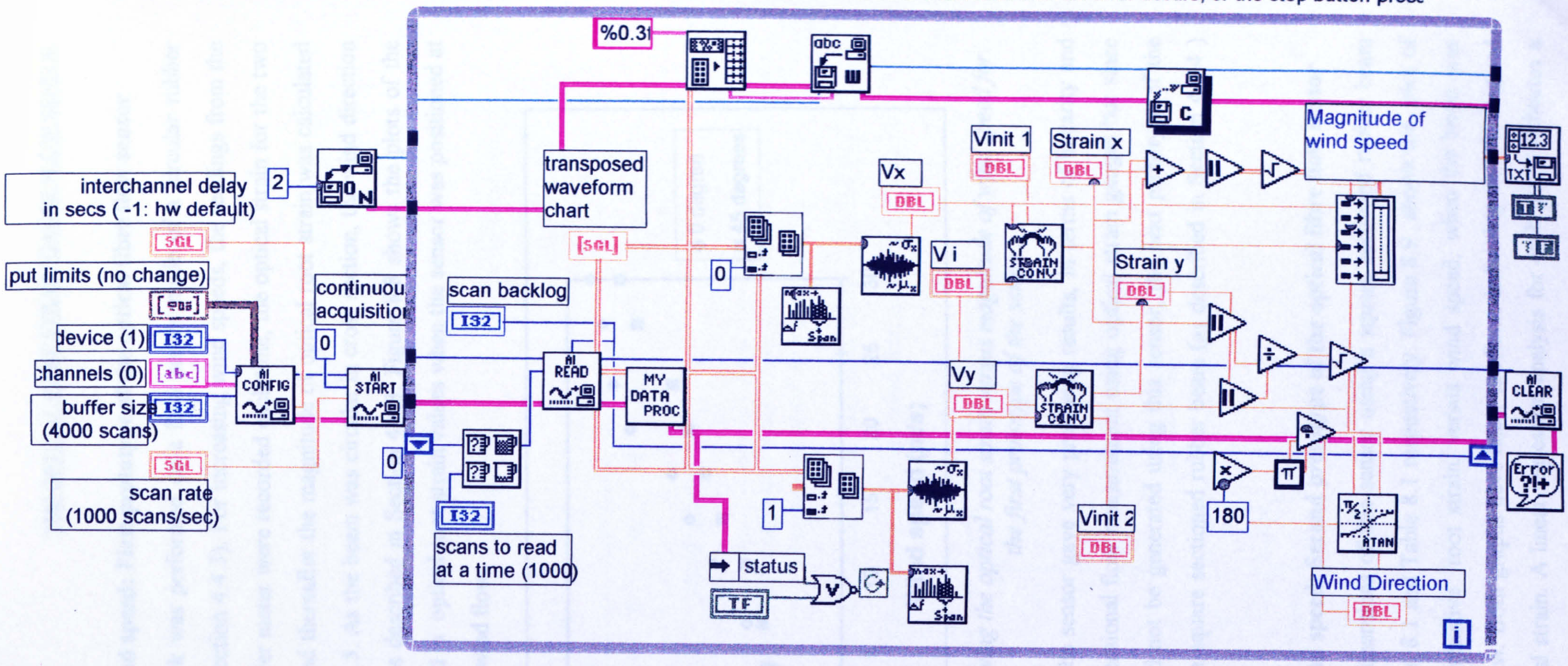

Figure 8.7: The virtual instrument program created with Labview used to acquire, process, store and display the optical strain gauge signals from the power meter.

8.3.2 Magnitude of wind speed: First prototype of the optical fibre flow sensor

Initial experimental work was performed on a flow sensor made of a circular rubber beam (as described in Section 4.4.3). For increasing wind speeds, the readings from the two channels of the power meter were recorded each time, the optical strain for the two fibres were calculated and thereafter the magnitude of optical root strain was calculated according to Equation 8.5. As the beam was circular in cross section, the wind direction could not be obtained as described in Section 4.4.3. Figure 8.8 shows the plots of the magnitude of wind speed in optical root strain values when the sensor was positioned at 0 and 45 degrees to the wind flow.

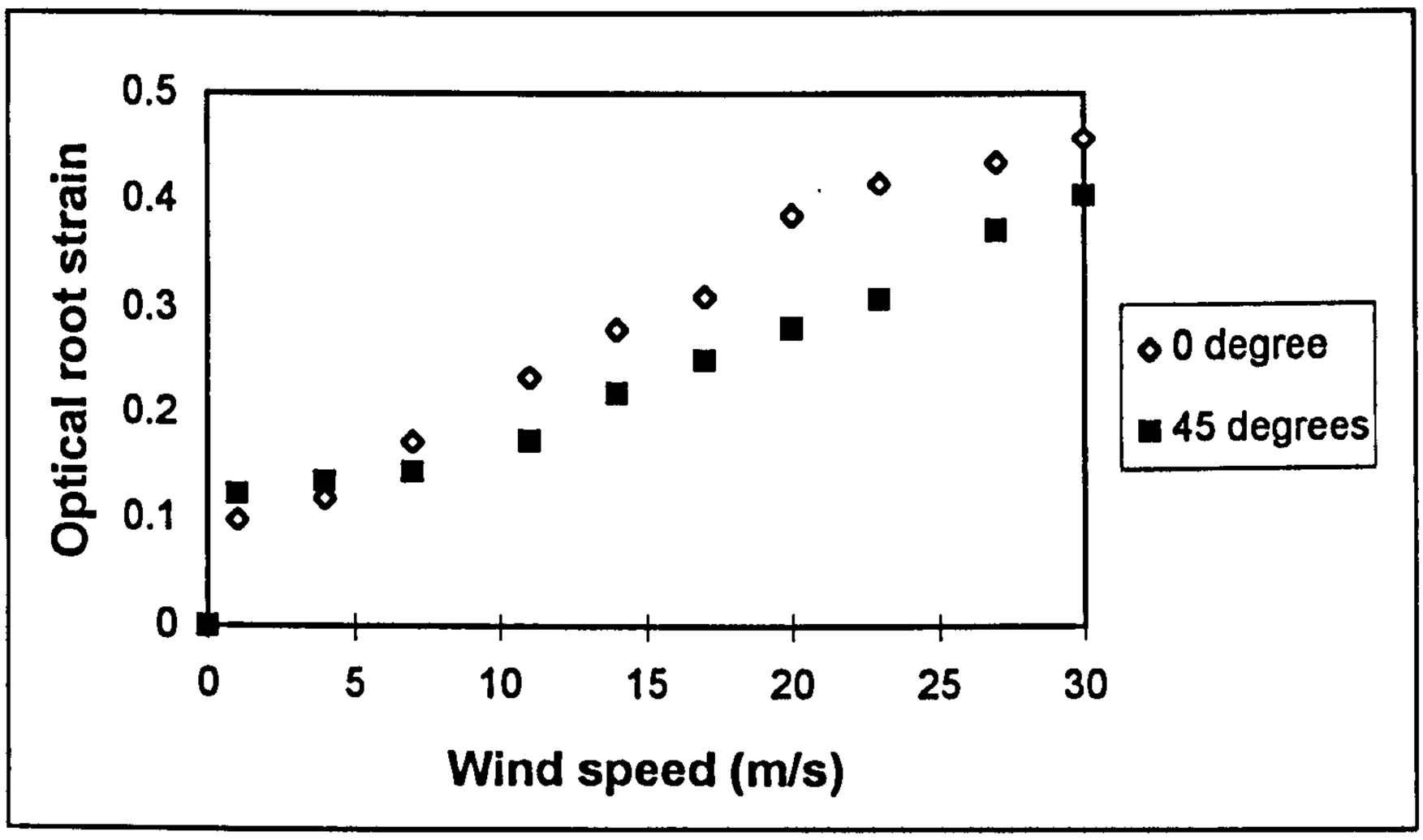

Figure 8.8 : Plots showing the optical root strain versus magnitude of wind speed for the first prototype of the sensor.

This first prototype of the sensor gave very promising results, in terms of linearity and sensitivity, for two dimensional flow measurement using optical strain gauges but since the wind direction could not be generated using this sensor, the next prototype of the flow sensor which had a square sectioned rubber beam (as described in Section 4.4.4) was developed.

8.3.3 Magnitude of wind speed: Second prototype of the optical fibre flow sensor

The construction and dimensions of this sensor using a square sectioned rubber beam were specified in Section 8.1 and Table 8.1 respectively. Figure 8.9 shows the plot of optical root strain and resistive root strain, versus wind speed, when the beam was oriented 45^0 to wind flow. Both graphs have linear gradients indicating that wind speed is proportional to optical strain. A linear regression analysis for each graph indicates a

sensitivity of 0.005±0.0004 optical root strain / (m/s) and a resolution (optical) of 1.3 m/s, and a sensitivity of 0.0065 ±0.0001 resistive root strain / (m/s), and a resolution (resistive) of 0.4 m/s for wind speeds up to 30 m/s.

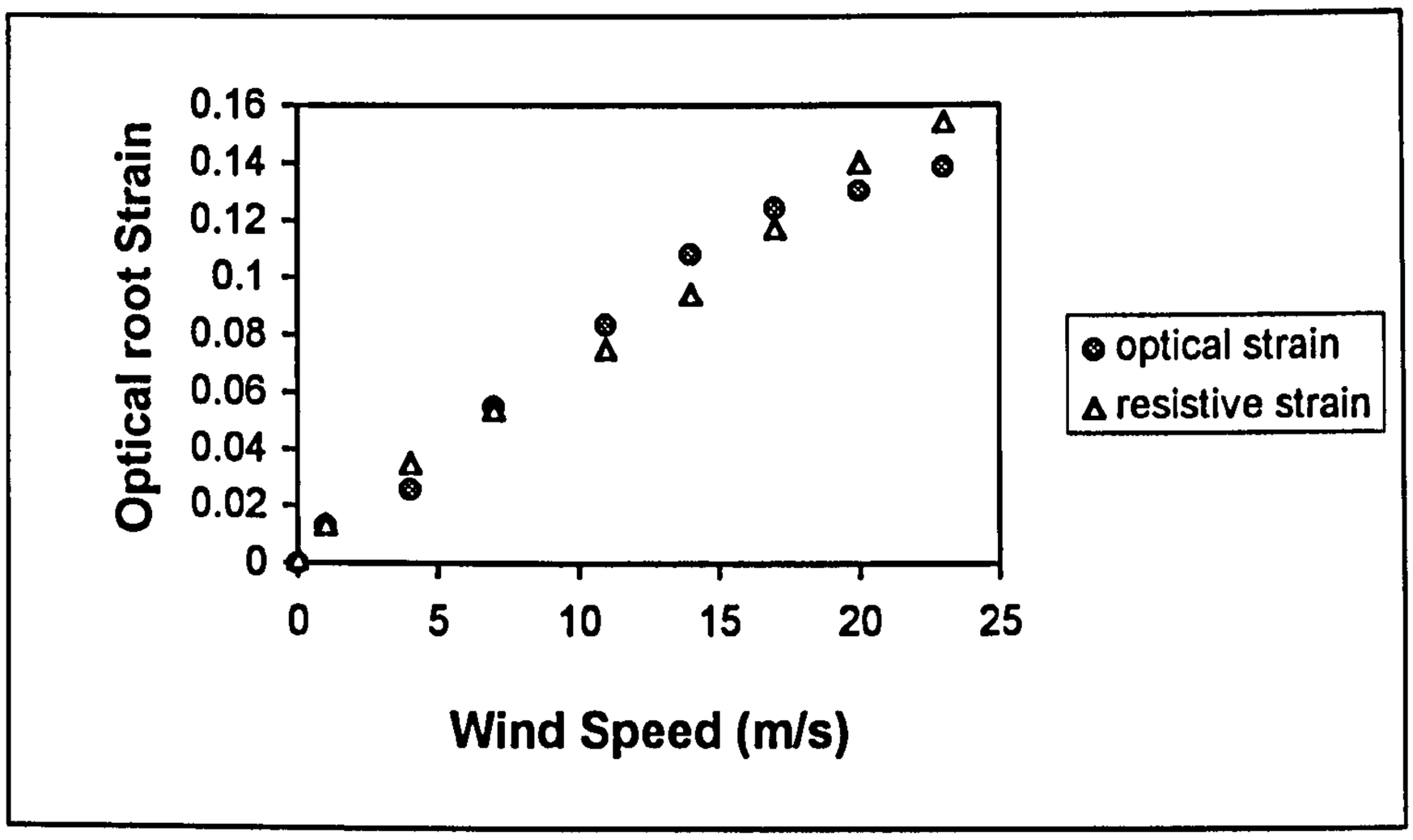

Figure 8.9: Comparison of the resistive and optical root strain versus wind speed for orientation of 45° to wind flow.

Figure 8.10 shows the top view of the optical fibre flow sensor with the two fibres to illustrate the orientation of the sensor to different wind directions from 0^0 to 360^0.

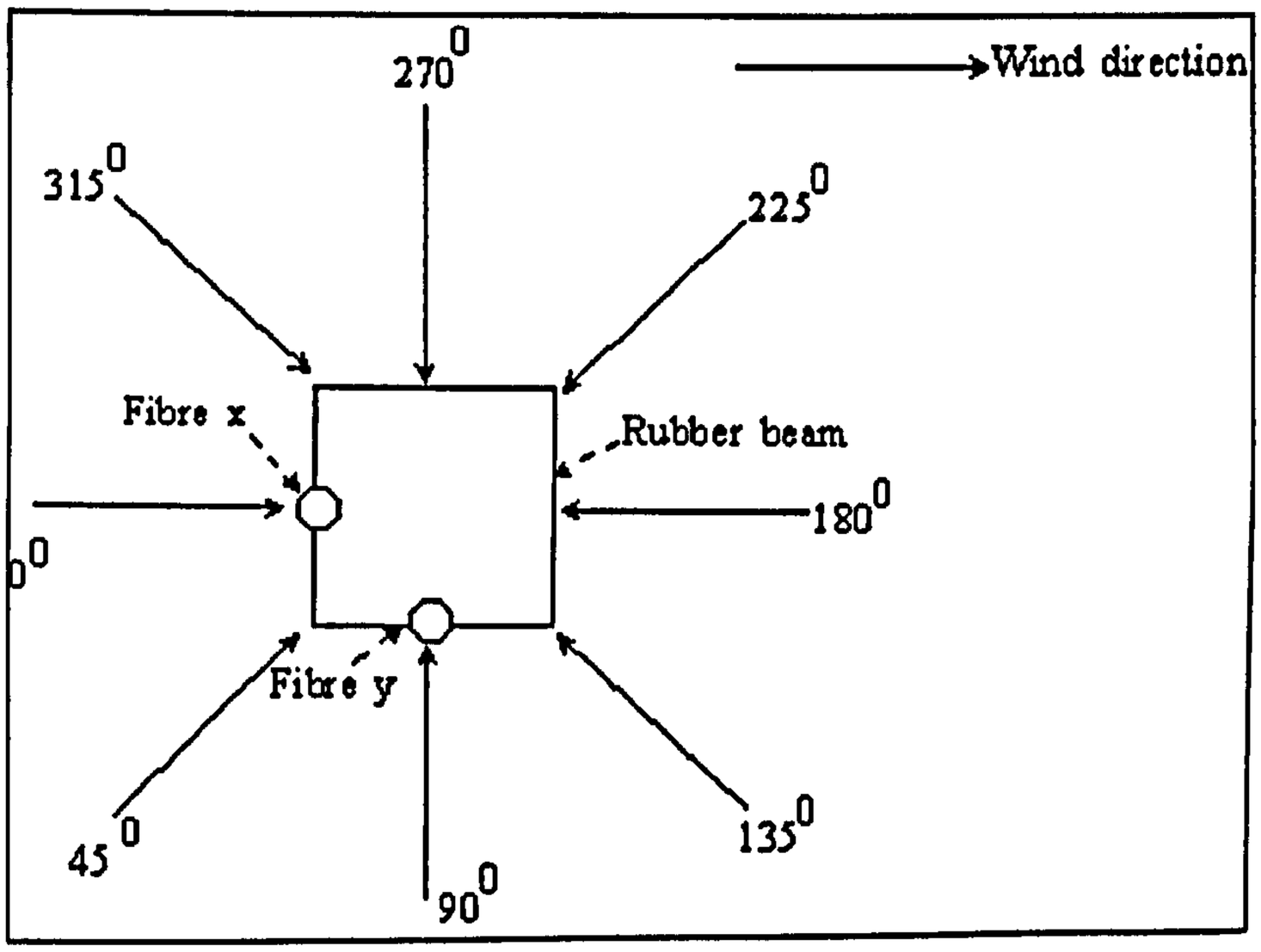

Figure 8.10: Top view of the optical fibre flow sensor showing its orientation to different wind directions

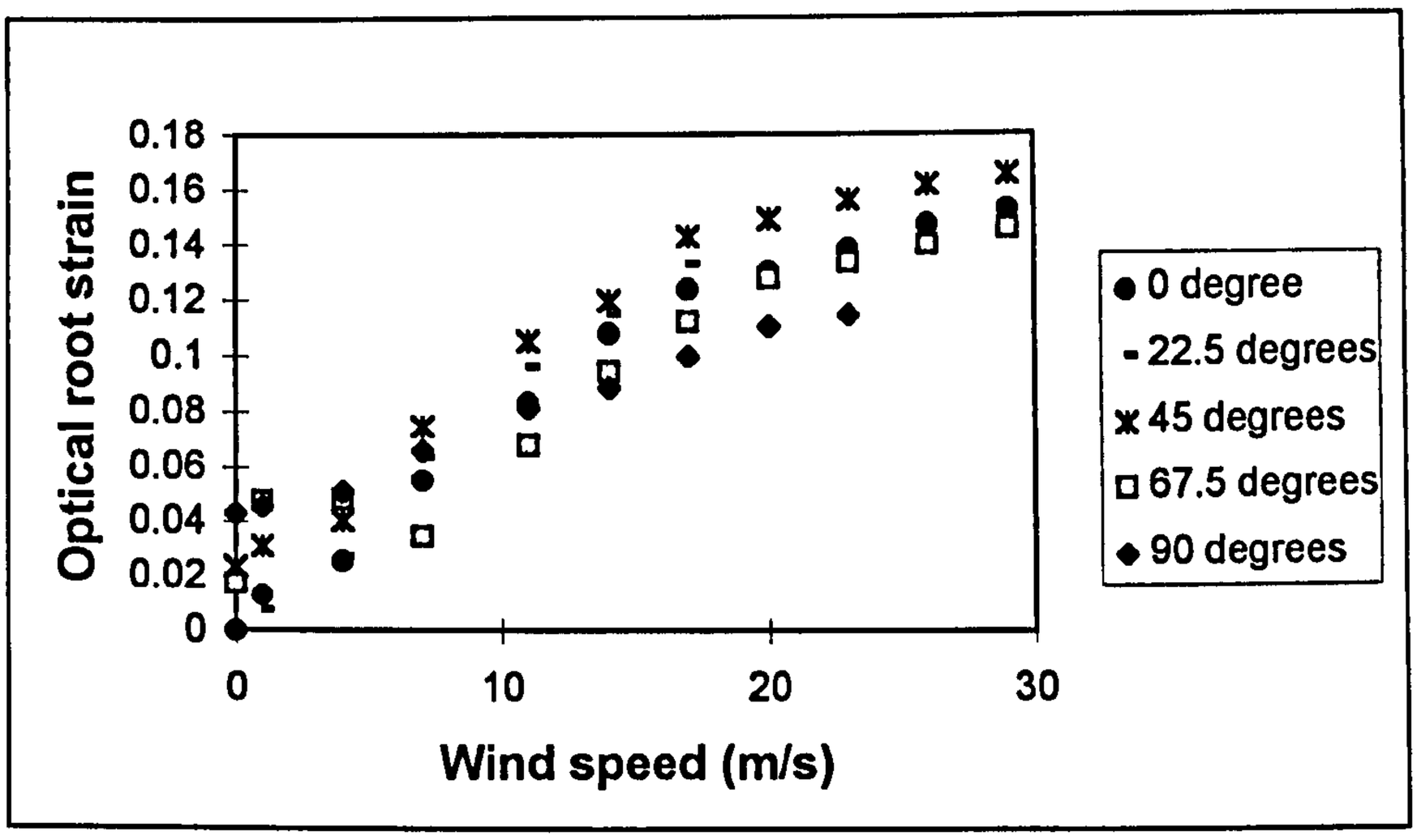

Figure 8.11 : Plots showing the optical root strain versus magnitude of wind speed for various orientation angles.

Figure 8.11 shows a plot of optical root strain versus wind speed when the elastic beam was oriented at different angles to the airflow. The sensor is independent of angle of orientation of the beam to the direction of airflow. Therefore all the data presented in Figure 8.11 can be used to obtain a calibration curve for the sensor that will be valid for multi-directional airflow. When a linear regression was performed on all the data for the optical strain gauges, the sensitivity was found to be 0.0050 ± 0.0002 optical root strain s/m and the resolution to be 1.4 m/s. This analysis has already been performed for the conventional strain gauges set-up [Chapter 4.3.4].

Figures 8.12 (a), (b) and (c) shows the plots for 90^0 (positive axis) and 270^0 (negative axis) positions of the sensor when the direction of wind velocity was reversed (or the sensor rotated through 180°) causing the sensor to deflect with the grooved area first facing towards the airflow, and then facing away from the airflow. These three plots indicate the need for vectorial addition of the x and y-components of strain. Figure 8.12(a) shows the plot of the optical strain in the x-direction ($strain_x$) versus wind speed, for the forward and reverse airflows. The plots have a R^2 value of 0.8965, which does not indicate very good linearity.

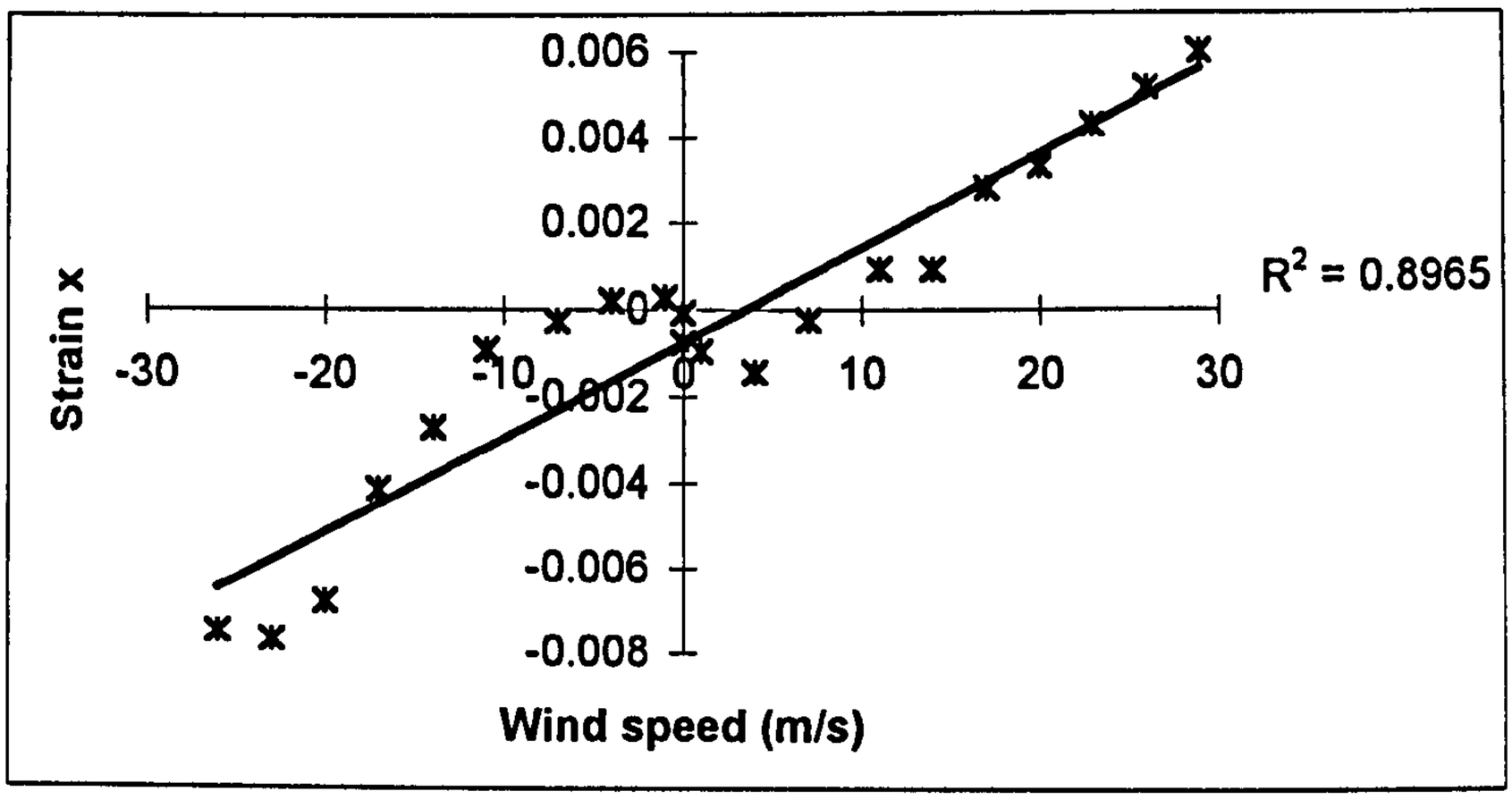

Figure 8.12(a): Optical strain(x-component) versus wind speed for forward and reverse airflow (90^0 and 270^0)

Figure 8.12(b) shows the plot of optical strain in the y-direction ($strain_y$) versus wind speed, for the above mentioned forward and reverse airflows. The R^2 value of 0.9623 is much better compared to that of Figure 8.12(a) as the optical fibre generating this y-component of the optical strain is perpendicular to the airflow. In Figure 8.12(a) the fibre is parallel to the airflow and gives a non-linear plot. Figure 8.12(c) is the plot obtained by combining the x- and y-components of the optical strain vectorially (vector strain) versus wind speed. There is an improvement in the linearity (R^2 value of 0.9784) compared to the previous two values, thereby proving the importance of measuring wind speed in two dimensions rather than in one.

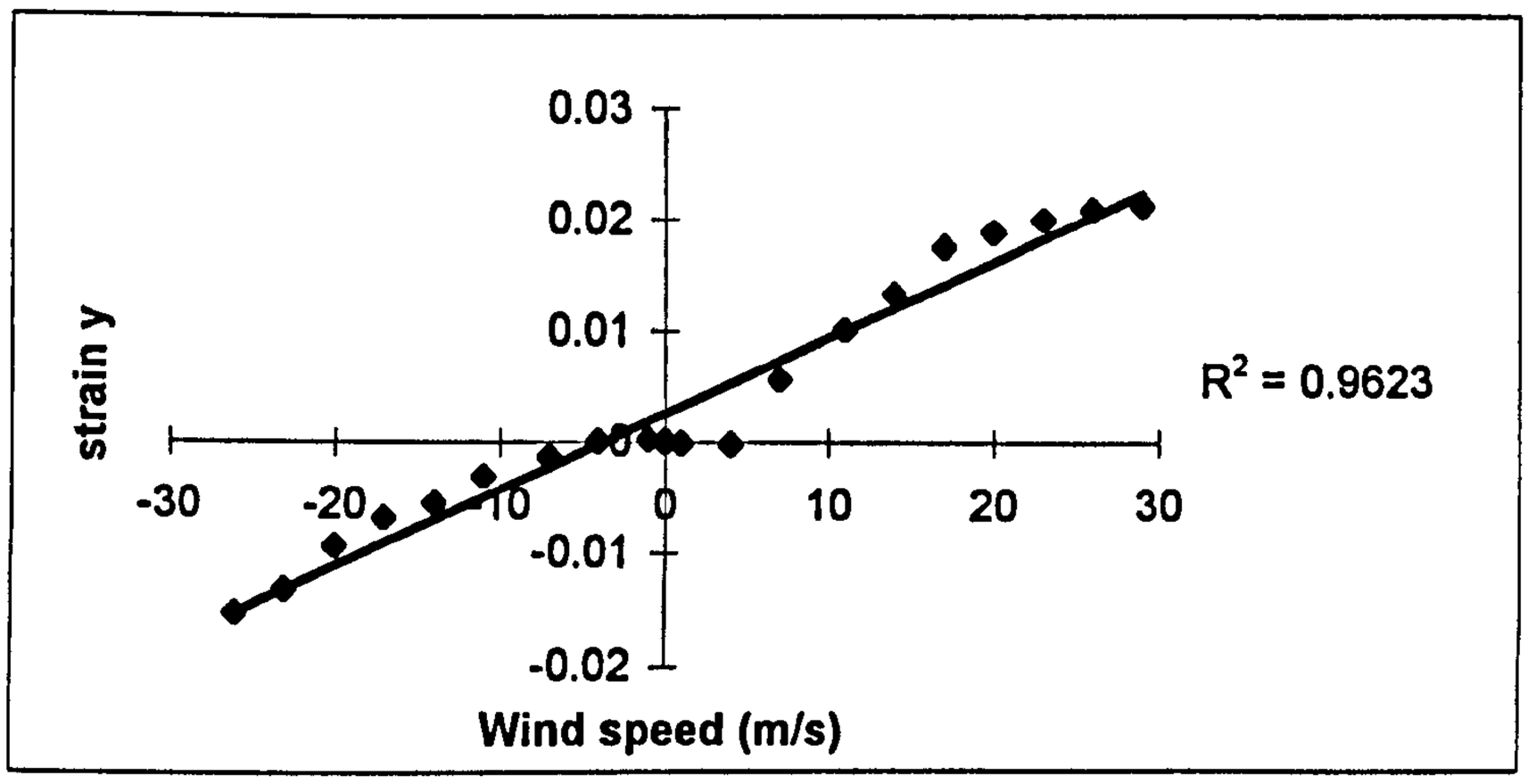

Figure 8.12 b: Optical strain(y-component) versus wind speed for forward and reverse airflow (90^0 and 270^0)

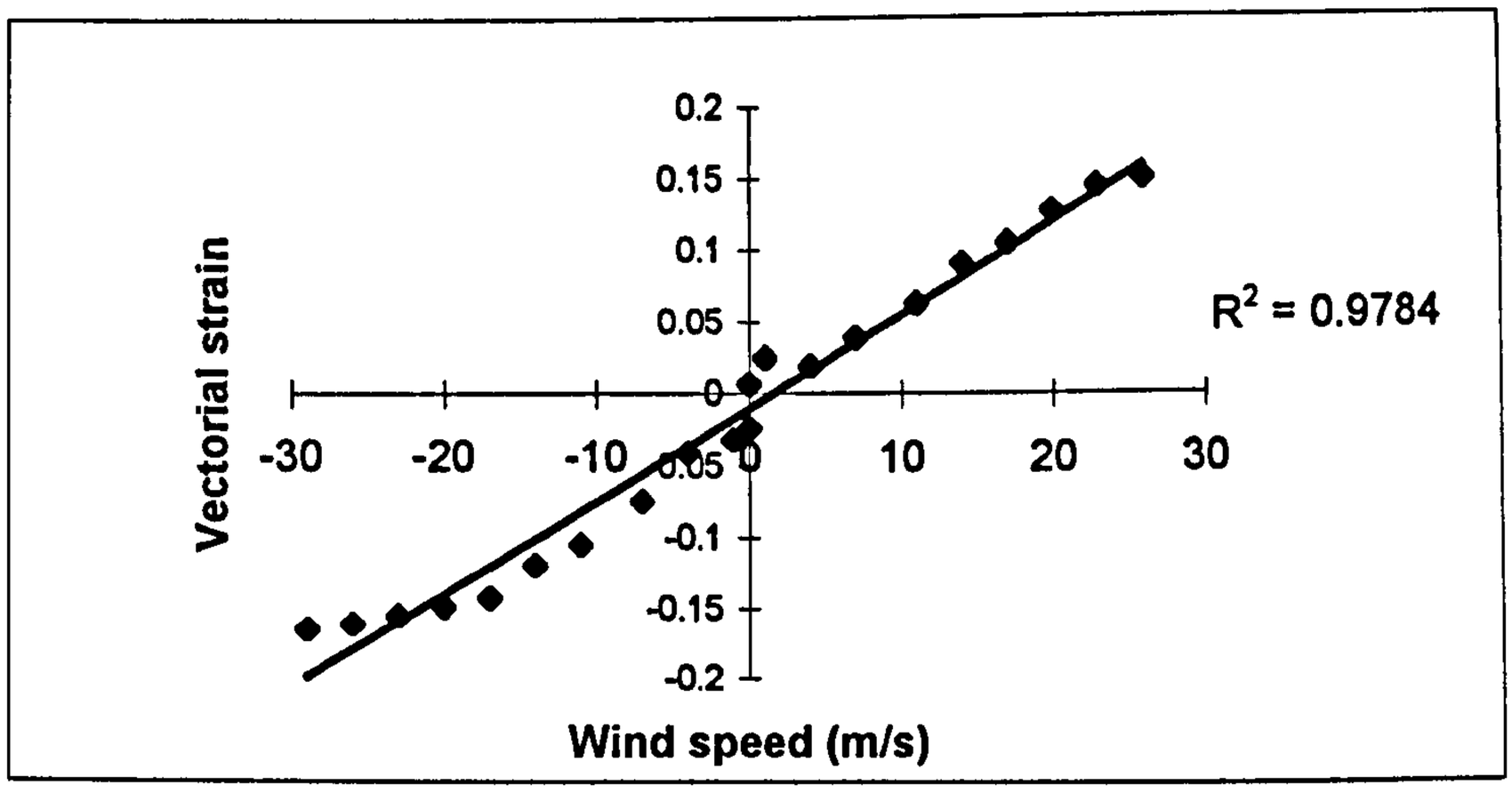

Figure 8.12 c: Optical root strain(vectorial strain) versus wind speed for forward and reverse airflow (90^0 and 270^0)

Figure 8.13 shows the plots when the sensor was oriented at 45^0 (negative axis) and 225^0 (positive axis) to the wind flow. When the sensor was oriented at 225^0 to the wind flow, the fibres were facing the wind flow, causing the grooves to open as the wind speed increased. At 45^0 to the wind flow, the flow was reversed causing the grooves to close. The effect of the closing and opening of the grooves on the light intensity transmitted through the fibre was discussed in Chapter 7. The plots of Figures 8.12(c) and 8.13 indicates that the sensor behaves similarly in forward and reverse directions and so is able to cope with multi-directional airflow. The range of operation of the optical fibre flow sensor is limited by the bending of the sensor which in turn is limited by the Young's modulus of the rubber beam and the inherent strength of the POF.

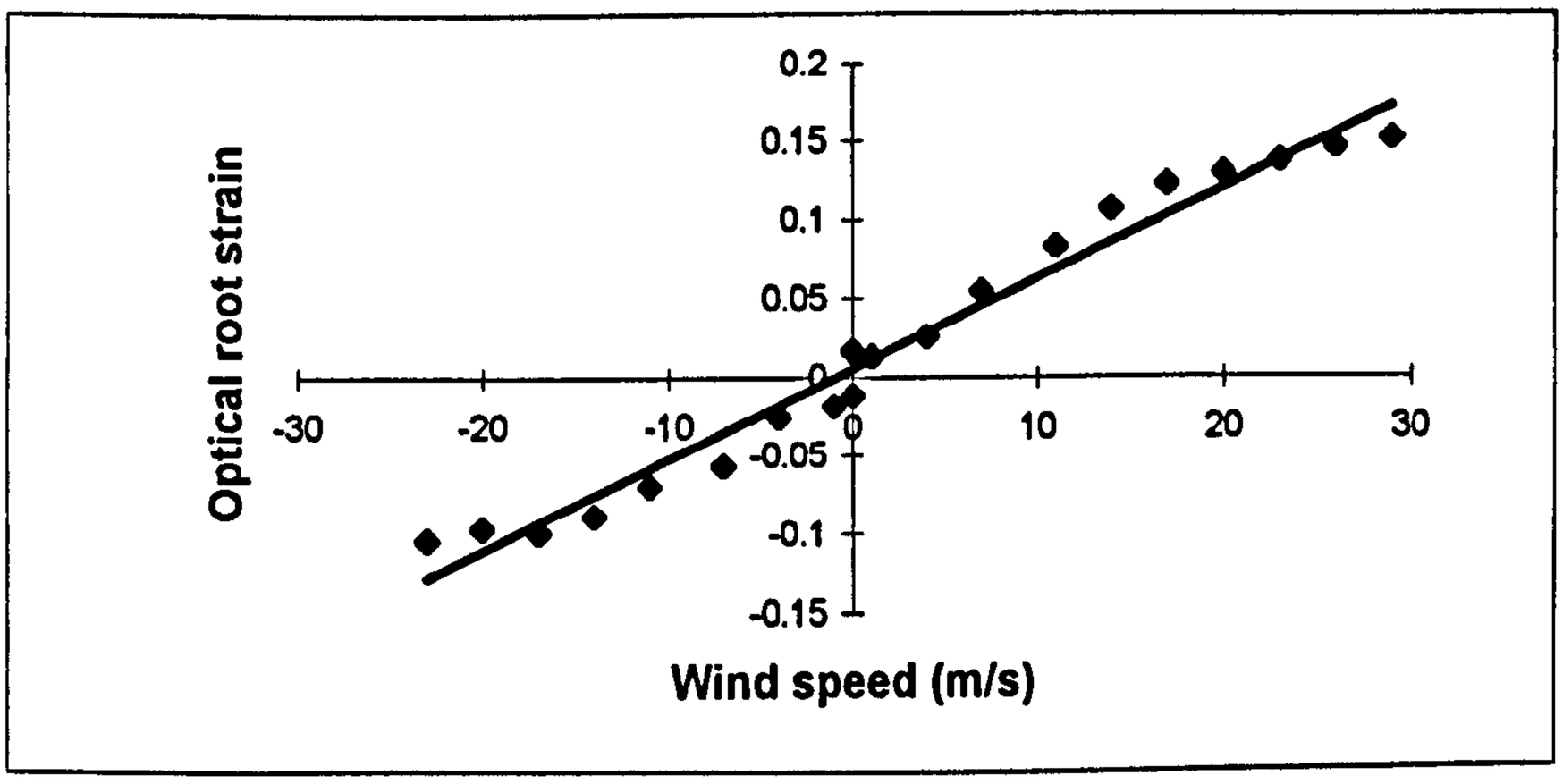

Figure 8.13: Optical root strain versus wind speed for forward and reverse airflow (45^0 and 225^0)

8.3.4 Direction of wind velocity

The direction of wind velocity for various wind speeds was calculated using Equation 8.6 for the different sensor positions in a plane perpendicular to the longitudinal axis of the rubber sensor from 0 to 180^0. Figure 8.14 shows the plots obtained from 11 m/s to 30 m/s. Several authors have stated that it is difficult to calculate the wind direction accurately at low wind speeds. The situation is similar in this case and the readings became more accurate as the wind speed increases (in this case 11 m/s and above). The wind direction repeats itself in cycles of 90^0 rotation and a similar curve was obtained for the 180 to 360^0 sensor positions.

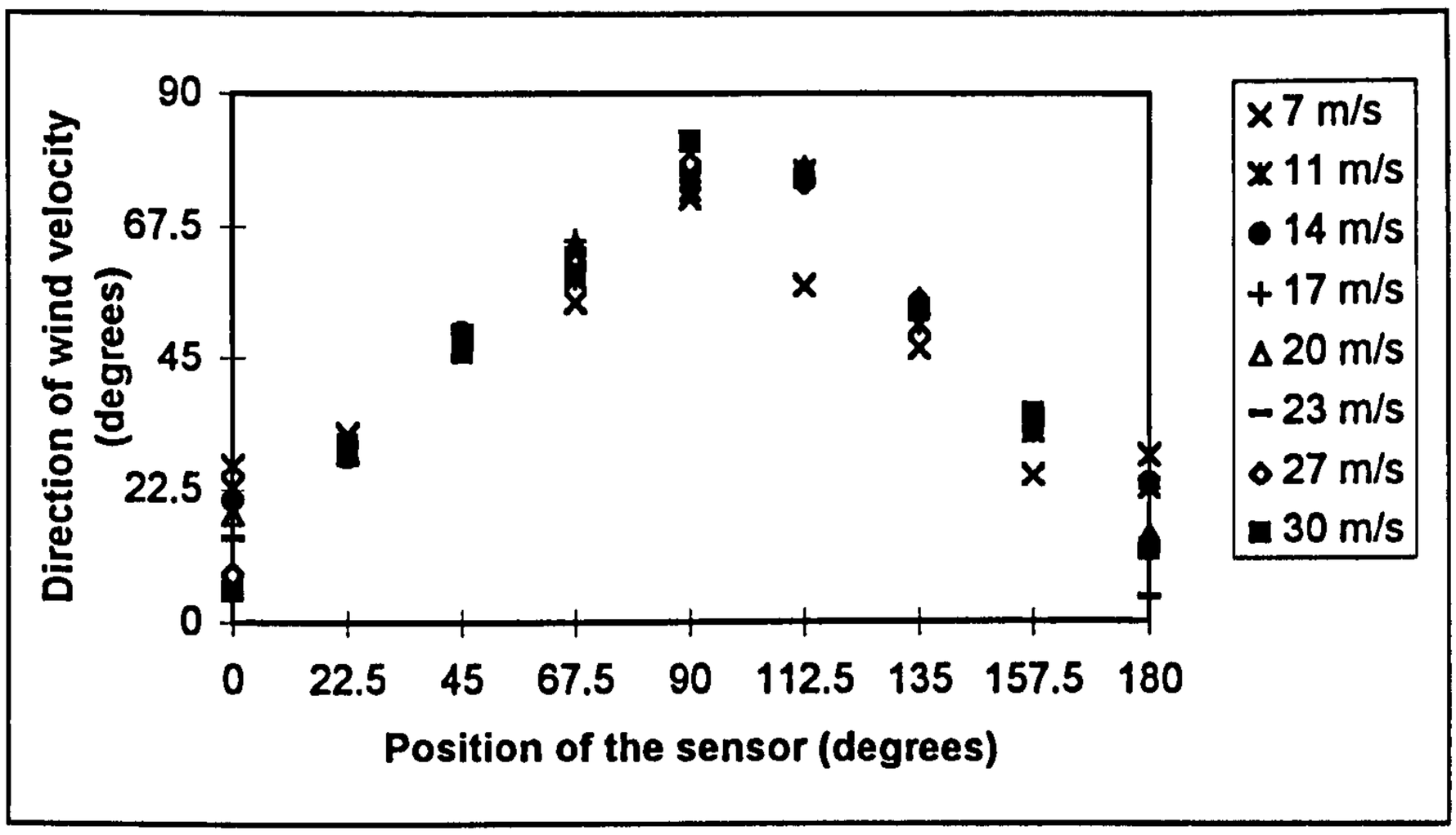

Figure 8.14: Direction of wind velocity for different wind speeds.

The wind direction sensitivity was found to be 0.81 ± 0.05 degrees and the resolution was found to be 5.9 degrees by performing a linear regression on all the data.

One important conclusion was obtained from experiments conducted to measure the wind direction. Initially, for the sake of convenience, the two optical fibres were each placed on the two edges and on the same side of the rubber beam, as shown in Figure 8.15(a). This was an improper alignment as the components of the wind velocity generated by the two fibres were parallel to each other. This arrangement was able to indicate the wind speed but gave no indication of the wind direction. When the two fibres were moved to the two adjacent longitudinal faces of the rubber beam (as illustrated in Figure 8.15(b)), the x and y-components of the wind velocity that were generated from this alignment enabled the detection of wind direction as well as

indicated in Figure 8.14. Hence *the position and alignment of the fibres on the flow sensing beam is important for the indication of the wind direction.*

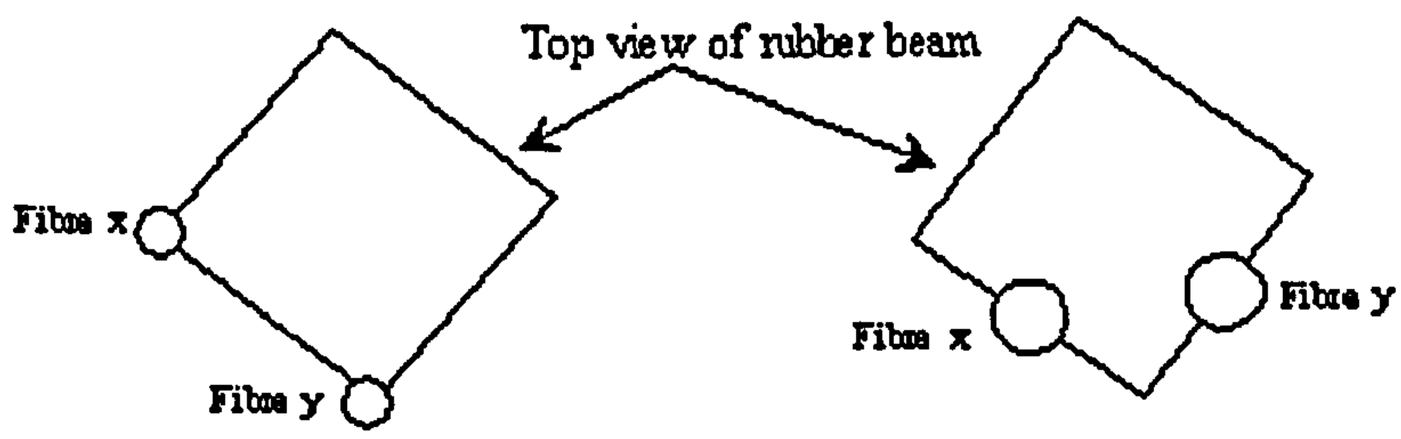

(a) Improper alignment *(b) Proper alignment*

Figure 8.15: Improper and proper alignment of the fibres on the rubber beam

8.4 STATIC CHARACTERISTICS OF THE OPTICAL FIBRE FLOW SENSOR

In the design of any instrument, it is essential to consider the parameters such as sensitivity, resolution, linearity, hysteresis and repeatability (defined in Sections 5.3 and 5.4) which are collectively known as the static characteristics of the instrument. This section discusses the results of the experiments conducted in the wind tunnel to explore these parameters for the optical fibre flow sensor.

Sensitivity and resolution have been discussed earlier in Section 8.3. The linearity of this flow sensor is derived from Figure 8.12(c). For the plots discussed in this figure, the correlation co-efficient was 0.9784, thereby indicating a linearity of ± 2.2 %.

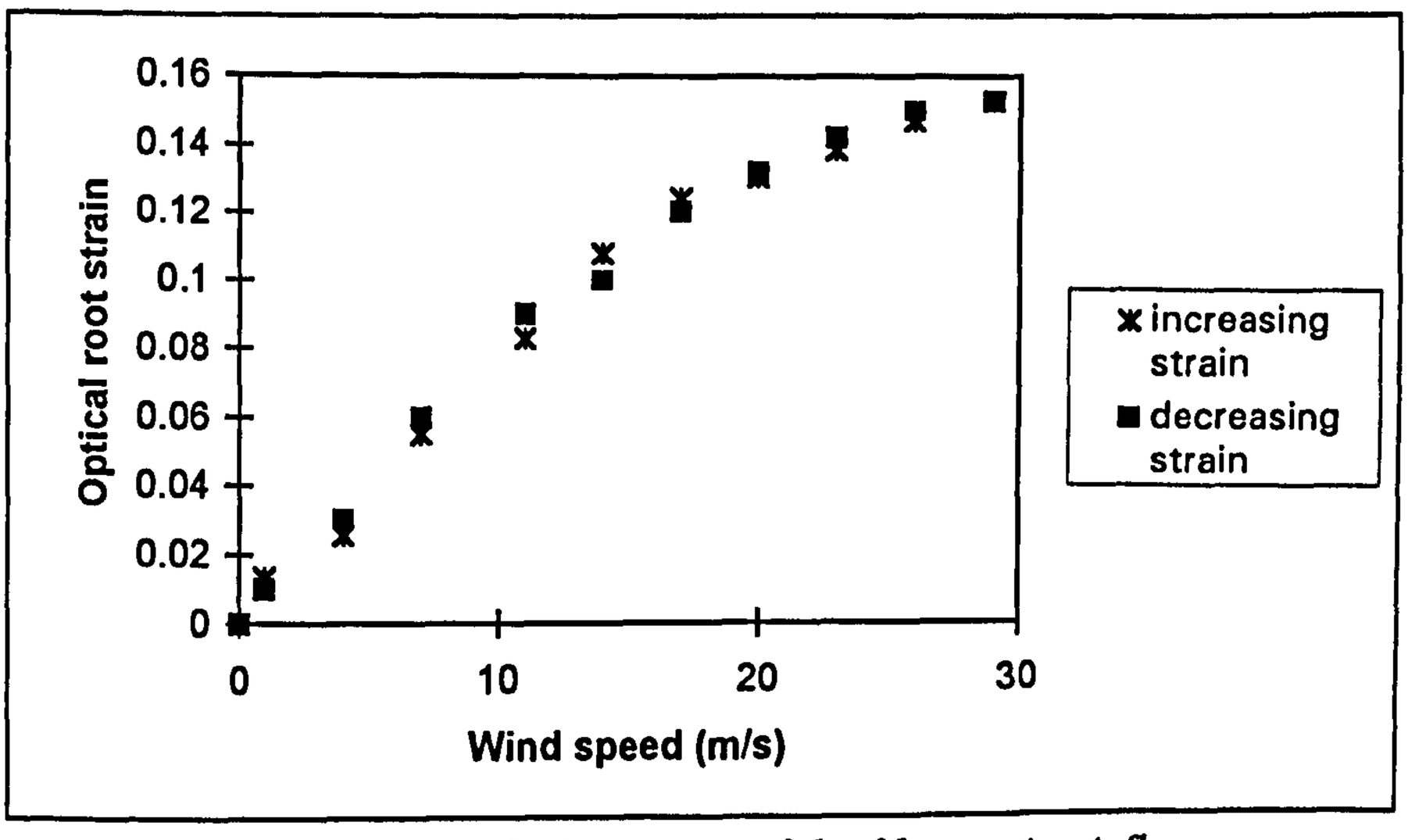

Figure 8.16: Test for hysteresis of the fibre optic airflow sensor

In order to conduct experiments to demonstrate the hysteresis of the flow sensor, the wind speed was steadily increased from 0 to 30 m/s and then steadily reduced to 0 m/s.

The co-incidence between the loading and unloading curves of Figure 8.16 indicates a very stable sensor which has negligible hysteresis.

Repeatability describes the closeness of output readings when the same input is applied repetitively over a short period of time, with the same measurement conditions, same instrument and observer, same location and the same conditions of use maintained throughout. In order to test the repeatability of the optical fibre flow sensor, the sensor was subjected to repeated increase in wind speeds from 0 to 30 m/s several times. Figure 8.17 shows the plots obtained during three such tests. From these results, this flow sensor had a repeatability of 0.36%.

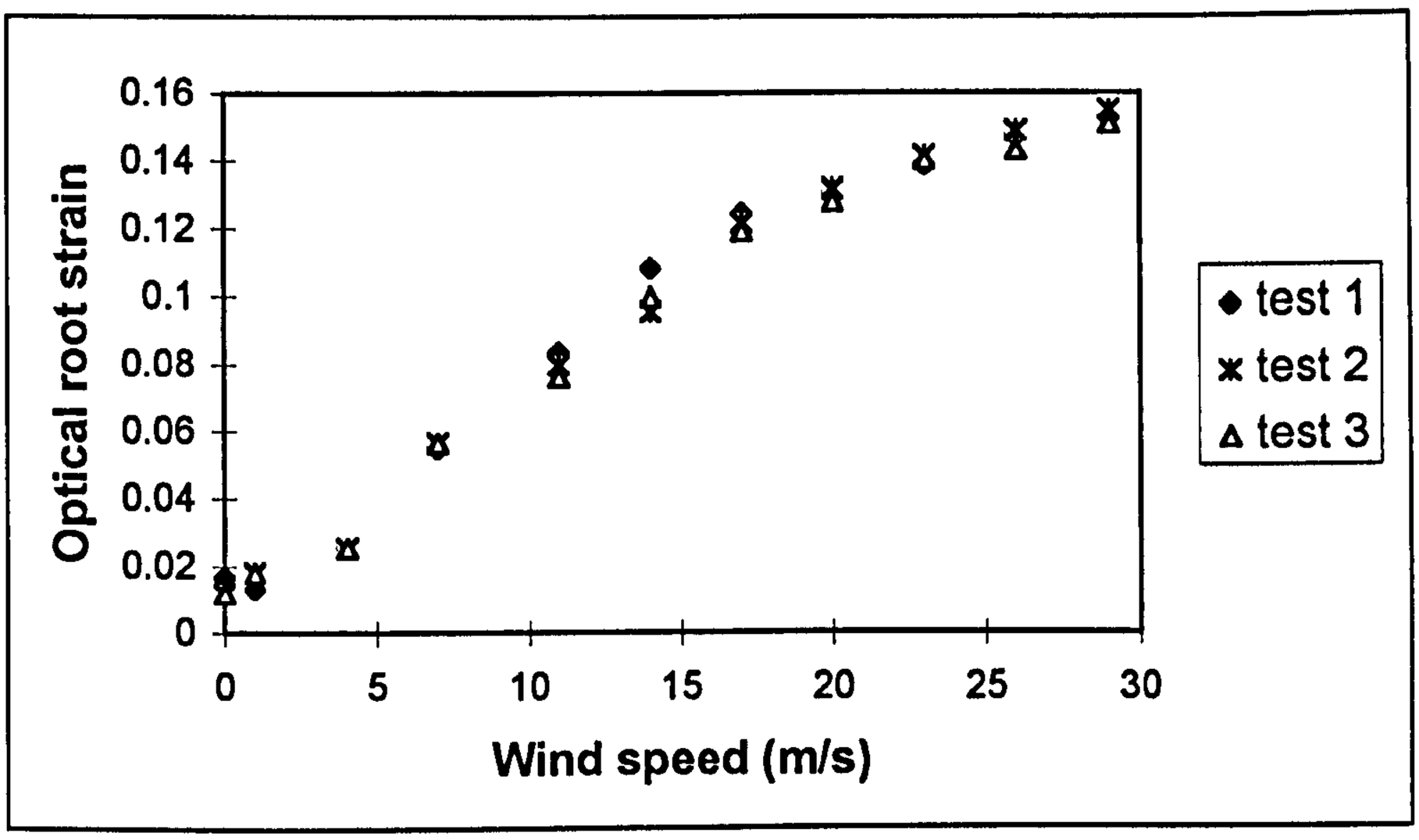

Figure 8.17: Tests for repeatability of the fibre optic airflow sensor

In order to test the stability of the response, the wind speed in the wind tunnel was set to a constant value (14 m/s) and the voltage output from the power meter, which was equivalent to the optical power from the optical fibre flow sensor were acquired by Labview using the VI shown in Figure 5.1 and sent to a spreadsheet file every second. Figure 8.18 indicates the response obtained for the first 300 seconds.

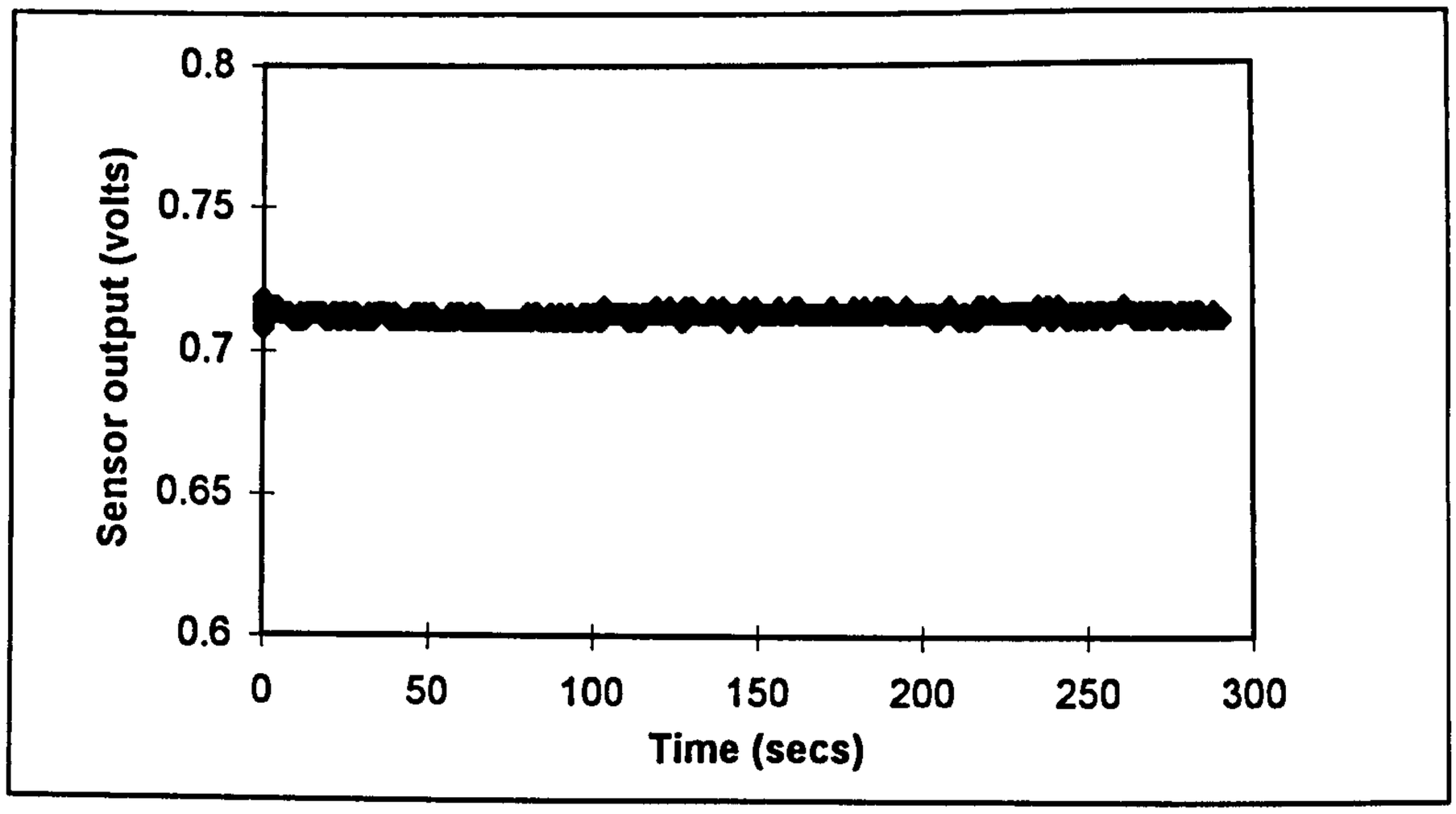

Figure 8.18: Testing the stability of the response

Table 8.2 indicates the results of descriptive statistical analysis performed on this plot. The mean and standard deviation were 0.7128 and 0.0017 respectively. The tests were performed at different wind speeds and only small variations were observed.

Table 8.2: Descriptive statistical analysis of Figure 8.18

Mean	0.712819
Standard Error	4.03E-05
Median	0.712891
Mode	0.712891
Standard Deviation	0.001708
Range	0.01709
Minimum	0.703125
Maximum	0.720215
Sum	1282.361
Count	1799
Confidence Level(95 %)	8.89E-05

The histogram of the plot of Figure 8.18 is shown in Figure 8.19. From Table 8.2 and the Histogram (Figure 8.19), for a mean value of 0.713 volts, the minimum and maximum values were 0.703 volts and 0.72 volts respectively indicating a standard error

of 4 E-05. These readings have indicated that the sensor has a very stable response within the limits of quantization error.

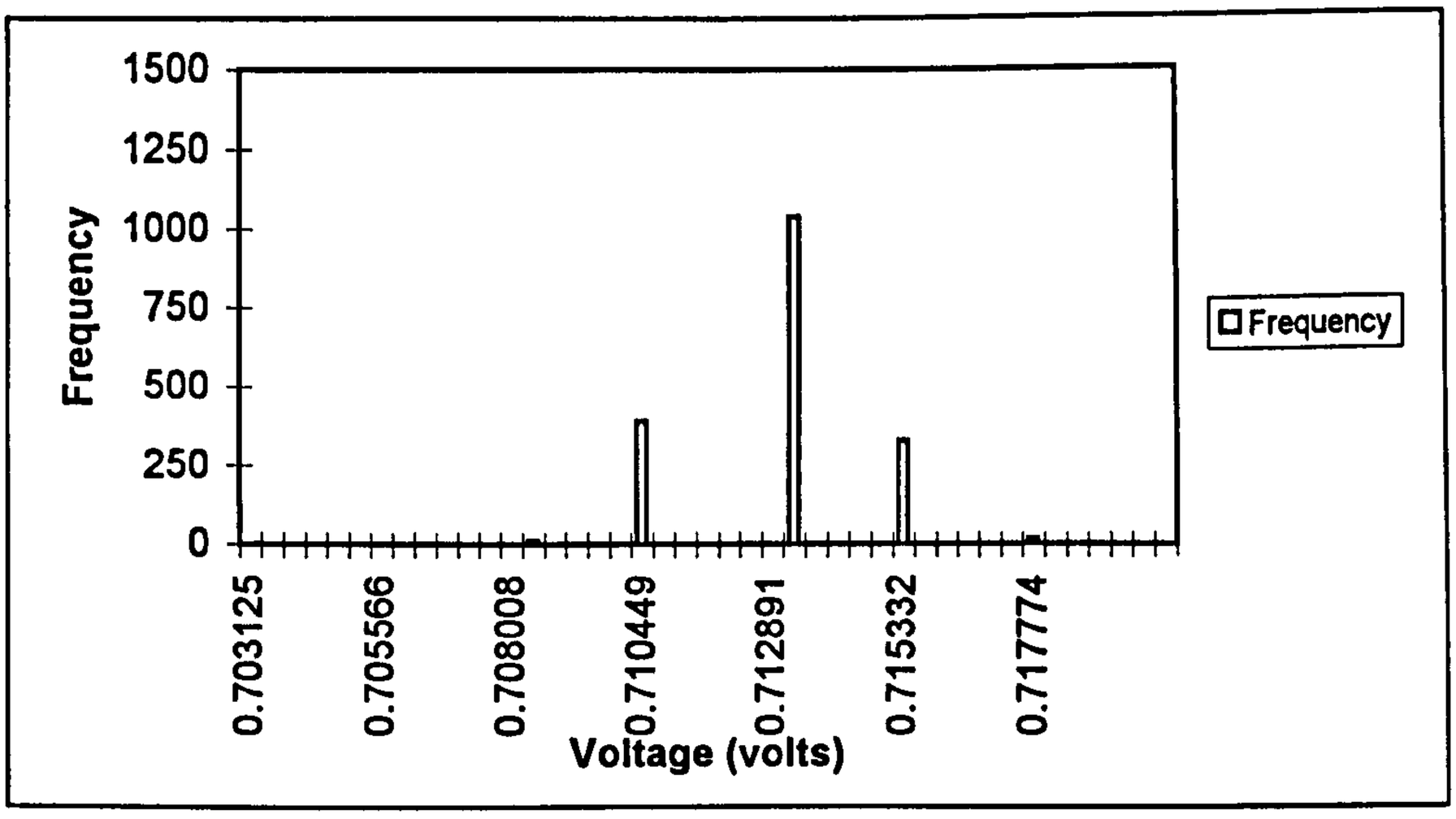

Figure 8.19: Histogram obtained from the stability tests

8.5 DYNAMIC CHARACTERISTICS OF THE OPTICAL FIBRE FLOW SENSOR

Dynamic characteristics describe the performance of a measuring instrument when the measured variable is changing rapidly. An open ended wind tunnel with a maximum wind speed of 33 m/s was used for the investigation of the transient response of the sensor. A shutter mechanism was specially designed to provide a step input to the flow sensor. The response of the sensor was acquired by the 12 bit DAQ-card 1200 and transferred to a spreadsheet file using Labview. The block diagram of the VI used for this purpose is the same as that used for the resistance strain gauge flow sensor shown in Figure 5.10. Data was acquired every 0.01 seconds for a period of 10 seconds by setting the sampling frequency to 100 Hz (f_s) and the number of samples to 1000.

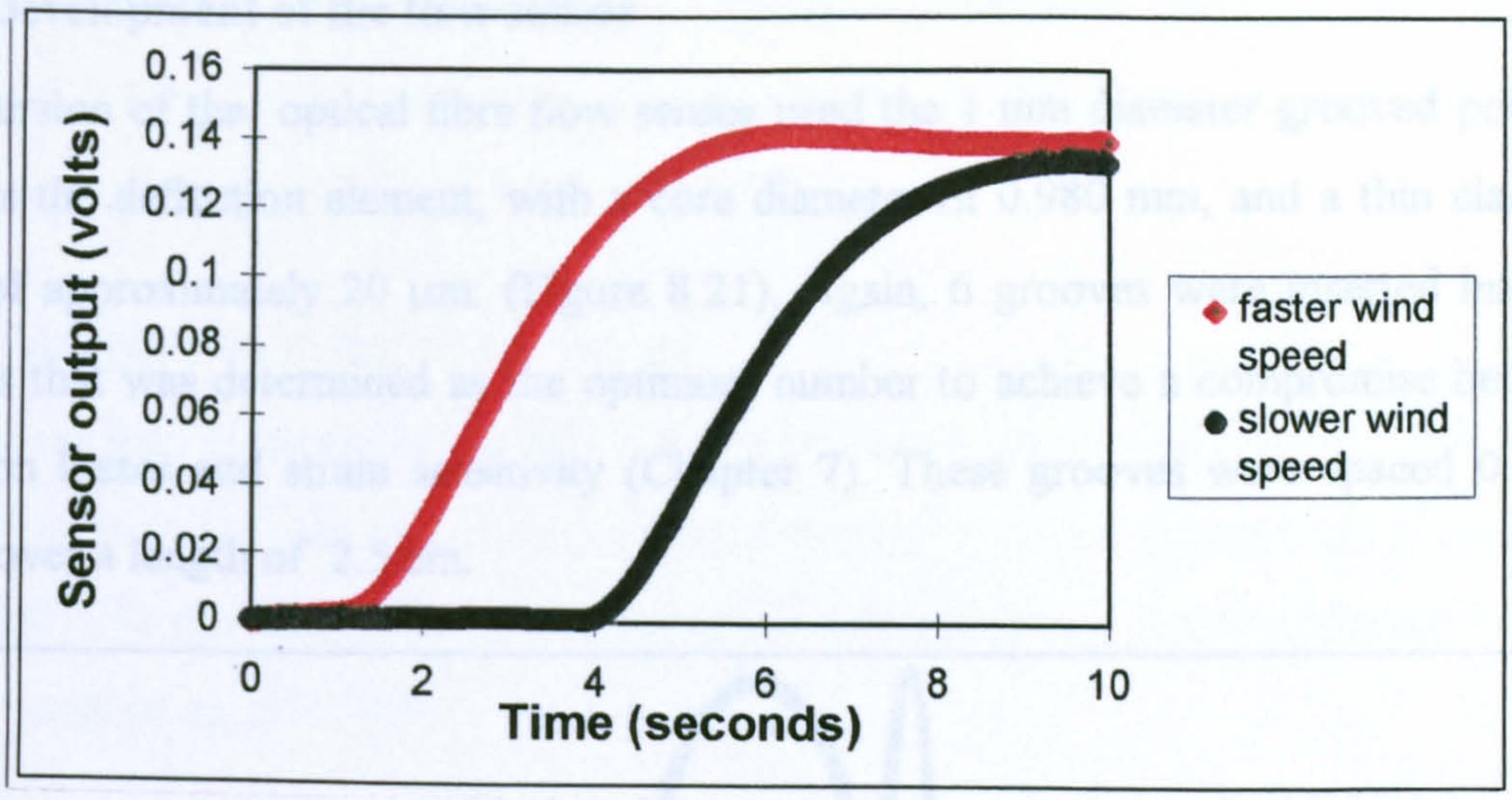

Figure 8.20: Response of the optical fibre flow sensor at two wind speeds

The optical fibre flow sensor was mounted in the wind tunnel and with the shutter mechanism closed, the wind tunnel was set at a particular wind speed. Since the shutter door was closed, the sensor did not undergo any deflection. When the shutter was opened, the deflection and hence the response of the sensor was detected and analysed using Labview. Figure 8.20 shows the response obtained at two different wind speeds. The sensor indicated a 95% response time of 5.4 seconds, a 10% to 90% rise time of 4.6 seconds and a 63.2% time constant of 3.6 seconds. The sensor response could probably be much faster than what was obtained here. The shutter mechanism was by itself quite slow (about 2 seconds) and this could be the reason for the response time that was obtained. If an alternative experimental arrangement, similar to the one described in Section 5.5.3, could be designed and set up, the sensor could indicate a faster response time, probably in terms of milliseconds.

8.6 AN OPTICAL FIBRE FLOW SENSOR WITHOUT RUBBER CANTILEVER.

The work presented in this section shows how an optical fibre strain gauge by itself can be used to measure fluid flow in two dimensions. Previous work used a rubber beam as the deflected device with conventional [8.2] or optical fibre strain gauges [8.3] attached to the deflected beam, but it was found in Section 8.3.3 that the performance characteristics of the resistance strain gauge flow sensor was better than the optical fibre flow sensor with the rubber cantilever. Hence to improve the characteristics of the optical fibre flow sensor, an unsupported sensitised 1 mm diameter plastic optical fibre without the rubber cantilever was used to measure the fluid flow.

8.6.1 Development of the flow sensor

This version of the optical fibre flow sensor used the 1 mm diameter grooved polymer fibre as the deflection element, with a core diameter of 0.980 mm, and a thin cladding layer of approximately 20 μm. (Figure 8.21). Again, 6 grooves were inserted into the fibre as that was determined as the optimum number to achieve a compromise between insertion losses and strain sensitivity (Chapter 7). These grooves were spaced 0.4 cm apart, over a length of 2.5 cm.

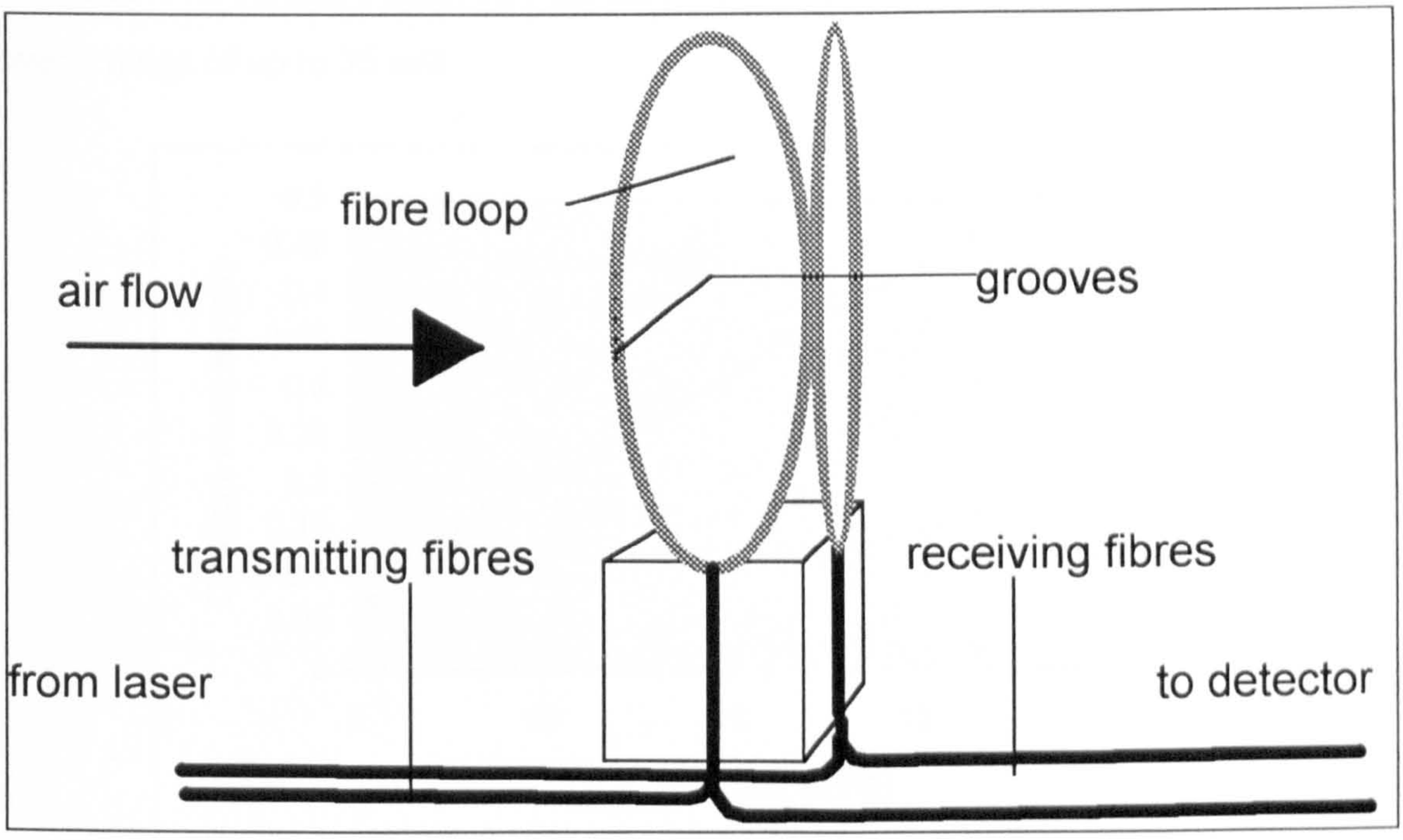

Figure 8. 21: Optical fibre deflection flow sensor.

In order to measure strain in two orthogonal directions, perpendicular to the longitudinal axis of the fibre, two fibres were used, as shown in Figure 8.21, with the grooves oriented at 90° to each other. This was achieved by positioning the fibres on two adjacent faces of a beam of square cross-section. This beam was short enough to prevent any restriction to the deflection and yet long enough to hold and support the optical fibres. The fibres were looped round so that the looped ends acted as drag elements. The grooved portion of the fibre was unsupported and free to deflect in the air stream. Light from a 1 mW helium neon laser at 633 nm, was split 50: 50 using a cubic beam splitter, and coupled into each fibre using microscope objectives. (Figure 8.4) The transmitted intensity through each fibre, was monitored using a power meter, giving intensities P_x and P_y. The power loss was calculated in optical root strain, $\Delta P/P_o$ by measuring maximum power, P_o at zero deflection, and $\Delta P = P_o - P_v$ where P_v is the

power measured at wind velocity, V m/s. Optical root strain was therefore calculated for the x and y fibres and combined vectorially to give magnitude and direction of optical strain, using Equations 8.5 and 8.6 respectively.

8.6.2. Experiments in the Wind Tunnel

The sensor was mounted in the 460 x 460 mm closed circuit wind tunnel. The optical fibre flowmeter was clamped on a turn table and rotated around its longitudinal axis from 0° to 360°. At various angles, ΔP_x and ΔP_y were measured as a function of wind velocity over a range of up to 35 m/s.

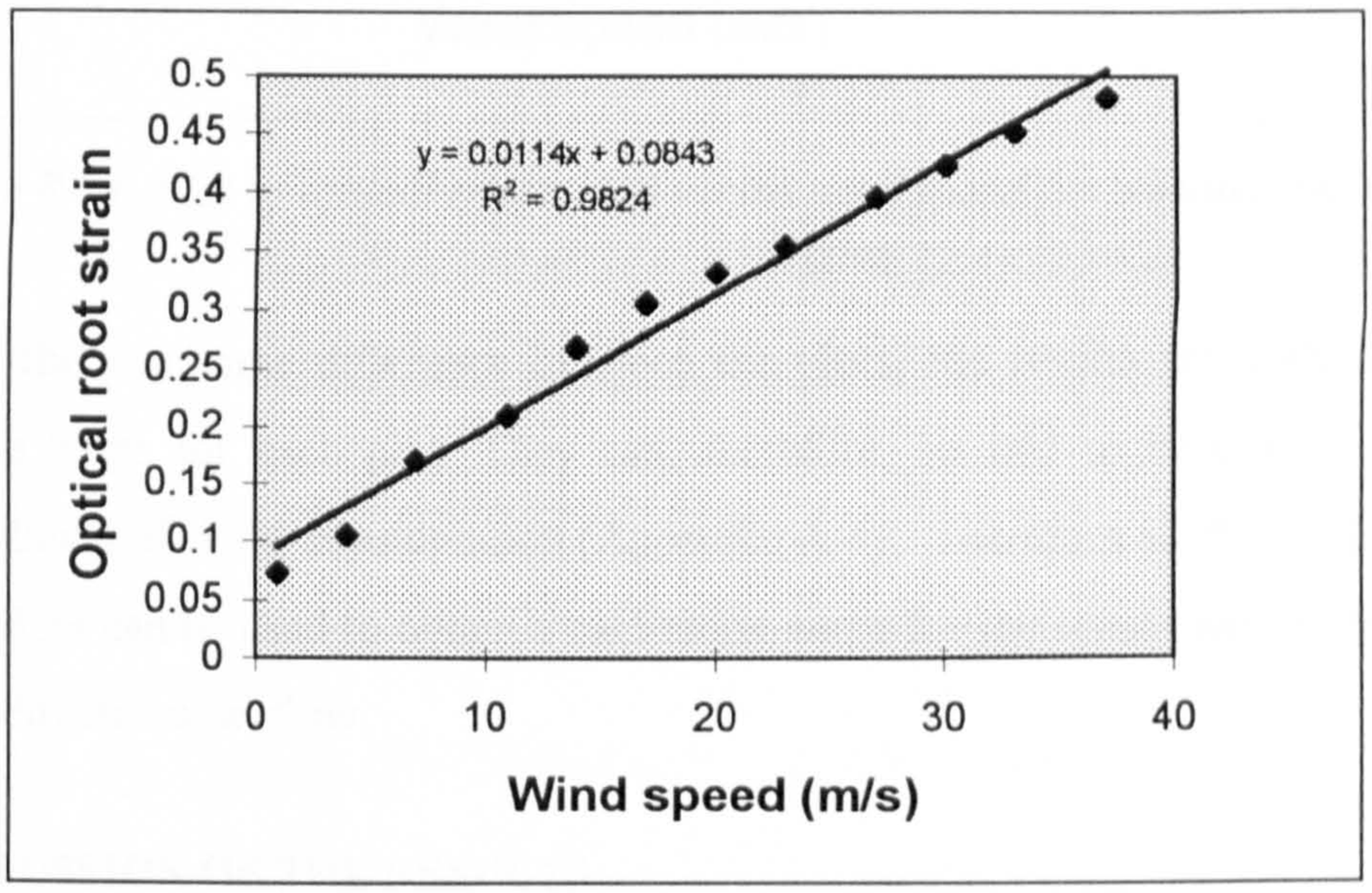

Figure 8.22: Plot of optical root strain versus wind speed for orientation of 60°.

Figure 8.22 shows a plot of optical root strain versus wind speed, when the optical fibre flowmeter was oriented at an angle of 60°. The graph has a linear gradient indicating that optical strain is proportional to the square of the wind speed. A linear regression analysis indicates a sensitivity of 0.01 ± 0.0005 optical root strain s/m, and a resolution of 0.96 m/s for windspeeds up to 35 m/s. Preliminary experiments indicate that the sensor will operate up to 50 m/s.

Figure 8.23 shows a plot of optical root strain versus wind speed when the elastic beam was oriented at different angles from 0^0 to 90° to the airflow.

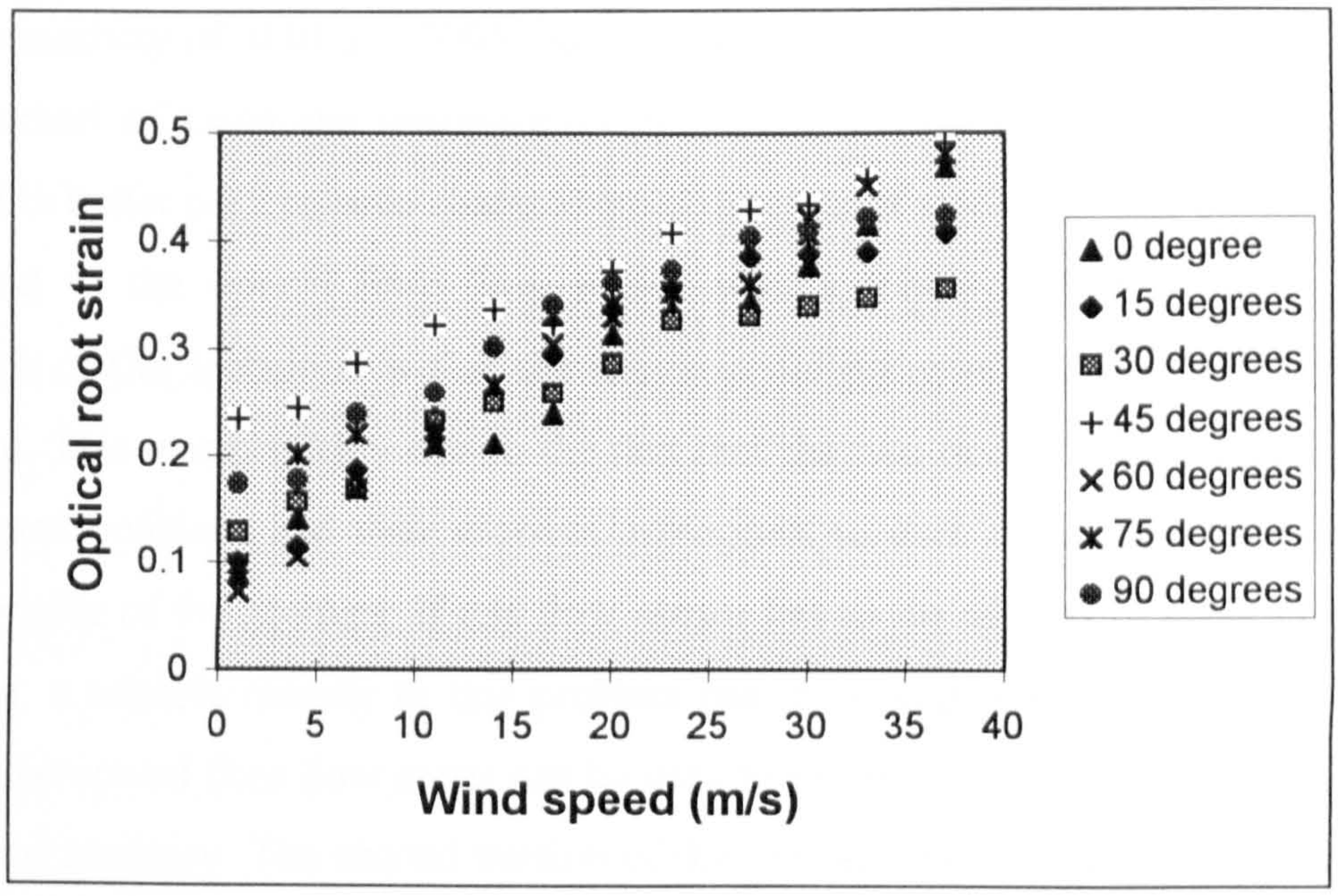

Figure 8.23: Plot of optical root strain versus wind speed for various orientation angles.

Although there is some difference between the plots, the results are within the 95% confidence limits for each plot. They can, therefore, be said to be coincident within statistical limits of 95% consideration.(Appendic A-4). Therefore all the data presented in Figure 8.23 can be used to obtain a calibration curve for the sensor which will be valid for multi-directional airflow.

8.7 DISCUSSION OF THE RESULTS

A novel technique for the measurement of two dimensional fluid velocity, using two versions of an optical fibre flow sensor have been demonstrated.

The first version used a rubber beam with two grooved plastic optical fibres on the two adjacent sides of the rubber beam. The sensor had a sensitivity of 0.005±0.0004 optical root strain and a resolution (optical) of 1.3 m/s while measuring the wind speed for wind speeds up to 30 m/s. While measuring the wind direction, the sensitivity of the sensor was found to be 0.81 ± 0.05 ^{0}/degree and the resolution was found to be 5.9^0. A similar sensor was developed and discussed in Chapter 4 to measure fluid flow using conventional electrical strain gauges. The electrical flow sensor had a sensitivity of 0.0065 ±0.0001 resistive root strain s/m, and a resolution (resistive) of 0.4 m/s.

To improve the performance characteristics of the optical fibre flow sensor, an all-optical fibre sensor has been demonstrated for wind velocity, over a range of 0m/s to 35m/s,

with a sensitivity of 0.01 ± 0.0005 optical root strain s/m and a resolution of 0.96 m/s. This method of using the unsupported optical fibre itself to undergo deflection has resulted in better performance characteristics in terms of resolution and sensitivity when compared to the optical fibre flow sensor with a rubber cantilever. But a major drawback of this technique is that the sensor could not give an indication of the wind direction. This was probably due to the fact that the two optical fibres, although in the undeflected positions had their grooves orthogonal to each other, could not retain the orthogonality of the grooves. If this flow sensor has to be utilised to measure the wind direction, a suitable remedy to this problem has to be implemented. Nevertheless, this type of the optical fibre flow meter can be used to sense the two dimensional fluid speed with good accuracy. The second version of the optical fibre flow sensor could be used for measuring flow in small pipes (as small as 15 mm diameter), which could be useful for the water industry where the direction of flow is not of any consequence.

CHAPTER 9

CONCLUSION: SENSOR FEATURES AND APPLICATION AREAS

This thesis has described the design, development and calibration of three flow sensors, all of which are based on the principle of elastic beam deflection. The first flow sensor has used conventional resistance strain gauges while the latter two have used optical fibre strain gauges to sense the deflection. The development, optimisation and calibration of the optical fibre strain gauge has also been discussed in this thesis in Chapter Seven. Chapter One has given an account of the flow sensors that have been developed in the past while optical fibre flow sensors in particular were reviewed in Chapter Six.

9.1 NOVEL FEATURES OF THE FLOW SENSORS

These flow sensors come under the general category of target flow sensors or the drag-force flowmeters. This is because the moving fluid exerts a force on the drag element of the sensor causing the sensing beam to deflect. The compression and extension resulting from the deflection is measured by strain gauges, both electrical and optical, attached to the surface of the beam. Hence the name target or drag-force flow meters.

9.1.1 The novelty of the research undertaken to develop the target flow sensors

The three target flow sensors that have been developed in this project measure two dimensional wind and water flow. Successful calibration has been performed for two dimensional air flow measurement and preliminary calibration has been performed for one dimensional water flow measurement.

A further advantage of the instrument is that it can be made to generate a measurement of flow direction in two dimensions, or even in three dimensions. Provided that the deflecting forces are independent in the sensing directions, the resulting outputs can be added vectorially to generate values for speed and direction of fluid flow which are independent of each other. This approach of vectorially adding the fluid components to generate both the speed and direction of the fluid flow is a novel drag-force sensing technique when compared to the existing techniques [1.14-1.19] used in target flow sensors.

A literature survey has indicated that none of the optical fibre flow sensors developed to date have used plastic multimode optical fibres to measure two dimensional flow. The method of measuring the strain by inserting radial grooves into the fibre to make the fibre lossy is yet another novel and unique approach.

The removal of the rubber beam for the third flow sensor, resulting in better performance characteristics, has enabled the use of the optical fibre itself as the drag element. A similar approach has been used to develop a vortex shedding flowmeter. But the uniqueness in the technique adopted in this project is that the bare optical fibre has been used to detect the drag-force exerted by the fluid, and hence the velocity of the fluid, without the problems associated with oscillations. There are no known publications as yet using this technique.

9.1.2 Improved features of these flow sensors over others

There are many different techniques of measuring flowrate and none will offer a solution to every flowmetering problem. The target flow sensors developed in this Ph.D project are very versatile and reliable flow measurement devices. The flowmeters are compact, and requires no infrastructure, other than a rigid support. The advantages of these devices over rotating flowmeters are lower inertia enabling measurements of gusts and rapid changes in windspeed, absence of mechanical parts, and robustness. They are easy to maintain and simple in operation, thereby reducing the maintenance and operational costs. They can cope with fluids containing solid matter, such as sludge or slurries. Compared with vortex shedding and Doppler devices based on ultra-sonics, the proposed instruments are cheaper, allowing multiple-headed sensing. Hot wire anemometers are affected by raindrops, but these instruments are rugged and less susceptible to moisture. The compactness of the device, and the fact that both speed and direction are measured by the same transducer at the same place and time, offers advantages for the measurement of flow which varies over small distances, such as winds close to the ground. The flow sensors have no rotating parts and this makes the instrument suitable for conditions where abrasion, contamination or corrosion make more conventional instruments unsuitable. Finally, the optical fibre flow sensors developed have the advantages of being immune to electromagnetic interference and can be used in hazardous environments.

9.2 APPLICATION AREAS

The sensors were primarily intended for environmental applications, but could be used for industrial applications as well. The main areas of application envisaged are:

9.2.1. Meteorology

Measurement of short term gusts and turbulence close to the surface and to obstacles (natural and artificial) is an important matter in understanding wind loads on structures such as buildings and wind turbines, and can also be significant in introducing or replacing vegetation in windy areas for amenity, erosion control or economic forestry. The proposed instrument has very small inertia, and would possibly be able to follow the profile of gusts, although tests have not been conducted to prove this.

9.2.2. Hydrology

The flow of water in rivers is affected by the topography of the river bed, and it is thought that fish are able to make use of regions of fast or slow flow, as appropriate to their activity and direction of travel. Artificial drainage work on natural rivers, to make them into arterial drains, reduces the roughness of the river bed and banks and this is thought to lessen the range of habitats available to fish. There is a need, therefore, for a simple, robust and inexpensive transducer which can be placed at a series of depths and positions across a river, or as a matrix of several transducers at different sites for simultaneous measurements of velocity and flow direction. Measurement of flow direction close to river channel beds or of velocity gradients in the channel cross-section are also important in studies of sediment movement in channels, undertaken by engineering geologists and geomorphologists.

9.2.3. Marine studies

There is considerable interest in the post-breaking movement of waves horizontally at right angles to the shore. Conventional instruments are often insufficiently robust for this purpose, especially when abrasion by sand or gravel is likely. In addition, submarine cables and pipelines can be abraded and damaged by current-borne sand particles. Thus the measurement of movement of sea-water, especially close to the sea-bed, is important to an understanding of the coastal environment and its interaction with man-made structures. The proposed instrument would be suitable for such measurements.

9.2.4 Oil and gas industry

The production of oil and gas provides a classic example where metering accuracy can be related directly to income and perhaps for this reason a wide range of problems have been identified which need to be tackled. With proper selection and design of the sensing beam material (Chapter 3) and calibration, the target flow sensor developed could probably be used to measure the oil flow rate due to its ease of installation and high reliability.

9.2.5 Automobile Industry

Single- and multi-point injection systems offer the possibility of improving engine parameters such as torque, power, emissions, fuel economy and driveability. To do this the air/fuel ratio must be carefully controlled and this control is achieved by measurement of the air flow rate; the appropriate petrol flow rate is then provided. The air flow rate is measured in most systems by the Bosch air vanemeter (Chapter 1.4.2) which again belongs to the category of target flowmeters. There is a need for the response time of the meter to be fast enough to follow the engine speed but not so fast as to follow 'noise' in the flow. Also, turn-down ratio of 40:1 is required to cover the range between idling and full throttle. Overall, therefore, for a two-litre engine, air flowrates in the range of 2.5-100 g/s have to be measured over periods as short as 0.01 second in a 500 mm pipe.

There is thus a tremendous potential for a successful air fuel meter, which is also cheap and the solution could possibly be one of the flow sensors described in this thesis. Flow of diesel fuel, gasoline and transmission fluid could also be measured. Turbine flowmeters have previously been used, but they do not have the response and viscous immunity at low flows as does the target flowmeter.

9.2.6 Domestic water metering

Of all the changes and innovations taking place in flowmetering in the UK at the present time, one of the most important and challenging area arises from the likely introduction of widespread domestic water metering. Greater demands are being placed on water meters. The water industry have showed interest in both the resistive and optical flow sensors developed. They are looking for a cheap but low - accuracy network of meters to get an overall idea of water flow on domestic mains and they consider that the sensors

developed could meet their requirements. Section 9.3 outlines the suggestions for further work to be undertaken to meet these needs of the water industry.

Another challenge is in meter reading. Access for meter readers can be difficult and manual reading of meters is costly. Remote meter reading systems offer advantages both for centralised data collection and customer billing and for control of water consumption through the application of variable tariffs. The resistance strain gauges have the option of using remote measurements of the signals and so this could be another area of application for this flow sensor.

9.2.7 Steam measurement

Measurement of saturated or superheated steam is critical in today's energy conscious environment. Conventional flowmeters are not practical due to the damaging effects of condensate that can occur in saturated steam. The design of the target flowmeter permits the addition of an overrange stop to limit the possibility of damage to the primary sensing element.

9.2.8 Multi-phase flow

Multi-phase flow covers a variety of situations but the widest current interest is in the flowrate of gas/liquid mixtures. Historically this has been a problem only in power generation with small bore boiler tubes carrying steam/water mixtures but is now a major concern of the oil and gas industry. The key requirement to achieve successful metering of multi-phase flow would be to condition the flow so that the phases are either separated or the flow is homogeneous i.e. the various phases flow with the same velocity. The target flowmeter would appear capable of handling multi-phase flow, but has not been tested under these conditions.

Advance in resistance and optical fibre strain gauge technology and procedures and the use of new materials with improved physical properties offer future application opportunities. It should be noted, however, that the application potential of the target flowmeter as it is presently configured has not been fully explored.

9.3 SUGGESTIONS FOR FURTHER WORK

The most important area to pursue would be to continue with the calibration of the resistance and optical fibre flow sensors to measure water flow. Preliminary measurements have been performed in a water tank to measure water using the resistance strain gauge flow sensor in the range of 0 to 0.4 m/s with a resolution of 0.02 m/s, thereby providing a turn down ratio of 23:1. Further calibration runs have to be performed to extend the range of the flow sensor and hence the turn down ratio. Once this has been successfully undertaken for one dimensional flow measurement, this could be extended by using two pairs of resistance strain gauges for two dimensional flow measurement, thereby generating both the magnitude and direction of water velocity. The water industry have specified particular needs relevant to them where they would like to see if this sensor could measure water flow in a 15 mm pipe. This would mean that the sensor would have to be designed accordingly by reducing overall dimensions (both length and width) of the flow sensing beam and the drag element and then calibrated in the water rig in a 15 mm pipe. If the problem of dirt build up on the drag element occurs, the solution to the problem would be to redesign the drag element. The drag element could probably be a circular disk supported in the centre of the pipe or conduit so that it forms an annulus between the drag element and the pipe wall. The annulus provides a space for the dirt to pass freely beneath the disk and gas bubbles over it.

Another possible area to work on would be to calibrate the optical fibre flow sensor without the rubber cantilever to measure water flow. Optical systems present problems of contamination and of refractive index variation. These issues need to be investigated thoroughly. If this sensor provides promising results while measuring water flow, a series of carefully instrumented calibration runs will need to be performed. This sensor could be redesigned to improve the performance characteristics of the sensor by replacing the fibre loop with a single plastic fibre having a reflective coating or mirror at the free end which could reflect the signals back to the power meter or a detector. This modification of the optical fibre flow sensor could then be used to measure fluid flow. One of the disadvantages of the fibre optic strain gauge is that the grooved optical fibres present problems of contamination. One possible solution to this problem is to replace the fibre

groove with bragg gratings [9.1] inserted into the fibre which can then be tested as a flow sensor. A simpler alternative is to sheath the grooved area of the fibre.

A major advantage of the target flow meter is that it can be extended to measure the flow of other fluids like oil, steam, hydrocarbons, etc. By having a knowledge of the fluid to be metered and the temperature range that would be encountered during a particular flow measurement, the sensing beam material could be selected (reviewed in Chapter 3) and used to redesign the sensor. Having performed successful calibration runs to measure wind and water flow, the measurement of other fluids should not be a problem. Equation 4.23 shows the method of theoretically calculating the speed of an unknown fluid using the results of the calibration runs in a known fluid. The ability to calibrate the target flowmeter in a safe and easy-to-handle fluid like water and to provide a solution with high accuracy for hazardous applications, where a calibration with the actual fluid may not be possible, is one of the major benefits of this flowmeter.

The data acquisition and analysis package - Labview, supplied by National Instruments has been invaluable during the calibration runs that were performed. This sophisticated package is very expensive and it would be a good idea to replace it with a battery driven microcontroller. This would reduce the overall cost of the sensor and furthermore would facilitate in its usage as a stand alone instrument. Thereafter a series of these sensors could be used as in a quasi-distributed system. Preliminary programming has been performed on a microcontroller, the C-Port 552 based around the Philips 80C552, by the author, to convert the two analog signals from the sensor into digital form and then to add them and to take the square root of the sum. Further work could not be pursued on this as the microcontroller was not capable of generating the floating point value of the square root of a number. Work is being done on a PIC - microcontroller (16C71) as an undergraduate project to do the necessary acquisition and analysis of the signals. [9.2]. Once that is completed, a stand alone, portable and low cost flow sensor would be available for commercial exploitation.

REFERENCES

[1.1] Schlichting, H; Boundary layer theory, 6th edition, 1968.

[1.2] Heywood, KJ; Fluid flows in the environment: an introduction; *Physics Education*; vol. 28, 1993, pages 43-51.

[1.3] O. Reynolds; An experimental investigation of the circumstances which determine whether the motion of water shall be direct or sinuous, and of the law of resistance in parallel channels. *Phil. Trans. Royal Society* 174, 935-982 (1883), Scientific papers 2, 51.

[1.4] Barnes, H T and Coker E G; The flow of water through pipes. *Proc. Royal Society*, London, 74, 341 (1905).

[1.5] Schiller L; Untersuchungen uber laminaer und turbulente Stromung. Forschg. Ing. Wes, Heft 428 (1922)

[1.6] Ekman V W; On the change from steady to turbulent motion of liquids. *Ark. f. Mat. Astron. och Fys* 6, No 12 (1910).

[1.7] Baumeister T; "Mechanics of fluids", Mark's standard handbook of Mechanical Engineers, 8th edition.

[1.8] Brain T J S and Scott R W W; "Survey of pipeline flow meters", *Journal of Physics, E: Scientific Instruments*, Vol. 15, 1982.

[1.9] Furness R A and Heritage J E; " Commercially available flow meters and future trends", *Measurement and Control*, June 1986.

[1.10] Orlando V A and Jennings F B, 1954, 'The momentum principle measures true mass flow rate'; *Transactions of the American Society of Mechanical Engineers*, 76, pp. 961-965

[1.11] Al-Khazraji, 1979; Electromagnetic flow meters with large electrodes; PhD Thesis, London University.

[1.12] Doebelin E O; 1990, Measurement systems, Application and Design; McGraw-Hill International Editions.

[1.13] Escudier M P; 1983, "The instrumentation of a modern fluid mechanics research laboratory (Part 1)", *Measurement and Control*, Vol 16, June 1983.

[1.14] Clarke W T;1986, " *Design and operation of target flowmeters*" , Encyclopaedia of fluid Mechanics, Gulf Publishing company, USA.

[1.15] Robert L Mott; Applied Fluid Mechanics, Second edition, Prentice Hall.

[1.16] Hoerner S F; 1965, Fluid dynamic drag; Practical Information on Aerodynamic drag and Hydrodynamic resistance. Hoerner, Midland Part, N.J.

[1.17] Krause L N and Fralick G C; "Miniature drag force anemometer", 1977, NASA TM X-3507.

[1.18] De Carlo J P; Fundamentals of flow measurement, ISA Learning module, Instrument Society of America, North Carolina, USA; 1984.

[1.19] Waldron H N, Main I C, Jongens A W D, Brundrit G B; " A semiconductor strain gauge probe to measure turbulence in the water column", *Journal of the S.African Acoustics Institute*, Vol. 6, pp 80-95.

[2.1] BS6888: 1988, Bonded Electrical Resistance strain gauges calibration.

[2.2] W Thomson (Lord Kelvin), On the electrodynamic qualities of metals, *Proceedings of the Royal Society*, London, 146 (1856), 649-751.

[2.3] Window A L and Holister G S ; Strain gauge Technology, Applied Science Publishers (1982).

[2.4] Kobayaski A, Handbook on experimental mechanics, 1987, pt 6, Prentice Hall.

[2.5] Optimising strain gauge excitation levels, Measurements group Technical note, TN-502 (1979).

[2.6] Student Manual for strain gauge Technology, Measurements group, Bulletin 309B (1983).

[2.7] Transducer applications, Issue 1, March 1986, Measurements group.

[2.8] Perry C C and Lissner H R, The strain gauge primer, McGraw Hill (1962).

[3.1] Bolton W (1989); Newness Engineering Materials Pocket Book.

[3.2] Nagdi K (1993); Rubber as an engineering material: guideline for users, Hanser Publishers.

[3.3] Lindley P.B, Engineering design with natural rubber, NR Technical Bulletin, Malaysian Rubber producer's Research Association, Fourth edition (1974).

[3.4] Gary R. Hamed (1992), "Materials and compounds", *Engineering with rubber: How to design rubber components*, Edited by Alan N.Gent, Hanser Publishers.

[3.5] Philip Freakley, (1996), "Rubber processing: evolution and challenges", *Materials World*, vol. 4, number 4, April 1996.

[3.6] Pilkey W. D, (1994) Formulas for Stress, strain and structural matrices, John Wiley and Sons.

[3.7] Bragg G.M, (1974), Principles of Experimentation and measurement, Prentice Hall.

[3.8] D. Cumberland (1983), Panama Weathering Study, Dupont Technical Report 515.

[4.1] Newman F H and Searle V H L(1948); The general properties of matter. Edward Arnold.

[4.2] Labview Reference Manuals(1992); National Instruments Corporation.

[4.3] Dudzinski T J and Krause L N (1969); "Flow direction measurement with fixed position probes", Report No. *NASA TM X 1904*.

[4.4] Bryer D W and Pankhurst R C; Pressure-probe methods for determining wind speed and flow direction, National Physical Laboratory.

[4.5] Transducer Applications, Measurements Group, Inc; Issue 1, March 1986.

[4.6] Tom Clarke: 1986, '*Design and operation of target flowmeters*' ; Encyclopaedia of Fluid Mechanics;Vol 1; Gulf Publishing company, USA.

[4.7] Encyclopaedia of Fluid Mechanics (1986);Vol 1; Gulf Publishing company, USA.

[4.8] Arnold Sommerfield: Partial differential Equations in Physics. Academic Press Inc., 1949, pp 303.

[5.1] Davies O L and Goldsmith P I; Statistical Methods in Research and Production; 1972;Oliver and Boyd.

[5.2] Shapiro, B H, "Putting strain gauge pressure transducer stability in perspective", Dynisco Co, Norwood, MA (1983 reprint).

[5.3] Alan S Morris, Principles of Measurement and instrumentation, Prentice-Hall,1993.

[5.4] H K P Neubert; Instrument transducers: An introduction to their performance and design; second edition; Clarendon Press, 1975.

[5.5] F C Kinghorn, Analysis and assessment of data *in developments* and flow measurement, Applied Science Publishing, Editor: R W W Scott, 1982.

[5.6] British Standards Institution, Precision of test methods, Part 1,Guide for the determination of repeatability and reproducibility for a standard test method, BS 5497;1979.

[5.7] Barry E Jones (1985), Instrumentation, measurement and feedback, Tata Mc-Graw Hill

[5.8] Robert N Bateson (1989), Introduction to control system technology, third edition.

[5.9] Cerni R H and Foster L E; Instrumentation for Engineering measurement. John Wiley and Sons, Inc, New York, London (1962).

[5.10] Fraser C J and Milne J S, Microcomputer applications in Measurement systems, pp19, Macmillan (1990).

[5.11] Ginsburg B.R, "Flow rate measurements for spacecraft thrusters," Rocketdyne Division of North American Aviation (1983).

[6.1] Alan S Morris (1993); Principles of measurement and instrumentation, Prentice Hall.

[6.2] Vali, V and Shorthill R W (1976) Fiber ring interferometers. *Applied Optics*, 15, 1009.

[6.3] Rogers, A J (1977) Optical methods for measurement of voltage and current at high voltage. *Optical laser technology*, 273.

[6.4] Eric Udd (1991), Fiber optic sensors: An introduction for Engineers and Scientists, John Wiley.

[6.5] Scully, P J (1991), PhD Thesis, University of Liverpool.

[6.6] Grattan, K T V and Meggitt, B T (1995), Optical Fiber sensor Technology, Chapman & Hall.

[6.7] Lagakos N, Litovitz T, Macedo P, Mohr R and Meister R(1981), Multimode optical fiber displacement sensor. *Applied Optics*, 20, 167-168.

[6.8] Jeff Hecht (1993), Understanding Fiber Optics, Sams Publishing.

[6.9] Busurin, V I, Semenov A S and Udalov N P (1985) Optical and fiber optic sensors (review). *Soviet Journal of Quantum Electronics* **15**(5), 595-621.

[6.10] Medlock R S (1986) Review of modulating techniques for fiber optic sensors. *Journal of Optical Sensors*, 1(1), 43-68.

[6.11] Sheem S K and Cole J H (1979), Acoustic sensitivity of single mode optical power dividers, *Opt. letters*, **4**, 322-324.

[6.12] Brian Culshaw and Dakin J, (1989), Optical Fiber sensors: Systems and applications, vol 2.

[6.13] Sharma M and Brooks R E (1980), Fiber optics sensing in cryogenic environments, *Proc. SPIE*, **224**, 46-52.

[6.14] Rogers, A.J, (1979), "Optical measurement of current and voltage on Power systems", *IEE Journal of Electrical Power application*, vol 2, 120-124.

[6.15] Ivan Andonovic and Deepak Uttamchandani (1989), Principles of modern optical systems, Artech House.

[6.16] Wickersheim K A and Alves R V (1982), Fluoroptic thermometry: A new RF-Immune Technology in biomedical thermology. Aln R L, Liss Inc. New York, 547-554.

[6.17] Hocker. G B, (1979); "Fiber optic sensing of pressure and temperature", *Applied Optics*, vol 18, 1445-1448.

[6.18] Butter C D and Hocker G B, (1978), "Fiber optic strain gauge"; *Applied Optics*, vol 17, 2867-2869.

[6.19] Yariv A and Windsor H V; (1980) "Proposal for detection of magnetic fields through magnetorestrictive perturbation of optical fiber", *Optic letters*, vol 5, 87-89.

[6.20] T.Liu, F.Al-Khodairi, M.Wu, M.Irle, G.F. Fernando;(1996) "In-situ monitoring in composites using an embedded extrinsic Fabry-Perot interferometric sensor and a CCD detection system", *Photonics, SPIE conference*, China.

[6.21] Baker R C and Morris M V; "The suitability of flowmeters for optical techniques", *Proceedings of the International Conference on Optical techniques in Process Control*, The Hague, June 1983 (BHRA).

[6.22] Dickinson, "Design considerations for optical flowmeter sensors", *Second International conference on flow measurement*, London, May 1988.

[6.23] Smart M G,(1985), UK Patent GB 2 144 216 A.

[6.24] Norton, P (1983), UK Patent GB 2 111 196A.

[6.25] Place J D and Maurer R, (1986), " A non-invasive fiber optic pick-up for a turbine flowmeter", Proceedings of the fourth international conference on fiber optics, London, *SPIE* vol 630, pp 226-232.

[6.26] Barnard R H, (1984), UK Patent GB 2 082 765B.

[6.27] Tsuruoka M and Miyoshi N, (1986), UK Patent GB 2 103 795B.

[6.28] Sovik R E, (1985), " Flow measurement - some new considerations", Mechanical Engineering, May 1985, pp 48-52.

[6.29] Theoderescu, H N, Sofron E, Baciu I and Schiopu L, (1981), "Low cost sensors based on liquid crystals", *Proceedings of the conference on Electronics for Ocean Technology*, Birmingham, September 1981 (IERE), pp 75-80.

[6.30] Nord H, (1981), " A new solution to an old flow measuring problem", *ISA Transactions*, vol 20, no. 2, pp 11-14.

[7.1] A.L Harmer, "Optical Fiber strain gauge", US Patent, 4 163 397, Aug 7, 1979.

[7.2] C K Asawa et al, "High sensitivity fiber optic strain sensors for measuring structure distortion" , *Electron letters*, vol 18, pp362, 1982.

[7.3] D C Marvin and N A Ives, "Wide range fiber optic strain sensor", *Applied Optics*, vol 23, pp 4212-4217, 1984.

[7.4] The Photonics Design and Applications Handbook. Pittsfield, MA:Laurin Publishing company, 1986, p.H-210.

[7.5] N F Schmitt, Private communcation.

[7.6] Measurement Group, Micro-Measurement Division, Technical Data, Part B, 1988.

[8.1] Murtaza G and Senior J M, "Schemes for referencing of intensity-modulated optical sensor systems", Optical Fibre Sensor Technology, Chapman & Hall (1995).

[8.2] Chandy R., Morgan R. and Scully P.J, Multidirectional air-flow measurement using strain gauges. *International Conference on Signal Processing Applications and Technology '95.Boston, USA, 24-26 October 1995* .

[8.3] Chandy R., P.J.Scully and R.Morgan, "Elastic beam deflection flowmeter using optical and conventional strain gauges", *Applied Optics and Optoelectronics conference, Reading, UK, September 1996.*

[9.1] Brady G P, Hope S, Lobo Ribeiro, Webb D J, Reekie L, Archambault J L and Jacson D A (1994); "In-fibre grating temperature and strain sensors". Tenth International Conference on Optical Fibre Sensors, Glasgow, Sept 1994.

[9.2] N F Schmitt, E Lewis, P Scully; 'UV Photo Induced grating structures on POF', *POF'96*, Paris, France.

[9.3] Keith Dunbell, Private Communication

APPENDICES

Derivation of dA/A

The term dA represents the change in cross-sectional area of the conductor resulting from the applied load. For the case of a uniaxial tensile stress state,

$$\varepsilon_a = \frac{dL}{L} \qquad \text{(A-1)}$$

$$\varepsilon_t = -\nu\,\varepsilon_a = -\nu\frac{dL}{L} \qquad \text{(A-2)}$$

where ε_a is the axial strain in the conductor

ε_t is the transverse strain in the conductor

ν is Poisson's ratio of the material used for the conductor.

If the diameter of the conductor is d_0 before application of the axial strain, the diameter of the conductor d_f after it is strained is

$$d_f = d_0\left(1-\nu\frac{dL}{L}\right) \qquad \text{(A-3)}$$

From Equation A-3 it is clear that

$$\frac{dA}{A} = -2\,\nu\frac{dL}{L} + \nu^2\left(\frac{dL}{L}\right)^2 \qquad \text{(A-4)}$$

Table A-1: Table showing the acquired strain gauge signals and the calculated magnitude of wind speed for the electrical strain gauge flow sensor set at 45° to flow direction.

Fan speed (rpm)	**Wind speed (m/s)**	**$strain_x$ (strain)**	**$strain_y$ (strain)**	**$(strain_x+strain_y)^{1/2}$ (root strain)**
0	0	0	0	0.00127
100	1	-0.00008	0.0001	0.01344
200	4	-0.0006	0.00063	0.03502
300	7	-0.00156	0.00131	0.0535
400	11	-0.0029	0.00276	0.0752
500	14	-0.00441	0.00437	0.0937
600	17	-0.00617	0.00753	0.11708
700	20	-0.00817	0.01138	0.13982
800	23	-0.01019	0.01361	0.15427

Table A-2: $(strain_x+strain_y)^{1/2}$ at different angles to wind flow for the electrical strain gauge flow sensor.

Wind speed (m/s)	**$(Strain_x+strain_y)^{1/2}$ (root strain)**					
	15°	30°	45°	60°	75°	90°
0	0.00206	0.00213	0.00127	0.00469	0.00255	0.00462
1	0.01502	0.01241	0.01344	0.01883	0.03101	0.01503
4	0.04186	0.03181	0.03502	0.04094	0.04889	0.0385
7	0.06529	0.04891	0.0535	0.06034	0.06113	0.05098
11	0.07478	0.07122	0.0752	0.08098	0.07199	0.072
14	0.09396	0.0918	0.0937	0.09762	0.09548	0.0945
17	0.10667	0.12211	0.11708	0.11649	0.10546	0.1062
20	0.12172	0.13439	0.13982	0.14584	0.12489	0.1285
23	0.12722	0.14757	0.15427	0.16005	0.13455	0.1365

Methods for statistical analysis of experimental data

Two variables x and y can be related by a linear equation of the form:

$$y = mx + c \qquad \text{(A-5)}$$

where m is the slope and c is the intercept of the y axis.

Once a linear relationship has been established between two variables, the variability of the data about the fitted line can be described in terms of the confidence limits placed around the line. Typically, 95% confidence limits [3.7] are used where

$$95\%\ \text{confidence interval is}\ \bar{x} \pm \frac{1.96\,\sigma}{\sqrt{n}} \qquad \text{(A-6)}$$

where $\bar{x}$ is the sample mean, σ is the standard deviation, n is the total number of observations in the sample. The confidence interval is a range on either side of a sample mean.

For the tests conducted in this PhD project, the 95% confidence limits were used to ascertain if a set of n samples of data were co-incident. Described below is an illustration of how this was done. For the data presented in Table A-2 in the Appendix, (the corresponding plots are shown in Figure 4.12) the data for the 75^0 and 90^0 positions of the sensor are taken and a regression analysis is performed separately for each of the two positions where x is the wind speed (m/s) and y is root strain. The following values were obtained for the lower 95%, m and upper 95% for both the sets of data.

Regression analysis

Position of the sensor	75^0	90^0
Lower 95%	0.004	0.0053
m	0.005	0.0057
Upper 95%	0.006	0.0061

It can be observed that the value of m at 75^0 (which is 0.005) lies between the Lower 95%-75^0 and Upper 95%-75^0 and also between Lower 95%-90^0 and Upper 95%-90^0. Likewise, the value of m at 90^0 (which is 0.0057) lies between Lower 95%-90^0 and Upper 95%-90^0 and also between the Lower 95%-75^0 and Upper 95%-75^0 .Hence it can be said that the plots at 75^0 and 90^0 are coincident [5.3]. Similar analysis was performed for all the other positions of the sensor and all the plots were found to be coincident.

Table A-3 : Theoretical strain vs. Experimental strain

Wind speed (m/s)	Theoretical strain	Experimental strain
0	0	0
1	3.1E-06	1.9E-06
4	4.9E-05	1.4E-05
7	0.0001	0.0002
11	0.0003	0.0004
14	0.0006	0.0007
17	0.0009	0.001
20	0.0012	0.0013
23	0.0016	0.0016
26	0.0021	0.002
29	0.0026	0.0025
32	0.0031	0.003
35	0.0037	0.0039
38	0.0044	0.005

Table A-4: Table showing the velocity of water predicted from air flow measurements

Sensor output (root of microstrain)	Air speed (m/s)	Water speed (m/s): Equation 4.24
0	0	0
3.46	1	0.03
7	4	0.126
11.83	7	0.22
16.18	11	0.347
20.07	14	0.44
24.08	17	0.53
29.40	20	0.63
33.12	23	0.727
35.93	26	0.82
39.17	29	0.91
42.92	32	1.01
46.46	35	1.10
49.47	38	1.20
51.96	41	1.29
54.68	44	1.39
56.56	47	1.48
57.84	50	1.58

List of Publications

[1] "The drag force flowmeter", *The Measurement, Instrumentation and Sensors Handbook*, CRC Press Inc. Publication; 1997. (To be published)

[2] R Chandy., Morgan R. and Scully P.J. "Elastic beam deflection flowmeter for environmental applications", *Sensors and their Applications VII. Dublin, Ireland, 10-13 September 1995.*

[3] R Chandy., Morgan R. and Scully P.J. "Multidirectional air-flow measurement using strain gauges". *International Conference on Signal Processing, Applications and Technology, Boston, USA, 24-26 October 1995* .

[4] R Chandy., Morgan R. and Scully P.J. "Multidirectional air-flow measurement using strain gauges". *Data Acquisition and Exposition conference '95, Boston, USA, 24-26 October 1995.*

[5] Schmitt N.F., Morgan R. Scully P.J., Lewis E. and Chandy R. "Flow sensor using optical fibre strain gauges", SPIE volume 2508, *Chemical, Biochemical and Environmental Fibre Sensors VII.*

[6] R Chandy., Scully P.J., Schmitt N.F., Lewis E. and Morgan R; "Optical fibre deflection flow sensor for measurement of air velocity"; *Optical Fiber Sensors: Advanced sensing Photonics, Sapporo, Hokkaido, Japan. May21-24 1996.*

[7] R. Chandy, P.J.Scully and R.Morgan, "Elastic beam deflection flowmeter using optical and conventional strain gauges". *Applied Optics and Optoelectronics conference, Reading, UK, September 1996.*

[8] R Chandy, R Morgan, P J Scully, "Theoretical and experimental investigation of the static characteristics of a strain gauge based air flowmeter". *International conference on Material Engineering, Gallipoli-Lecce, Italy*, September 6-8, 1996.

[9] P J Scully, R Chandy, R Edwards, E Lewis, D F Merchant, R Morgan N F Schmitt, F H Zhang; "Plastic Optical Fiber sensors for environmental monitoring", *Plastic Optical Fiber sensors '96- The fifth international conference on Plastic optical fibers and applications, Paris, France*, October 1996. pp 28-29.

[10] P J Scully, B Deboux, R Chandy, R Edwards, J Grabowski, E Lewis, D F Merchant, R Morgan, N F Schmitt and F H Zhang; "Optical Fiber sensors for environmental monitoring", *Optical sensing and its applications, IOP Optical group, Dublin, Ireland*, November 1996. pp6

[11] R Chandy, P J Scully, R Morgan; "Multidirectional air flow sensing using optical fiber strain gauges", *Photonics '96, Madras, India*, December 1996.